Investigation and Modelling of Ice Processes in the Nelson River's Outlet Lakes Area

---

by

KEVIN DANIEL RIDLEY LEES

Thesis submitted to the Faculty of Graduate Studies
of the University of Manitoba
in partial fulfilment of the requirements for the degree of

DOCTOR OF PHILOSOPHY

Department of Civil Engineering
University of Manitoba
Winnipeg, Manitoba, Canada

Publications associated with this research

Peer Reviewed Publications:

Lees, K., Clark, S.P., Malenchak, J., Chanel, P. 2021. Characterizing freeze-up iccover formation on the regulated Upper Nelson River. Journal of Cold Regions Engineering, 35(3).

Lees, K., Clark, S.P., Malenchak, J., Knack, I., Shen, H.T. 2021. Numerical simulation of freeze-up jamming in a skim ice regime. Cold Regions Science and Technology, 191.

Peer Reviewed Publications (in review):

Lees, K., Clark, S.P., Malenchak, J., Chanel, P. (submitted). A novel methodology to quantify winter conveyance through an ice-impacted lake outlet system. Cold Regions Science and Technology.

Conference Proceedings:

Lees, K., Clark, S.P., Malenchak, J., Chanel, P. 2021. Numerical Simulation of Winter Conveyance through the Outlet Lakes Area (Upper Nelson River). 21st Workshop on the Hydraulics of Ice Covered Rivers, CRIPE (virtual conference), Saskatoon, SK, August 29 - September 1.

Lees, K., Clark, S.P., Malenchak, J., Chanel, P. 2019. Two-Dimensional Modelling of Freeze-up Conditions Near Jenpeg Generating Station. 20th Workshop on the Hydraulics of Ice Covered Rivers, CRIPE, Ottawa, ON, July 14 - 16.

Abstract

Ice is a prominent characteristic of water bodies in cold regions. For rivers regulated for hydropower operations, the production of ice particles can result in obstructions and subsequent performance issues during energy production. Rough and thickened ice covers resulting from high flow conditions can also lead to substantial hydraulic losses. While ice formations impact hydropower operations, a river's flow hydrograph also influences ice processes from freeze-up through break-up. Research investigations into the influence of regulation on ice processes benefits not only hydropower practioners, but also those who are impacted by hydropower operations. Further, understanding these cause-and-affect relationships supports design of innovative tools to quantify the impact of ice on river hydraulics.

In this study, a detailed characterization of ice processes is presented for the regulated Upper Nelson River region located at the outlet of Lake Winnipeg in Northern Manitoba, Canada. With a focus on freeze-up and mid-winter processes, this characterization informed design of a 2D numerical modelling methodology to simulate ice-affected winter hydraulics. Model development included simulation of both thermal and dynamic ice phenomenon, which relied on derivation of numerous site-specific hydraulic functions. The presence of significant skim ice runs in this region inspired development of a novel treatment to simulate freeze-up jamming of skim ice floes on very mild-sloped rivers.

The modelling methodology shows strong performance in simulating both freeze-up and mid-winter hydraulics, which is a signficiant contribution considering the complexity of this lake-outlet system. A quantitative evaluation of the effects of climate change on river ice hydraulics is included, with future projection of shorter and warmer winters leading to greater cumulative discharge from Lake Winnipeg. While discharge increases may lead to increased power production in future years, concurrent projections of increased inter-annual variability may present new operational challenges. Findings from this original research can be applied not only to the Nelson River, but also other regulated regions that are impacted by river ice.

Acknowledgements

Upon completion of this thesis I have many people to thank. Firstly, I would like to acknowledge that this research was funded by support from Manitoba Hydro, NSERC, University of Manitoba, Northern Scientific Training Program, and Research Manitoba.

To my research advisors Dr. Shawn Clark and Dr. Jarrod Malenchak, I am truly grateful for your guidance at every step of this journey. Your tireless dedication and helpful advice were a driving force in me being able to finish a thesis I am proud of. To my committee members – Dr. Tricia Stadnyk, Dr. Mark Tachie, and Dr. Lindenschmidt – thank you for your constructive and supportive feedback. The time and support of my entire committee have helped improve the quality of this thesis.

Thank you to Dr. Hung Tao Shen and Dr. Ian Knack, who provided valuable input on river ice modelling aspects of this research. Also thank you to Paul Chanel, Kevin Gawne, Milan Bijeljanin, Phillip Slota, and Mike Vieira for their expertise on Manitoba Hydro's systems. Thank you also to Alexander Wall, as well as Mike Baron and Manitoba Hydro hydrometrics, who provided logistical support and expertise in all things field monitoring.

To my fellow graduate students - thank you for the research talks, fun and games, and support along the way.

To my family - thank you for your endless support and understanding. Thank you also for tolerating every river ice conversation. You always believed in me, even when I struggled to do the same. I hope I have made you proud.

Table of Contents

List of Figures

List of Tables

Notation

$\lvert X_{LW} - X_{704} \rvert$	stream-wise distance from Lake Winnipeg to station 05UB04; where X is stream-wise location
$\lvert X_{704} - X_{FB} \rvert$	stream-wise distance from station 05UB704 to Jenpeg forebay; where X is stream-wise location
A_1, A_2, A_3	polynomial regression coefficients (Fig. 5.7)
a_1, a_2	polynomial regression coefficients (Fig. 4.3)
AAD	average absolute deviation
AE	absolute error
Air	Euclidean distance between inlet and outlet of channel
A_O	open-water surface area
a_S	Stefan formula coefficient
A_{XS}	cross-sectional area
b_1, b_2, b_3	polynomial regression coefficients (Fig. 4.5)
b, b_Y	intercept accompanying Sen's slope
B_0	boundary flux
b_w	empirical coefficient
C	Chezy coefficient
c_1, c_2	polynomial regression coefficients (Fig. 4.7)
C_c	fractional cloud cover
C_d	wind drag coefficient

$CDDF$	cumulative degree-days of freezing
$CDDF_{TOT}$	total cumulative degree-days of freezing over winter
$CDDT$	cumulative degree-days of thawing
$CDDW$	cumulative degree days of warming
$CDDW_{MIN}$	minimum cumulative degree days of warming for warming onset
CL	streamwise length of channel
C_m	melt coefficient
c_p	heat capacity of water
C_T	coefficient relating bed shear stress to turbulent fluctuation velocity
C_w	water-ice drag coefficient
C_{w*}	coefficient accounting for efficiency of wind effects on turbulence
D	hydraulic depth
d_1, d_2	polynomial regression coefficients (Fig. 4.7)
D/S	downstream
DD_R	forebay drawdown rate
D_{local}	flow depth at highest velocity point along cross-section
d_n	nominal diameter of ice particles
DOY_{FO}	nth day (1-365) of freeze-up onset relative to October 1st

DOY_{WM}	nth day (1-365) of warming onset relative to October 1st
d_w	water depth
DY_{WM}	number of mid-winter warming days (January 1st to DOY_{WM})
E	energy
e_1	polynomial regression coefficient (Eq 4-4)
e_a	vapour pressure
e_s	saturated vapour pressure
$Err.$	relative error
F	Froude number
F_{CR}	critical Froude number
F_{local}	Froude number at highest velocity point along cross-section
$F_{R_{approach}}$	Froude number from equilibrium ice cover equation
F_S	dimensionless buoyant velocity ratio
g	gravitational constant
H	operating head
H'	water depth under ice cover
h_{crit}	minimum sheet ice thickness for freezing
h_i	ice thickness
h_{floe}	ice floe thickness
H_{IA}	ice-air heat transfer coefficient

h_s	snow thickness
$h_{s_{max}}$	maximum snow thickness prior to ice cover flooding
h_{sheet}	sheet ice thickness
h_{SOG}	depth of snow-on-ground where subscript *OBS* = observed; *CALC* = calculated
$h_{SOG_{max}}$	seasonal maximum depth of snow-on-ground
$h_{SOG_{mean}}$	seasonal mean depth of snow-on-ground
H_{WA}	water-air heat transfer coefficient
H_{WI}	water-ice heat transfer coefficient
IF	ice factor where subscript *ERIA* = empirical river ice approach; *CRIM* = coupled river ice model; *HIST* = historical; *OBS* = observed
IQR	inter-quartile range
k	empirical constant
k_i	thermal conductivity of ice
k_s	thermal conductivity of snow
L	stream-wise distance from ice front to upstream open water section
LEC	leading edge celerity
LEP	leading edge position
M	daily snowmelt

MAE	mean absolute error
N	surface ice concentration
N_{max}	maximum surface ice concentration
n_i	Manning's ice roughness coefficient
n_b	Manning's bed roughness coefficient
n_c	Manning's composite roughness coefficient
$p_{ensemble}$	ensemble probability value
p_j	porosity of ice jam
POW	power
P_{SIG}	significance proportion
P_{SNOW}	total cumulative precipitation converted to snow
P_{TOT}	total cumulative precipitation where subscript *OBS* = observed; *SIM* = simulated
Q	discharge where subscript *OBS* = observed discharge; *SIM* = simulated discharge; *O-W* = 3D rating curve equivalent calculated discharge; *FINAL* = end-of-winter discharge; *TARGET* = winter discharge target; *ADCP* = field measured discharge; *MIN* = minimum discharge; *HYPE* = Hudson Bay Hydrologic Predictions for the Environment; *G* = generator discharge; *adj* = adjusted; *HIST* = discharge calculated using a historical ice factor; *inflow* = assigned inflow to model; *outflow* = assigned outflow from model boundary
$\vec{q}_{uc}$	under cover ice discharge capacity

R	local energy ratio
R^2	coefficient of determination
Ri_f	flux Richardson number
R_H	hydraulic radius
R_{SNOW}	regional snow coefficient
R_t	albedo
S	water surface slope where subscript *LOC* = local; *REG* = regional; *o-w* = open-water; *TOT* = total
s_i	specific gravity of ice
S_N	sinuosity
SS, SS_Y	Sen's slope
SAE	sum of absolute error
t	time where subscript *start,IS* = start of ice stabilization; *start,IS* = end of ice stabilization; *start,FD* = start of forebay drawdown; *end,FD* = end of forebay drawdown; *start,DD* = start of discharge decline; *end,DD* = end of discharge decline; *FO* = freeze-up onset; *WM* = warming onset; end_sim = end of simulation
T_{AIR}	air temperature (Celsius)
$T_{AIR_{JAN}}$	average January air temperature (Celsius)
T_{AIR_k}	air temperature (Kelvin)

T_{CR}	critical surface water temperature (Celsius)
t_i	ice thickness
$t_{i_{min}}$	minimum ice thickness for stability
T_{MIN}	minimum air temperature (Celsius)
T_m	melting point (Celcius)
T_S	water surface temperature (Celsius)
T_{S_k}	water surface temperature (Kelvin)
T_W	bulk water temperature
T_{WM}	base temperature for warming
U	depth-averaged velocity
u_*	friction velocity
U/S	upstream
$\vec{v}$	velocity
v_z'	vertical turbulence velocity
v_b	average rise velocity of frazil ice
$\vec{v}_{CR}$	threshold velocity for border ice formation
$\vec{v}_{crit}$	critical freezing velocity
$\vec{v}_{ice}$	ice floe velocity
V_f	ice volume
$\vec{v}_{local}$	flow velocity at highest velocity point along cross-section

$\vec{v}_{parcel}$	parcel velocity
w_{dir}	wind direction
w_{mag}	wind speed
WSE	water surface elevation where subscript *FB* = forebay; *LW* = Lake Winnipeg; *704* = station 05UB704; *703* = station 05UB704; *o-w* = open-water; *w-e* = wind-eliminated; *CALC1* = forcing at model boundary UB1; *CALC2* = forcing at model boundary UB2; *CALC3* = forcing at model boundary DB3; *SIM1* = simulated model boundary UB1; *SIM2* = simulated at model boundary UB2; *SIM3* = simulated at model boundary DB3; *ERIA* = empirical river ice approach; *CRIM* = coupled river ice model; *HYPE* = Hudson Bay Hydrologic Predictions for the Environment
X_1	net change in WSE_{LW}
X_2	number of days where $T_{MIN} \leq$ -15°C
X_3	WSE_{LW} at start of winter
X_{MED}	median value of explanatory variable
X_Q, Y_Q	proportions of total discharge
XS	cross-section
Y	response variable
Y_{25th}	25th percentile of response variable
Y_{75th}	75th percentile of response variable
Y_{MED}	median value response variable

z	distance above the ground surface
α_i	fraction of water depth affected by ice friction
β	empirical heat flux coefficient
ΔH	hydraulic head where subscript *LOC* = local; *OBS* = observed; *REG* = regional; *SIM* = simulated; *TOT* = total; *TARGET* = complete forebay drawdown condition; o-w = open-water; *1* = intermediate calculation quantity (Fig. 4.1); *HIST* = predicted using historical ice-factor
Δh_{sheet}	change in sheet ice thickness
Δt	change in time
Δt_h	hydrodynamic timestep
Δt_{ice}	ice dynamic timestep
Δt_{intvl}	coupling timestep
ΔQ	winter discharge decline
$\Delta Q/\Delta t$	normalized winter discharge decline
ε_a	emissivity of air
ε_w	emissivity of water
θ	dimensionless flow strength
θ_c	dimensionless critical flow strength
κ	von Kármán constant
λ	latent heat of fusion of ice

η	efficiency
ρ_a	air density
ρ_i	density of ice
ρ_w	water density
σ	Stefan-Boltzmann constant
τ_i	flow shear stress at ice cover
$\emptyset$	internal friction angle of ice rubble
$\emptyset_*$	net heat flux
$\emptyset_B$	net long-wave radiation flux
$\emptyset_{cl}$	clear-sky short-wave radiation flux
$\emptyset_G$	groundwater seepage heat flux
$\emptyset_L$	latent heat flux
$\emptyset_{precip}$	precipitation heat flux
$\emptyset_R$	net short-wave radiation flux
$\emptyset_S$	sensible heat flux
$\emptyset_{wa}$	total heat flux at air-water interface
$\emptyset_{wa}$	heat loss at the air-water interface
$\emptyset_R$	net short-wave radiation
ω	buoyancy velocity of ice particles

Chapter 1: Introduction

1.1 Background and Motivation

Ice processes are an important attribute of water bodies in cold regions. These water bodies include not only lakes and rivers, but also constructed features like canals and reservoirs. Ice processes have considerable implications for both anthropogenic and natural environments. For instance, in communities at high latitudes humans may rely on ice roads for safe transport and remote site access. Ice covers also present opportunities for mid-winter recreation, including activities such as skating, hockey and ice fishing. For aquatic and terrestrial habitats, the annual transition between open-water and ice-covered conditions is important for physical, chemical and biological processes. Ice-affected flow conditions also facilitate transport of sediment, which can lead to erosive and depositional conditions that control the morphology of water bodies.

Relative to ice processes in quiescent water bodies such as lakes, ice processes in rivers are considerably more complex due to the movement of water. River ice processes are generally site-specific, dynamic, and both spatially and temporally variable. Even at onset of ice formation during the start of winter, river ice can result in material backwater conditions (i.e., water level change) that are driven by an increased channel resistance to flow. In the event of ice jam formation leading to severe flow restrictions, substantial backwater can result in flooded conditions that are potentially catastrophic for infrastructure and public safety.

Highly dynamic and consequential events such as ice jam floods are an important motivator for knowledge advancement of the field of river ice engineering. Aside from flooding concerns, river ice researchers and practitioners have also focused on the impacts of ice on energy generation, which includes hydropower systems on regulated rivers. An example of these impacts is a reduction in flow from a reservoir due to the formation of an ice restriction, which may compromise energy production.

River ice research continues to advance our common understanding of the formation, evolution and breakup of ice covers. This research has included laboratory experiments at various scales, as well as physical and numerical modelling. Research efforts also include adapting new technologies and monitoring techniques to support

in-situ observations of ice processes. These technologies can also mitigate the safety risks associated with winter field work. The following sections provide general descriptions of ice cover formation and evolution through winter, as well as information on interactions between ice and regulated hydropower systems.

1.1.1 Thermal Processes

In natural environments, the formation of ice on a water body relies on two primary conditions: (1) supercooling, and (2) nucleation. Supercooling refers to the process of reducing the temperature of water past its freezing point (approximately 0°C for fresh water) without changing state. Once supercooling is achieved, crystals can form resulting in ice generation and latent heat release. For a water body to become supercooled it must lose energy to its surrounding environment. This energy exchange is characterized by a net heat flux ($\emptyset_*$), which can be quantified using a complete energy-budget equation that typically includes only the most significant energy quantities (Eq 1-1).

$$\emptyset_* = \emptyset_{\boldsymbol{R}} + \emptyset_{\boldsymbol{B}} + \emptyset_{\boldsymbol{S}} + \emptyset_{\boldsymbol{L}} + \emptyset_{\boldsymbol{precip}} + \emptyset_{\boldsymbol{G}} \qquad \text{Eq 1-1}$$

Short-wave radiation ($\emptyset_R$) is derived from the sun's energy and is termed *solar insolation* upon arriving at the Earth's surface following atmospheric interactions (Ashton, 2013). Short-wave radiation plays an important role in ice cover decay, as well as ice processes impacted by diurnal heat flux patterns. Net long-wave radiation ($\emptyset_B$) is the balance of energy exchanged between the Earth's surfaces and the atmosphere, in accordance with Boltzman's Law. The magnitude of long-wave radiation contributions to net heat loss can be significant, even when air temperatures are only moderately cold. Sensible heat flux ($\emptyset_S$) is important throughout winter and is driven by gradients of temperatures and wind-speed (Ashton, 2013), while latent heat flux ($\emptyset_L$) can be significant during evaporation or sublimation. Secondary fluxes include heat transfer from precipitation ($\emptyset_{precip}$) and groundwater seepage ($\emptyset_G$), although these are typically of smaller magnitude relative to other quantities.

Estimating a net heat flux using Eq 1-1 requires detailed measurements of many quantities, which can be impractical for some applications. A simplified method

commonly applied in river ice calculations utilizes a water-air heat transfer coefficient (H_{WA} [W m^{-2} °C^{-1}]) as shown in Eq 1-2:

$$\emptyset_* = H_{WA}(T_S - T_{AIR}) \quad \text{Eq 1-2}$$

where T_{AIR} is air temperature [°C]. The water surface temperature (T_S [°C]) is often approximated using the bulk water temperature (T_W [°C]), which is a quantity easily measured by using monitoring instrumentation (i.e., temperatures sensors). The typical range of H_{WA} reported in the literature is $15 - 25$ W m^{-2} °C^{-1}, although factors such as windspeed can result in highly variable conditions (Marcotte, 1975; Prowse, 1995). A constant value of H_{WA} is often applied in river ice studies, such as those involving numerical simulations, despite this known variability (USACE, 2006).

Transport of thermal energy in rivers can be approximated by a depth-averaged form of the heat transport and conservation equations (Eq 1-3):

$$\frac{\partial T_w}{\partial t} + U\frac{\partial T_w}{\partial x} \cong \frac{\emptyset_*}{\rho_w c_p D} \quad \text{Eq 1-3}$$

where t is time [s], U is depth-averaged velocity [m s^{-1}], ρ_w is water density [kg m^{-3}], D is hydraulic depth [m], and c_p is the heat capacity of the water [J kg^{-1} °C^{-1}]. Application of Eq 1-3 assumes well-mixed conditions, which may not apply to deep rivers with a vertical temperature gradient and thermal inertia. Deep water bodies generally take a long time to reach equilibrium with cold atmospheric conditions.

1.1.2 River Ice Formation

Using an analytical approach (Eq 1-4; Beltaos, 1995), the volume of ice (V_f [m^3]) generated in a water column can be determined through an integration of heat loss from the water column over time:

$$V_f = \frac{1}{\rho_i \lambda}\int_{t_1}^{t_2} A_0 H_{WA}(T_W - T_{AIR})dt \quad \text{Eq 1-4}$$

where ρ_i is the density of ice [kg m^{-3}], λ is the latent heat of fusion of ice [J kg^{-1}], and A_0 is open-water surface area [m^2]. While Eq 1-4 yields a reasonable approximation of ice quantities generated in natural water bodies, the transport and fate of this ice depend on numerous conditions. These conditions can result in a variety of ice processes as illustrated on Fig. 1.1.

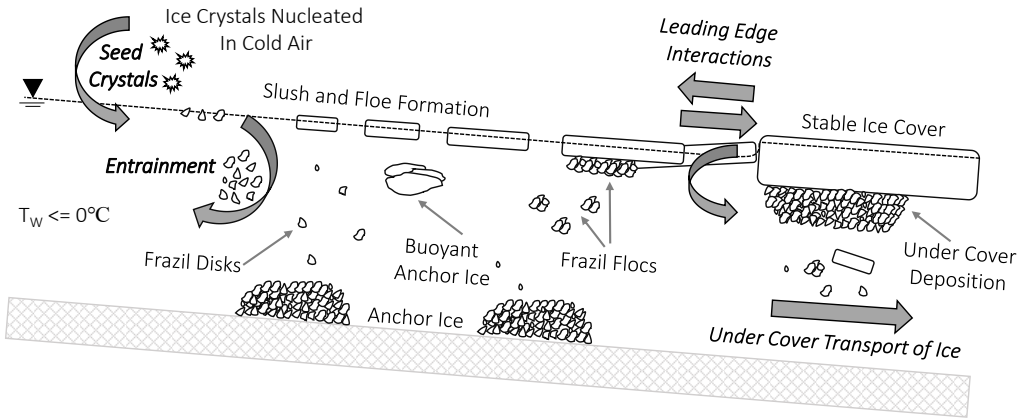

Fig. 1.1 - Profile view of a simplified evolution of river ice processes (adapted and modified from Daly (2013).

As previously mentioned, a primary condition for ice formation in natural water bodies is supercooled temperatures. The secondary condition for ice formation is nucleation, which can take one of two forms. If supercooled water temperatures reach -38°C or less, *spontaneous nucleation* can occur. However, this is specifically a lab-controlled occurrence and does not happen in natural water bodies (Daly, 1984). Instead, *heterogenous nucleation* involves ice particle formation via initiation by a *seed crystal*, such as a snowflake or air bubble.

In a calm water body such as a lake, ice formations are generally smooth with uniform properties. On the contrary, river ice formations can be highly variable and usually appear in stages. At the onset of winter, early river ice formations include *border ice*, which is surface ice that initiates in areas of low turbulence with attachment (e.g., along shorelines) and grows laterally into the channel. Ice that initiates in the form of ice sheets away from shorelines is termed *skim ice run*; a term that describes a collection of ice pieces referred to as *skim ice floes*. Factors

contributing to skim ice run formation include low turbulence and high heat loss, which can result in growth of ice floes with high buoyancy and large surface area.

Early river ice studies (i.e., Michel, 1967) noted that with the introduction of turbulence, via either wind or water movement, surface ice particles may become entrained into suspension. As a result, ice particles transform into a sticky and slushy material referred to as *frazil ice*. The turbulence-induced forces that entrain ice particles are countered by buoyant forces. After entrainment of enough ice particles, conglomerates of frazil ice gain sufficient buoyancy in the form of *frazil flocs.* These frazil flocs will float to the river's surface where they take form of *frazil pans*. These frazil pans gain additional ice mass through both thermal growth and mechanical interactions with other pans or border ice edges (process of *buttering*). Mobile units of ice (e.g., skim ice floes, frazil ice pans) contribute to the formation of ice jams (discussed further in Section 1.2.1.2). Suspended frazil ice may also adhere to the channel bed to become *anchor ice*, which can lead to intermittent release events resulting in the formation of *buoyant anchor ice*.

1.1.3 Ice Effects on River Regulation

River regulation refers to the control of water levels and/or discharge variability in a water body to meet demands ranging from domestic water supply to industrial applications. Regulation is generally accomplished by construction and operation of hydraulic structures such as dams. For regulated rivers that supply hydropower operations, ice conditions can present numerous complications. In essence, the presence of an ice cover increases the total hydraulic resistance of a river, leading to either increased backwater or reduced flow (or both) as a result of energy losses.

Strategies to manage river ice are generally classified as either *structural* and *non-structural* (Tuthill, 1999). Structural approaches include the permanent installation or annual deployment of ice booms to initiate ice cover formation (example on Fig. 1.2).

Fig. 1.2 – Example of an ice boom (oblique view on top, plan view on bottom), located upstream of Jenpeg Generating Station in Northern Manitoba. [Images by Kevin Lees]

Another example is rock groynes (example on Fig. 1.3), which are in-stream structures that support ice cover formation and reduce the likelihood of cover collapse which leads to undesirable ice thickening.

Fig. 1.3 – Rock groyne (stream-wise rock-structure partition) in the Ominawin Bypass Channel in Northern Manitoba. [Image courtesy of Manitoba Hydro]

Non-structural approaches are mainly focused on flow control, which involves strategic manipulation of river hydraulics to control ice cover formation. The hydro-meteorological conditions unique to a sample of flow control programs world-wide are summarized on Fig. 1.4.

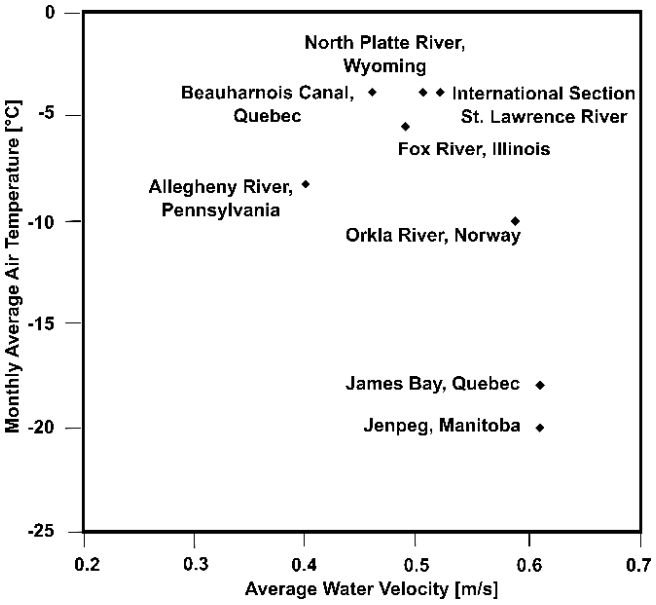

Fig. 1.4 – Examples of flow control programs worldwide (adapted from Tuthill, 1999); estimates for the Orkla River derived from Stickler and Alfredson (2010) and Gebre et al. (2014).

It is notable that flow control programs in Canada, and in particular Manitoba, are characterized by exceptionally cold sub-arctic temperatures.

The start of winter presents an especially critical time for ice management. Considering there is usually limited ice coverage in early winter, the onset of cooling conditions can promote supercooling and the formation of substantial amounts of ice in expansive open-water areas. This ice is subject to transport under the limited ice cover, which may lead to *under cover deposition* resulting in increases to under-ice roughness and thickness. Ice may also deposit at downstream hydraulic structures leading to congestion on hydropower intake components (i.e., trash racks), resulting in considerable head-losses and operational difficulties.

As a mitigation to reduce frazil ice risks, an effective strategy is to suppress ice production at the source by promoting formation of a stable insulating ice cover as early as possible. This is achieved through temporary flow reductions, which reduce flow velocities and increase the likelihood that ice floes accumulate in the upstream direction to form an ice cover. It is important that these flow reductions are as short as possible to minimize impacts to flow supplies and waterway users.

While flow reductions may lead to immediate reductions in power generation, net benefits in the form of improved flow conveyance through winter can be substantial. For instance, on the Nelson River it is estimated that freeze-up flow control at Jenpeg Generating Station (Jenpeg) contributes to annual savings on the order of two million dollars per year (Zbigniewicz, 1997). A conceptual visualization of the benefits of a temporary flow reduction (or *cutback*) is shown on Fig. 1.5.

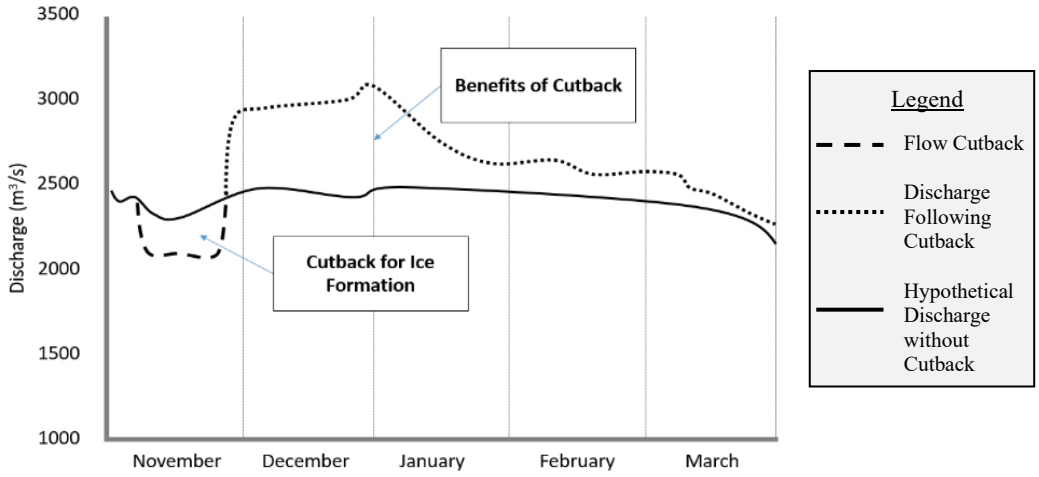

Fig. 1.5 – Visualization of the conveyance benefits achieved by a temporary flow reduction or *cutback* (adapted from Zbigniewicz, 1997).

Procedures followed for river ice control generally rely on site-specific monitoring data and heuristics guided by professional expertise. To further support these practices, there is considerable research interest in advancing development of models that can simulate pertinent river ice processes and their impact on river hydraulics. While these tools present opportunities for present-day operational support, they can also provide far-future projections of climate impacts on local ice conditions.

A regulated hydropower area of interest to many stakeholders is the *Outlet Lakes Area* (*OLA*) of the Upper Nelson River in Manitoba, Canada. This area regulates outflows from Lake Winnipeg through control at Jenpeg Generating Station (Jenpeg), in tandem with other structures and channels developed in the 1970s as part of *Lake Winnipeg Regulation*. As described by Manitoba Hydro, Lake Winnipeg Regulation was pursued to achieve two key objectives: (1) reduce shoreline flooding on Lake Winnipeg, and (2) support hydroelectricity generation to meet the growing

demand in Manitoba (Manitoba Hydro, 2014). Lake Winnipeg Regulation components and OLA water bodies are shown on Fig. 1.6, with the general flow direction being north.

Fig. 1.6 – OLA facilities and control structures (red squares), constructed channels (red lines) and water bodies involved in Lake Winnipeg Regulation. Copyright image used with permission granted by Manitoba Hydro (J. Malenchak, personal communication, January 25, 2022).

Through hydraulic control by Jenpeg and other Lake Winnipeg Regulation components (e.g., Two-Mile Channel, Eight-Mile Channel, Ominawin Bypass Channel, etc.), the outflow from Lake Winnipeg is harnessed for power generation

on the Nelson River. Flows from Lake Winnipeg, along with flows from the Burntwood River and Grass Rivers further downstream on the Nelson River, supply power generation at six hydropower stations (including Jenpeg). Together, these stations supply 75% of Manitoba Hydro's total electricity generation (Manitoba Hydro, 2014). The OLA provides an excellent setting to both advance knowledge of river ice processes in regulated river settings, as well as design tools to simulate these processes. Aside from the economic importance of this system, the OLA features diverse river ice processes, an active hydrometric monitoring network, and complex open-water and ice affected hydraulics.

[Author's note: throughout this thesis the terms *Outlet Lakes Area* and *Upper Nelson River* may be used interchangeably, however without exception these terms are intended to describe the same geographic region.]

1.2 Literature Review

1.2.1 Freeze-Up and Mid-Winter Ice Processes

1.2.1.1 Border Ice and Ice Floe Formation

In early winter when supercooling occurs, first ice formation initiates in slow-moving water. In the case that this ice initiates at a support such as a shoreline or stationary structure, it is termed *border ice*. This ice type is also referred more generally as *static ice cover*, especially in the case of a lake or other relatively still water body that becomes completely ice-covered via thermal ice processes.

While most rivers are generally well-mixed, a steep temperature gradient exists at the upper layer of the water column near the air-water interface, meaning a supercooled surface layer can form with sufficient heat loss. Matoušek (1984a) developed an empirical approach to estimate the temperature of this near-surface layer (T_S [°C]) using bulk-water temperature (T_W [°C]), air temperature (T_{AIR} [°C]), an air-water heat transfer coefficient (H_{WA} [W m^{-2} °C^{-1}]), depth-averaged flow velocity (U [m s^{-1}]), and wind-speed (w_{mag} [m s^{-1}]) (Eq 1-5):

$$T_S = T_W - \frac{H_{WA}(T_W - T_{AIR})}{1130U + b_w w_{mag}} \quad \text{Eq 1-5}$$

where b_w is a channel width coefficient [-]. Border ice formation can be predicted using T_S by comparing with a critical value (T_{CR} [°C]). Documented site-specific values of T_{CR} in the literature include -1.1°C for the River Ohre (Matoušek, 1984a), -0.5 °C for the St. Lawrence River (Liu and Shen, 2011), and -0.15 °C to -0.25 °C for the Nelson River (Bijeljanin, 2013; Malenchak, 2011). This considerable range of site-specific values is owed mainly to differences in river conditions and calibration approaches.

Field studies have investigated border ice characteristics on a variety of rivers, with a particular focus on critical velocity thresholds and rates of border ice growth. Northern river investigations have included the Red River and Assiniboine River (Simoes et al., 2020), the Nelson River (Newbury, 1968) and the Burtwood River (Miles, 1993). More southern river investigations have focused on the St. Anne River (Michel et al., 1982) and the Ottauquechee River (Calkins and Gooch, 1982). Limited studies have focused on border ice formation in small rivers, although notable exceptions include Matoušek (1984b) and Hirayama (1986). Among the findings of these studies is the recognition that both channel hydraulics and heat fluxes contribute to border ice formation and growth.

If surface ice forms away from attachment areas, mobile ice floes will form. The tendency for these ice floes to remain on the water surface depends on the balance of ice buoyancy (characterized using *buoyant velocity* or v_b [m s^{-1}]) and turbulence (characterized using *vertical turbulence velocity* or v_z' [m s^{-1}]). While the magnitude of v_b can be estimated based on the magnitude of T_S (Matoušek, 1992), additional lab (e.g., McFarlane et al., 2014) and field (e.g., Morse and Richard, 2009) studies feature more rigorous investigations of frazil buoyancy. Values for v_z' are usually determined through empirical equations that consider flow and channel properties, while some approaches also incorporate the influence of wind-induced turbulence (Lal and Shen, 1989).

If ice particle buoyancy is sufficient, ice particles will remain at the surface in the form of *skim ice floes.* These ice floes are thin upon formation and have the appearance of grease or glass ice (Matoušek, 1984b; Marcotte, 1984). Field observations of substantial skim ice runs are limited, and include study areas in the regions of the St. Lawrence River (Marcotte, 1984b), the Peace River (Jasek et al.,

2013), and the Tanana River (Osterkamp and Gosink, 1983). Laboratory experiments have included investigations into the conditions that result in different types of ice floe formations. These include a study of turbulence in a cold-lab counter-rotating flume (Unduche, 2008), and assessment of velocities in a cold-lab re-circulating channel (Hammar et al., 2002). Additional related studies include a theoretical analysis of turbulence effects on surface ice formation (Andreasson et al., 1998) and a field investigation of water column mixing (Richard, 2011).

One of the most widely-referenced frameworks describing the delineation of conditions that result in static ice cover, skim ice run, or frazil ice formation was developed by Matoušek (1984b). This framework uses depth-averaged flow velocity, heat flux and channel properties (expressed through a Chezy coefficient) together to predict ice type formation. The approach was developed and verified using observations from relatively small rivers (Prague-Podaba, Ohře River, and Middle Lab) under moderate net heat fluxes (Q_{OBS} = 104 to 242 m^3 s^{-1}; $\emptyset_*$= -148 to -289 W m^{-2}). In this light, there exists opportunity to evaluate this framework for other types of rivers, including large regulated sub-arctic rivers.

1.2.1.2 Ice Jam Formation and Undercover Transport of Ice

There are several types of ice jams that occur in nature. In the case of tranquil flow conditions, a *surface jam* may form from a single layer of ice floes (Beltaos, 1995). A more dynamic scenario is the formation of a *wide-channel jam* or *narrow-channel jam* (Section 1.1.2) as described by Pariset et al. (1966), resulting in thicker ice conditions relative to a surface jam. Wide-channel jams are characterized as an accumulation of ice mass that is prone to collapse and thickening due to applied forces and ice cover failure (a process referred to as *consolidation*). The process of repeated ice cover collapse and upstream advance of the ice cover is referred to as *telescoping* (Beltaos, 1995).

Narrow-channel jams are formed and thicken because of ice that submerges at a leading ice edge, in accordance with the hydraulics of the river. The upstream progression of a narrow-jam is referred to as *frontal progression* (Michel, 1984). Regulated rivers are typically operated: (1) to achieve narrow-channel jam formation, and (2) to minimize risk of consolidation. In general, it is advantageous

for regulated rivers to have an ice cover with low hydraulic resistance. It should be noted that the factors contributing to the characteristics of ice jams are numerous, and include the quantity of ice supply, characteristics of active ice floes, integrity of the existing ice cover, channel geometry, and hydraulic conditions (Matoušek, 1984a,b; Uzuner and Kennedy, 1972; Pariset and Hausser, 1961).

Studies by Pariset and Hausser (1961) and Pariset et al. (1966) laid the foundation to describe behaviour of ice floes at a leading edge, such as an upstream ice boundary or ice boom. This includes differentiating between conditions resulting in ice floe submergence from those resulting in ice floe arrest and upstream propagation. These studies focused on ice cover progression based on a h_{floe}/d_w (ice floe thickness/water depth) ratio and the incoming velocity of the ice floe. Michel (1971) evaluated the forces acting on an ice floe at a leading edge, yielding derivation of a modified form of the equilibrium ice cover equation proposed by Pariset et al. (1966) (Eq 1-6):

$$F_{R_{approach}} = (1 - \frac{h_{floe}}{d_w}) \sqrt{2(1 - s_i)(1 - p_j)(\frac{h_{floe}}{d_w})} \quad \text{Eq 1-6}$$

where s_i is the specific gravity of ice [-], and p_j is the porosity of the ice jam [-]. This research gave rise to the use of a critical Froude number (F_{CR}) to predict the likelihood of ice floe submergence during ice jamming. Many factors contribute to the reliability of a critical Froude number, including channel properties and geometric/strength characteristics of incoming ice floes. An early publication by Kivisild (1959) reported an estimated range of $0.06 \leq F_{CR} \leq 0.09$, similar to a finding by Shen and Ho (1986) who noted F_{CR} to be 0.09.

While F_{CR} thresholds are widely-applied in engineering applications, this metric may be less dependable in some regulated rivers with a small *ice thickness-to-flow depth* ratio (Tuthill and Mamone, 1998). On these rivers, streamwise velocity may be a more reliable metric for predicting ice floe submergence. Laboratory observations by Perham (1983) yielded a critical streamwise velocity for submergence to be 0.7 m s^{-1}. More recent studies have investigated the fundamental physics governing ice floe submergence, including pressure effects at leading ice edges (Dow Ambtman et al.,

2011). Other relevant studies related to ice floe behaviour include Ashton (1974); Countermash and McGilvary (1994, 1993); Daly and Axelson (1990); Hara et al. (1996); Larsen (1975); Uzuner and Kennedy (1972).

In the event of ice floe submergence, ice particles may be briefly transported only to deposit under the ice cover in low velocity areas. These resulting under-ice formations are referred to as *hanging dams*, and the hydraulic energy losses associated with these collections of ice particles can be substantial. The presence of open-water areas, especially those that remain open throughout winter (example shown on Fig. 1.7), can increase risks of ice generation and hanging dam formation.

Fig. 1.7 – Open-water area at Manitou Rapids section of the OLA in Northern Manitoba, with flow direction being towards the bottom of the image. [Image courtesy of Manitoba Hydro]

Shen and Wang (1995) characterized the movement of under ice particles by coupling erosion and depositional processes, which are governed by the ice supply and carrying capacity of the flow area under the ice cover (Eq 1-7 and Eq 1-8):

$$\varphi_i = 5.487(\theta - 0.041)^{1.5} \qquad \text{Eq 1-7}$$

$$\varphi_i \equiv \frac{\vec{q}_{uc}}{F_S d_n \sqrt{(1 - s_i) g d_n}} \; and \; \theta \equiv \frac{\tau_i}{\rho_w F_S^2 (1 - s_i) g d_i} \qquad \text{Eq 1-8}$$

where $\vec{q}_{uc}$ is the ice discharge capacity per unit width [m^2 s], F_S is a dimensionless buoyant velocity ratio [-], τ_i is the flow shear stress at the underside of the ice cover [N m^2], ρ_w is the density of water [kg m^{-3}], d_n is the nominal particle diameter [m]. If θ exceeds 0.041 (or another chosen critical value), under cover deposits will erode to a further downstream location according to the ice discharge capacity of the flow.

The effects of ice on river hydraulics depend both on the nature of initial ice jam formation, as well as evolution of the ice cover throughout winter. An ice cover formed in relatively calm conditions may have an Manning's ice roughness coefficient (n_i) of 0.01 to 0.015 (Beltaos, 2013), while these values can increase considerably based on the jam thickness and properties of ice floes that comprise the jam (Nezhikhovskiy, 1964). Several studies (e.g., Ashton and Nufelt, 1991; Beltaos, 2011) describe the various mechanisms that decrease ice cover roughness over winter, including the downward growth of a solid ice layer from the interstices of the ice cover, and thermal erosion at the underside of the ice cover. While these processes result in a smoother ice conditions over winter, a continuous supply of ice particles that thicken hanging dams may serve to increase ice roughness. Ice roughness estimates for hanging dams reported in the literature include 0.03 (St. Lawrence River; Shen and Van DeValk, 1984) and 0.04 (Smokey River; Beltaos and Dean, 1981). Characterizing and simulating the impacts of ice on river hydraulics should consider the cumulative effects of both ice jam formation and under ice deposition.

1.2.1.3 Ice Growth and Decay

Both individual ice floes and expansive ice covers are subject to thermal growth and decay. Growth and decay rates are governed by heat fluxes and other environmental conditions, including the presence of insulating materials such as snow. A practical equation often employed to estimate ice thickness (h_i) is the Stefan formula, as described by Michel (1971) (Eq 1-9):

$$h_i = a_s\sqrt{CDDF} \qquad \text{Eq 1-9}$$

here a_S [m °$C^{-0.5}$ $day^{-0.5}$] is a calibrated coefficient with typical values ranging from 0.007 to 0.035, depending on wind and snow conditions (Michel 1971). Cumulative

degree-days of freezing (*CDDF*) is a measure of departure of T_{AIR} from a base temperature (typically selected as 0ºC) (Boyd, 1979). A more comprehensive method of calculating ice growth employs differential equation that accounts for heat fluxes through ice and snow layers (Ashton, 2013) (Eq 1-10):

$$\frac{dh_i}{dt} = \frac{H_{IA}(T_m - T_{AIR}) - \emptyset_R}{\rho_i \lambda H_{IA}\left(\frac{h_i}{k_i} + \frac{h_s}{k_s} + \frac{1}{H_{IA}}\right)} \qquad \text{Eq 1-10}$$

where T_m [°C] is the melting temperature, h_s is the snow depth [m], and k_i and k_s are the thermal conductivities [W m^{-1} °C^{-1}] of ice and snow, respectively. While Eq 1-9 and Eq 1-10 are well-established, there are complicating factors that affect their reliability. Among these factors are spatial variation in snow thickness and river hydraulics, as well as concurrent thickening of an ice cover via mechanical processes (i.e., ice cover consolidation or under-ice deposition).

The role of snow during ice growth and decay has been the focus of numerous studies in the literature. The thermal resistance of snow (0.04 to 1.0 W m^{-1} °C^{-1}; Arenson et al., 2014) is considerably less than that of ice (2.7 W m^{-1} °C^{-1}; Arenson et al., 2014), meaning that the presence of snow slows ice growth and decay rates. In the event that a snow layer on an ice cover exceeds the cover's buoyancy, the interface between snow and ice becomes submerged and flooded. Ashton (2011) described the phenomenon of ice cover flooding as a state of *isostacy*, where a head differential drives water upward forming slush. As this slush layer re-refreezes, the result is *snow ice* formation. This snow ice layer is discussed by numerous sources in the literature (Adams and Prowse, 1981; Beltaos, 2008; Michel, 1971). The presence of various snow and ice layers complicates application of Eq 1-10 due to the differences in thermal properties between materials.

Predicting rates of ice decay using Eq 1-10 can be a more complicated endeavour, especially in the presence of a snow layer. This is due to the complex partitioning of energy gains by the snow and ice layers during melt (Ashton, 2011). In an extensive study by Bilello (1980), empirical methods were applied to characterize river and lake ice decay using cumulative degree-days of warming (*CDDW*), which accounts for the insulating effect of snow during ice decay. Shen and Yapa (1984) later proposed a unified degree-day method to estimate both thermal growth and decay of

an ice cover. For regulated rivers with significant snowfall, proper treatment of snow is necessary for accurate estimation of ice thicknesses, and the subsequent impact of that ice on channel hydraulics.

1.2.2 River Ice Modelling and Ice Forecasting

River ice models can be broadly classified as either physical or numerical. In the case of numerical models, these tools can range in complexity from analytical equations to comprehensive two-dimensional models. On the spectrums of academic to commercial and physically-based to empirical, river ice models are typically academic and empirical. However, these models are not limited to academic environments, and have supported real-world endeavours including engineering design, industry operation, and environmental impact assessment (Petryk, 1995).

River ice models in the literature are generally site-specific and formulated under simplifying assumptions. Early river ice models applied historical records and simplified mathematical/empirical equations (Ashton, 1986). These models have since progressed to resolve more complex equations through advanced computing platforms. While simulation capabilities vary between models, the physical processes that are represented by model calculations can be categorized as: *supercooling*, *ice generation and transport*, *ice jamming and consolidation*, *under cover erosion and deposition*, *thermal ice growth and decay*, and *ice cover breakup* (Petryk, 1995).

The following sections describe the pertinent one-dimensional and two-dimensional river ice models described in the literature, along with notable applications of these models.

1.2.2.1 One-Dimensional River Ice Models

One-dimensional (1D) river ice models are designed using uniform cross-section conditions (e.g., average flow velocity). Quantities relevant to river ice calculations, such as water temperatures, ice concentrations and ice forces are also represented by cross-section values. A 1D river ice modelling approach cannot account for the effects of transverse flow distribution on river ice processes, however these models are advantageous due to their computational efficiency, availability for use (see descriptions of *RIVICE* and *RIVER1D*), and relative ease of implementation. The

following is a brief description of prominent 1D river ice models mentioned in the literature.

ICEDYN/ICESIM (Carson et al., 2003; Petryk, 1995; Simonsen and Carson, 1977)

ICESIM was initially developed by Acres International Limited in the 1960s as part of engineering design on the Nelson River. This steady state model can simulate both freeze-up and break-up processes that influence the characteristics of a water surface profile, including ice generation, ice jamming, under cover deposition and transport, border ice growth, and anchor ice processes. ICEDYN functions as an extension to ICESIM to facilitate unsteady simulations. These capabilities were motivated by a need for evaluation of hydropower peaking scenarios.

RIVICE (Lindenschmidt, 2017; Martinson et al., 1993)

RIVICE was initially developed by a Canadian consortium and is currently housed at the Global Institute for Water Security (University of Saskatchewan). RIVICE is unique in that it is among the few open-source river ice models available for prospective users. The model is described as fully-dynamic wave model, and similar to ICESIM/ICEDYN, is capable of simulating ice jamming, ice consolidation, and under cover deposition and transport processes. RIVICE also facilitates calculations of thermal processes such as border and skim ice formation. Applications of RIVICE have focused mainly on ice jam simulations both in Canada (e.g., Red River, Athabasca River, Peace River, Yukon River) and abroad (Tornionjoki River, Oder River). The model's short computation times allow for stochastic modelling endeavours, such as those involving a Monte-Carlo framework.

RIVER1D (Blackburn and She, 2019)

RIVER1D is a public domain model developed and housed at the University of Alberta. The goal of the RIVER1D research initiative is to create a comprehensive river ice processes model that is capable of simulating dynamic ice processes in natural systems. RIVER1D can accommodate natural channel geometry and simulate both thermal and dynamic ice processes. Developers note that the model's current treatments of anchor ice evolution and under cover ice processes are ongoing.

Notable applications of RIVER1D have included study areas on the Susitna River and Peace River.

MIKE-ICE (Thériault et al., 2010)

MIKE-ICE is a river ice add-on module to the Danish Hydraulic Institute's (DHI) hydraulic model MIKE11. MIKE-ICE is capable of unsteady simulations that account for a variety of thermal and dynamic ice processes. Applications of MIKE-ICE in the literature are limited, however the model has been applied for hydropower applications on the Romaine River.

RICEN (Shen et al., 1991, 1995; Shen, 2010)

The RICEN model was developed at Clarkson University with the intention of providing comprehensive river ice simulation capabilities. The model is capable of unsteady simulations that include thermal and dynamic ice processes such as supercooling, ice generation, border and skim ice growth, anchor ice growth, ice jamming, under cover deposition and transport, and thermal ice growth and decay. A novel aspect of the RICEN model is the formulation of a two-layer ice transport framework, where suspended ice and surface ice are evaluated individually. Many of the RICEN formulations form the basis of the more advanced CRISSP2D model (discussed in Section 1.2.2.2).

1.2.2.2 Two-Dimensional River Ice Models

Two-dimensional (2D) river ice models are considerably more complex than 1D models. These 2D models employ a finite element method (FEM) solving approach, which includes a triangular mesh to facilitate calculations. The advantages of these models over a 1D solving approach is that 2D models can account for effects of transverse flow distribution on river ice processes. However, the main disadvantage of these models is that their computational efficiency can be low, which limits applications. Models with 2D simulation capabilities may be useful for environments with flow splits and braided or meandering channels, such as deltas or regions flooded for hydropower generation. To date, there are two primary 2D river ice models frequently mentioned in the literature, although there are others in development (e.g., TELEMAC; Bourban et al., 2018).

RIVER2D (Katopodis and Ghamry, 2007; Steffler and Blackburn, 2002 Wojtowicz et al., 2009)

RIVER2D, a 2D version of the previously mentioned RIVER1D model, was initially a hydraulic model but has since been adapted to facilitate simulations of supercooling, border ice formation, frazil ice processes, ice bridging and frontal progression. The current state of RIVER2D development is unclear from the literature, and documented applications of RIVER2D have been limited to the Athabasca River.

CRISSP2D (Liu et al., 2006; Shen, 2010, 2002)

Two-dimensional Comprehensive River Ice Simulation System Project (CRISSP2D) functions as an extension of DynaRICE (Shen et al., 2000a) and RICEN (Shen et al., 1995). The model was developed to address multiple issues faced by hydropower operators in North America. CRISSP2D remains one of the only 2D river ice models in active development and is comprehensive in the types of river ice processes that can be simulated. Study rivers where CRISSP2D has been applied are numerous and include the Odra River (Kolerski, 2021), the Saint John River (Knack and Shen, 2018), the St. Lawrence River (Shen, 2010), the Assiniboine River (Simoes et al., 2020), the Hay River Delta (Brayall and Hicks, 2012), the Dauphin River (Wazney, 2019), and the Nelson River (Bijeljanin and Clark, 2011; Malenchak et al., 2006). A more detailed description of CRISSP2D is provided in Section 3.5.

1.2.2.3 Model Applications on Regulated Rivers

Hydropower operation decisions are based largely on conservative strategies informed by observed conditions (Timalsina et al., 2013). The development and application of predictive tools (e.g., numerical models) can be helpful to assist ice management. Uses of models to simulate regulated river conditions include development of a freeze-up forecasting tool by Shen et al. (1991) for the Ohio River. This tool uses combination of weather forecasts, as well as channel and flow properties to predict ice conditions. Modelling effects of a major hydropower development on ice regimes was the focus of a 1D modelling study by Jasek and Pryse-Phillips (2015) for the Peace River. In Norway, Timalsina et al. (2016) applied a coupled model to simulate effects of flow control on river ice in the Orkla Basin.

This included an evaluation of numerous scenarios to assess effects of various flow control strategies on ice conditions.

Research by Bijeljanin (2013) provided an important foundation for this thesis, as the study included initial design of a CRISSP2D model specific to the Lake Winnipeg outlet near Jenpeg. Main contributions by Bijeljanin (2013) were consolidation of historical bathymetric datasets, model mesh development, and preliminary model application to simulate freeze-up ice conditions. The following findings were included among the outcomes of the research:

1) identification of discrepancies between simulated and observed hydraulics in open-water conditions, attributed to inaccuracies in bathymetry data or model boundary configuration;
2) observation of mixed model performance during ice-affected conditions, especially in the case of unsteady discharges; and,
3) description of poor model performance during periods of warming air temperatures.

The research presented in this thesis builds upon work completed by Bijeljanin (2013), and among its contributions addresses all three findings mentioned. While most hydropower applications have employed analytical or 1D models, the research in this thesis presents continued development of a 2D modelling tool to simulate the most important aspects of the Lake Winnipeg outlet's ice regime.

1.2.3 Climate Change and River Ice

As described in Section 1.2.1, various hydro-meteorological factors drive river ice formation and evolution. Many simulations of river ice processes focus on capturing conditions of past or near-future events. Evaluating effects of climate change on river ice involves projections of long-term future conditions. A thorough collection and interpretation of site-specific baseline data helps to characterize present day conditions, which is a fundamental step to navigating the uncertainty and consequences associated with a changing ice regime. As such, climate change assessments generally build off present-day knowledge and numerical tools.

The implications of changing climate conditions for hydropower operations in cold regions are uncertain, as the environmental response to climate change is regionally

dependent (Schleussner et al., 2016). In northern regions of Canada, climate change is associated with an increase in precipitation (Cherry et al., 2017), albeit with a high degree of uncertainty. In the event that higher discharge conditions result from climate change, open-water areas resulting from higher velocities may inhibit surface ice cover leading to increased frazil ice production (Timalsina and Alfredsen, 2015). Temperature increases along with an increased frequency of rain-on-snow events may affect ice cover stability, leading to risk of mid-winter breakup events (Beltaos, 2013).

Numerical models provide a valuable means of projecting future conditions resulting from climate change. Numerical simulations of river ice processes generally require model coupling between river ice models and climate and/or hydrologic models (Das and Lindenschmidt, 2021). Model coupling facilitates use of hydro-meteorological forcing data that these other types of models can provide. Climate models include Global Climate Models (GCMs) and Regional Climate Models (RCMs); from which climatic parameters such as air temperature and precipitation can be derived through downscaling (Gebre et al., 2014a). Hydrologic models provide valuable inputs of stage or discharge, based on their representation of watershed processes.

Studies focused on quantifying climate change impacts on river ice range in complexity, with many taking the form of a sensitivity analysis. Huokuna et al., (2009) assessed frazil risk days using discharge and air temperatures in an analytical model, which the authors acknowledged was accompanied by an oversimplification of both hydrodynamic calculations and effects of surface ice covers on suppression of frazil ice formation. More complex studies have applied 1D and 2D models for more detailed accounting of river ice processes. One challenge noted in the literature is the issue of scale, as river ice models are developed at local scales, often with a fine resolution required to resolve the governing equations for ice dynamics. Climate and hydrologic models are designed at larger scales, as they account for more expansive geographic areas.

The Orkla Basin in central Norway has been the focus of some of the most extensive numerical studies exploring climate change effects on river ice. HEC-RAS was employed in this region for an environmental assessment to evaluate effects of climate change on the local river ice regime (Timalsina et al., 2016). HEC-RAS was

also coupled with other models to evaluate effects of operational decisions on river ice regimes. For a separate study in the Orkla basin, MIKE-ICE was coupled with two models: (1) rainfall-runoff model HBV (Gebre et al., 2014a) and (2) reservoir operations model *MyLake* (Timalsina and Alfredsen, 2015). This study highlighted both positive effects (e.g., reduced ice season duration and static ice loading) and negative effects (e.g., increased freeze-thaw events and unstable ice conditions) associated with climate change (Gebre et al., 2014a).

Analysing a suite of relevant winter variables can provide a holistic description of anticipated changes to river ice conditions, as in some cases analysis of a single variable is not sufficient. Examples of relevant variables include duration of ice cover season (Andrishak and Hicks, 2008; Gebre et al., 2014a), ice front position (Andrishak and Hicks, 2008; Jasek and Pryse-Phillips, 2015), ice thickness (Gebre et al., 2014a; Jasek and Pryse-Phillips, 2015), quantity of frazil production (Huokuna et al., 2009; Timalsina and Alfredsen, 2015), and duration of freeze-up (Timalsina and Alfredsen, 2015).

Numerical evaluations of climate change effects have been limited to select regions and have focused mainly on analytical and 1D models. As the predictive capabilities of numerical river ice models improve, 2D tools can be leveraged to assist in projection efforts. Projections of climate change effects on the ice-affected hydraulics of the OLA compared to baseline conditions is an unexplored area in the literature and is a component of this thesis.

1.3 Research Objectives

River ice processes can have wide-ranging impacts on environmental and human environments, and for hydropower generation the result can be considerable losses to efficiency. Water resources that supply hydropower systems can be subject to a variety of ice processes (Section 1.2.1), all of which are governed by hydro-meteorology and site-specific conditions. To support hydropower operations and planning, improving numerical modelling capabilities to simulate ice processes remains an evolving area of the literature (Section 1.2.2). Tools such as numerical models serve an important role in facilitating projections of the impacts of climate change in the cryosphere (Section 1.2.3).

The OLA presents a favourable environment to facilitate an original contribution to the knowledge of ice processes in northern regulated rivers. Design and application of novel modelling approaches in the OLA can yield short-term predictions and long-term projections of regional ice-affected hydraulics, with transferable utility to other regulated rivers. To this end, the specific objectives of this research are as follows:

Objective 1: To gain a comprehensive understanding of CRISSP2D and demonstrate simulation of freeze-up processes using an ideal channel and Jenpeg-specific model.

Objective 2: To characterize freeze-up patterns in the OLA through historical data and documentation, satellite imagery and a river ice monitoring program.

Objective 3: To develop and implement a river ice forecasting tool to predict ice conditions and winter hydraulics in the OLA under prescribed hydrologic and meteorological conditions.

Objective 4: To simulate and describe the potential effects of changing climatic conditions on both the OLA ice regime and Lake Winnipeg discharge.

1.4 Organization of Thesis and Contributions of Authors

Chapter 2

Chapter 2 provides a description of OLA ice conditions using both a consolidated historical dataset and 2D hydraulic model. This chapter contributes to thesis Objectives 2 and 3. This chapter is an extended version of a paper published in the journal *Cold Regions Engineering* entitled "Characterizing ice cover formation during freeze-up on the regulated Upper Nelson River". This article was written in collaboration with Dr. Shawn Clark (University of Manitoba), Dr. Jarrod Malenchak (Manitoba Hydro), and Paul Chanel (Manitoba Hydro).

The primary author (Kevin Lees) designed the methodology, performed calculations and analysis, and developed the manuscript independently with guidance from the three co-authors. Manitoba Hydro provided hydrometric and imagery data through designated project advocates. Field work was conducted both by study authors (including the primary author), field technician Alexander Wall, and Manitoba Hydro hydrometrics. Peer review and journal comments were addressed by the

primary author with suggestions from other co-authors. The final manuscript was accepted on February 20, 2021.

Additions added to Chapter 2 beyond the journal paper are data from a net radiometer that could not be retrieved in a timely manner due to delays associated with COVID-19. These data are presented in a section entitled *Site-Specific Radiation and Albedo Measurements*, which includes Fig. 2.5 through Fig. 2.7. Also added to the thesis is Appendix A, which provides a complete summary of deployed instrumentation (types and dates) as part of the OLA river ice monitoring program.

Chapter 3

Chapter 3 outlines a treatment of skim ice run during freeze-up jamming in CRISSP2D using an ideal trapezoidal channel. This chapter contributes to thesis Objective 1. This chapter is an adapted version of a journal paper published in the journal *Cold Regions Science and Technology* entitled "Numerical simulation of freeze-up jamming in a skim ice regime". This article was written in collaboration with Dr. Shawn Clark (University of Manitoba), Dr. Jarrod Malenchak (Manitoba Hydro), Dr. Hung Tao Shen (Clarkson University) and Dr. Ian Knack (Clarkson University).

The primary author (Kevin Lees) designed the methodology and implemented coding modifications, performed simulations and post-processed results, and developed the manuscript independently with guidance from the three co-authors. Peer review and journal comments were addressed by the primary author with suggestions from other co-authors. The final manuscript was accepted on July 6, 2021. No material differences exist between Chapter 3 and the publication in *Cold Regions Science and Technology*.

Chapter 4

Chapter 4 of the thesis describes design and application of a novel methodology to calculate ice-affected hydraulics at the Lake Winnipeg outlet. This chapter contributes to thesis Objectives 1 and 3. This chapter is an extended version of a manuscript submitted to the journal *Cold Regions Science and Technology* entitled "A novel methodology to quantify hydraulic conveyance through an ice-impacted lake-outlet system" on December 10, 2021. This manuscript was written in

collaboration with Dr. Shawn Clark (University of Manitoba), Dr. Jarrod Malenchak (Manitoba Hydro), and Paul Chanel (Manitoba Hydro).

The primary author (Kevin Lees) designed the methodology, performed model simulations and post-processing, and developed the manuscript independently with guidance from the three co-authors. Manitoba Hydro provided hydrometric data and other site-specific information through designated project advocates. Peer review and journal comments will be addressed by the primary author with suggestions from co-authors. This manuscript remains with reviewers assigned by *Cold Regions Science and Technology*.

An addition to Chapter 4 beyond the submitted manuscript is a sensitivity analysis of pertinent parameters. Specifically, this is Section 4.6.7, which also includes Fig. 4.19. Also added to this thesis are three additional appendices (Appendix B, C and D). Application of a slope-area method to estimate ice roughness throughout the OLA is summarized in Appendix B. Estimation of an acceptable error range for numerical simulations performed in Chapter 4 is outlined in Appendix C (specifically Fig C.3). At least one mention of each appendix was added to the main body of this thesis.

Chapter 5

Chapter 5 of the thesis is a quantitative assessment of climate change impacts to the ice-affected hydraulics of the Lake Winnipeg outlet. This chapter contributes to thesis Objective 4. This unpublished chapter is entitled "Quantifying future changes to winter discharge potential in a northern regulated river". The author (Kevin Lees) designed the methodology, performed model simulations and post-processing, and developed the chapter independently with input from Dr. Shawn Clark (University of Manitoba), Dr. Jarrod Malenchak (University of Manitoba), Dr. Tricia Stadnyk (University of Calgary) and Mike Vieira (Manitoba Hydro). Hydrologic data inputs for this study were shared by Dr. Tricia Stadnyk based on research conducted in the Hudson Bay River Basin (HBRB) as part of BaySys (Braun et al., 2021; Stadnyk et al., 2020; Tefs et al., 2021).

Chapter 6 provides a summary of the contributions of this original work, which take the form of both knowledge advancement in the river ice research sphere and insight

for those with interest in hydropower operations and water resources modelling. Areas for future research are included in the categories of *field studies and monitoring*, *numerical modelling*, and *interdisciplinary collaboration*.

Chapter 2: Paper 1 – Characterizing ice cover formation during freeze-up on the regulated Upper Nelson River, Manitoba

2.1 Abstract

Flow control programs on regulated rivers can improve winter flow conveyance for hydropower operations. On the Upper Nelson River, station flows at Jenpeg Generating Station are reduced during freeze-up to promote formation of a smooth ice cover in often turbulent upstream areas. This ice cover reduces the risk of frazil generation, which could otherwise result in blockages and subsequent energy losses. In this study, a characterization of freeze-up conditions for the Upper Nelson River is presented through 15 years of historical observations, supplemented by a short-term detailed monitoring program (2015-2018). Observations of rapid leading edge celerity are associated with increased ice production under dampened hydraulic conditions. Analysis of ice cores and drone footage highlights the role of skim ice runs in early cover formation; while predictions of skim ice formation show agreement with ice floe taxonomy from the literature. Establishing a baseline of freeze-up conditions for the region will assist in the development of predictive tools, such as numerical models, to optimize flow control decisions for this significant hydropower system.

2.2 Introduction

The presence of river ice can pose significant challenges to hydropower operations in cold regions. Regulation of the annual flow hydrograph is accomplished by hydraulics structures, and the resulting flow patterns affect ice processes from freeze-up through break-up. In turbulent reaches, frazil ice formation occurs under supercooled conditions. This ice can migrate and deposit under an existing ice cover or at hydropower station intakes, with the potential consequences of head losses (Daly, 1991), increased maintenance and reduced system efficiency.

The objective of this paper is to present a summary of freeze-up conditions on the Upper Nelson River for 2004 to 2018, with a specific focus on frontal progression. A novel feature of this study is the most comprehensive summary of freeze-up patterns

for this region, which when paired with hydraulic calculations and estimates of ice production, yields a quantitative assessment of conditions during 15 years of flow control (Section 2.4.1, 2.4.2). A secondary contribution is the insight provided regarding skim ice run formation on large rivers (Section 2.4.3). The role of cold temperatures and interstitial freezing between ice layers is also discussed in the context of maintaining cover stability through freeze-up (Section 2.4.3). These contributions further the understanding of the outcomes of flow control practices, which will facilitate development of more comprehensive tools (e.g., numerical models) to assist river ice management for all waterway users.

2.2.1 Background

Implementing controls to mitigate risks associated with frazil ice is an integral part of cold regions hydropower operations. Conventional river ice controls include structural (e.g., ice booms) and non-structural interventions (Tuthill, 2013). An example of the latter is flow control programs, whereby discharge and water level are manipulated to promote favourable ice cover formation. Potential of high frazil concentrations is reduced through insulation of the water column by the ice cover, viscous dissipation due to flow effects at the ice cover, and latent heat release from any frazil growth that occurs (Daly, 2013).

Flow control programs have been employed on various rivers in North America (Tuthill, 1999) and abroad. River ice formation in all of these regions can have significant economic, cultural and ecological implications. Jenpeg Generating Station (Jenpeg), located 100 km from the outlet of Lake Winnipeg, functions to both generate power (125 MW) and control outflows from Lake Winnipeg for the purposes of flood control and power generation (Manitoba Hydro, 2014). Flow control in Manitoba is unique compared to other regulated regions described in the literature, based on the high latitude and low-temperature conditions.

Zbigniewicz (1997) described the history and operational practices undertaken during flow control at Jenpeg. Through this, they underlined the net economic benefit of flow reductions despite the associated costs. Studies investigating ice processes near Jenpeg include Bijeljanin and Clark (2011), who focused on applying a numerical freeze-up model for the region. This study was comprised of model

development, simulation of hydrodynamic conditions, and predictions of freeze-up timing and ice type (Bijeljanin, 2013). While these efforts provided an overview of ice processes for the Upper Nelson River, extensive freeze-up monitoring has been conducted since for more detailed characterization.

Freeze-up phenomenon observed near Jenpeg includes *frontal progression* in dynamic reaches, which refers to the accumulation of several layers of ice floes at a leading edge. Through frontal progression, an ice cover will advance to an upstream leading edge position (LEP; the most upstream interface of competent ice cover). An ice cover may also undergo a series of frontal progression, collapse and thickening events, through a process referred to as *telescoping* (Beltaos, 1995). In deep rivers with a mild slope, such as the Upper Nelson River, discharge and channel geometry, as well as weather conditions, dictate frontal progression (Shen and Ho, 1986) and backwater effects. Hydraulic conditions at a leading edge are typically classified using a Froude (F) number; whereby ice floes become entrained when a threshold is exceeded. Factors affecting this threshold include ice floe integrity based on weather conditions, with values ranging from 0.06 (Perham, 1983) for mild temperatures to 0.1 (Kivisild, 1959) or greater for colder conditions leading to more competent ice floes. A conceptual diagram of this process is shown on Fig. 2.1, whereby the leading edge progresses upstream from $LEP_{t_{i-1}}$ at cross section 1 (*XS1*) to LEP_{t_i} (*XS5*) between time t_{i-1} and t_i.

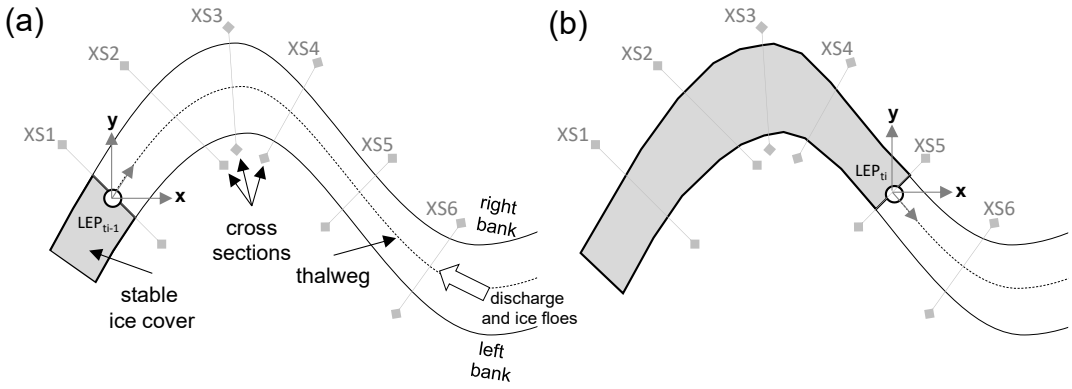

Fig. 2.1 - Conceptual diagram of frontal progression from LEPt$_{i-1}$ to LEPt$_i$ between time (a) t$_{i-1}$ and (b) t$_i$.

In addition to ice floe integrity, *F* threshold is governed by geometry of ice floes (Pariset and Hausser, 1961). Given supercooled conditions in low turbulence reaches, large and thin surface ices floes known as *skim ice run* will form (Matoušek, 1984b). These ice floes have been documented on other northern rivers such as the St. Lawrence River (Marcotte, 1984b), Peace River (Jasek et al., 2013), and Tanana River (Osterkamp and Gosink, 1983). Understanding conditions under which these ice floes form and contribute to frontal progression is an important consideration for flow control on the Upper Nelson River.

2.3 Design and Methodology

2.3.1 Study Area

The region of interest for this study was the Upper Nelson River, spanning from Lake Winnipeg to Jenpeg (Fig. 2.2).

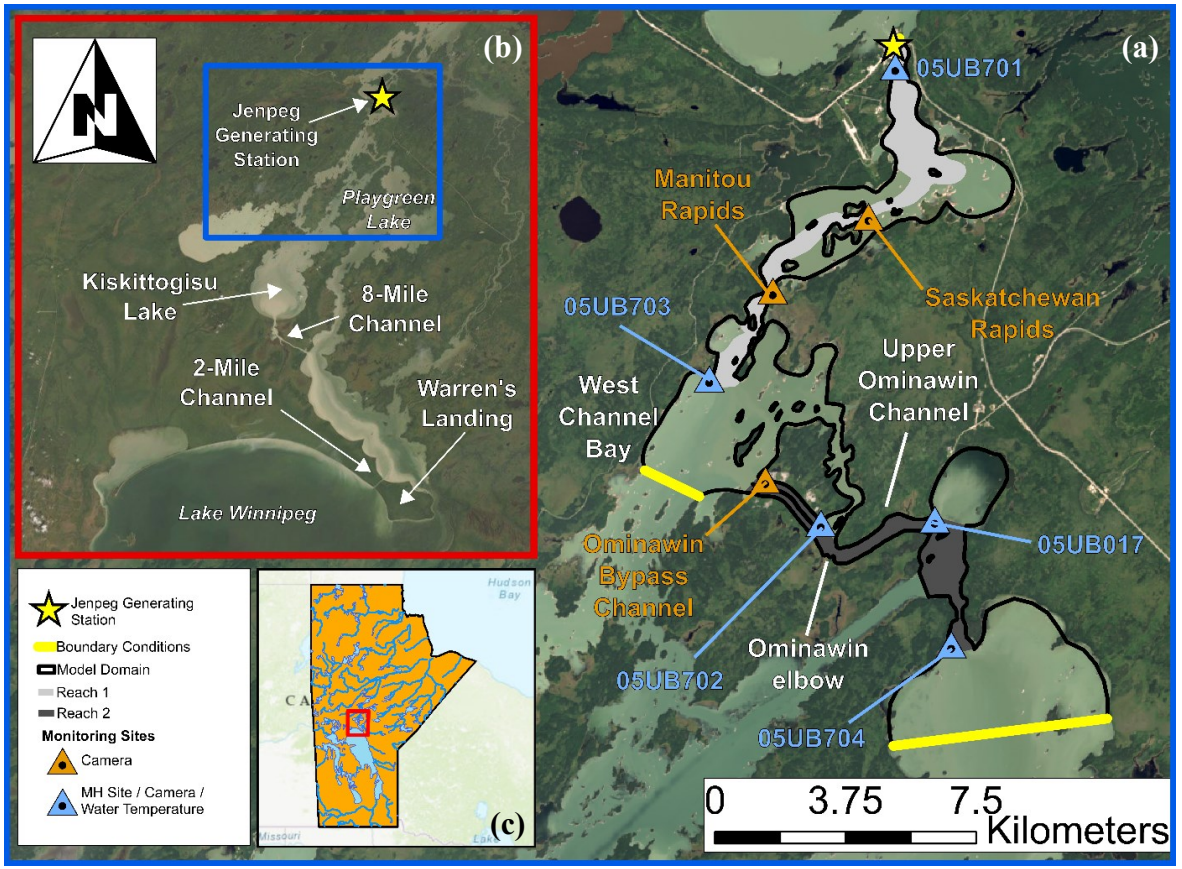

Fig. 2.2 - Study area, hydraulic model domain, monitoring sites and study reaches. [Image in (a) courtesy of the USGS, Landsat; base map in (b) from ArcGIS World Imagery, Surface Layer Credits: Source: Esri, DigitalGlobe, GeoEye, Earthstar Geographics, CNES/Airbus DS, USDA, AeroGRID, IGN, and the GIS User Community; vector data in (c) from Government of Manitoba 2001, Government of Canada 2017.]

Lake Winnipeg serves as a critical reservoir that, on average, contributes about 40% of the total storage across the Manitoba Hydro system (Manitoba Hydro, 2014). Outflow from Lake Winnipeg enters the Nelson River through Warren's Landing and the 2-Mile diversion channel. Approximately 85% of this outflow is routed through the West Channel of the Nelson River, with the remaining 15% passing through the East Channel (Manitoba Hydro, 2014). Flow through the West Channel is routed either through Playgreen Lake or the 8-Mile diversion channel towards Kiskittogisu Lake. Several downstream flow splits are present at Metchanais Rapids and Kisipachewuk Channel, as well as Ominawin Bypass Channel and the Lower Ominawin Channel. Flows eventually converge in West Channel Bay, and progress through a series of rapids prior to arrival at Jenpeg.

The morphology of the Upper Nelson River varies spatially, with channels ranging in top-widths of hundreds of meters to over 1 km. Further, flow depths vary from relatively shallow (e.g., approximately 5 m) to more than 40 m deep in some locations. These natural and constructed channels, as well as the connecting quiescent water bodies, comprise a complex hydraulic network. Total flow in these channels is based on historical records at Jenpeg, where median total station flow was 2,100 $m^3 s^{-1}$ (1977-2018) with 90% of all flow records being within the range of 1,500 to 2,700 $m^3 s^{-1}$. This study focuses mainly on the 50 km reach from Jenpeg upstream to Playgreen Lake (05UB704), as ice processes in this region are most dynamic and have the highest potential to affect winter flow capacity. While historical monitoring efforts have also focused on Cross Lake ice processes downstream of Jenpeg, this area is considered outside the scope of this study.

2.3.2 Freeze-Up Processes and Ice Stabilization

Lake Winnipeg Regulation has resulted in formation of shallow regions (back bays) that flank areas including Saskatchewan Rapids, Manitou Rapids and the West Channel Bay. Stationary ice growth in these back bays may reach its full extent of growth within one night. Operational experience suggests that freeze-up begins in these regions at about 50 cumulative degree-days of freezing ($CDDF$), calculated as a measure of departure of the mean daily temperature from a base temperature (selected as 0ºC) (Boyd, 1979). This $CDDF$ condition has occurred in November during each of the last 15 years.

Flow control at Jenpeg occurs during the Ice Stabilization Program, which includes temporary flow cutbacks to reduce velocities in upstream reaches. Reduced velocities have the most significant impact in two dynamic reaches near Jenpeg (Reach 1 and Reach 2; see Fig. 2.2). These reaches convey high flow volumes and present the greatest risk of frazil generation during winter. This risk is mainly attributed to turbulent flow conditions in shallower and narrower portions of the reaches, due to the entrainment of frazil ice that can occur in these areas. Historical observations show that significant under-ice blockages may occur in these areas without flow control measures (Zbigniewicz, 1997).

The mechanism of cover formation varies between reaches. In Reach 1, a floating ice-retention boom positioned directly upstream of Jenpeg (station 0 m of Reach 1) resists incoming ice floes, thereby initiating cover formation and retaining ice throughout winter (Abdelnour et al., 2012). Secondary bridging is observed during select years near the islands of Saskatchewan Rapids, which promotes further progression but also restricts ice floes from travelling downstream. Progression in Reach 1 eventually ceases due to high velocities at Manitou Rapids (station 9000 m of Reach 1), which create unstable conditions for incoming ice floes. In Reach 2, the formation of stationary ice in West Channel Bay (station 0 m of Reach 2) is a necessary condition for forming an ice cover in Reach 2. The eventual infilling of this area occurs either due to thermal growth or surface congestion of ice floes from upstream, and from here frontal progression continues until termination at the Ominawin Elbow or the inlet of the Upper Ominawin Channel (station 6000 m of Reach 2). Significant consolidation or recession of ice covers in these reaches is not observed during most flow years. This is due both to flow regulation and also the sufficient strength of the ice cover to resist applied forces.

2.3.3 Monitoring Data

2.3.3.1 Hydrometric and Meteorological Conditions

Manitoba Hydro maintains an active hydrometric monitoring network in the study area (MH Site*;* Fig. 2.2), which provided hourly water surface elevation (WSE) at a number of locations, water temperature (where available) and best estimates of total station flow at Jenpeg. Water temperature records lacked the accuracy to identify

the onset and magnitude of supercooling; as such, this condition was assumed to occur upon plateauing of the time-series near 0°C for heat flux calculations.

Meteorological data was sourced from Norway House station (Climate ID: 5062040, located 65 km southeast of Jenpeg; available record for years 1968 to present), which was selected for its proximity to the study area and the availability of hourly data. Fractional cloud cover observations (C_c) for heat flux estimates were provided by the Plymouth State Weather Center (Plymouth State Weather Center, 2019) for Norway House Airport. Both hydrometric and meteorological datasets were infilled by applying linear interpolation in the event of a data gap.

2.3.3.2 Regional Ice Conditions

Selecting a meaningful metric for characterizing freeze-up required consideration of local conditions and data availability. Leading edge position (LEP) in the study area was identified through manual review of low-altitude digital images captured from a helicopter as part of operational monitoring. These photographs document ice conditions from the outlet of Playgreen Lake to Jenpeg, with images available for morning and afternoon (approximately 10:00 and 15:00, respectively) flights for most freeze-up dates. Approximately 24,000 images were reviewed for this study, comprising years 2004 through 2018. Low-altitude images were supplemented with optical imagery from Landsat and Sentinel-2 satellites obtained from U.S. Geological Survey's *EarthExplorer* (2019). Ice conditions were also assessed in RADARSAT-2 imagery, as shared by Natural Resources Canada (2015-2017). In all cases, observations of LEP were compiled into a database with attributes of geographic location (i.e., easting, northing) and time of observation. In the event that a leading edge did not follow a straight line across the channel, the average location of the ice front along the channel width was taken as the LEP.

2.3.3.3 Ground Level Observations

Ground level observations were collected to supplement the existing monitoring network and to characterize local ice conditions between 2015 and 2018. Trail cameras were attached to trees or weighted metal poles to identify ice run events, while Sea-Bird temperature sensors (± 0.002°C accuracy, from -5 to +35°C; Sea-Bird Scientific, 2019) were deployed to accurately identify the timing and magnitude

of supercooling events. Locations of these instruments is shown on Fig. 2.2 (*Camera* and *Water Temperature*), with a summary of deployment dates on Table 2.1.

Table 2.1 - Deployment dates for freeze-up monitoring program.

Freeze-Up Season	Monitoring Location							
	05UB701	05UB703	05UB702	05UB017	05UB704	Ominawin Bypass Channel	M. Rapids	S. Rapids
pre-2015	○	○	○	○	○	-	-	-
2015	○●⊙	○●	○●	○●	○●	-	●	-
2016	○●⊙	○●	○●	○●	○●	-	-	-
2017	○●⊙	○●⊙	○●	○●	○●⊙	●	●	-
2018	○●⊙	○●⊙	○●⊙	○●⊙	○●⊙	●▲◇	●	●▲◇

Notes:
○Manitoba Hydro sensors (water level and temperature)
●Trail camera
⊙Sea-Bird temperature sensor
▲Ice Core
◇Drone Footage

Drone flights were also completed at an altitude of 100 m above Reach 1 (at Saskatchewan Rapids) and Reach 2 (near 05UB702) on November 8 and 9, 2018 using a DJI Phantom 4 PRO equipped with a 20 MP camera (SFOC #18-19-00025697). Footage was first reviewed qualitatively to observe ice floe behaviour at leading ice edges. This footage was taken at an elevation of 100 m above the water surface. Estimates of ice floe velocity ($\vec{v}_{ice}$) were then derived by measuring pixel displacement using Tracker® (Brown, 2019), and assuming that ice floe and surface velocities are equivalent (Beltaos, 1995) (Eq 2-1):

$$\vec{v}_{ice} = 1.15 v_{local} \quad \text{Eq 2-1}$$

Surface velocity was estimated from simulated depth-averaged velocity ($\vec{v}_{local}$) using a scaling factor of 1.15. Ice cores were also taken at these two drone flight locations in January 2019 using a Kovacs *Mark II* ice corer (diameter = 0.09 m) and power auger. Cores were transported to the cold room laboratory at the University of Manitoba (T_{AIR} = -10°C), and processed by applying a methodology based on Gherboudj et al. (2007). Cores were cut length-wise using a band saw, followed by lateral cuts to obtain 2 cm slices that were photographed under cross-polarized light to document ice structure.

2.3.4 Frontal Progression Characterization

The following sections outline the methodology applied to assess the hydraulic and meteorological conditions that contribute to different frontal progression rates. The development and application of a numerical model to quantify reach hydraulics is discussed. Further, the heat flux equations and approach to estimating ice production volumes are described. A schematic outlining the coupling of these components is shown on Fig. 2.3.

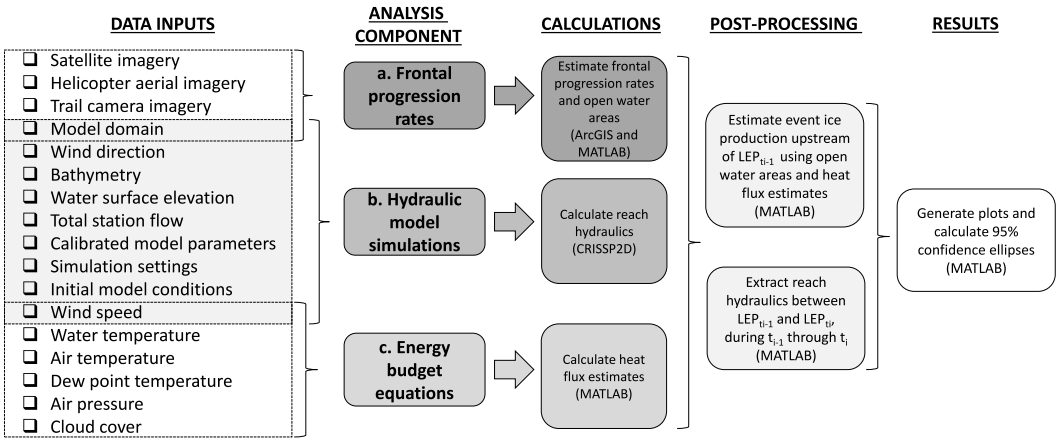

Fig. 2.3 - Summary of methodology for characterizing frontal progression event.

2.3.4.1 Frontal Progression Rates

Leading edge celerity (LEC [m s^{-1}]) was calculated to assess the frontal progression rate between observations (Eq 2-2):

$$LEC = \frac{LEP_{t_i} - LEP_{t_{i-1}}}{t_i - t_{i-1}} \qquad \text{Eq 2-2}$$

In the event the ice cover stalled between time t_{i-1} and t_i, Eq 2-2 yields a value of zero. An instance of frontal progression is illustrated in imagery on Fig. 2.4, whereby cold overnight temperatures coincident with a flow cutback of approximately 300 m^3 s^{-1} between November 24 and 25 progressed the cover within the Ominawin Bypass Channel to the point that it was upstream of the channel groyne by November 26.

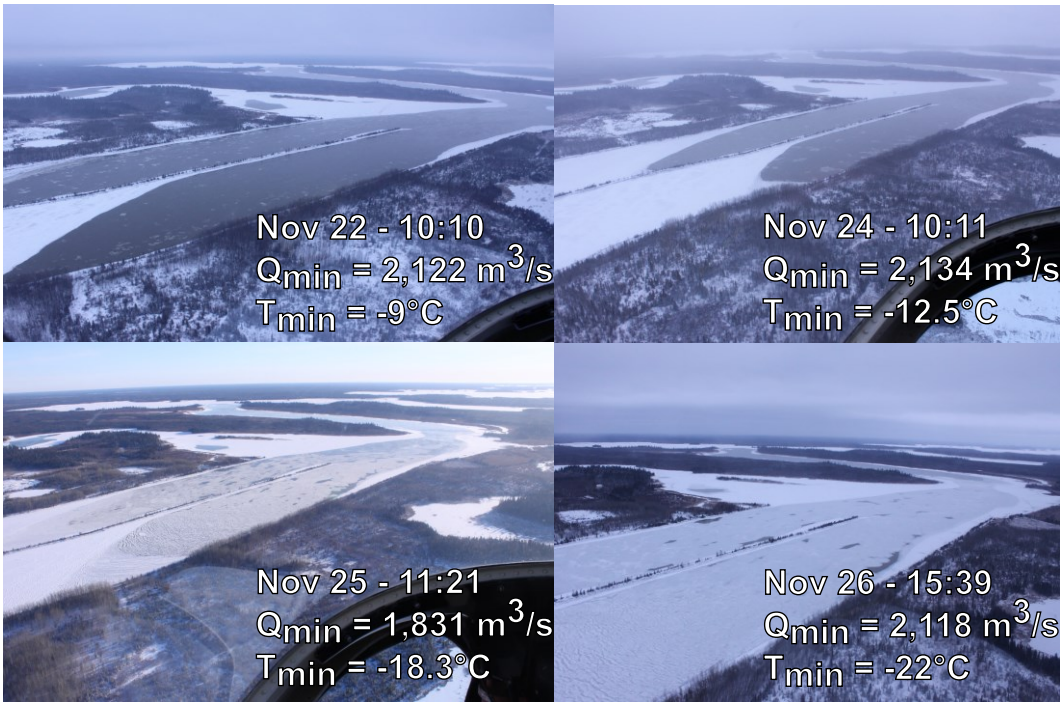

Fig. 2.4 - Observation of frontal progression in Reach 2 (November 2015), including minimum air temperature and minimum station flow between observations. [Images courtesy of Manitoba Hydro.]

2.3.4.2 Hydraulic Model Simulations

Model Set-Up, Calibration and Validation

Frontal progression is affected by channel hydraulics, as high velocities can result in entrainment of ice floes under the leading ice edge, and telescoping of the ice cover. Reach hydraulics were estimated using Comprehensive River Ice Simulation System Project (CRISSP2D), developed at Clarkson University (Liu and Shen, 2011); as this two-dimensional model can account for the flow splits, islands and meanders near Jenpeg. Hydraulic calculations within the model domain (Fig. 2.2) were performed using a finite element mesh, comprising 12,325 nodes and 22,640 elements; a density which provided reasonable continuity error across the domain (~1-2%). The mesh had an irregular grid size, with grid cells ranging in size from 50 m^2 to 150,000 m^2. Simulation settings were selected in consideration of model stability and the model's wet-dry bed treatment (Malenchak, 2011).

Accurate river bathymetry is a prerequisite to achieving accurate hydrodynamic results (Merwade et al., 2008). A composite bathymetric surface was generated using historical cross-section data from Jenpeg's construction (Bijeljanin, 2013); pre-Lake Winnipeg Regulation Survey data; Playgreen Lake bathymetry from 2013; and supplemental data collected in Reach 1 and Reach 2 using a SonTek/YSI RiverSurveyor M9 in 2017 and 2018 by the University of Manitoba and Manitoba Hydro (Lees et al., 2019). Boundary conditions of outflow at Jenpeg, and upstream water level boundaries at West Channel Bay (west boundary; forced with 05UB703) and Playgreen Lake (east boundary; forced with 05UB704) were selected after testing various configurations. Between boundaries, the domain was partitioned into 19 reaches, as informed by documented bed characteristics (Mann and Vogel, 1973) and previous studies (Bijeljanin, 2013).

Hydrodynamic calibration included modifying Manning's coefficients from downstream towards upstream reaches. WSE at 05UB701 during the 2008 open-water period (June to October) was selected as the calibration period. The final calibrated model yielded a root mean squared error (RMSE) of 2.6 cm during this time. The model was validated by comparing measured (Q_{OBS}) and simulated (Q_{SIM}) open-water discharge at two locations: 8-Mile Channel (assumed equal to the inflow at the west boundary) and Ominawin Bypass Channel. Most simulated flows fell within the 10% margin of error considered standard for field discharge measurements (Moriasi et al., 2007). These results indicate a reasonable simulation of water levels and discharge used to calculate open-water reach hydraulics.

Model Scenarios

The numerical model was applied to calculate freeze-up hydraulics for 2004 through 2018 seasons. For this study, simulation of ice processes was excluded from model scenarios, due to the complexity that this would introduce into simulations. While CRISSP2D is capable of simulating many aspects of river ice processes including the coupling of hydrodynamic and ice processes, the presence of several concurrent site-specific ice phenomenon during the freeze-up period (e.g., substantial skim ice runs, significant border ice zones, ice cover strength due to solid crust formation) make ice dynamic simulations in the study area particularly challenging and a primary area for further model development. For this study, an analytical approach

was applied to estimate ice production volumes (Section 2.3.4.4), in order to compare the relative contributions of ice generation and local hydraulics in advancing the ice cover. The effect of ice on hydraulics was accounted for in part by forcing the model with observed ice-affected water levels from 05UB703 and 05UB704. A reasonable RMSE was calculated for the remaining three gauges during all freeze-up years, ranging from less than 1 cm at 05UB017 to a maximum of 8.5 cm at 05UB702.

To further assess the suitability of hydraulics simulated for this study, simulated velocities and drone-derived velocities were compared. Maximum ice floe velocities derived from drone footage on November-8-2018 were 0.82 m s^{-1} and 0.57 m s^{-1} for Reach 1 and 2, respectively. Maximum simulated water surface velocities were estimated to be 0.80 m/s and 0.59 m/s for these reaches by converting depth-averaged velocities using Eq 2-1. Along with the reasonable RMSE achieved for water levels, this comparison of surface velocities indicates that even without simulating ice processes, the model provides a suitable approximation of reach hydraulics for this study.

Results from the numerical model mesh were interpolated to Reach 1 and 2 using a MATLAB post-processing procedure. Each reach was partitioned into cross-sections (conceptual example shown on Fig. 2.1) spaced 20 m apart and comprising 11 points. Hydraulic variables for each point were extracted from the closest finite element node using a minimum distance search. The main flow path through the reach was established by identifying the point with the highest velocity in each cross-section. At these local nodes, hydraulic values for depth-averaged velocity ($\vec{v}_{local}$) and flow depth (D_{local}) were extracted to characterize frontal progression events and conditions. A local Froude number (F_{local}) was calculated using Eq 2-3.

$$\mathrm{F_{local}} = \frac{\boldsymbol{v_{local}}}{\sqrt{\boldsymbol{g D_{local}}}} \qquad \text{Eq 2-3}$$

Conventional approaches for predicting ice formation include applying average cross-section conditions (Kivisild, 1959; Michel, 1984), however use of local hydraulic values have been justified for assessing frontal progression events (Shen and Ho, 1986). For each event, all local hydraulic values were extracted for cross-

sections between $LEP_{t_{i-1}}$ and LEP_{t_i}, between time t_{i-1} and t_i. The median of these values was applied to characterize frontal progression events, as this is representative of reach hydraulic conditions. This median value is referred to henceforth as the *reach velocity* and *reach Froude number*.

2.3.4.3 Energy Budget Calculations

Energy fluxes at the air-water interface are a primary driver of heat loss from a water column and subsequent ice production. For this study, a full heat-budget approach was selected to characterize freeze-up events, to account for the diurnal variations that are not captured in the more simplified semi-empirical heat transfer method. Equations applied are those programmed into CRISSP2D (Liu and Shen, 2011) and described in comprehensive detail in other works (e.g., Malenchak, 2011). The pertinent calculations were coded and computed using MATLAB to bypass the computation time associated with 2D model simulations. Net heat flux at the air-water interface ($\emptyset_*$) comprises several components, including

$$\emptyset_* = \emptyset_{\boldsymbol{R}} + \emptyset_{\boldsymbol{B}} + \emptyset_{\boldsymbol{S}} + \emptyset_{\boldsymbol{L}} \qquad \text{Eq 2-4}$$

where a negative value for $\emptyset_*$ [W m^{-2}] was interpreted as heat loss from the water surface and cooling of the water column. Heat fluxes due to precipitation, frazil ice formation and groundwater were neglected, as were heat exchanges at the water-bed and water-ice interfaces. This is considered a reasonable assumption for this study, as the heat loss at the air-water interface is the primary driver of ice production in the water column. Net short-wave radiation ($\emptyset_R$) was estimated using (Kennedy, 1944) (Eq 2-5):

$$\emptyset_R = (1 - R_t)\emptyset_R(1 - 0.0065C_c^2) \qquad \text{Eq 2-5}$$

where $\emptyset_{cl}$ [W m^{-2}] is short-wave radiation reaching the earth surface at the study site under clear sky conditions calculated using several astronomical and geographical relationships (Liu and Shen, 2011); R_t is the albedo of open-water (R_t = 0). Net long-wave radiation ($\emptyset_B$) is the balance of energy emitted from the water and received from the overlying atmosphere and nearby objects. This balance was estimated as (Liu and Shen, 2011):

$$\emptyset_B = \varepsilon_w \sigma [T_{S_k}^4 - \varepsilon_a (1 + kC_c^2) T_{AIR_k}^4] \quad \text{Eq 2-6}$$

where σ is the Stephen-Boltzman constant (taken as = 5.67x10^{-8} W m^{-2} K^{-4}); T_{S_k} [K] is the surface water temperature; ε_a and ε_w are the emissivity of the air (0.03) and water (0.97), respectively; T_{AIR_k} [K] is the air temperature 2 m above the surface; and k is an empirical constant (k = 0.0017). Sensible ($\emptyset_S$) and latent ($\emptyset_L$) heat fluxes were calculated using the Rimsha and Donchenko (1957) formulations (Eq 2-7 and Eq 2-8).

$$\emptyset_S = \left(\frac{4.1855}{8.64}\right)\left[\left(8 + 0.35(T_S - T_{AIR})\right) + 3.9 w_{mag}\left(\frac{2}{z}\right)^{0.15}\right](T_{S_k} - T_{AIR\_k}) \quad \text{Eq 2-7}$$

$$\emptyset_L = \left(\frac{4.1855}{8.64}\right)\left[\left(1.56(8 + 0.35(T_S - T_{AIR})\right) + 6.08 w_{mag}\left(\frac{2}{z}\right)^{0.15}\right](e_s - e_a) \quad \text{Eq 2-8}$$

where T_S and T_{AIR} are the surface water and air temperature [°C], respectively; w_{mag} is the observed wind speed [m s^{-1}] at a distance z [m] above the surface; and e_s [mb] and e_a [mb] are the saturated vapor pressure and vapor pressure, respectively. Vapor pressures were calculated using the Goff-Grath-Murray formulation, as outlined in Liu and Shen (2011). Both air and water temperatures were obtained from historical datasets, and as discussed previously, water temperatures were assumed to be 0ºC at the onset of supercooling.

Site-Specific Radiation and Albedo Measurements

Site-specific measurements of net solar radiation ($\emptyset_R$) and net long-wave radiation ($\emptyset_B$) were obtained using a four-component net radiometer consisting of incoming/outgoing pyranometer and pyrgeometer pairs. Using these data, albedo (R_t) was calculated in the form of a time-series. The Apogee SN-500-SS radiometer was installed at the Jenpeg weather station (coordinates in Appendix A) through coordination with Manitoba Hydro and the Province of Manitoba.

A comparison of observed long-wave radiation and values calculated using Eq 2-6 are shown on Fig. 2.5.

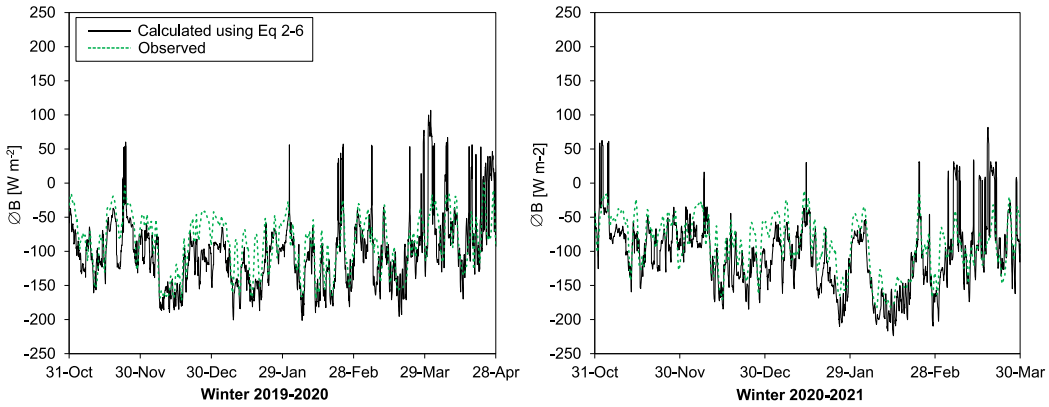

Fig. 2.5 – Comparison of calculated and observed net long-wave radiation for winters 2019-2020 and 2020-2021.

Although the general trends of long-wave radiation datasets are consistent, variations in the magnitude of hourly values is observed. This is attributed to both the sensitivity of Eq 2-6 to air temperatures and the estimation of cloud cover C_C from interpretations of airport monitoring data.

A comparison of observed short-wave radiation and values calculated using Eq 2-5 are shown on Fig. 2.6.

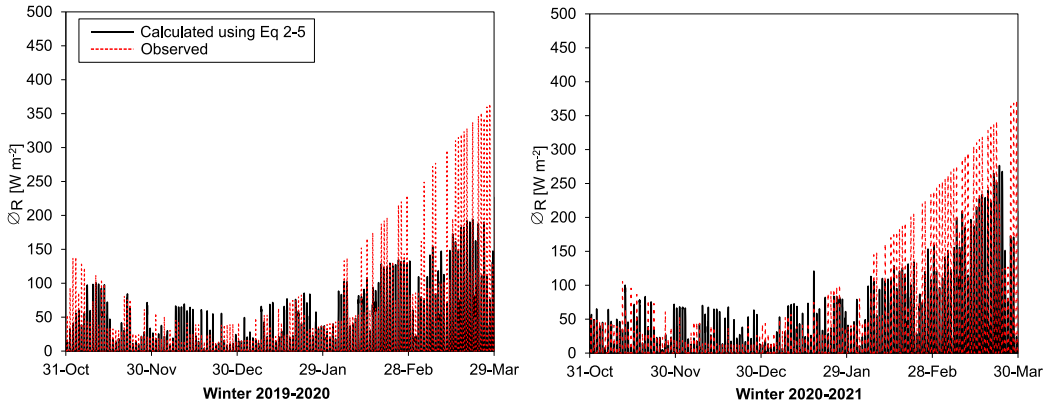

Fig. 2.6 – Comparison of calculated and observed net short-wave radiation for winters 2019-2020 and 2020-2021.

Distinct and significant differences are observed between net short-wave radiation datasets. As discuss by Peters (2021), this is attributed to limited performance of Eq 2-5 and other supporting equations when applied to estimate solar radiation at high

latitudes. Fortunately, for this study the focus is on freeze-up calculations (November and December) when solar radiation quantities are small, meaning that discrepancies between dataset are of low consequence for calculations.

Lastly, a visualization of observed albedo and snow-on-ground data are shown on Fig. 2.7.

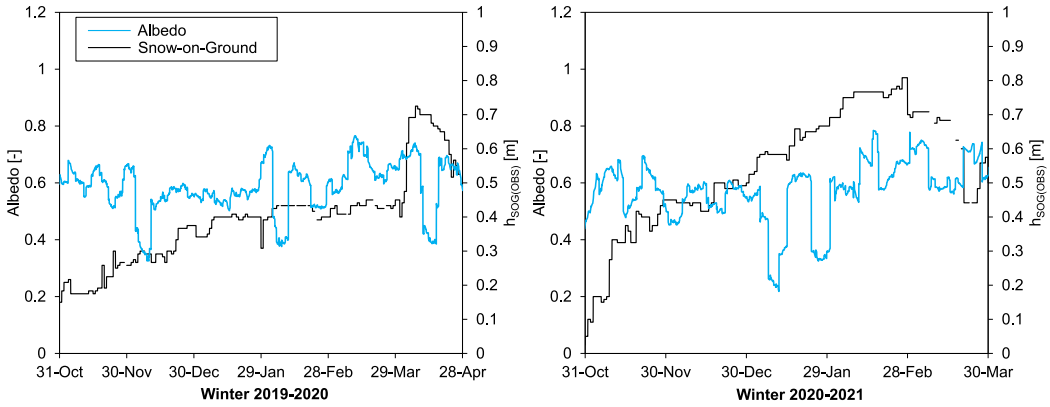

Fig. 2.7 – Visualization of observed albedo and snow-on-ground for winters 2019-2020 and 2020-2021.

Albedo shows fluctuations throughout winter, corresponding mainly with changes in snow water equivalent and surface moisture in response to atmospheric conditions. For both winters 2019-2020 and 2020-2021, average albedo fluctuates around 0.5, with an approximate range for most values being within 0.4 and 0.6.

These site-specific observations are helpful to understanding the error involved in applying equations Eq 2-5 and Eq 2-5 to estimate heat flux quantities, and what factors may contribute to these discrepancies, such as spatial and temporal variations in snow albedo.

2.3.4.4 Post-Processing

Estimating ice production upstream of the ice front was a necessary post-processing step in MATLAB, as ice volume (V_f [m^3 s^{-1}]) is a function of both heat flux and open water area. The analytical formulation by Beltaos (1995) was applied (Eq 2-9):

$$V_f = \frac{1}{\rho_i \lambda} \int_{t_1}^{t_2} (L \emptyset_*) dt \qquad \text{Eq 2-9}$$

where ρ_i and λ are the density and latent heat of fusion of ice (taken as 920 kg m^{-3} and 333,400 J kg^{-1}, respectively), and L [m] is the stream-wise distance from the ice front to the open water extent in the upstream reach. Integrating equation Eq 2-9 yielded an estimate of ice production volume per unit width of the channel, which allows for comparison between progression events.

Data outputs from historical ice observations, hydraulic simulations and ice production calculations provided the components required for event analysis. A script developed in MATLAB paired each frontal progression event with its associated reach hydraulics and unit width ice production estimate (as shown on Fig. 2.3). These datasets were plotted by grouping frontal progression events based on magnitude [m s^{-1}] with a 95% confidence ellipse calculated for each group. Formal definitions of these ovals vary in the literature, however they are generally described as an ellipse-shaped region for two parameters, whereby a larger confidence level results in a larger confidence ellipse (Alexandersson, 2004). These ellipses allow identification for trends in grouped data for purposes of discussing historical trends.

2.3.5 Ice Run Characterization

Freeze-up events can be characterized based on the quantity of ice available, and also the qualities of the ice floes. Taxonomy of ice floes can vary between regions, while a conventional approach includes classes of *stationary ice*, *skim ice run*, and *frazil ice run* (Matoušek, 1984b). Imagery with significant ice cover progression (i.e., $LEC \geq 0.01$ m/s) was assessed to classify ice floe type present during those events. Characteristic examples of active ice floes are shown on Fig. 2.8.

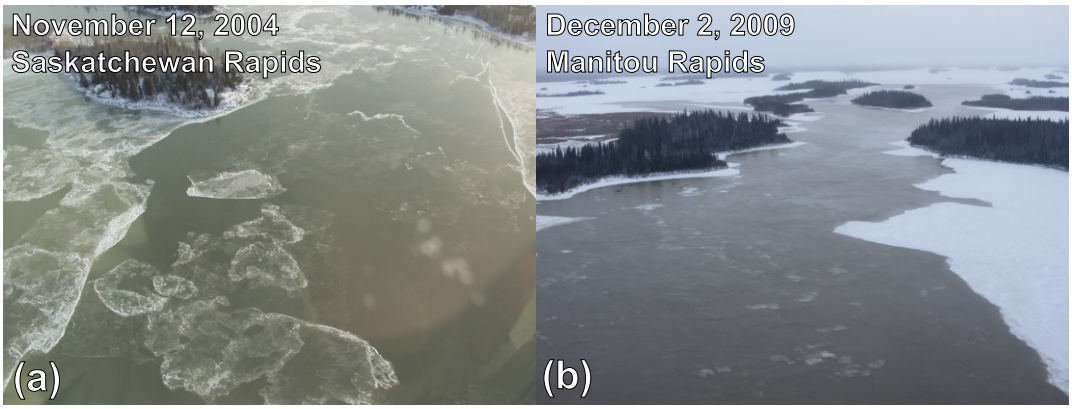

Fig. 2.8 - Observations of (a) skim ice run and (b) frazil ice run. [Images courtesy of Manitoba Hydro.]

In addition to frontal progression events, static border ice was identified in two regions significant for frontal progression: (a) the back bay flanking Reach 1 near Saskatchewan Rapids and (b) West Channel Bay. These events occurred quickly after the start of freeze-up, meaning that ice growth could be attributed to have occurred over a specific night.

Observations of active and stationary ice were compared to literature delineations of ice types, based on mean velocity and maximum heat flux. The partition between stationary ice and skim ice run was generated by applying assumptions outlined by Matoušek (1984b), while the skim ice and frazil ice division was calculated as (Eq 2-10):

$$\emptyset_* = \left(\frac{\sqrt{9.81}\vec{v}_{local}}{5\sqrt{C(0.7C+6)}} - 0.005\right)\left(1130U + b_w w_{mag}\right)(-0.025)^{-1} \qquad \text{Eq 2-10}$$

where b_w is an empirical coefficient, and the delineation Eq 2-10 is valid for Chezy coefficients (C) between 10 and 60. Chezy coefficients were calculated for all progression events using local flow depth (D_{local}) and reach Manning's coefficient (n_b) (Eq 2-11).

$$C = n_b^{-1} D_{local}^{1.3\sqrt{n_b}} \qquad \text{Eq 2-11}$$

2.4 Results and Discussion

2.4.1 Implications for Freeze-Up Operations

Predicting the optimal timing and duration of flow cutbacks by operators requires a number of strategies, including monitoring of WSE observations, weather forecasts and current ice conditions (Tuthill, 1999; Zbigniewicz, 1997). Assessing forecasted minimum air temperatures and station flows is an approach employed at Jenpeg, as these variables are surrogate parameters for ice production and channel hydraulics, respectively. These observed conditions are plotted along with LEC on Fig. 2.9.

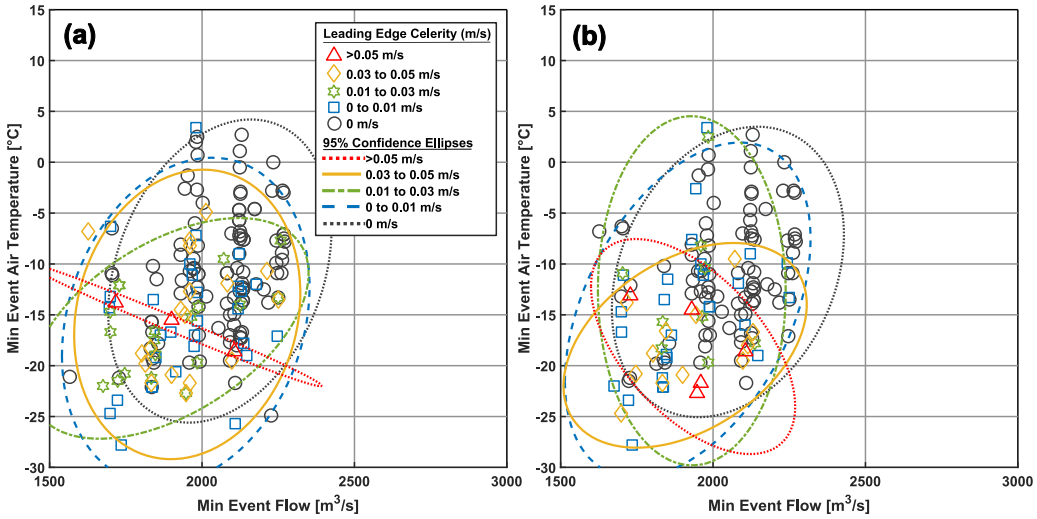

Fig. 2.9 - Observed frontal progression events using observed flow and minimum air temperature for (a) Reach 1 and (b) Reach 2, including leading edge celerity (shapes) and 95% confidence ellipses (lines).

The overlap of ellipses through a wide range, especially between -5°C to -20°C and 1,800 m^3/s and 2,250 m^3/s, indicates uncertainty in predicting the effect that flow cutbacks will have on advancing the ice cover. This is attributed to low correlation between station flow and local reach velocity (R^2 = 0.03 and 0.36 for Reach 1 and 2, respectively) during frontal progression events. This low correlation is due to the complex hydraulic relationship between forebay conditions at Jenpeg and upstream water levels in Lake Winnipeg, which are further complicated by ice effects between these two locations. As such, predicting local reach conditions from station flow alone is limiting. Further, the analysis shown excludes consideration of ice production area. These limitations are addressed, in part, through real-time monitoring of WSE records and monitoring the presence of open-water areas through helicopter flights. The following sections discuss a more detailed approach which considers ice production potential and local hydraulics in characterizing progression events.

2.4.2 Cumulative Effects of Flow Cutback and Ice Production

The primary effect of flow cutbacks at Jenpeg on upstream channel hydraulics is evident by assessing reach *F*. Visualizations illustrating the effect of flow cutbacks coincident with heat loss from the water column are shown on Fig. 2.10 and Fig. 2.11.

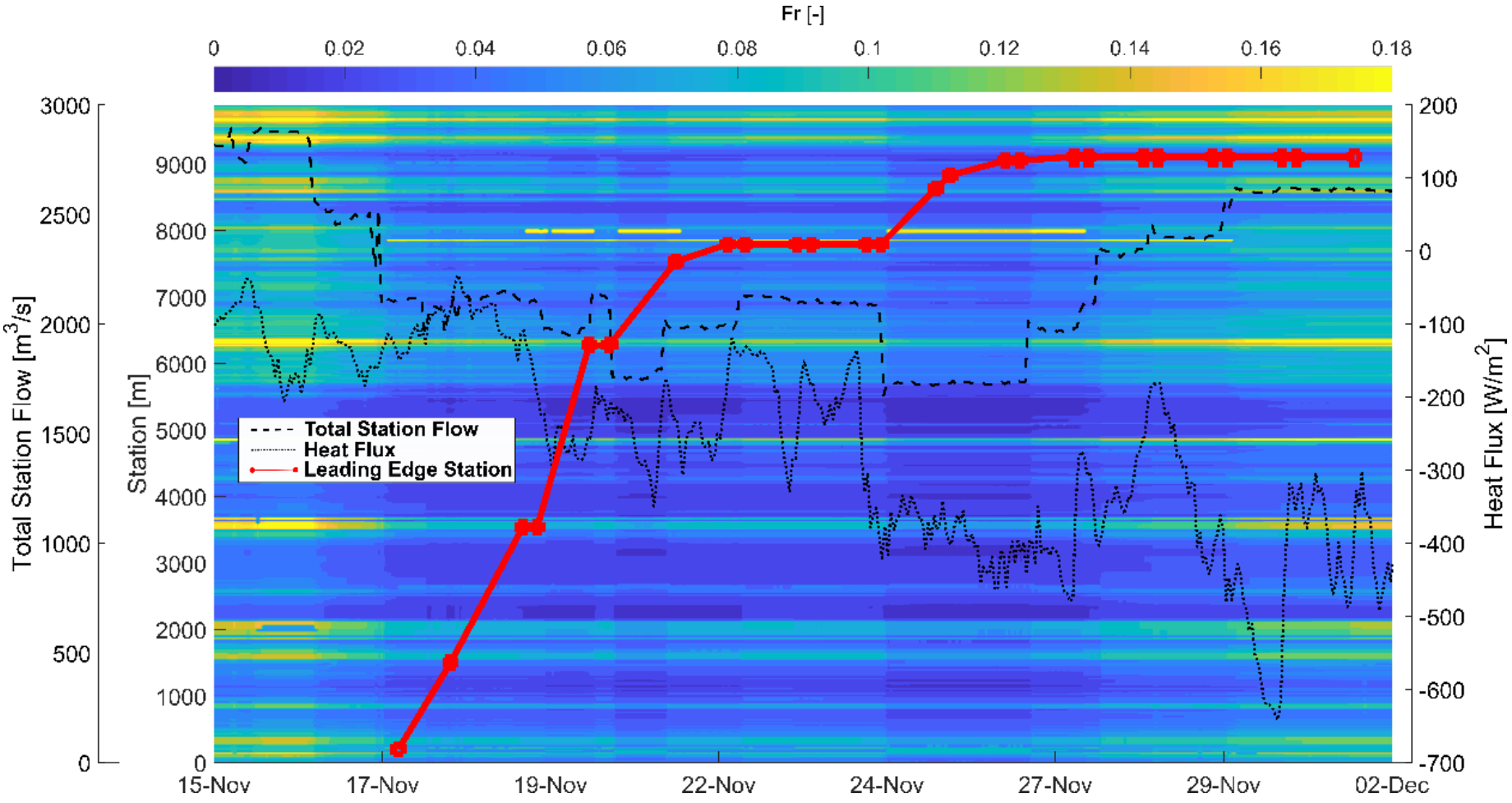

Fig. 2.10 - Visualization of frontal progression, channel hydraulics and heat flux during freeze-up in Reach 1 (2007 freeze-up).

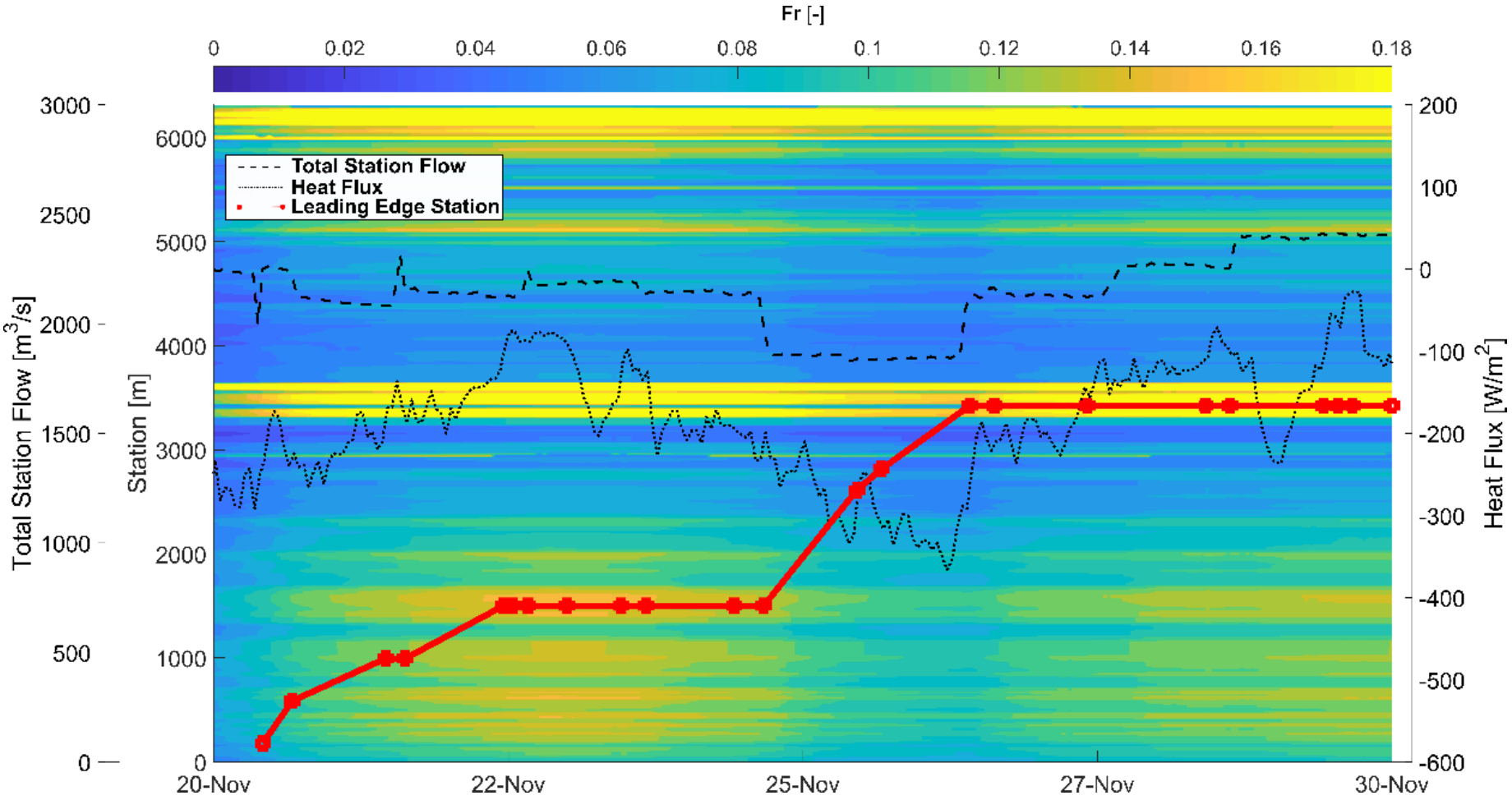

Fig. 2.11 - Visualization of frontal progression, channel hydraulics and heat flux during freeze-up in Reach 2 (2015 freeze-up).

0

As a typical example note the concurrent decrease in discharge and F on November 17 on Fig. 2.10. These cutbacks allowed the leading edge to progress past rapid sections (e.g., station 3700 m and 6300 m), where it may otherwise have stalled due to ice entrainment. After several cutbacks, the ice cover reached its final stable position near station 9000 m on November 26. Several instances of stalling or retreat were observed, including November 22 to 24, where LEC was 0 m s^{-1} due to insufficient upstream ice production caused by less heat loss and smaller open water area. Frontal progression in Reach 2 was also affected by flow cutbacks (Fig. 2.11), despite its further proximity from Jenpeg. Frontal progression occurred between November 25 and 26, after which the cover reached its stable position at station 3500 m (Ominawin elbow; Fig. 2.2). Fast closure of the ice front to its furthest upstream position is a key component of mitigating frazil ice risk. An analysis of all frontal progression events is shown on Fig. 2.10, in lieu of presenting individual summaries of each freeze-up year.

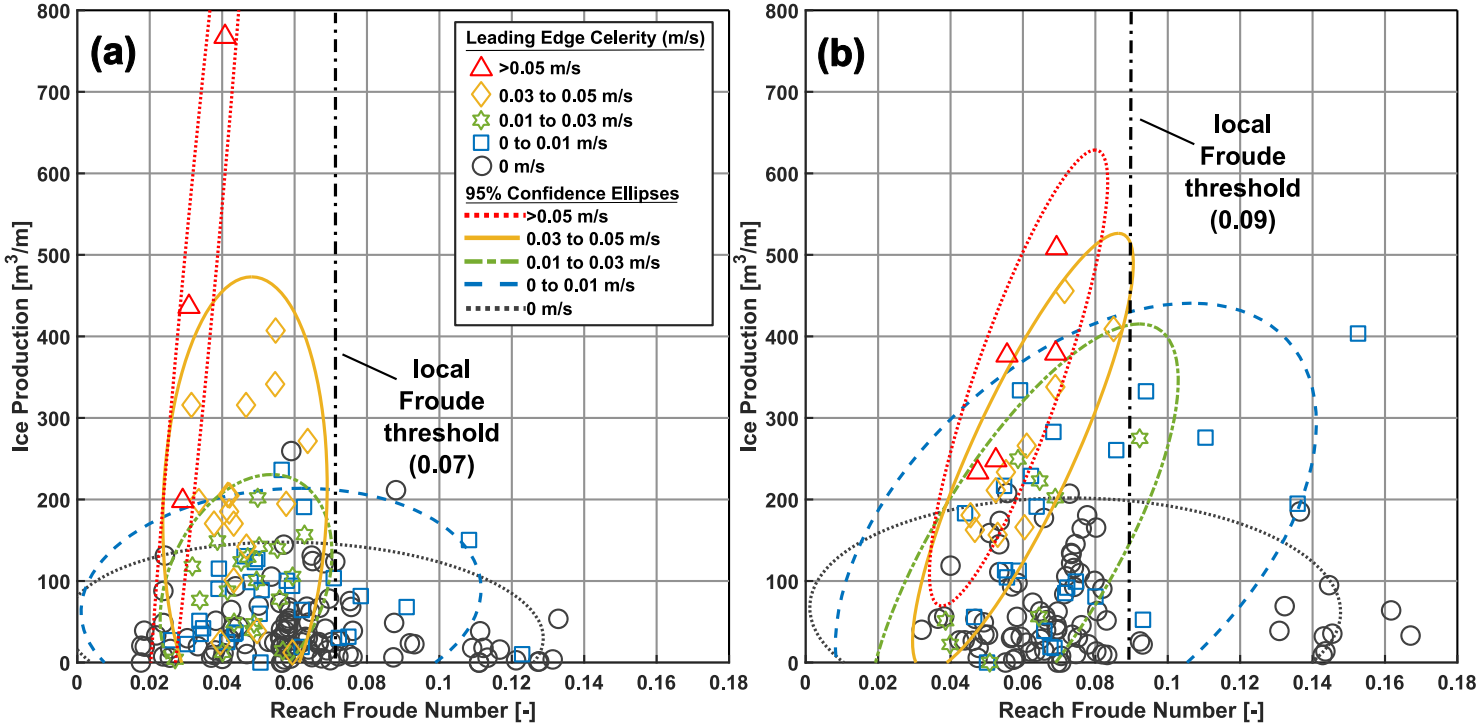

Fig. 2.12 - Frontal progression events using reach Froude number for (a) Reach 1 and (b) Reach 2, including leading edge celerity (shapes) and 95% confidence ellipses (lines).

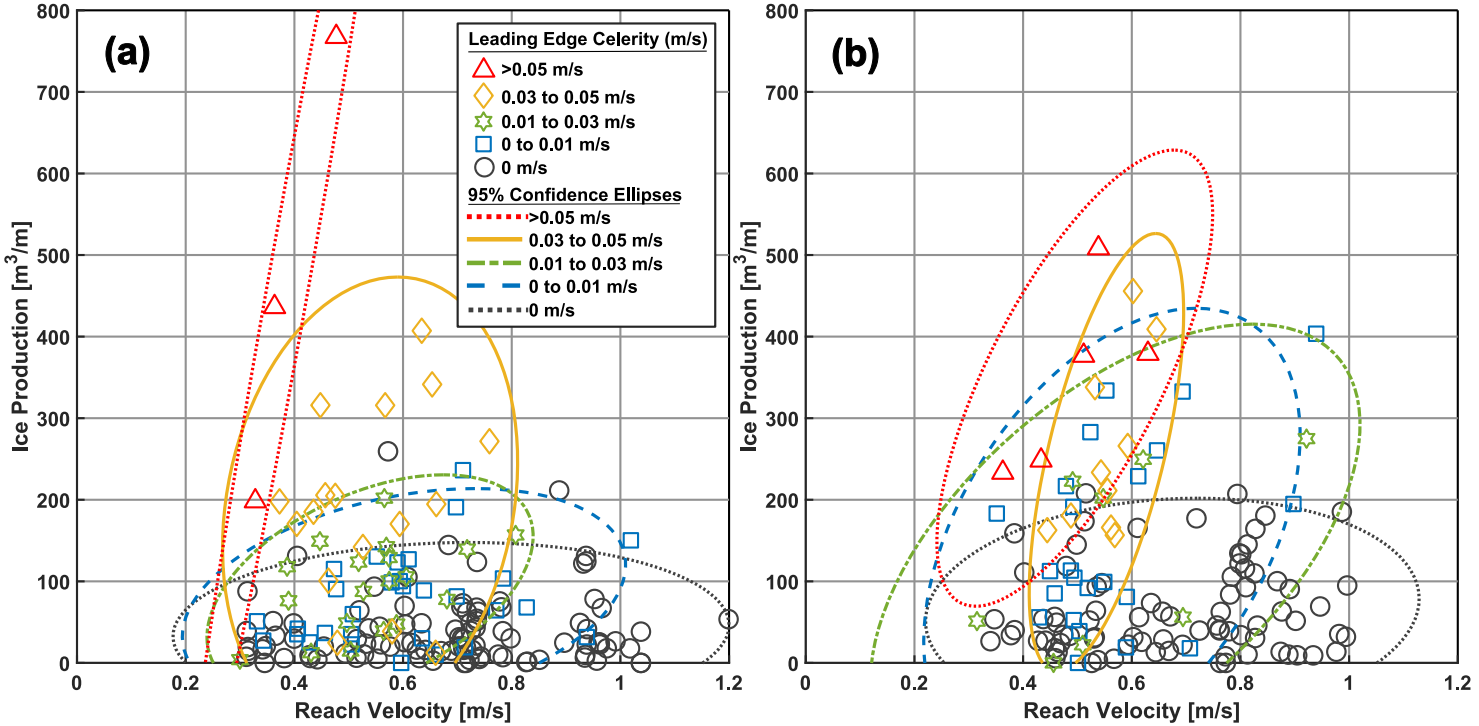

Fig. 2.13 - Frontal progression events using reach velocity for (a) Reach 1 and (b) Reach 2, including leading edge celerity (shapes) and 95% confidence ellipses (lines).

0

Occurrences of stalled leading edge (black ellipse; LEC = 0 m s^{-1}) are clustered mainly in the low ice production region (V_f < 200 m^3 m^{-1}) for all hydraulic conditions. Notably, other ellipses overlap in this low ice production region, suggesting that the effect of flow cutbacks is uncertain under mild air temperatures and/or cloudy sky conditions.

The shape of ellipses for moderate progression events (0.01 m s^{-1} to 0.05 m s^{-1}) shift upward and to the left. The most intense progression events (LEC > 0.05 m s^{-1}) occur only under high ice production (V_f > 200 m^3 m^{-1}) and lower reach Froude number. Several studies suggest that frazil ice buoyancy increases during periods of high heat loss (Matoušek, 1984a; Shen and Ho, 1986). Ice formed during these events includes large skim ice floes, which are more resistant to entrainment at an ice edge due in part to their geometry (Pariset and Hausser, 1961; Perham, 1983).

General patterns of ellipses are consistent between Reach 1 and 2, with increased LEC corresponding with narrowing ellipses that shift upwards and to the left. This aligns with the premise of flow control efforts, whereby frontal progression is accelerated by flow cutbacks corresponding with high heat loss conditions. Most events in these reaches occur below the generally accepted threshold for progression (F = 0.1; Kivisild, 1959). Interestingly, a difference in local Froude thresholds between Reach 1 (F = 0.07) and Reach 2 (F = 0.09) was observed, and remains unexplained. By applying reach velocity as the hydraulic variable (Fig. 2.13) rather than reach Froude number, ellipse ranges became arguably more comparable between reaches. Further, local velocities during some events in Reach 1 even exceed the accepted velocity criteria for progression ($\vec{v}$ = 0.7 m/s; Perham, 1983).

This discrepancy in outcomes when applying reach Froude number and velocity is attributed to differences in channel geometry. Local flow depths during freeze-up in Reach 1 (12.3 to 41.6 m) are more than twice that of Reach 2 (5.0 to 19.5 m). Despite similar reach velocities, Froude numbers vary between reaches due to these significant differences in flow depths. In the case of identical ice floes with the same velocities, we may expect similar behaviour between them despite having different local Froude numbers. Higher ice floe velocities have greater inertial forces, which must be resisted by the leading edge as ice floes decelerate and become stationary.

Buoyancy of the incoming ice floes also contributes to this resistance. These observation aligns with work by Tuthill and Mamone (1998), who suggest that Froude criteria is less important than velocity in deep rivers where ice thickness is a small fraction of the total flow depth.

2.4.3 Skim Ice Run Events in the Upper Nelson River

A secondary effect of flow cutbacks is the quiescent conditions that allow increased skim ice production. These floes can break up upon interacting with rapid sections (resulting in *brash ice*) but can also grow up to hundreds of meters to more than a kilometer in width (Marcotte, 1984b). A summary of ice floe observations compared to literature ranges is shown on Fig. 2.14 and Fig. 2.15 for Reach 1 and 2, respectively.

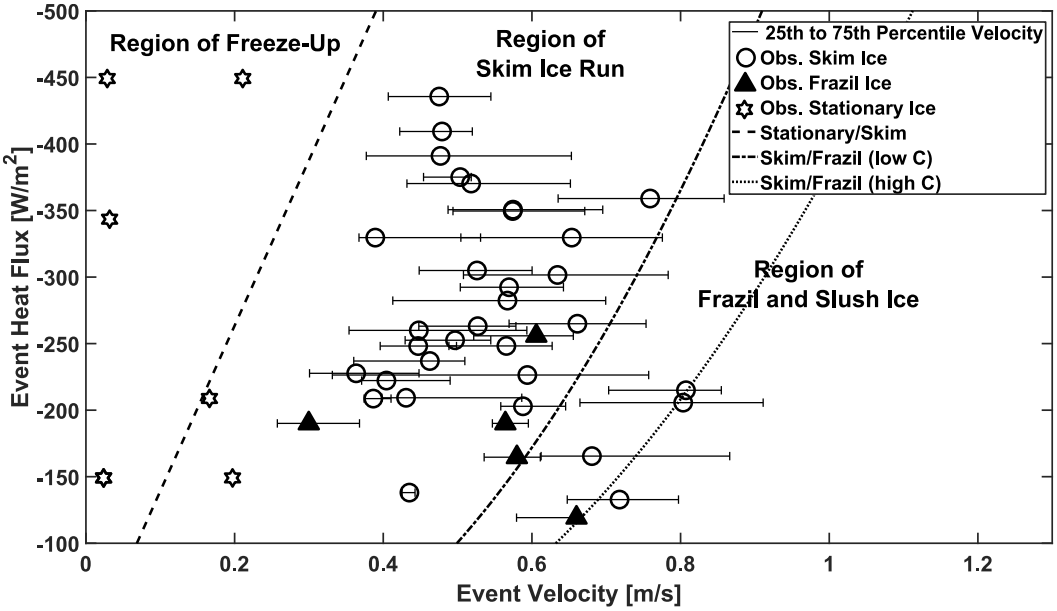

Fig. 2.14 - Ice floe observations (shapes) compared to literature criteria (Matoušek, 1984b) for Reach 1 and stationary ice areas. Three ice regions are differentiated by lines, horizontal bars indicate range of local velocities during frontal progression event.

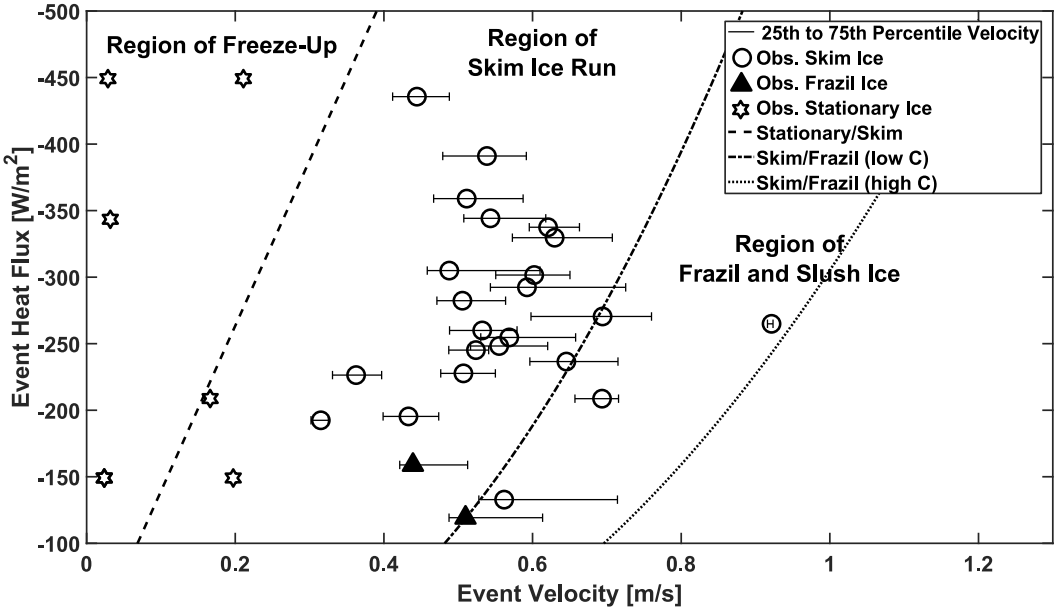

Fig. 2.15 - Ice floe observations compared to literature criteria (Matoušek, 1984b) for Reach 2 and stationary ice areas. Three ice regions are differentiated by lines, horizontal bars indicate range of local velocities during frontal progression event.

A range of Chezy coefficients encompassing 90% of events was considered appropriate for plotting purposes; with ranges of 36-52 and 34-60 selected for Reach 1 and 2, respectively. These skim ice observations, along with event heat flux and local velocities, show agreement with the floe taxonomy proposed by Matoušek (1984b). The frazil floes observed in this area (Fig. 2.8b) exist as unconsolidated slush, and lack the competent circular shape characteristic of frazil pans (*pancake ice*). As a result, there is uncertainty in identifying differences between skim ice run and frazil ice, leading to frazil ice observations in the *region of skim ice run*. This discrepancy may be due to the conditions under which the original framework was developed. Specifically, that the data was sourced from a small river (Q_{OBS} = 104 to 242 m^3 s^{-1}; Matoušek, 1984b) during milder conditions ($\emptyset_*$= -148 to -289 W m^{-2}; Matoušek, 1984b). Thus, further investigation may be needed to adapt this framework for application on larger northern rivers such as the Upper Nelson River.

The ice floes observed in this region result in distinct patterns in ice covers. An ice core profile from Reach 1 (Fig. 2.16) shows striations of initial formation layers.

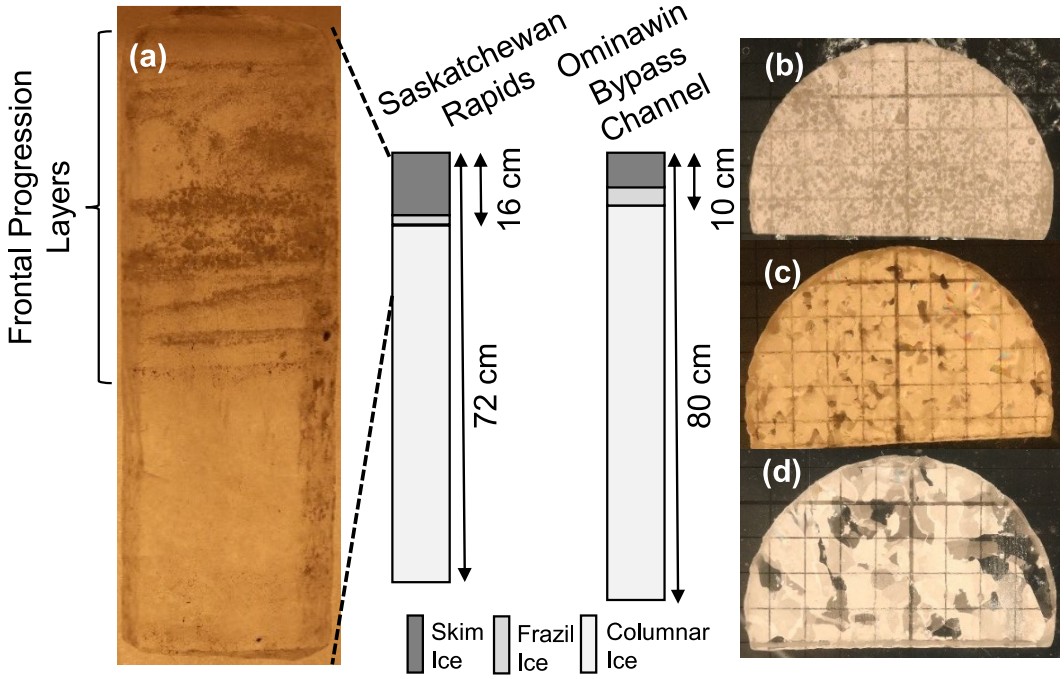

Fig. 2.16 - Ice core profiles from two locations (January 2019). Includes: (a) lengthwise profile showing skim ice striations and illustration of identified (b) skim ice, (c) frazil ice and (d) columnar cross-sections.

These patterns form due to the partial 'stacking' of ice floes during formation, which occurs due to deceleration of ice floes upon contact with the leading edge (as observed in the drone footage). This allows the ice cover to progress upstream over time. Despite a small initial thickness (16 cm and 10 cm for Reach 1 and Reach 2, respectively), the ice cover remains stable throughout freeze-up and under increased stresses when station flow is increased (e.g., after November 26 on Fig. 2.10 and Fig. 2.11). The freezing of interstitial water between stacked floes enhances cover resistance to consolidation (Michel, 1978); a phenomenon that when combined with frictional resistance of interlocking ice floes, leads to a synergistic effect on the overall resistance of the cover (Wazney et al., 2019a). As such, it can be said that cold conditions which promote interstitial freezing are imperative to efficient flow control in this region.

2.5 Conclusion

Flow regulation at Jenpeg has a significant impact on ice formation in the Upper Nelson River. The summary of freeze-up conditions presented indicates that frontal

progression of an ice cover through dynamic reaches of this river is most efficient under suppressed hydraulic conditions and high ice production. Stalling of the ice cover is attributed primarily to insufficient ice production, which could result in larger open water areas that over time, may increase risk of frazil generation. The overlap of frontal progression rates during low ice production events indicates that the effect of flow control decisions is uncertain during mild winter conditions. Selecting hydraulic metrics for predicting frontal progression, such as reach velocity and Froude number, requires consideration of channel morphology. In deep rivers such as the Upper Nelson River, channel velocity may be a more suitable metric than Froude number due to the dominance of inertial forces on floes at the leading ice edge. Results from this study also illustrate the advantage of considering reach-specific conditions to predict frontal progression patterns.

Skim ice floes are an integral component of stable cover formation near Jenpeg. Observations of these floes shows agreement with an established framework from the literature. Discrepancies in the identification of frazil ice events are attributed to a difference in hydraulic conditions between study rivers. The mechanism of ice cover formation was observed via stacking of ice floes at the leading edge, resulting in an initial cover that is relatively thin. In addition to downward growth of columnar ice, the cover resists consolidation due to freezing of interstitial water between ice layers.

Decisions regarding timing and duration of flow cutback require consideration of ice generation potential and local reach hydraulics. The outcome of flow cutback effects on the ice cover is most uncertain when ice production is low. Current strategies for ice management in this reach of the Nelson River include on-going monitoring of ice conditions and real-time monitoring records, tracking forecasted air temperatures, and planning cutback flow targets. Development of additional tools, such as numerical models, can assist in the optimization of flow control actions (magnitude and duration).

2.6 Chapter Summary

This chapter presents a detailed characterization of ice conditions in the Upper Nelson River. The identified cause-and-affect relationships during freeze-up are

important both for regulation practices and numerical model development. Results also provide insight into the role of channel morphology on both the nature of ice floes formation and the selection of suitable metrics to predict frontal progression rates and ice floe submergence behaviour. Observations of skim ice runs on this very mild sloped river, and the behaviour of skim ice floes during freeze-up jamming, form the foundation for the model treatment presented in Chapter 3.

Chapter 3: Paper 2 - Numerical simulation of freeze-up jamming in a skim ice regime

3.1 Abstract

Freeze-up jamming on regulated rivers is an important aspect of cold regions hydropower operations. The timing and nature of freeze-up jamming has a role in reducing effects to winter discharge conveyance. In northern regions with mild-sloped rivers, skim ice run is of considerable importance to formation of a thin and stable cover with low hydraulic resistance. This paper presents a detailed review of skim ice run, including quantitative methods for predicting skim ice formation and a description of its behavior during freeze-up jamming. The review is supplemented by site observations from a large Northern regulated river which experiences significant skim ice runs during winter. Following this, a treatment of skim ice run during freeze-up jam simulations is presented for a two-dimensional river ice model (Shen, 2010). The treatment includes implementation of empirical equations to establish skim ice run formation thickness, estimate skim ice floe strength as a function of thermal growth, and facilitate ice cover formation under varying discharge and air temperature conditions. Simulations illustrate the role of temporary discharge reductions on both the formation rate and thickness of the ice jam. Further, these simulations highlight that ice jam profiles formed under cold conditions show smaller final thicknesses relative to those formed under warmer conditions, due to the reduced strength of ice floes formed in warm weather. A brief sensitivity analysis evaluates the cumulative effect of concurrent changes to air temperature and discharge, as well as the impact of varying channel characteristics (i.e., sinuosity and bed slope). Enhancing capabilities of the model to simulate freeze-up jams creates potential for industrial applications, where anticipating the effects of discharge and air temperature on ice jam formation is often of paramount importance for river ice management.

3.2 Introduction

For hydropower operations on regulated rivers, freeze-up processes can pose considerable challenges (Gebre et al., 2014a; Huokuna et al., 2020a; Tuthill, 1999).

Energy losses can result from thickened and rough ice covers, which may form under either high operational discharges or localized flow velocities (Tuthill, 1999). Formation of freeze-up jams with a small thickness and smooth texture results in lower flow resistance, relative to thicker ice jams that have undergone significant consolidation. Further, maintaining cover stability is beneficial for providing hydropower generating potential during colder months where power demand is high, while maintaining safety for waterway users (Zbigniewicz, 1997). Factors contributing to the characteristics of freeze-up jams are numerous, and include the quantity of ice supply, characteristics of active ice floes, integrity of the existing ice cover, channel geometry, and hydraulic and wind conditions (Pariset and Hausser, 1961; Uzuner and Kennedy, 1972).

In Northern, mild-sloped rivers with slow-moving reaches, *skim ice runs* can be observed during freeze-up and throughout winter. A skim ice run is comprised of a collection of ice pieces which travel in the direction of flow. These individual ice pieces form from growth of surface ice crystals and are referred to in this study as *skim ice floes*. While limited by the width of the open-water area in a channel, lateral dimensions of these skim ice floes can exceed hundreds of meters (Lees et al., 2021; Marcotte, 1984b). Skim ice floes are differentiated from frazil ice floes, which are formed through an accumulation of frazil slush into a single moving unit. Despite the relatively small quantity of ice volume in skim ice run compared to what may be observed in a run of frazil ice floes, the large size of skim ice contributes to rapid freeze-up of a river. In some cases, this rapid formation process can occur in a matter of hours (Clark, 2013).

On regulated rivers, flow control of stage and discharge at a hydraulic structure helps to create satisfactory conditions for stable ice cover formation during freeze-up. This typically occurs through temporary reductions in channel discharge (Tuthill, 1999). For instance, reducing discharge at the Moses-Saunders Power Dam on the St. Lawrence River slows water velocities at a time with favorable weather condition to promote a smoother ice cover formation with less open water areas by reducing potential for consolidation events (Shen, 2011). In the Upper Nelson River region, reaching 100 km upstream of Jenpeg Generating Station (Jenpeg) at the Lake Winnipeg outlet, cold temperatures lead to significant skim ice runs during freeze-up

(Lees et al., 2021b). Flow control at Jenpeg has implications for ice integrity and water supply to stations downstream on the Nelson River hydropower network, which comprises the majority of hydropower potential in Manitoba (Zbigniewicz, 1997). To supplement monitoring of freeze-up conditions during flow control, river ice models can assist in assessing the cumulative effects of meteorological and hydraulic conditions on ice cover formation.

Improving capabilities of river ice models to predict freeze-up jamming in different river environments, including those with skim ice runs, has wide-ranging benefits for optimal flow control decisions. The first objective of this paper is to present a description of the physical processes involved in skim ice formation and jamming, from both the literature and site-specific observations of the phenomenon. This includes topics of skim ice floe qualities, formation criteria, and behavior during freeze-up jamming. The second objective of this paper is to outline an accompanying treatment of skim ice during freeze-up simulations in a two-dimensional river ice model. Aspects of this treatment include assigning an initial skim ice thickness and accounting for skim ice floe strength based on calculation of ice thickening due to thermal growth. Further, a minimum ice thickness parameter is introduced to simulate thin cover formation, while also allowing sufficient parcel interactions during calculation of ice dynamics. Demonstration of the model treatment is presented using an ideal trapezoidal channel, with a focus on skim ice floe properties and the resulting ice jams that form. The stand-alone and cumulative effects of varying discharge and heat loss conditions on skim ice floe formation and jamming are assessed, although with a brief discussion of the role of channel morphology on these processes.

3.3 Background

3.3.1 Literature Review

Several lab and field studies have investigated the thermal and hydraulic conditions under which skim ice forms. A summary of the main studies discussed in this paper is provided in Table 3.1.

Table 3.1 - Studies with relevant skim ice information.

Study Author(s) & (Year)	Study Type	Flume/Channel Description	Range of Thermal Conditions	Range of Hydraulic Conditions
Lees et al. (2021)	Field	Upper Nelson River	T_{AIR}= -30 to 5ºC	U = 0 to 1 m s^{-1} Q = 1,500 to 2,700 m^3 s^{-1}
Marcotte (1984b)	Field	St. Lawrence River	T_{AIR} = -25 to 5ºC	U = 0.3 to 3 m s^{-1} Q = 8,400 m^3 s^{-1}
Matoušek (1984a,b)	Field	Middle Labe & Prague-Podbaba	$\emptyset_*$ = -148 to -289 W m^{-2}	U = 0.24 to 0.73 m s^{-1} Q = 104 to 242 m^3 s^{-1}
Unduche (2008)	Lab	Counter-rotating flume (4.3 x 4.3 x 2.7 m)	T_{AIR} = -15.7 to -11ºC	U = 0.13 to 0.4 m s^{-1}
Hammar et al. (2002)	Lab	Re-circulating flume (section of 22 x 0.6 x 1 m)	T_{AIR} = -15.7 to -11ºC.	U = 0.06 to 0.883 m s^{-1}

3.3.2 Qualities of Skim Ice Runs

During freeze-up, border ice is often the first ice type to form, as it originates from the interface between the water and channel bank and grows laterally towards the channel centerline (Clark, 2013). While similar to border ice, skim ice floes are formed by ice particles that nucleate in slow moving flow conditions without attachment to the channel banks. Conglomerates of surface ice crystals result in flat aggregates of surface ice that travel downstream through advection, provided that wind and flow-induced turbulence is not sufficient to entrain particles into the water column (Matoušek, 1984a). With an initial thickness on the order of millimeters and horizontal dimension on the order of metres (or even hundreds of metres); skim ice floes can have the appearance of grease or glass ice (Matoušek, 1984b; Marcotte, 1984b). These thin floes become more translucent as they thicken, typically reaching a few centimeters. The pertinent equations describing thin ice growth are outlined by Ashton (2013, 1989).

3.3.3 Quantitative Prediction of Skim Ice Run Formation

Formation requires the presence of a supercooled surface layer, which may develop even if the bulk water temperature exceeds 0ºC (Hammar et al., 2002; Unduche, 2008). Matoušek (1984a) derived an empirical formula to quantify the temperature of the stratified surface layer as a function of bulk water temperature, heat loss, wind and channel characteristics. This surface water temperature represents the degree of supercooling, which is applied to estimate size and buoyancy of ice particles formed. Further study by Matoušek (1992) provided more quantitative estimates of surface temperature, including observation of initial ice formation at a surface temperature of -0.18ºC. Richard (2011) later described the state of water column mixing in terms of a flux Richardson number (Ri_f [-]), defined as the ratio of absorption of energy buoyancy to turbulent energy generation by momentum transfer (Eq 3-1):

$$Ri_f = \frac{B_0}{u_*^3/kd_w} \qquad \text{Eq 3-1}$$

where B_0 is the buoyancy flux [$m^3\ s^{-2}$], which is a function of heat flux and various fluid properties; u_* is the friction velocity [$m\ s^{-1}$]; κ is the von Kármán constant (κ =

0.4); and d_w is the water depth [m]. A stratified water column may be present if Ri_f exceeds 0.28, meaning that factors leading to stratification include high heat flux, low friction velocity, and large depth. Andreasson et al. (1998) conducted a theoretical study on the effects of surface turbulence on ice formation, with focus on flow depth and friction velocity. An upper threshold of u_* = 0.05 m s^{-1} was identified for skim ice formation, although this limit would vary between sites based on channel characteristics. Below this threshold, thermal processes influence ice floe properties (e.g., surface concentration, growth rate) with potential for larger floe formation proportional to a greater flow depth (Andreasson et al., 1998).

3.3.4 Field Observations of Skim Ice Runs

Field sites with documented skim ice run events include several large rivers. On the St. Lawrence River, Marcotte (1984b) described skim ice floes upstream of the Lachine Rapids. The high surface ice concentration of these floes, and the subsequent reduction in heat loss from the water column, contributed to reductions in regional anchor ice formation (Marcotte, 1984a). On the St. Lawrence River, Marcotte described formation of skim ice in an area immediately downstream of a regulated lake (Lake St. Louis). From these observations, a *limiting velocity for skim ice run* was established, which indicates that skim ice can form in higher velocity conditions given sufficient heat loss. This classification is similar to the classification of ice producing regions ('Frazil and Slush Ice', 'Skim Ice Run', and 'Stationary Ice') defined by Matoušek (1984b) based on hydro-meteorological conditions. These classes are presented on Fig. 3.1, along with the hydro-meteorological conditions during field and lab observations of skim ice (see Table 3.1).

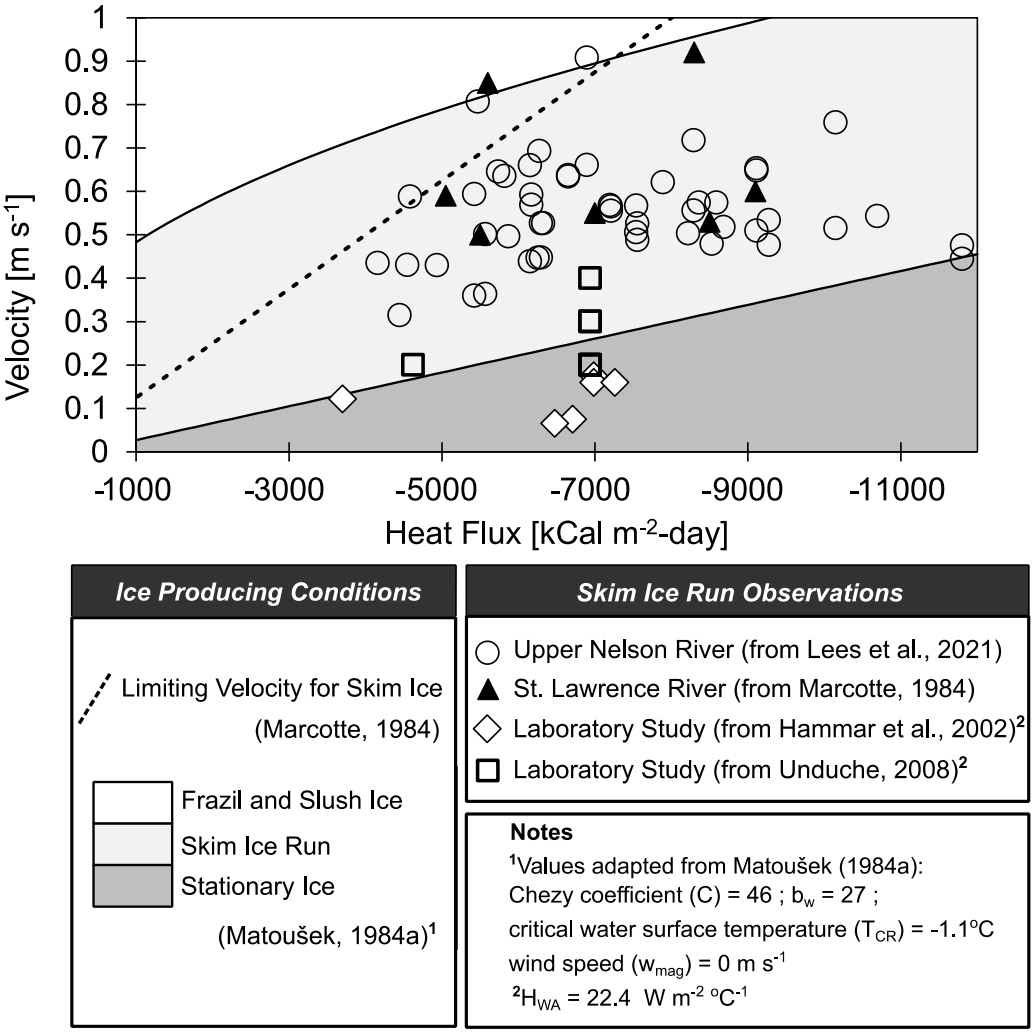

Fig. 3.1 - Summary of skim ice conditions in historical field and lab studies (overview in Table 3.1).

A noticeable contrast is seen between lab and field observations of skim ice run. While almost all field observations of skim ice run fall within the *Skim Ice Run* region (Fig. 3.1), laboratory observations of skim ice runs (Hammar et al., 2002; Unduche, 2008) generally occurred at lower velocities. Considering the difference in size between the flumes and channels in these studies, scale may have been a contributing factor. These studies highlight the need for further lab and field observations to validate empirical descriptions of skim ice formation and evolution.

3.3.5 Freeze-Up Jam Formation

In general, freeze-up jamming occurs either by congestion or by initiation from a downstream cover front, ice boom or other obstruction (Beltaos, 1995). Under very calm conditions, incoming skim ice floes may simply juxtapose leading to rapid frontal progression. Marcotte (1984b) described superimposition ('stacking') of skim ice floes as the mechanism of freeze-up jamming. Jasek et al. (2013) identified formation patterns of 'ridging' on the Peace River, where rough edges are visible at the boundaries of jamming skim ice floes due to ride-up and collapse into brash ice (i.e., small ice fragments). Brash ice may also result when weak skim ice floes collapse at the ice front. This phenomenon stalls frontal progression and thickens the leading ice edge, which has implications for numerical modelling of a skim ice regime (Jasek et al., 2013). Matoušek (1984b) noted that skim ice floes collapse into brash ice in the presence of rapids or hydraulic structures.

In the presence of significant changes to air temperature or discharge, consolidation may occur leading to thickening (Jasek et al., 2013) and stalling of ice cover advance. Related to this, it is established that the primary modes of fracture for floating ice 'sheets' is buckling and crushing (Ashton, 1986). Skim ice floes may also submerge under an existing cover if their inertia is sufficiently high. The mechanism of this submergence is vertical displacement, where floes sink and deposit at some distance downstream. The tendency for floes with a small thickness to flow depth ratio ($\frac{h_{floe}}{d_w} < 0.1$) to sink is attributed to the uniform pressure reduction beneath the ice floe, leading to minimal rotation (Larsen, 1975; Uzuner and Kennedy, 1972). Considering the typical width to thickness ratio of skim ice floes, and also that skim ice run events typically occur in low water velocities, submergence is a less likely outcome during freeze-up jamming.

3.4 Field Observations of Skim Ice Run in the Upper Nelson River

The hydro-meteorological conditions in the Upper Nelson River region in Northern Manitoba, Canada, allow for the presence of substantial skim ice runs during freeze-up. These skim ice runs contribute to accelerated frontal progression, with leading edge celerity (LEC) increasing to 0.05 m s^{-1} or greater during cold overnight conditions with sufficient open-water area (Lees et al., 2021b). Site observations

from the Upper Nelson River also provide insight into the nature of freeze-up jamming. Consistent with the studies mentioned previously, site observations show the presence of ridging and partial superimposition of large skim ice floes, as they decelerate at a leading ice edge (Fig. 3.2).

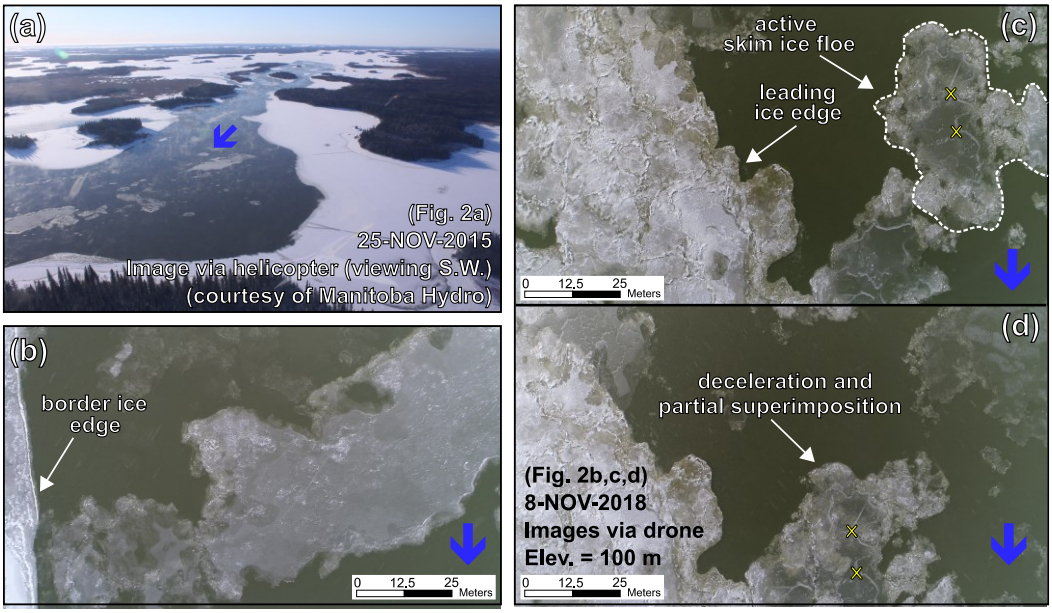

Fig. 3.2 - Observations of skim ice run from the Upper Nelson River; including (a) active skim ice floes between border ice cover; sequence of drone stills viewing down, including (b) partial view of large skim ice floe; and deceleration and partial imposition of skim ice floes during frontal progression (Δt = 90 s between (c) and (d)). Flow direction shown by blue arrows, yellow 'x' indicates an identifiable feature of the ice floe to compare images. Image (a) courtesy of Manitoba Hydro.

The presence of crushing failure is also observed in the case of weak skim ice run (Fig. 3.3), with an increase in ice roughness resulting from brash ice indicated by the bright white appearance of the ice cover in RADARSAT-2 imagery.

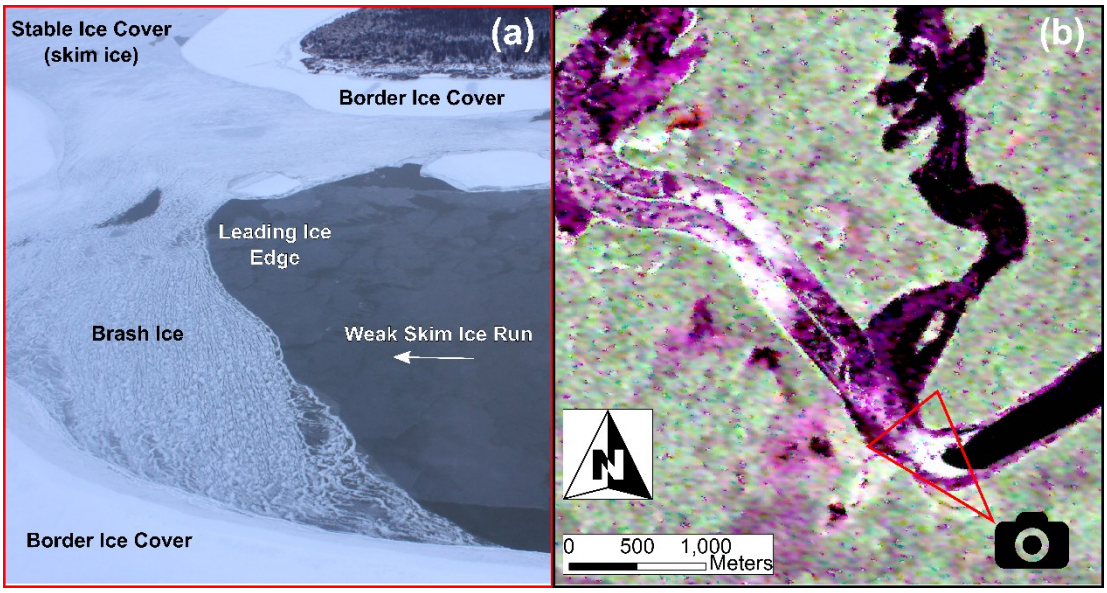

Fig. 3.3 - Crushing failure leading to rough ice texture at the Ominawin Channels, as shown in (a) helicopter image courtesy of Manitoba Hydro (2015), and (b) RADARSAT-2 imagery shared by Natural Resources Canada (2015).

Formation and jamming of skim ice floes is a prominent characteristic of freeze-up on the Upper Nelson River, which is an important time for ice management of the entire Nelson River system. A primary motivation for this paper is to develop an enhanced model treatment of this phenomenon for future application in complex two-dimensional model domains.

3.5 Overview of CRISSP2D

Two-dimensional Comprehensive River Ice Simulation System Project (CRISSP2D) functions as an extension of DynaRICE (Shen et al., 2000b) and RICEN (Shen et al., 1995). The model was developed to address multiple issues faced by hydropower operators in North America. CRISSP2D remains one of the few 2D river ice models, and is comprehensive with regard to the types of river ice processes that can be simulated. These include a variety of thermal and ice dynamic processes from freeze-up through break-up (Knack and Shen, 2018; Liu et al., 2006; Shen, 2016, 2010, 2002;). The main advantage of 2D modelling is an accounting of the effects of transverse flow distribution on the transport of river ice, which is important for many

river settings. The model's modular structure allows for adaptation of subroutines to features of a particular study area.

A more thorough description of the model is provided by Shen (2010). The following section focuses on description of thermal and ice dynamic calculations during surface ice transport and freeze-up jamming, as well as skim ice formulations in the model. The model is coupled with mass and energy exchanges occurring between hydrodynamic, thermal and ice dynamic modules. Hydrodynamic calculations employ a 2D depth-averaged form of the shallow water wave equations, which are solved through finite element calculations using an explicit upwind Petrov-Galerkin approach. Ice transport and dynamic interactions are simulated through the Lagrangian Discrete Parcel Method (DPM) based on the Smoothed Particle Hydrodynamics (SPH) (Shen et al., 1993). In this model, river ice is treated as a continuum of individual parcels, each with mass, momentum and energy. These individual parcels are composed of open-water and ice areas, with the latter partitioned into solid ice and porous frazil ice.

The ice mass of parcels is conserved from initial generation through freeze-up jamming. As parcels interact they undergo an increase in parcel mass density and surface concentration (up to a user-specified limit of N_{max}). Once the surface concentration (N) reaches N_{max}, additional increases in mass density serve to increases a parcel's ice thickness (t_i) through the process of mechanical thickening. External and internal forces on a parcel are resolved through a Lagrangian form of the surface ice momentum equation (Shen et al., 2000b), which considers the acceleration of an ice parcel, wind and water drag forces, the weight of the ice attributed to the water surface slope, and the internal ice resistance. This resistance is calculated with a Kelvin-Voight viscoelastic constitutive model, along with a Mohr-Coulomb yield criteria that governs the stress state of a parcel. If a parcel is in a plastic stress state, mechanical thickening will occur until an increase in internal ice resistance allows the parcel to return to a viscoelastic stress state.

Recent model adaptations have included incorporating the effect of freezing water between rubble ice floes to increase ice cover resistance to consolidation (Wazney et al., 2019b). This formulation tracks the growth and decay of a solid crust layer once a parcel begins jamming, and accounts for the cumulative strength due to rubble

friction and this solid crust layer. Provided the cumulative strength exceeds the externally acting forces, the parcel will remain in a viscoelastic stress state to inhibit mechanical thickening. The proposed treatment in this study adapts elements of the above described formulation to account for the strength attributed to skim ice floe growth.

The inception of a parcel in CRISSP2D most commonly occurs via formation of suspended frazil, and subsequent mass transfer to the river surface. This mass transfer rate is governed primarily by the suspended ice concentration and average rise velocity of frazil ice to the surface (v_b). In a skim ice dominant river, ice grows primarily at the surface without much entrainment into the suspended water column. In this scenario, a secondary type of parcel can be introduced through 'skim ice' elements, as described by Shen (2010), in the presence of a supercooled surface water layer. The focus of this study is on treatment of these particular skim ice parcels.

CRISSP2D applies Matoušek's formulation (Matoušek, 1984a), which includes calculation of vertical turbulence (v_z') (Eq 3-2) and buoyancy of ice particles (v_b) (Eq 3-3):

$$v_z' = \left[\left(C_T^{0.5} g^{0.5} \frac{U n_b}{\sqrt[6]{R_H}}\right) + C_{w*}\left(C_d \frac{\rho_a}{\rho_w}\right)^{\frac{3}{2}} w_{mag}^3\right]^{\frac{1}{3}} \quad \text{Eq 3-2}$$

$$v_b = -0.025 T_S + 0.005 \quad \text{Eq 3-3}$$

where C_T is the coefficient relating bed shear stress to turbulent fluctuation velocity [-]; g is the gravitational constant [m s^{-2}]; U is the depth-averaged water velocity [m s^{-1}]; n_b is the Manning's bed roughness; and R_H is the hydraulic radius [m]. Eq 3-2 includes the effect of wind on vertical turbulence (Lal and Shen, 1989), where C_{w*} accounts for wind effects on turbulence; C_d is the wind drag coefficient [-]; ρ_a and ρ_w the air and water density [kg m^{-3}], respectively; and w_{mag} is the wind speed [m s^{-1}]. The buoyancy of ice particles is defined as a function of the degree of supercooling in the surface layer, represented by a surface water temperature [T_S] (Eq 3-4):

$$T_S = T_W - \frac{\emptyset_*}{1130U - b_w w_{mag}} \quad \text{Eq 3-4}$$

where T_W is the depth-averaged water temperature [ºC]; $\emptyset_*$ is the heat loss at the air-water interface [W m^{-2}]; and b_w is a coefficient accounting for the width of the river [-].

3.6 Methodology

3.6.1 Treatment of Skim Ice Run

Simulation of freeze-up jamming involves aspects of hydrodynamic, thermal and ice dynamic modules in the model. Descriptions of these processes will include references to several model time steps: hydrodynamic (Δt_h), ice dynamic (Δt_{ice}), and coupling (Δt_{intvl}). The following sections outline aspects of the proposed treatment of skim ice runs from formation through to freeze-up jamming, as summarized on Fig. 3.4.

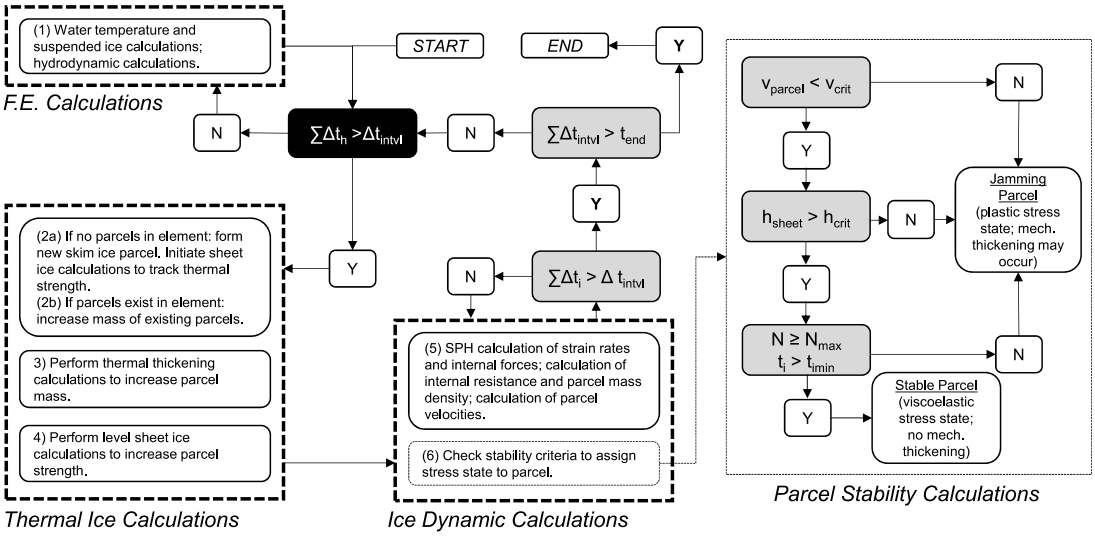

Fig. 3.4 - Overview of key model processing, coupling of times, and procedure to assess parcel stability during ice dynamic calculations.

3.6.1.1 Finite Element and Thermal Ice Calculations

Skim ice parcels are introduced in the model on elements of the finite element mesh that are comprised of nodes that satisfy the following criteria: (1) $v_b > v_z'$, (2) $T_{CR} <$

T_S < 0ºC, and (3) the element is not covered in stationary ice. Condition (1) accounts for the entrainment of ice particles if turbulence is too strong, while condition (2) allows for skim ice formation when the surface water temperature is between 0ºC and T_{CR} (i.e., the empirically-derived lower limit for skim ice formation). Provided that a supercooled surface layer is present, skim ice can form even when the bulk water temperature is not supercooled. There is currently no practical method for determining ice volume production in the supercooled surface layer, which is a requirement to determine initial thickness of the ice floes. Values from the literature and preliminary model testing indicate that an initial thickness of one millimeter is a suitable value for the proposed treatment. Skim ice parcels are introduced at Δt_{intvl}, with a high initial surface concentration and an area corresponding to the element in which they were generated.

Parcel ice thickness will change through growth or decay according to heat exchanges with the atmosphere and underlying water. In the case of frazil floes and loose frazil slush, open-water areas between floes facilitate increased suspended ice concentration in the event of net heat loss. In contrast, a large skim ice floe has a high surface concentration, meaning that a net heat loss will result in thickening of the floe. Skim ice floes can gain considerable strength and stability due to their growth during transport. To account for this strength, a sheet ice calculation (Ashton, 2013) is initiated for each parcel upon generation and is updated every Δt_{intvl} (Eq 3-5):

$$\Delta h_{sheet} = \frac{1}{\rho_i \lambda}\left(\frac{H_{IA}(T_m - T_{AIR}) - \emptyset_R}{\left(\frac{H_{IA} h_{sheet}}{k_i}\right) + 1}\right)\Delta t_{intvl} \qquad \text{Eq 3-5}$$

where H_{IA} is the ice-air heat transfer coefficient [W m^{-2}]; ρ_i is the ice density [kg m^{-3}]; λ is the latent heat of fusion of ice [J kg^{-1}]; h_{sheet} is the initial sheet ice thickness [m]; T_m is the temperature at the ice/water interface [ºC]; and $\emptyset_R$ is the net short-wave radiation [W m^2].

3.6.1.2 Ice Dynamic Calculations

Parcels will decelerate and converge as they approach an ice boom or leading ice edge. As a parcel decelerates below a user-specified critical threshold ($v_{parcel} < v_{crit}$), it is considered a candidate for jamming as described by Wazney et al (2019b). Instead of checking for ice stability at Δt_{intvl}, conditions for jam stability are checked at each ice dynamic time step (Δt_{ice}). As outlined on Fig. 3.4, requirements for a parcel to remain in a viscoelastic stress state are as follows: (1) a parcel's ice thickness must exceed a user-specified minimum thickness ($t_i > t_{i_{min}}$), and (2) the sheet ice thickness of a parcel must exceed a user-specified critical threshold ($h_{sheet} > h_{crit}$). These conditions account for two characteristics of freeze-up jamming by skim ice run:

1) Skim ice covers may achieve stability at a thickness less than what would be calculated by the Mohr-Coulomb yield criteria. The treatment bypasses the need for an ice jam to achieve stability by frictional resistance before thermal effects are incorporated into the jam's total resistance.

2) The ice jam profile should reflect the properties of the skim ice floes that comprise the ice supply. When compared to frazil ice floes, skim ice floes formed under cold conditions have higher stability and are less likely to collapse during jamming, leading to thinner cover formation and faster frontal progression. In the event that $h_{sheet} > h_{crit}$ is not satisfied, a parcel will continue to mechanically thicken until that condition is met.

In a real-world context, mechanical thickening is considered to occur primarily due to the collapse of skim ice floes into brash ice. A secondary form of mechanical thickening is complete superimposition of skim ice floes. These two physical processes are lumped together in the model treatment as they are far too complex to differentiate, and the net result of both is stalled frontal progression and thickening of leading ice edges.

In this treatment, the compounding effect of freezing interstitial water between skim ice floes is assumed to be coupled into the parameter h_{sheet}. Based on field observations, an assumption in the treatment is that once a stable jam is formed by skim ice run, it will not experience severe consolidation events. This is in part

attributed to the strength of individual skim ice floes that comprise the cover. In the existing formulation (Wazney et al., 2019b), parcel consolidation is simulated as external forces exceed the resistance of a parcel. During consolidation, h_{sheet} is reset to zero, potentially leading to significant mechanical thickening of the cover due to the loss of the 'solid crust layer'. To account for the strength of individual skim ice floes in this study, h_{sheet} is not reset to zero during mechanical thickening. This detail is required to limit the mechanical thickening that occurs, and most importantly, to prevent collapse of the ice jam in accordance with field observations.

3.6.2 Numerical Simulations - Ideal Trapezoidal Channel

The proposed treatment is presented through simulations in an ideal trapezoidal channel (flow direction, right-to-left), shown on Fig. 3.5.

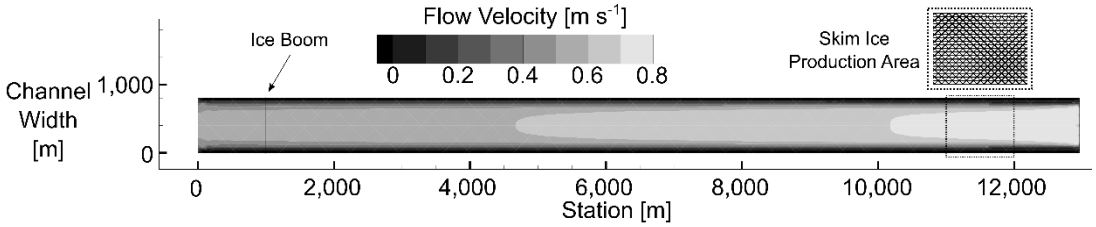

Fig. 3.5 - Trapezoidal ideal channel geometry.

The channel design was informed by conditions on the Upper Nelson River. The channel had a mild grade (0.02%), top width of 800 m, side slopes of 1:40 (H:V), and a total length of 13 km. An ice boom was positioned 1 km from the channel outlet, and was parameterized to restrict movement of all incoming parcels. During simulations, two types of hydrodynamic boundary conditions were applied to illustrate versatility of the treatment. In the case of variable discharge tests, boundary conditions of upstream inflow and downstream fixed water level were applied. Water surface profiles during these tests reflect the upstream staging that results from ice jam formation, with the focus of these simulations being the change in upstream velocity. Alternatively, boundary conditions of downstream outflow and upstream fixed water level were applied during variable air temperature tests. This condition reflects a scenario where outflow is controlled by a hydraulic structure

(i.e., hydroelectric dam), and upstream water levels reflect stage in a large reservoir that undergoes gradual and relatively minor water level changes.

A 0.8 km^2 *skim ice production area* was designated at the upstream end of the model, which provided a controlled region for ice generation between tests. This scenario is similar to a skim ice producing area at the outlet of a lake. In a case where this area was not constrained, the presence of skim ice producing area would be governed by the criteria for skim ice elements. The result of this is that during very cold conditions, skim ice producing areas may be expansive, resulting in more ice production and faster frontal progression. Variation in ice production area is not included in these simulations, and instead test conditions evaluated the effect of variable air temperature, variable discharge, and channel morphology on ice jam formation (see Table 3.2).

Table 3.2 - Testing conditions for ideal channel simulations, including upstream (U/S) and downstream (D/S) boundary conditions (BC).

Category of Test	T_{AIR} [ºC]	Q[1] [m^3 s^{-1}]	D/S BC	U/S BC	Bed Slope	Sinuosity
Variable Discharge (Fig. 3.8)	-15	1,980 2,120 2,265 2,405 2,550 2,690	WSE[2]	Q_{inflow}[3]	0.02%	1.0
Variable Air Temperature (Fig. 3.9)	-25 -20 -15 -10 -7.5 -5[5]	2,265	$Q_{outflow}$[4]	WSE[2]		
Variable Air Temperature and Discharge (Fig. 3.10)	-10 -10 to -15 -10 to -25	2,265 to 1,980	$Q_{outflow}$[4]	WSE[2]		
Variable Bed Slope (Table 3.5)	-20	1,980	WSE[2]	Q_{inflow}[3]	0.02% 0.03% 0.05%	1.0
Variable Sinuosity (Table 3.5)	-20	1,980	$Q_{outflow}$[4]	WSE[2]	0.02%	1.1 1.2 1.3

Notes:
[1]Q = discharge
[2]WSE = assigned water surface elevation at boundary
[3]$Q_{outflow}$ = assigned outflow from model
[4]Q_{inflow} = assigned inflow to model boundary
[5]No thermal strength included in this scenario (base case for comparison purposes)

Five additional channels were designed to accommodate simulations with different bed slope (0.03% and 0.05%) and sinuosity (1.1, 1.2 and 1.3). Aside from changing bed slope and sinuosity, the properties of these five channels (i.e., top width, side slopes, boom position, stream-wise length) remain similar to those of the channel on Fig. 3.5. In the case of sinuous channels, the model mesh was modified to accommodate a curved shape. This curve was defined by select values for sinuosity (S_N), which is defined as (Mueller, 1968):

$$S_N = \frac{CL}{Air} \qquad \text{Eq 3-6}$$

where CL is the stream-wise length of the channel (13 km), and Air is the Euclidean distance between the inlet and outlet of the channel (km). Discharges selected are based on operating conditions during flow control on the Upper Nelson River. Parameter values were selected through a combination of field data, pertinent literature, and satisfactory values based on preliminary model testing. Values held constant across all simulations are summarized in Table 3.3.

Table 3.3 - Relevant parameters across simulations.

Parameter	Description	Value
$t_{i_{min}}$	Minimum ice thickness for freezing	0.2 m
$\vec{v}_{crit}$	Critical freezing velocity	0.05 m s^{-1}
h_{crit}	Critical sheet ice thickness	0.01 m
$\emptyset$	Internal friction angle of ice rubble	46º
H_{WA}	Heat transfer coefficient	22.4 W m^{-2} $ºC^{-1}$
n_i	Manning's coefficient for ice	$0.02 \sim \begin{cases} 0.02, & t_i \leq 0.2\ m \\ 0.06, & 0.2\ m \leq t_i \leq 0.6\ m \\ 0.06, & n_i = 0.06\ for\ t_i \geq 0.6\ m \end{cases}$

3.7 Results and Discussion

3.7.1 Effects of hydro-meteorological conditions on ice supply

3.7.1.1 Ice producing conditions

The type of ice floes that form during freeze-up depend on both hydraulic and thermal conditions. The approximate test conditions selected for the *skim ice production area* are shown on Fig. 3.6.

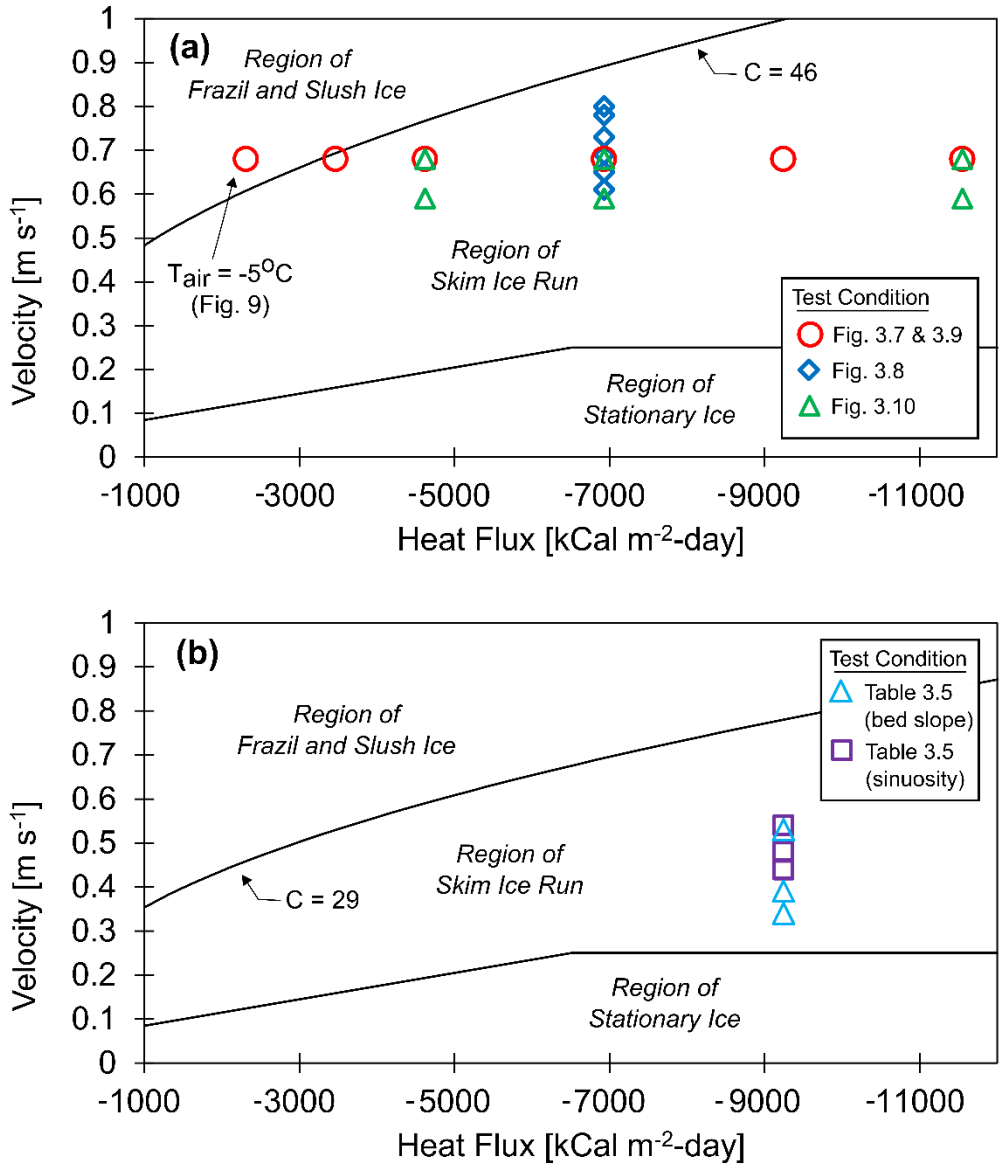

Fig. 3.6 - Approximate hydro-meteorological conditions relative to nomograph of ice producing regions (adapted from Fig. 3.1).

These test conditions are compared with the delineations of ice producing regions, which are defined based on the hydraulic characteristics of the channel. The partition between the *Region of Frazil and Slush Ice* and *Region of Skim Ice Run* varies primarily as a function of the Chezy coefficient of the reach. In a natural channel with varying bed roughness and hydraulic radius, potential for skim ice production can vary between reaches. Hydraulic conditions defined by a higher Chezy coefficient were applied for most tests (Fig. 3.6a), as these values are representative

of a large, slow moving river. Under these conditions, the region of skim ice production extends to higher velocity conditions at moderate heat fluxes. To accommodate simulations in the five channels with varying channel sinuosity and bed slope, a lower Chezy coefficient was applied (Fig. 3.6b). With a lower Chezy coefficient, formation of skim ice is restricted to high heat fluxes or low velocity conditions (Matoušek, 1984b).

Variation of test conditions in the vertical direction on Fig. 3.6 reflect different hydraulic conditions (discharge, bed slope, sinuosity), which result in different flow velocities in the channel. Important to note is that at relatively low heat fluxes and higher velocities, formation of frazil and slush ice will occur instead of skim ice. Lastly, at very low velocities, Fig. 3.6 shows the *Region of Stationary Ice*, which indicates formation of border ice. The horizontal line on top of the *Region of Stationary Ice* indicates an upper velocity limit for border ice formation ($\vec{v}_{crit}$; 0.25 m s^{-1} on Fig. 3.6), which can be derived from field observations (Shen, 2010).

3.7.1.2 Strength of skim ice floes

For the prescribed air temperatures, initial sheet ice thickness (h_{sheet}) associated with parcels ranged from 1-2 mm upon exiting the skim ice production zone. Sheet ice thickness growth rates are summarized on Fig. 3.7.

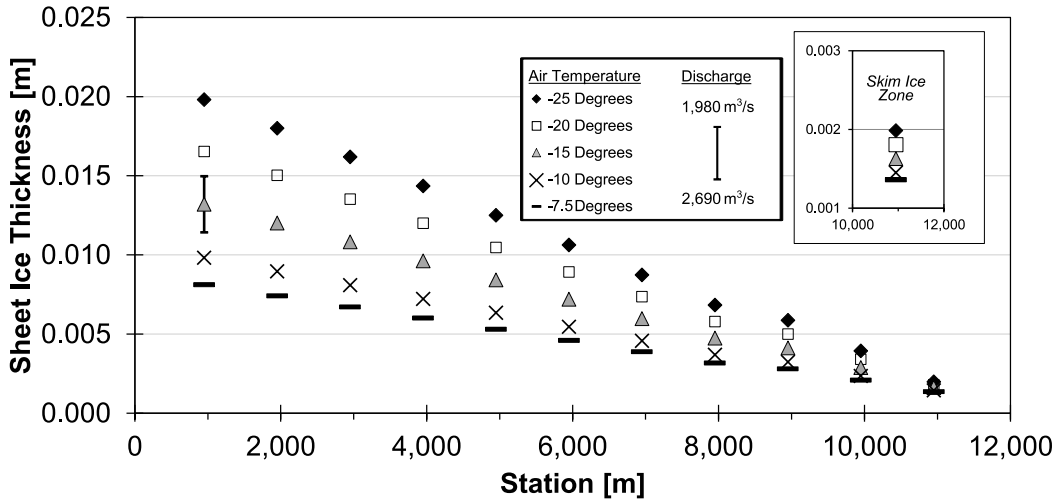

Fig. 3.7 - Sheet ice thickness (surrogate for strength) under variable air temperatures (Q = 2265 m^3 s^{-1}). Vertical bars @ station 1000 m indicate range in sheet ice

thickness for variable flows of 2690 m^3 s^{-1} (thin) to 1980 m^3 s^{-1} (thick). Inset figure shows ice thickness at station 11,000 m.

Despite this small initial thickness, skim ice floes continue to thicken during advection downstream, with variations in sheet ice thickening rate under different air temperature conditions. For instance, T_{AIR} = -10ºC results in a sheet ice thickness of 0.01 m upon arrival at the ice boom. Assuming a failure stress of 0.5 MPa (selected from a range derived from lab and field studies; e.g., (Wazney et al., 2019a, Andres, 1999), 5000 N m^{-1} of per unit width resistance during ice cover formation is achieved. By this same logic, skim ice floes formed when air temperatures are -25ºC will have almost two and a half times the strength of ice floes formed under -7.5ºC conditions. The vertical bar at x = 1000 m shows that the effect of flow changes on incoming skim ice floe strength.

3.8 Effects of hydro-meteorological conditions on ice jam profiles

3.8.1 Varying channel discharge

Channel discharge plays a primary role in ice cover formation, and is an important factor in river ice control on regulated rivers. This is particularly true for mild-sloped and deep rivers, where backwater effects do not significantly reduce leading edge Froude numbers, a process that facilitates ice cover formation in steeper rivers (Shen and Ho, 1986). By applying a fixed water level at the downstream end of the model, discharge is varied to change the water surface slope (and subsequent flow velocity) upstream. In real world systems, including large rivers, it is expected that some variation in downstream water level would accompany a change in discharge. These scenarios simplify this reality, as the focus of simulations was on evaluating the effects of changing flow velocities on jam formation.

For the following simulations, initial bulk water temperature, as well as upstream boundary temperature were set at 0.05ºC to represent the condition of slightly warm water underlying an ice cover. Starting from an open-water condition (Fig. 3.8a), ice jam formation occurs at different rates under different discharge conditions (Fig. 3.8b and Fig. 3.8c). Once each ice jam reaches the final upstream position, discharge

in all scenarios was increased to a maximum rate based on site conditions in the Upper Nelson River (2,690 m^3 s^{-1}; Fig. 3.8d).

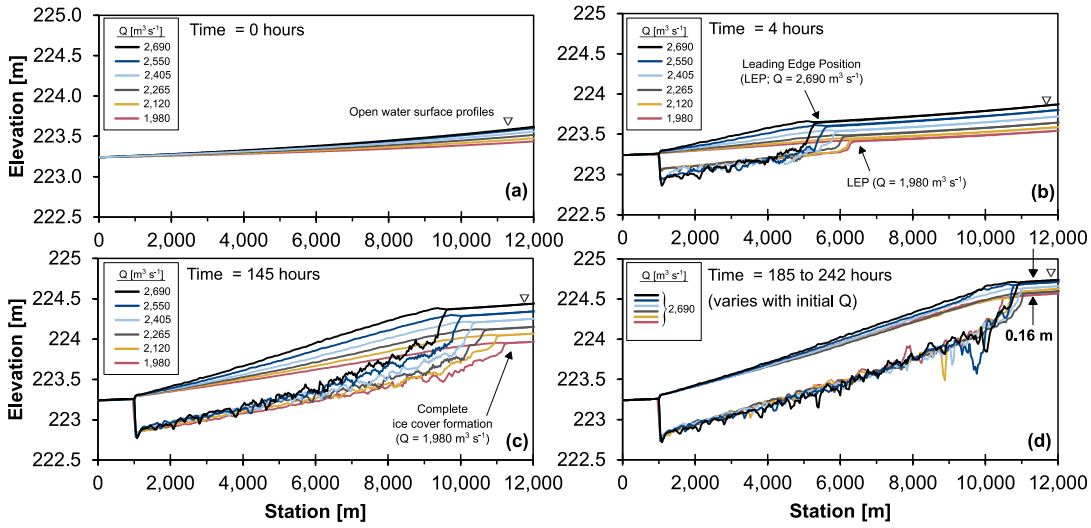

Fig. 3.8 - Stages of ice cover progression (T_{AIR} = -15ºC) from (a) open-water condition to (d) stable cover formation and flow increase.

To reflect practices in a flow control scenario, ice jams were permitted to thermally thicken for 24 hours once a complete stable cover formed (Leading Edge Position (LEP) = 11,000 m) before channel discharge was increased to 2,690 m^3 s^{-1} (Fig. 3.8d). This reduced potential for undesired consolidation events and downstream jam thickening when discharge was increased. Reducing discharge from 2,690 m^3 s^{-1} to 1,980 m^3 s^{-1} resulted in a 32% (2.8 day) reduction in time required for the *LEP* to reach 11,000 m. Upon complete formation, the average ice cover in the lowest discharge case was 20% thinner (corresponds with 23% less total ice volume) when compared to the highest discharge case. The result of this is a 14% reduction in backwater height upstream of the ice jam when compared to the highest discharge case.

The reduced backwater resulting from temporary flow reductions during simulations is attributed to two effects. The primary effect is an increase in travel time for parcels before they reach the ice front, which facilitates accumulation of ice mass and thermal strength. A secondary effect of reduced discharge is less time required for a parcel to decelerate below the critical threshold ($v_{parcel} < v_{crit}$). Not reflected

in these simulations is the effect of reduced discharge on channel features, where frontal progression may be limited by a localized high velocity region. Reduced discharge may also dampen upstream turbulence, thereby expanding skim ice production areas of the river.

3.8.2 Varying air temperature

Weather conditions (i.e., air temperature) have a multitude of effects on ice production, as well as on ice cover formation and stability. As with previous simulations, initial bulk water temperature and upstream boundary water temperature were set at 0.05ºC to represent the condition of slightly warm water underlying an ice cover. The effect of air temperature on ice jam formation is illustrated on Fig. 3.9, and statistics associated with each run are summarized in Table 3.4.

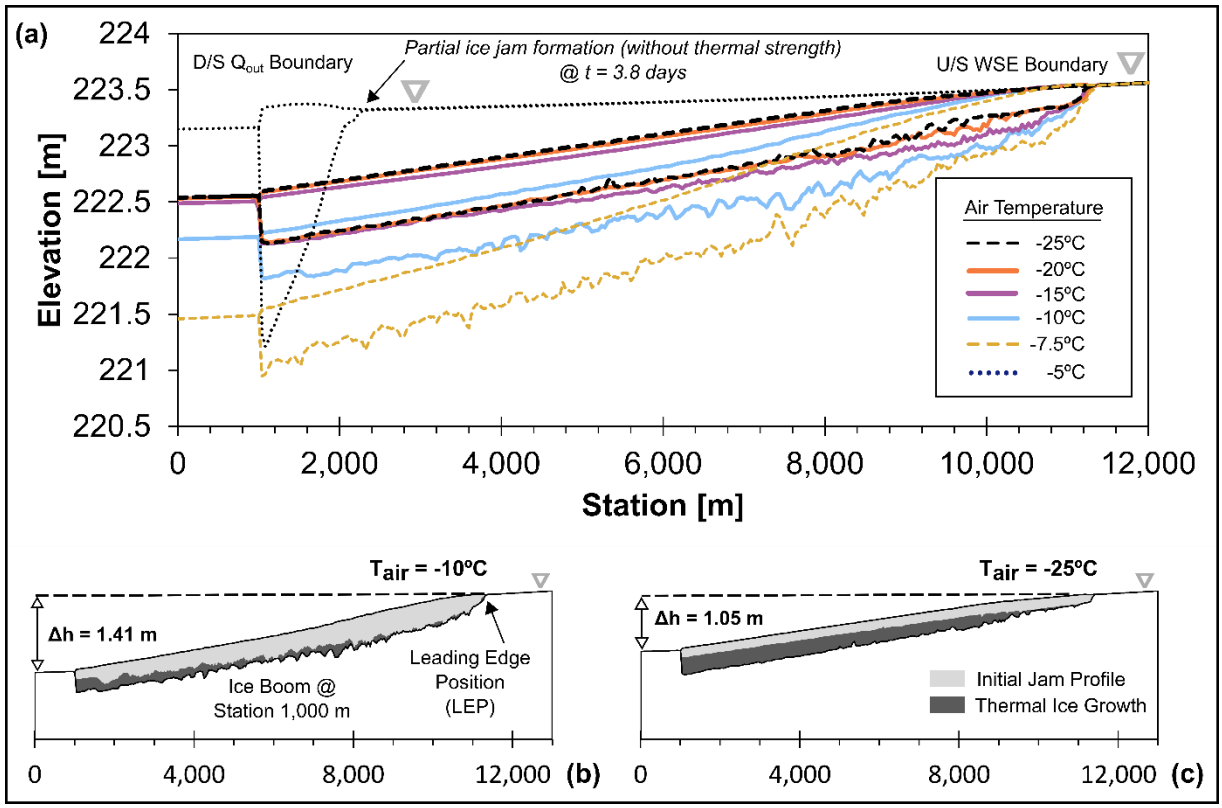

Fig. 3.9 - Ice jam profiles under varying temperature conditions (Q = 2265 m^3 s^{-1}), including detailed jam profiles for (b) T_{AIR} = -10ºC, and (c) T_{AIR} = -25ºC.

Table 3.4 - Run statistics for varying temperature conditions

Q	T_{AIR}	Time for stable ice cover formation (LEP @ 11,000 m)	Average Leading Edge Celerity	Average t_i	ΔH from U/S to D/S of jam formation
[m^3 s^{-1}]	[ºC]	[days]	[m hr^{-1}]	[m]	[m]
2,265	-25	3.8	114	0.37	1.05
	-20	4.7	92	0.37	1.05
	-15	6.2	70	0.38	1.09
	-10	10.3	41	0.48	1.41
	-7.5	16.7	25	0.52	2.12
	-5	>16.7	<25	>0.52	>2.12

A comparison of ice jams profiles formed under different heat losses (Fig. 3.9b and Fig. 3.9c) shows appreciable differences. Under colder air temperatures (T_{AIR} = -25ºC), h_{sheet} for incoming floes exceeds the minimum threshold (h_{crit} = 0.01 m) upon arrival at the ice front. As a result, parcels will only thicken to $t_{i_{min}}$ upon convergence with other parcels. The *initial jam profile* reflects this initial jamming thickness. As the LEP approaches the skim ice production zone, travel time is reduced, and h_{sheet} is less than h_{crit} upon a parcel's arrival at the ice front leading to mechanical thickening beyond $t_{i_{min}}$. Following initial jam formation, thermal growth of the ice cover continues, resulting in an average cover thickness of 0.37 m when T_{AIR} = -25ºC. Thermal thickening of the ice jam would continue until an equilibrium thickness is reached.

Under warmer conditions ($T_{AIR} \geq$ -10ºC), rate of growth of h_{sheet} is lower, meaning that h_{crit} is only satisfied for parcels arriving at the ice front after travelling most of the channel reach. As the LEP advances upstream, parcels converge and

mechanically thicken beyond $t_{i_{min}}$ until h_{sheet} exceeds h_{crit}. The result of this is a thickening of the initial jam profile in the upstream direction, and reduced LEC as the ice front approaches the skim ice production zone. A test case without any thermal strength is included (T_{AIR} = -5ºC), meaning that parcels did not transition from *jamming parcel* to *stable parcel* during the simulation (see 'Parcel Stability Calculations' on Fig. 3.4) In this case, the ice jam undergoes significant thickening during only a short period of time (3.8 days) to achieve stability. A significant amount of ice volume and time would be required to extend this ice jam up the entire channel, with the result being ice-induced head losses that far exceed any of the other test cases.

As summarized in Table 3.4, stable ice cover formation times increase significantly as air temperatures approach 0ºC. For instance, a 6.5 day difference in closure time is simulated between the -10ºC and -25ºC cases, and a 0.36 m difference in overall head difference across the jam is observed. It is also evident from Fig. 3.9. that properties of the jams become more consistent as temperatures decrease (<= -15ºC test cases). This is attributed to the selected value of h_{crit} (0.01 m), which results in fairly uniform profiles in the early stages of jam formation. As LEP approaches the upstream extent of the model (Station > 8,000 m), differential thicknesses are visible between these three test cases, although the range of ΔH across these three cases was only 0.04 m. An increase in h_{crit} would further differentiate jam profiles between cases. For instance, a simulation using h_{crit} = 0.012 m increased the range of ΔH to 0.25 m. A comparison of freeze-up patterns and hydrometric records for a specific site between years with different air temperatures may provide guidance on choosing a suitable value for h_{crit}.

3.8.3 Cumulative impact of hydro-meteorological conditions

The sensitivity of ice jam formation based on the cumulative impact of hydro-meteorological conditions is relevant to flow control during freeze-up, where the decisions regarding the timing and magnitude of flow reductions benefit from optimization. In the following scenarios, air temperature and discharge are changed concurrently at 48 hours after the start of simulation. Run statistics and the resulting jam profiles are summarized on Fig. 3.10.

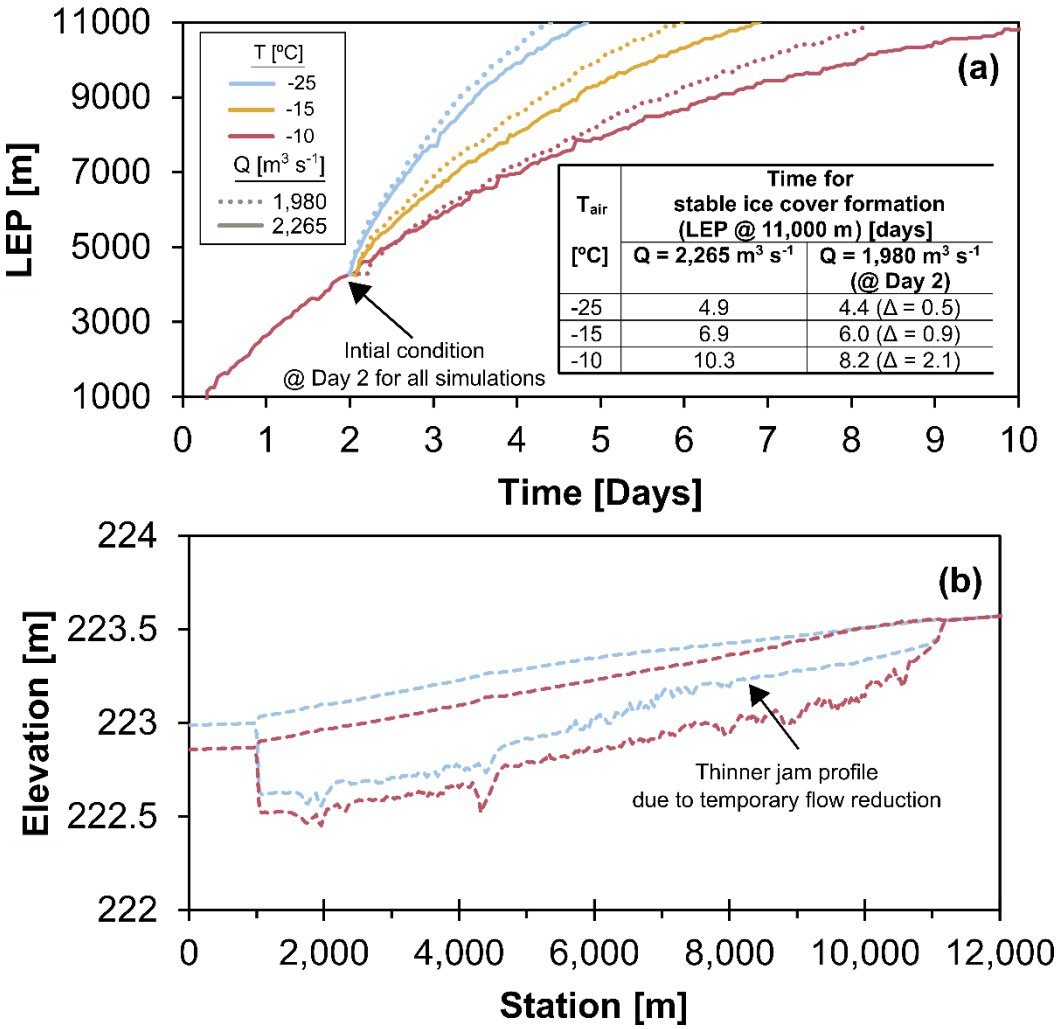

Fig. 3.10 - Effect of temporary flow reduction (-285 m s^{-1}) at t = 2 days under varying air temperature conditions on (a) leading edge celerity and (b) ice jam profiles.

From these figures, it is evident that heat loss (and subsequent ice production) is the primary factor in increased rates of frontal progression. A change in temperature from -10ºC to -25ºC at hour 48 results in a nearly 50% increase in LEC to an average of 0.03 m s^{-1}, consistent with the range of most frontal progression events observed for the Upper Nelson River (0.01 to 0.05 m s^{-1}). While flow reductions increase LEC in all scenarios, the effect is most pronounced as the LEP approaches the skim ice production zone. In a regulated river setting, an early flow reduction may have implications for power generation potential and waterway users, and as such these decisions require consideration of both forecasted weather conditions and reach-specific conditions (i.e., open-water area and local hydraulics). An example of this is

shown for the 2007 freeze-up on the Upper Nelson River, where a series of frontal progression events occurred between November 17 and 23 (average T_{AIR} of -9.8ºC). After three days of stalling, the combined effect of a flow reduction and cold overnight conditions (T_{AIR} < -20ºC) allowed for sufficient skim ice production and suitable hydraulic conditions for the ice cover to progress to its final upstream extent (Fig. 3.11).

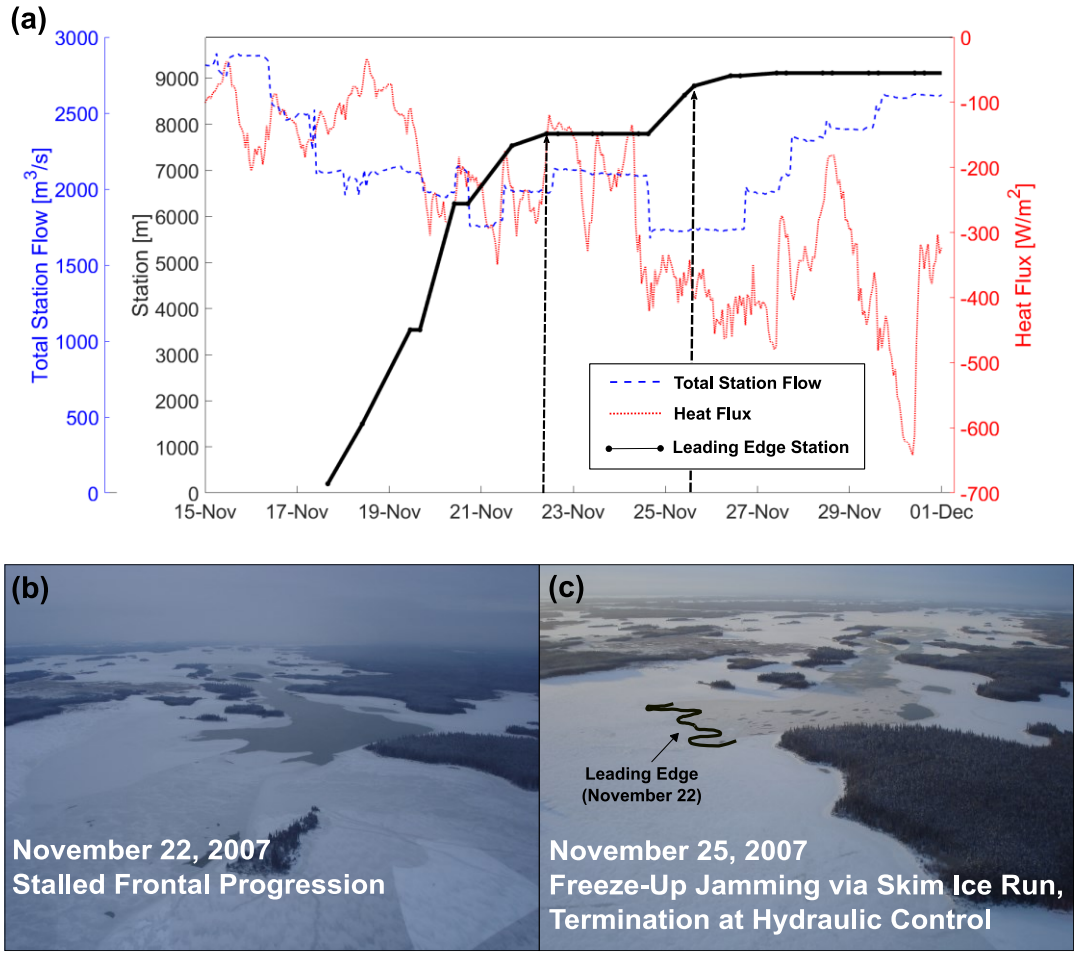

Fig. 3.11 - Conditions during the 2007 freeze-up on the Upper Nelson River during freeze-up, including site conditions (a), and frontal progression due to skim ice run between November 22 (b) and November 25 (c). Images courtesy of Manitoba Hydro.

3.8.4 Role of channel morphology

Channel features, such as meanders, constrictions and variable bed slopes can affect both ice production and freeze-up jamming processes. To evaluate the effect of sinuosity and changing bed slope on freeze-up jamming, a lower Chezy condition was applied (Fig. 3.6b). As such, a lower discharge and air temperature condition was chosen to allow for production of skim ice floes in these simulations. A comparison of run statistics for these channel conditions is shown in Table 3.5.

Table 3.5 - Run statistics for varying channel morphology conditions

Q	T_{AIR}	Bed Slope	Sinuosity	Mid-Channel Velocity (@ 3,000 m)	Time for stable ice cover formation (LEP @ 11,000 m)	Average Leading Edge Celerity
[m^3 s^{-1}]	[ºC]	[-]	[-]	[m s^{-1}]	[days]	[m hr^{-1}]
1,980	-20	0.02%	1.1	0.41	3.2	130
			1.2	0.45	3.8	109
			1.3	0.48	4.2	99
		0.02%	1.0	0.29	3.1	134
		0.03%		0.30	3.2	130
		0.05%		0.32	3.5	119

The primary effect of the presence of increasing bed slopes and meanders is an increase in flow velocity, which reduces frontal progression rates. For instance, the introduction of a meander with sinuosity of 1.3 increased the time required for stable ice cover formation by 31%. While the range in results was smaller for varying bed slope conditions, steeper bed slopes contributed to slower frontal progression. This has implications for frontal progression through a channel with irregular morphology

in the streamwise direction. It is noted also from Fig. 3.6b that in channels with a higher bed roughness or shallow flow depths, turbulence may limit production of skim ice to very cold conditions. In this case, suspended frazil ice is typically the dominant ice type during supercooled conditions.

3.9 Application and site-specific parameter values

The proposed treatment includes selection of several parameters, each governing different aspects of ice cover formation. The focus of simulations was on parameters that account for the role of heat loss and travel time on skim ice properties. In addition to h_{crit}, the $t_{i_{min}}$ parameter allows the ice cover to remain stable at a thickness less than that calculated by the Mohr-Columb failure criterion. Site-specific river ice monitoring programs may provide data for calibration of this value. For instance, ice cores extracted from multiple locations on the Upper Nelson River indicate an initial formation thickness of 0.10-0.16 m. Documentation also notes historical observations of 'white ice' (0.26 m; Manitoba Hydro, 2015) and 'snow ice' (0.1-0.5 m; Manitoba Hydro, 2018) in ice cores extracted from the Upper Nelson River. These data only capture some of the inter-annual and spatial variability of freeze-up conditions in the region, but do provide some guidance for a range of suitable values (0.1 to 0.5 m). Considerations for selecting a value for $t_{i_{min}}$ include that if set too low, parcels may not adequately interact with each other, resulting in simulated irregularities in the ice cover. Alternatively, if $t_{i_{min}}$ is set too high, the effect of thermal strength diminishes during simulations, resulting in thicker ice jams that rely primarily on frictional strength.

3.9.1 Mixed frazil-skim ice regime and termination of frontal progression

The results presented in this paper represent the scenario where ice jam formation results from a supply of skim ice from a localized upstream area ('skim ice production zone'). Even for freeze-up conditions where skim ice is the dominant ice type, mixed frazil and skim ice regimes can occur (Andreasson et al., 1998; Matoušek, 1992;). In a mixed frazil and skim ice regime, several frazil pans can be bonded together with a skim ice center, as was observed on the Tanana River during cold overnight conditions (i.e., < -15ºC) (Osterkamp and Gosink, 1983). This could

be addressed by simulating frazil ice deposition onto skim ice parcels between the skim ice production zone and stable ice cover. As a result, $t_{i_{min}}$ would be satisfied earlier as parcel mass would increase by both deposition and thermal thickening. A mixed ice regime may also result from advection of frazil ice pans from a steeper reach upstream of a skim ice producing zone, as observed on the Peace River (Jasek et al., 2013). These site-specific scenarios would require further adaptation of the treatment.

Another consideration for freeze-up jamming simulations is the presence of an upstream hydraulic control that terminates advancement of the cover. An example of this is on the St. Lawrence River, where frontal progression is noted to cease due to a high velocity region near Gallop Island (Shen and Ho, 1986). In the Upper Nelson River, a high velocity region (> 1 m s^{-1}) near Manitou Rapids typically limits frontal progression, and thus serves as a benchmark for flow control efforts (see Fig. 3.11c). In the current model, parcels can continue to achieve stability and progress until the entire skim ice zone is ice covered. In reality, frontal progression may be limited by an upstream hydraulic control. To account for this, frontal progression could be terminated by designating a 'rapids' zone that entrains parcels to increase suspended ice concentration, an approach similar to other modelling studies (Malenchak, 2011). An alternate approach is to set a hydraulic threshold, such as flow velocity in the case of deep rivers (e.g., U < 0.7 m s^{-1}; Perham, 1983), to limit frontal progression. A more complex approach involves including both a hydraulic threshold and characteristics of the ice supply, as larger skim ice floes may have sufficient stability to initiate frontal progression past a hydraulic control. Site-specific conditions would need to be considered to select an appropriate mechanism to account for these upstream controls.

3.10 Conclusion

On very mild sloped rivers in cold regions, skim ice runs can play an integral role in stable ice cover formation by freeze-up jamming. Given suitable hydraulic and meteorological conditions, skim ice run contributes to accelerated frontal progression of an ice cover. This study describes a proposed treatment using a two-dimensional river ice model to simulate ice jam formation in a skim ice dominant

freeze-up. During simulations, an initial skim ice thickness is established on the order of millimeters, consistent with lab and field studies describing ice growth. Through implemental of empirical equations, skim ice strength (simulated through sheet ice calculations) increases as a function of travel time and heat loss. Further, these equations account for the strength of ice floes when calculating ice cover thickness during ice dynamic simulations.

The focus of simulations in this study was evaluating the impact of changing hydro-meteorological conditions on freeze-up jamming. Variable discharge simulations illustrate the effect of temporary flow reductions on freeze-up jamming, as an increase in ice floe travel time leads to a thinner jam profile with less backwater. Simulations under varying air temperatures illustrate the tendency for thinner jam profiles to form during colder conditions. Further simulations assessing the cumulative effect of these two variables show that the efficacy of flow reductions is most effective as an ice floe's travel time decreases. Channel properties, such as bed slopes and meanders, impact ice floe formation and freeze-up jamming through variations in hydraulic conditions.

The proposed treatment of skim ice run was designed with consideration of the cumulative effects of heat loss and discharge on freeze-up jamming. For hydropower operations, enhancing capabilities of the model to simulate freeze-up jams can lead to decision-support tool development for improved ice management. This includes predicting the optimal magnitude and timing of temporary flow reductions, or predicting risk of frazil ice generation due to a delay in frontal progression. Application and adaptation of the proposed treatment for suitable river regions is of interest for further study.

3.11 Chapter Summary

This chapter presents a treatment of skim ice runs during freeze-up jamming in a 2D trapezoidal channel model. Frontal progression rates simulated were comparable with those associated with skim ice run events in the Upper Nelson River presented in Chapter 2. The designed treatment accounts for the effect of flow control on skim ice floe formation and strength, where strength is a function of both travel time and

magnitude of heat loss. This treatment was adapted for modelling of winter-long historical scenarios at the Lake Winnipeg outlet, as presented in Chapter 3.

Chapter 4: Paper 3 – A novel methodology to quantify hydraulic conveyance through an ice-impacted lake-outlet system

4.1 Abstract

River ice can pose considerable challenges to hydropower operations in cold regions. Relative to open-water conditions, the presence of ice in various forms contributes to lower hydraulic efficiency. At the outlet of Lake Winnipeg, maintaining winter conveyance through the channels of the Outlet Lakes Area (OLA) is of paramount importance for downstream energy production on the Nelson River. The complex hydraulic conditions of the OLA are attributed to various factors, including the influence of hydraulic system operation, flow routing through lakes and rivers with non-uniform attributes, and the presence of dynamic ice processes throughout winter. In this study, a methodology was designed to quantify the impacts of ice on the OLA hydraulics using a combination of numerical and statistical tools. This approach includes adaptation and configuration of a two-dimensional river ice model, selection of suitable performance metrics, and derivation of hydraulic datasets for model forcing using historical observations and statistical relationships. Numerical simulations feature treatments for predominant ice processes in the OLA, including freeze-up jamming, thermal growth and decay of a stable ice cover, and under cover transport and deposition of brash ice. The methodology was evaluated using historical winters 1996-1997 to 2020-2021, with most results falling within an acceptable performance range, even in response to varying hydro-meteorological conditions. Instances of error exceeding accepted thresholds were attributed mainly to factors outside of the study, including uncertainty in discharge estimation and the effects of mid-winter forebay operation. Influence of Lake Winnipeg water levels on winter hydraulics was identified as significant, as higher upstream Lake Winnipeg water levels can mitigate ice impacts by providing more hydraulic head for conveyance. As expected, ice restriction severity also varies in accordance with heat fluxes. Targeted areas for improvement of the methodology and future work are discussed, including enhancing the simulation of the thawing ('pre-breakup') period and field verification of flow split quantities during winter. The methodology

presented provides an estimate of ice impacted hydraulics conveyance which serves to benefit hydropower operators, regional water resources studies, and further investigations of river ice impacts related to climate change.

4.2 Introduction

The presence of river ice conditions in cold regions can pose significant challenges to hydropower operations. Risks associated with ice are numerous and site-specific, but can include reduced water supply from reservoirs, decreased net head across generating stations due to backwater effects from downstream, presence of frazil ice blockages, and formation of ice-jam release waves that threaten ice cover stability. These conditions can compromise energy supply and operational efficiency, which is problematic when power demand is typically high during winter. Increasing hydro-meteorological variability associated with climate change presents a compounding challenge, with respect to both energy supply forecasting and hydropower system planning.

Approaches to assess and predict river ice conditions generally rely on site-specific observations and empirical relationships. Numerous river ice models have been developed to facilitate these approaches, including RICEN (Shen et al., 1995), DYNARICE (Shen, 2010), River 1D (Blackburn and She, 2019; She et al., 2012), CRISSP2D (Shen, 2002), Mike-ICE (Thériault, 2011), ICESIM (Carson et al., 2003) and RIVICE (Lindenschmidt, 2017). Applications of these models on regulated rivers include evaluation of mechanical breakup on the Peace River in Canada (Ye and She, 2021), assessing effects of Orkla River hydropower operations on river ice processes in Norway (Timalsina et al., 2016), and quantifying potential risks of ice jams on the Odra River in Poland (Kolerski, 2021).

The Nelson River (455 km long) features the largest hydropower system in Manitoba, Canada, accounting for 75% of power generation in the province (Manitoba Hydro, 2014). Energy generation at six power stations during winter is challenged by local ice phenomena, including anchor ice and aufeis (Malenchak, 2011; Peters, 2021), as well as hanging dams (Hopper and Raban, 1980) and ice cover consolidation (Groeneveld et al., 2017). The Nelson River is primarily supplied by outflow from Lake Winnipeg, the majority of which is routed through a

series of rivers and lakes termed the 'Outlet Lakes Area' (OLA). River ice management strategies in the OLA include the year-round deployment of an ice boom (Abdelnour et al., 2012), permanent construction of the Ominawin Bypass Channel and other channel improvements (Manitoba Hydro, 2014), and implementation of a freeze-up flow control program (Tuthill, 1999; Zbigniewicz, 1997). Despite this multi-faceted approach, the inevitable impact of ice formation is an increase in ice-induced head loss through this approximately 100 km reach and reduced conveyance. These ice impacts are of significance for both hydropower operations and water resources investigations in the region (Beihagdar, 2019; Kim, 2020).

Rating curves describing open-water hydraulics in the OLA are fairly well-established, while ice-affected relationships are much less defined. Past studies to characterize ice-resistance in the OLA employed functions derived from meteorological variables (Wilson et al., 2020) and percentile-based statistics derived from historical hydrometric data (Beihagdar, 2019). Despite progress made by these studies, considerable uncertainty in prediction capabilities remains due to the complexity of ice processes, and the non-linear and unsteady hydraulic characteristics of the reach. This gap warrants continued improvement of ice condition prediction capabilities using more advanced hydraulic techniques.

The overall objective of this paper is to present a coupled numerical and statistical methodology to quantify winter conveyance through the OLA. This methodology includes derivation and application of several hydraulic relationships that quantify ice-induced head losses under a range of conditions. Adaptation and application of a two-dimensional numerical model to simulate ice processes in the OLA is also described. The coupled methodology is applied over a suite of historical years, with results compared to acceptable error thresholds. Lastly, a brief climate change scenario is presented to illustrate potential future applications.

4.3 Background

4.3.1 Ice Resistance and Channel Hydraulics

The presence of an ice cover increases the wetted perimeter of a river, thereby reducing the channel's discharge capacity. This discharge capacity is also affected

by ice cover roughness, which is a variable quantity both spatially and temporally. By applying an analytical equation describing flow conveyance in a channel (e.g., Manning's equation), total channel resistance can be described using a composite roughness value (n_c). Composite roughness is a function of ice roughness (n_i), bed roughness (n_b), as well as various channel and flow properties (Chow, 1959).

Commonly applied methods (e.g., Sabaneev equation; as described by Ashton (1986)) to calculate composite roughness are based on the assumption that flow in an ice-covered cross-section is divided into two regions, which are primarily influenced by either bed or ice friction. Such methods also assume uniform flow conditions in both of these regions, despite the unsteady and non-uniform flow regime characteristic of ice-covered rivers (Ghareh Aghaji Zare et al., 2016). A common simplification in ice-affected hydraulics is that of 'quasi-uniformity', which is defined by a lack of trend in hydraulic parameters (despite fluctuations) over a sufficiently long channel reach (Beltaos, 2011). Under the assumption of quasi-uniform flow, n_c and n_i can be back-calculated using hydrometric data, as well as known (or assumed) channel properties and ice conditions (Beltaos, 2011).

In an unregulated river scenario with natural controls, the presence of an ice-cover over winter will typically result in upstream backwater to accommodate the ice-induced head loss. Conversely, in a regulated scenario with a downstream control structure, ice-induced head loss can be compensated for by increasing the reach water surface slope via lowering of the downstream water level. Once downstream water levels reach a steady minimum operating level, a decrease in channel discharge from the upstream area will occur if ice resistance increases over time. Increases in ice resistance can occur due to under cover deposition of ice floes that form in upstream open-water areas, over winter ice cover thickening, and other mechanisms (e.g., ice cover consolidation). A study of ice resistance on the St. Claire River, which is controlled by both upstream and downstream reservoirs, observed a 0.6 m drop and 65% reduction in downstream water level and channel discharge, respectively, due to ice jamming (Derecki and Quinn, 1987).

4.3.2 Study Area, Hydraulic Variables and Spatial Scales

Lake Winnipeg (Fig. 4.1a) receives inflows from a drainage area of almost 1,000,000 km^2 (Province of Manitoba, 2021a), and functions as the main reservoir for power generation on the Nelson River.

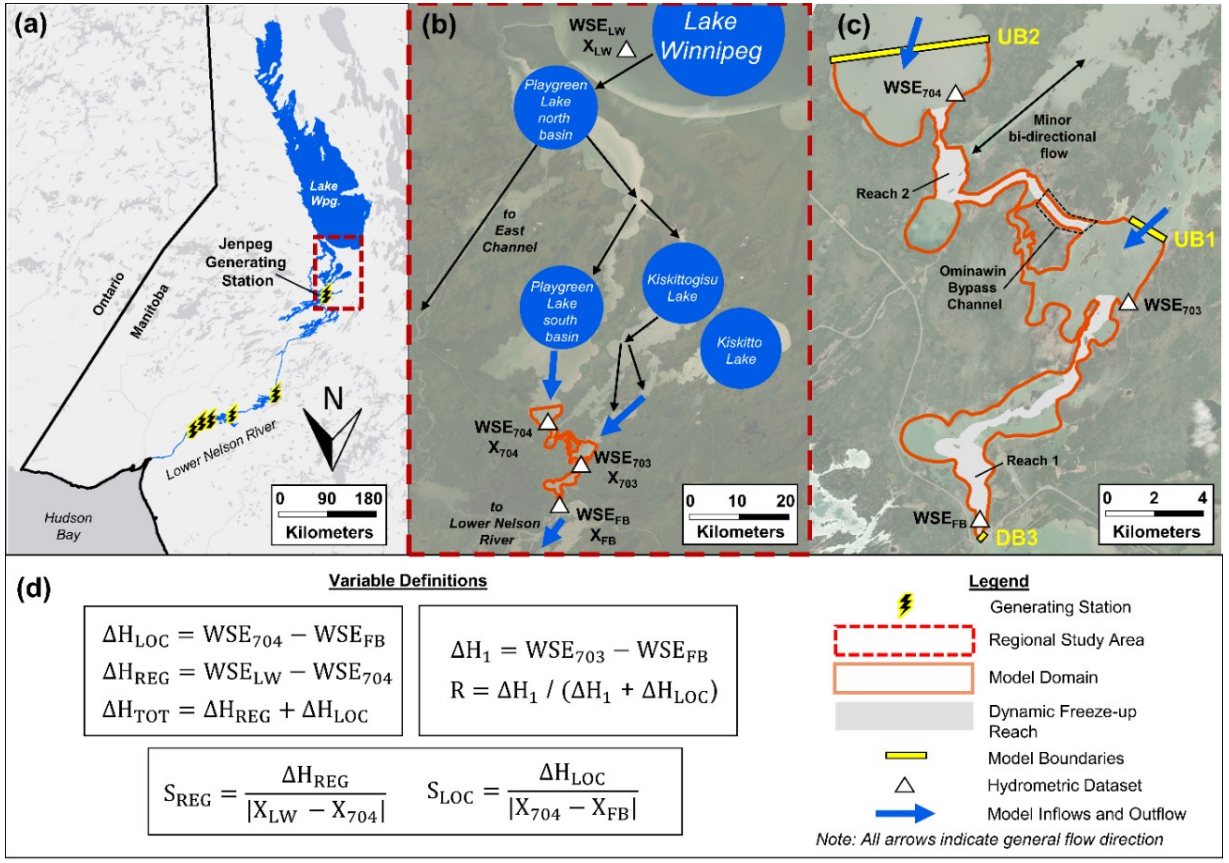

Fig. 4.1 - (a) Lake Winnipeg and Nelson River network; (b) regional study area; (c) local study area and model domain, and; (d) hydraulic variable definitions and map items legend. [Base map in (a) from Esri, HERE, Garmin, © OpenStreetMap contributors, and the GIS User Community; vector data in (a) from Government of Manitoba 2001, Government of Canada 2017; base map in (b) from from ArcGIS World Imagery, Surface Layer Credits: Source: Esri, DigitalGlobe, GeoEye, Earthstar Geographics, CNES/Airbus DS, USDA, AeroGRID, IGN, and the GIS User Community; image in (c) courtesy of the USGS, Landsat.]

The majority of outflow (85%) from Lake Winnipeg is routed through the OLA (Fig. 4.1b), while the remaining discharge naturally flows through the East Channel of the Nelson River. At the OLA outlet, outflow from Jenpeg is routed to the Lower Nelson River, which has a general flow direction of northeast towards Hudson Bay.

During open-water conditions, discharge through the OLA is a function of two main hydraulic controls - Lake Winnipeg water surface elevation (WSE_{LW}; upstream control) and the Jenpeg Generating Station (Jenpeg) forebay elevation (WSE_{FB}; downstream control). Fig. 4.1c outlines a highly-monitored and studied area near Jenpeg, where dynamic ice processes significantly impact OLA hydraulics and is the focus area of the present study.

Relevant hydraulic variables identified for this study (Fig. 4.1d) include *hydraulic head* (ΔH; difference in water surface elevation), *water surface slope* (S; stream-wise water surface gradient between two locations), and *local energy ratio* (R; discussed in Section 4.4.2.2). Select variables are further categorized by three spatial scales (Fig. 4.1b): (a) *total* (*TOT*; X_{FB} to X_{LW}); (b) *regional* (*REG*; X_{704} to X_{LW}); and (c) *local* (*LOC*; X_{FB} to X_{704}).

4.3.3 Stages of Winter Conveyance

The configuration of hydraulic controls in the study area results in four distinct conveyance stages during winter operations in OLA (Fig. 4.2), including *onset of freeze-up*, *ice stabilization*, *forebay drawdown,* and *discharge decline.*

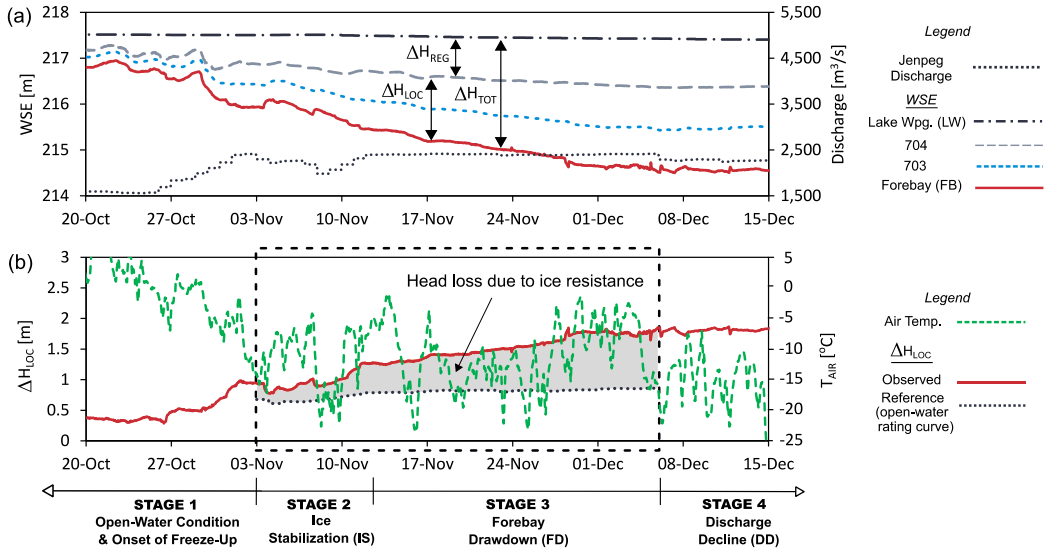

Fig. 4.2 - (a) Observed hydrometric data and illustration of hydraulic variables; and, (b) four stages of winter flow conveyance (shaded grey area illustrates ice-induced head losses).

For the purposes of this study, the winter period of interest spans from immediately prior to freeze-up to the onset of thawing conditions in spring. Note that throughout winter the large storage capacity of Lake Winnipeg ensures that WSE_{LW} experiences relatively minor fluctuations. At the *onset of freeze-up*, cumulative degree-days of freezing (CDDF) increase from zero, resulting in minor ice formation in shallow back bays and along shorelines. At this stage, OLA discharge is governed almost exclusively by ΔH_{TOT}, as ice resistance is minimal. Jenpeg discharge is incrementally increased in anticipation of flow control during the *ice stabilization* stage, which commences at the onset of dynamic ice conditions that occur at approximately 60 CDDF. The ice stabilization stage is characterized by temporary flow reductions (approximately 140 $ft^3\ s^{-1}$ intervals during the initial ice formation period) to facilitate formation of a smooth and stable ice cover upstream of Jenpeg. A primary focus area of ice stabilization is to achieve stable ice cover formation over two faster-moving reaches upstream of Jenpeg (see *Dynamic Freeze-Up Reach* on Fig. 4.1), while also considering the impact of changing discharge conditions on other areas upstream and downstream of Jenpeg.

Following ice stabilization, Jenpeg discharge is incrementally increased to a pre-established flow target (based on observed hydraulic conditions and energy system requirements), leading to the *forebay drawdown* stage. In a scenario involving no ice-induced head losses, WSE_{FB} and ΔH_{TOT} would remain constant under steady discharge conditions. In contrast, the presence of an ice cover requires the continual drawdown of WSE_{FB} to compensate for the increasing ice-induced head losses. An illustration of this ice resistance is shown in shaded grey on Fig. 4.2. In effect, the primary contribution of the methodology presented in this paper is to simulate this ice resistance across Stages 2 through 4. After the forebay is drawn to its minimum operating level, WSE_{LW} continues to govern discharge through the OLA. As ice conditions evolve, discharge through the OLA slowly declines until the onset of warmer temperatures in spring that will first reduce, and then eliminate ice-effects altogether.

4.3.4 Hydro-Meteorological Observational Data

This study applies hydro-meteorological data from within the OLA, supplemented by data from Norway House (ECCC ID: 5062040) and Thompson (ECCC ID: 5062921) airports. While Jenpeg station data (WSE_{FB} and Q_{OBS}) are available from 1977 to present, local hydrometric stations (05UB704 and 05UB703) were not installed until 1996. As such, 1996 to 2021 was selected as the study period of interest. A complete summary of hydro-meteorological data availability is summarized in Table 4.1.

Table 4.1 - Hydro-meteorological data availability for the study.

Time Period	Monitoring Location					
	Lake Winnipeg	Norway House	Thompson	05UB704	05UB703	Jenpeg GS
1977-1996	○	⊙	□	N/A	N/A	○●
1996-1998	○	⊙	□	○	○	○●
1998-2008[1]	○	●⊙	□	○	○	○●
2008-present[2]	○	●⊙	□	○⊗	○⊗	○●

Notes:
○Water Surface Elevation (Manitoba Hydro)
●Discharge (Manitoba Hydro)
⊗Water Temperature (Manitoba Hydro)
⊙Air Temperature, Dew Point Temperature, Wind Speed and Direction, Precipitation (Environment Canada, 2021)
●Cloud Cover (Plymouth State Weather Center, 2019)
□Snow-on-Ground (Environment Canada, 2021)
[1]Cloud cover prior to 1998 was estimated using qualitative weather descriptions.
[2]Additional detailed site-specific monitoring data is available, as outlined by Lees et al. (2021b) and Appendix A.

4.3.5 Two-Dimensional River Ice Model

To accurately account for ice processes in the OLA, this study includes adaptation of an existing two-dimensional river ice model previously developed using CRISSP2D (Lees et al., 2019; Shen et al., 1995a). CRISSP2D is a suitable model for the region, considering its comprehensive simulation capabilities of thermal and dynamic ice processes. The model uses a two-dimensional form of the depth-integrated free-surface shallow water flow equations to simulate hydraulics. This formulation considers discharge as two layers: the upper layer (ice cover and surface ice floes) and lower layer (water layer). In addition to shear stress at the channel bed, shear

stress at the ice cover is calculated as a function of water and ice velocities, water density and a drag coefficient (C_w; Eq 4-1):

$$C_w = \frac{n_i^2 g}{(\alpha_i H')^{\frac{1}{3}}} \quad \text{Eq 4-1}$$

where g is the gravitational coefficient [m s^{-2}], H' is the water depth under the ice cover [m], and α_i is the fraction of total depth affected by ice friction (Shen et al., 1990). Additional details of the formulation of hydrodynamic equations in the model are provided by Shen et al. (1990) and Lal and Shen (1989).

The OLA model domain encompasses 56 km^2 of water surface area (Fig. 4.1c). As a result, numerical model simulations only provide quantities for local hydraulic variables (ΔH_{LOC} and S_{LOC}). Ice resistance in the regional study area is considered secondary in importance relative to the magnitude of ice resistance in the local study area based on analysis of historical data. As such, the regional study area was strategically excluded from the model domain, as inclusion would require expansion of the model domain by 30 times. In addition to significant increases to model computation time, domain expansion would require bathymetric and hydrometric datasets not currently available. A coupled numerical and statistical approach is instead employed to provide quantities of regional hydraulic variables (ΔH_{REG} and S_{REG}).

4.4 Methodology

The following sections describe the coupled statistical and numerical approach to quantify the relevant hydraulic variables for the study area.

4.4.1 Regional Ice Resistance

Ice resistance across the regional study area was estimated based on hydrometric records. A regression of observed S_{LOC} and S_{REG} during winters 1996-1997 to 2018-2019 yielded a strong logarithmic correlation (at 10,000 ft^3 s^{-1} intervals; Fig. 4.3).

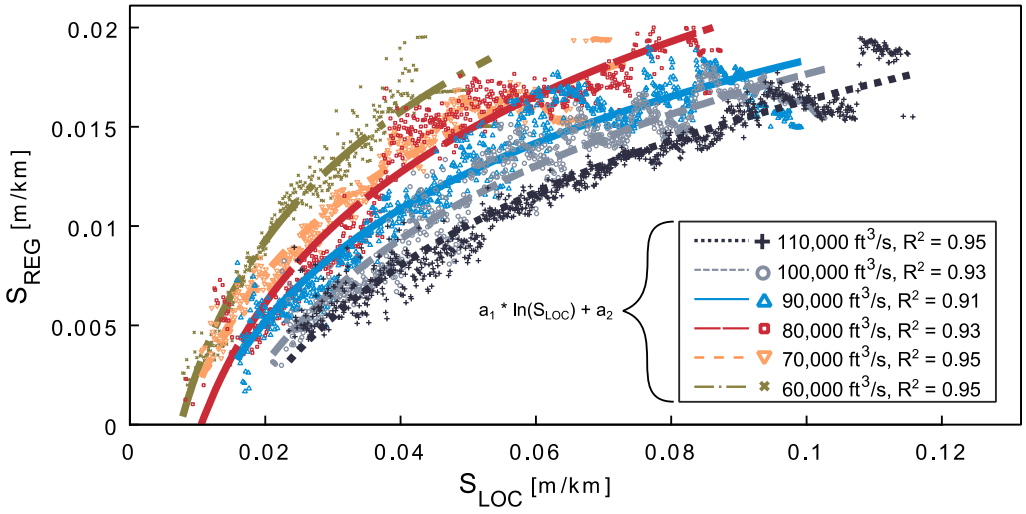

Fig. 4.3 - Estimation of regional water surface slope (S_{REG}) as a logarithmic function of local water surface slope (S_{LOC}) based on observed data.

The limits of each function on Fig. 4.3 are plotted according to ranges of observed datasets. The relative magnitudes of S_{LOC} and S_{REG} suggest higher ice impacts in the local study area, thus supporting the exclusion of the regional study area from the numerical model. The asymptotic trend of ordinate values with increasing S_{LOC} is expected, as the large upstream lakes (i.e., Playgreen Lake and Kiskittogisu Lake) of the regional study area undergo only small stage changes due to ice impacts.

4.4.2 Numerical Model Configuration

Quantities of local hydraulic variables (ΔH_{LOC} and S_{LOC}) are required to estimate regional hydraulic variables (see Section 4.4.1), which together yield quantities that describe the hydraulics across the entire OLA (ΔH_{TOT} and S_{TOT}). The following sections describe the configuration of the numerical model, which was applied to quantify local hydraulic variables.

4.4.2.1 Summary of Model Set-Up

Due to the complex hydraulics of the OLA and the limited model domain extents, considerable attention was given to the assignment of hydraulic boundary conditions. Forcing datasets assigned at upstream (UB1 and UB2) and downstream

(DB3) model boundaries, along with model outputs of interest, are summarized in Table 4.2.

Table 4.2 - Summary of hydraulic boundary conditions and model outputs at each stage. Bolded entries highlight interconnected quantities between stages.

Stage		Forcing Dataset			Simulation Output			Model Output of Interest
		UB1	UB2	DB3	UB1	UB2	DB3	
2	Ice Stabilization	WSE_{CALC1}	WSE_{CALC2}	$+Q_{OBS}$	$\mathbf{-X_Q Q_{OBS}}$	$\mathbf{-Y_Q Q_{OBS}}$	$\mathbf{WSE_{SIM3}}$	$\Delta H_{LOC(SIM)}$
3	Forebay Drawdown							
4	Discharge Decline	$\mathbf{-X_Q Q_{OBS}}$	$\mathbf{-Y_Q Q_{OBS}}$	$\mathbf{WSE_{CALC3}}$[1]	WSE_{SIM1}	WSE_{SIM2}	$+Q_{OBS}$	Q_{SIM}[1]

Notes:
[1]See Section 4.4.2.3 for derivation of WSE_{CALC3} and Q_{SIM}.
$+Q$ / $-Q$ = outflow from model / inflow to model
X_Q, Y_Q = simulated % of total Q_{OBS}, where $X_Q + Y_Q = 100\%$
Subscript definitions are as follows:
CALC - calculated using statistical relationships derived for this study
SIM - simulated by the numerical model
OBS - assigned using historical monitoring datasets

During Stages 2 and 3, simulated and observed hydraulic head were calculated as outlined in Eq 4-2 and Eq 4-3, respectively:

$$\Delta H_{LOC(SIM)} = WSE_{CALC2} - WSE_{SIM3} \quad \text{Eq 4-2}$$

$$\Delta H_{LOC(OBS)} = WSE_{704} - WSE_{FB} \quad \text{Eq 4-3}$$

4.4.2.2 Stage 2 and 3 Boundary Conditions

Assigning forcing data at boundaries UB1 and UB2 for Stage 2 and 3 simulations involved a multi-step process. While the process is complex, this effort was necessary to accommodate the limited model domain. A graphical summary of the datasets, hydraulic relationships, and procedural steps to derive UB1 and UB2 forcing data is provided on Fig. 4.4, which is referenced throughout this section.

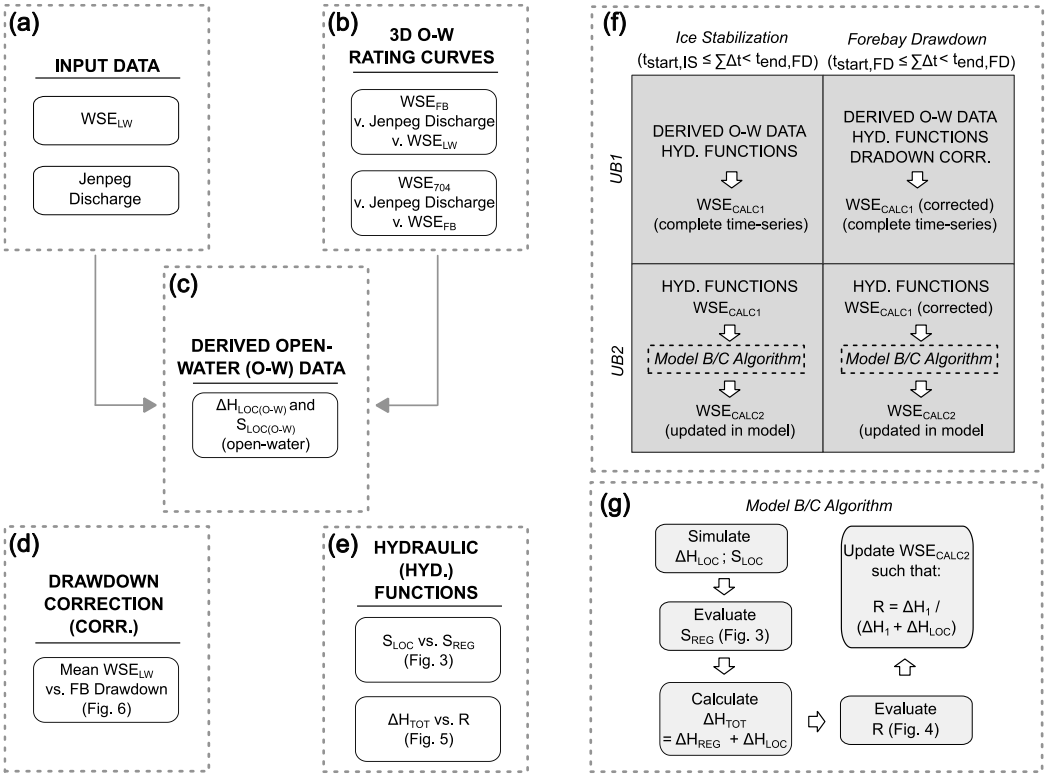

Fig. 4.4 - Flow chart illustrating: (a-e) datasets and hydraulic relationships, (f) procedure followed to calculate WSE_{CALC1} and WSE_{CALC2} at Stage 2 and 3, (g) algorithm applied to account for dynamic upstream flow split.

During Stage 2 and 3, Jenpeg outflow (Q_{OBS}) was assigned at the downstream boundary (DB3). However, at upstream boundaries UB1 and UB2, nearby observed WSE data at stations 05UB703 (WSE_{703}) and 05UB704 (WSE_{704}) were considered unsuitable for model forcing. These observed datasets inherently reflect ice resistance, which would result in over-simulation of ΔH_{LOC} by the numerical model. Synthetic WSE datasets were instead applied for model forcing at UB1 and UB2.

At UB1, a complete synthetic dataset (WSE_{CALC1}) was derived with two goals: (1) reflect an 'ice-free' condition, thus allowing the numerical model to properly simulate ice resistance, instead of imposing ice resistance through forcing datasets; and (2) account for the influence of the upstream hydraulic control (i.e., Lake Winnipeg), which is outside the numerical model domain, on the hydraulic efficiency in the OLA. At UB2, an algorithm was programmed into the model to calculate and update WSE_{CALC2} during simulations.

To reflect an ice-free condition, two sets of three-dimensional open-water (o-w) rating curves were employed (Fig. 4.4b). Using input datasets of WSE_{LW} and Q (Fig. 4.4a), rating curves yielded o-w values for: (*Set 1*) $WSE_{FB,}$ and subsequently (*Set 2*) WSE_{704}. *Set 1* rating curves were provided by Manitoba Hydro, while *Set 2* curves were derived using observed hydrometric data from 1996 to 2018. These curves yielded a local o-w hydraulic dataset for each historical winter (Fig. 4.4b; $\Delta H_{LOC(o\text{-}w)}$ and $S_{LOC(o\text{-}w)}$).

Additional hydraulic functions (Fig. 4.4e) were required to account for the effect of Lake Winnipeg on the hydraulic efficiency of the OLA. In addition to the curves on Fig. 4.3 that provide ΔH_{TOT}, the curves shown on Fig. 4.5 were developed to address the flow split (both open-water and ice-affected) at the upstream model boundaries.

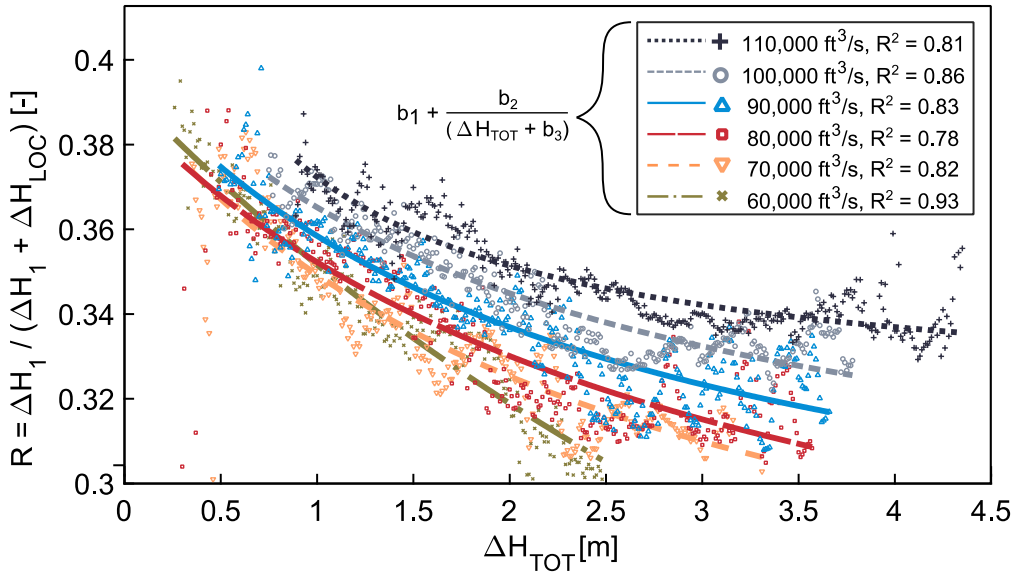

Fig. 4.5 - Local energy ratio (R) estimated as a hyperbolic function of total head (ΔH_{TOT}).

Neglecting minor continuity error that occurs during simulations, the proportion of total discharge received at these two boundaries (X_Q and Y_Q; Table 4.2), where the summation of terms equates to 100% of Q_{OBS}. Owing to the hydraulic efficiency of a constructed bypass channel (Ominawin Bypass Channel; Fig. 4.1c) that works as part of LWR to increase outflow from Lake Winnipeg up to 50% above natural levels (Manitoba Hydro, 2014), open-water ADCP discharge measurements indicate

a positive linear relationship between Q_{OBS} and discharge proportion through UB2 (Y_Q).

Unfortunately, an ice-affected relationship between Q_{OBS} and Y_Q cannot be calculated, as suitable winter ADCP discharge measurements are unavailable. Alternatively, a surrogate parameter *local energy ratio* (R; Fig. 4.5) was employed to simulate quantities of X_Q and Y_Q. R was selected to be the ratio of ΔH_1 to the sum of hydraulic heads across model boundaries, as this combination of variables yielded a strong hyperbolic correlation at 10,000 $ft^3\ s^{-1}$ intervals when plotted against ΔH_{TOT} (Fig. 4.3). While a direct conversion between R and Y_Q is not easily attained, a decrease in R generally corresponds with a decrease in Y_Q. Based on the tangential slopes of each curve, the effect of ΔH_{TOT} on Y_Q is most prominent at lower discharges and diminishes with increasing values of ΔH_{TOT} as the forebay is drawn down to a minimum operating level. Lastly, while not explicitly represented in these curves, Y_Q is also a function of ice restrictions from Lake Winnipeg to Jenpeg.

As summarized on Fig. 4.4f, a complete synthetic time-series for WSE_{CALC1} was developed prior to simulations by combining derived o-w data (Fig. 4.4c) and hydraulic functions (Fig. 4.4e). Conversely, WSE_{CALC2} values were calculated and updated hourly using WSE_{CALC1}, hydraulic functions (Fig. 4.4e), and a *Model B/C Algorithm* coded directly into the numerical model (Fig. 4.4g). This approach updates WSE_{CALC2} by accounting for the cumulative effect of Q_{OBS}, WSE_{LW}, and ice resistance, in order to accurately model dynamic inflow behaviour at the upstream boundaries.

Further summarized on Fig. 4.4f, a correction to WSE_{CALC1} was required during Stage 3 simulations. A *forebay drawdown rate* (DD_R [m day^{-1}]) factor was developed by analyzing the hydrometric records of historical winters (Fig. 4.6).

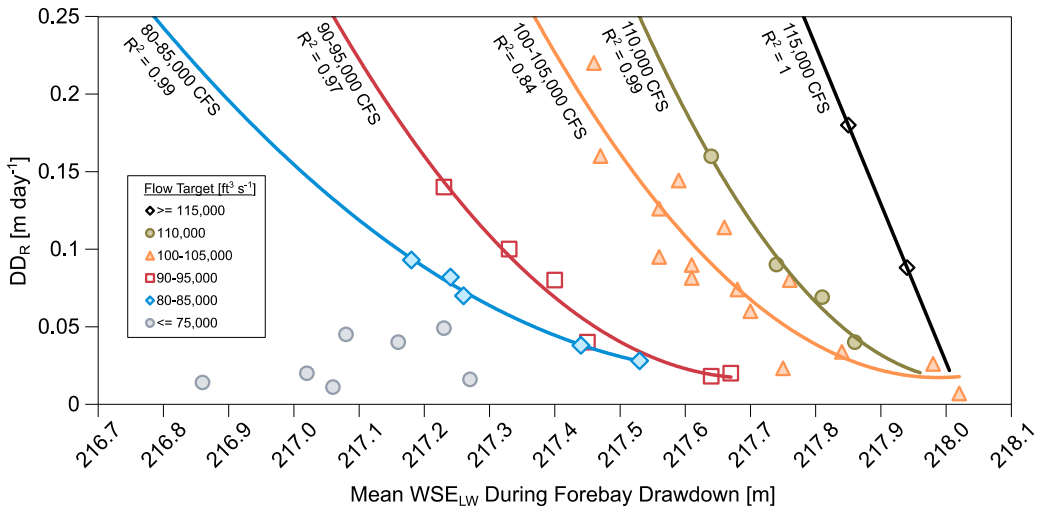

Fig. 4.6 - Effect of WSE_{LW} and discharge on forebay drawdown rate (DD_R) during Stage 3 (select years from 1984 to 2018). Second-order polynomial fit shown for all discharge ranges, except for 115,000 $ft^3\ s^{-1}$ (first-order polynomial fit due to data availability).

Trends illustrated by these curves are consistent with Nelson River hydraulics calculations completed prior to Jenpeg construction (Phelps and Coley, 1973). During moderate to high discharges ($Q \geq 80{,}000\ ft^3\ s^{-1}$), a distinct non-linear relationship is apparent. At higher WSE_{LW}, a decreasing tangential slope indicates that increased hydraulic head corresponds with improved hydraulic efficiency of the OLA, thus resulting in a lower DD_R to maintain discharge. Noteworthy also is that despite differing ice conditions between years, WSE_{LW} is clearly a dominant variable in predicting DD_R.

DD_R was calculated for each simulation using Q and WSE_{LW} and applied to nudge WSE_{CALC1} downward, resulting in a corresponding drop in simulated forebay level (WSE_{SIM3}). Without this correction, hydraulic head during Stage 3 would be greatly under-estimated, which results in an overestimate of winter discharge.

4.4.2.3 Stage 4 Boundary Conditions

Once the forebay is fully drawn down, Jenpeg station operators can no longer compensate for ice-induced head loss to encourage outflow from Lake Winnipeg. From this point onwards (i.e., Stage 4), WSE_{FB} remains fixed while WSE_{LW} may

fluctuate depending on conditions in the watershed. The magnitude of discharge decline during Stage 4 reflects both WSE_{LW} and the severity of ice restrictions in the OLA. Accordingly, the model output of interest during Stage 4 becomes Q_{SIM} instead of ΔH_{LOC}. Analysis of hydro-meteorological datasets during Stage 4 of each historical year illustrates the effect of ice and WSE_{LW} on flow decline. As shown on Fig. 4.7, a strong non-linear correlation is visible between magnitude of discharge decline (ΔQ), and both total change in WSE_{LW} and mean air temperature (taken as a surrogate for average heat loss).

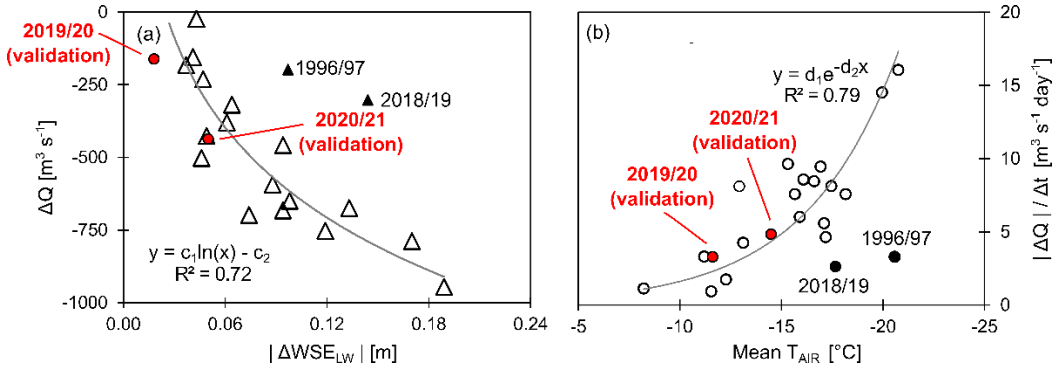

Fig. 4.7 - Effect of (a) change in WSE_{LW} and (b) average air temperature on discharge decline during Stage 4. Two years (1996/97 and 2018/19) are identified as outliers based on rising lake levels over these winters. Validation years (2019/20 and 2020/2020) are also included.

Greater average heat loss results in more ice production, leading to greater flow restriction in the OLA. Further, a decline in WSE_{LW} reduces hydraulic head across the OLA, which also results in lower discharge from Lake Winnipeg. Winters 1996-1997 and 2018-2019 were identified as outliers on Fig. 4.7, as an atypical increase in WSE_{LW} over these winters resulted in lower discharge decline than expected. It is notable that winter 1996-1997 was antecedent to one of the largest Manitoba floods on record, while rising water levels in winter 2018-2019 were attributed to a combination of East Channel ice effects and hydrologic conditions in the Nelson River watershed.

Boundary conditions during Stage 4 simulations were established with two goals: (1) reflect the impact of hydro-meteorological conditions on discharge decline, and (2) select a surrogate parameter suitable for discharge estimation. The model was forced with steady inflows ($-X_Q Q_{OBS}$ and $-Y_Q Q_{OBS}$) at UB1 and UB2, respectively, according to the model's hydraulic state at the end of Stage 3. As ice resistance in the model increased over Stage 4, backwater was simulated at boundaries UB1 and UB2 to maintain conveyance of the steady inflows. A first-order polynomial slope (e_1) was derived using hydrometric data to convert cumulative backwater at UB1 and UB2 to a decline in discharge (Eq 4-4):

$$\Delta Q_{SIM} = e_1[\sum_{i=2}^{n}[(WSE_{SIM1_i} - WSE_{SIM1_{i-1}}) + (WSE_{SIM2_i} - WSE_{SIM2_{i-1}}) \quad \text{Eq 4-4}$$

where n is the total number of simulated model hours. Coefficient e_1 [$m^3\ s^{1-}\ mm^{-1}$] yields approximately 1 $m^3\ s^{-1}$ decline in discharge for every 1 mm rise in backwater at upstream boundaries. At downstream boundary DB3, WSE_{SIM3} was assigned and adjusted based on changes in WSE_{LW}, where a decrease in WSE_{LW} is reflected by a proportional increase in WSE_{CALC3} (Eq 4-5).

$$WSE_{CALC3_i} = WSE_{SIM3} + (WSE_{LW_{i-1}} - WSE_{LW_1}) \quad \text{Eq 4-5}$$

While this configuration of boundary conditions does not mirror the natural system, it is a means to achieve an estimation of discharge decline given the constraints of the model. Finally, Stage 4 simulations were considered complete prior to the onset of breakup, as the methodology is only designed to assess freeze-up and mid-winter ice processes.

4.4.3 Simulated Ice Processes

Ice resistance in the OLA is the cumulative result of numerous freeze-up and mid-winter processes. The following sections describe treatment of these processes in the numerical model at each stage.

4.4.3.1 Stage 2: Ice Stabilization

The ice stabilization stage is characterized by short-term discharge changes that facilitate freeze-up jamming. The most important model treatments during this stage are those that govern ice jam formation and frontal progression. Stage 2 numerical simulations included dynamic ice jam calculations, where a Lagrangian discrete-parcel method (DPM) is employed in CRISSP2D (Shen et al., 1993). A recently developed treatment of skim ice in the model (Lees et al., 2021c) was implemented during simulations to account for the role of skim ice runs during frontal progression. Essentially, this treatment quantifies the strength and stability of large skim ice floes formed during cold weather events, which contributes to rapid frontal progression and thin ice cover formation.

Three *rapid zones* (Fig. 4.8) were generalized and delineated based on the extents of winter open-water areas observed in historical imagery.

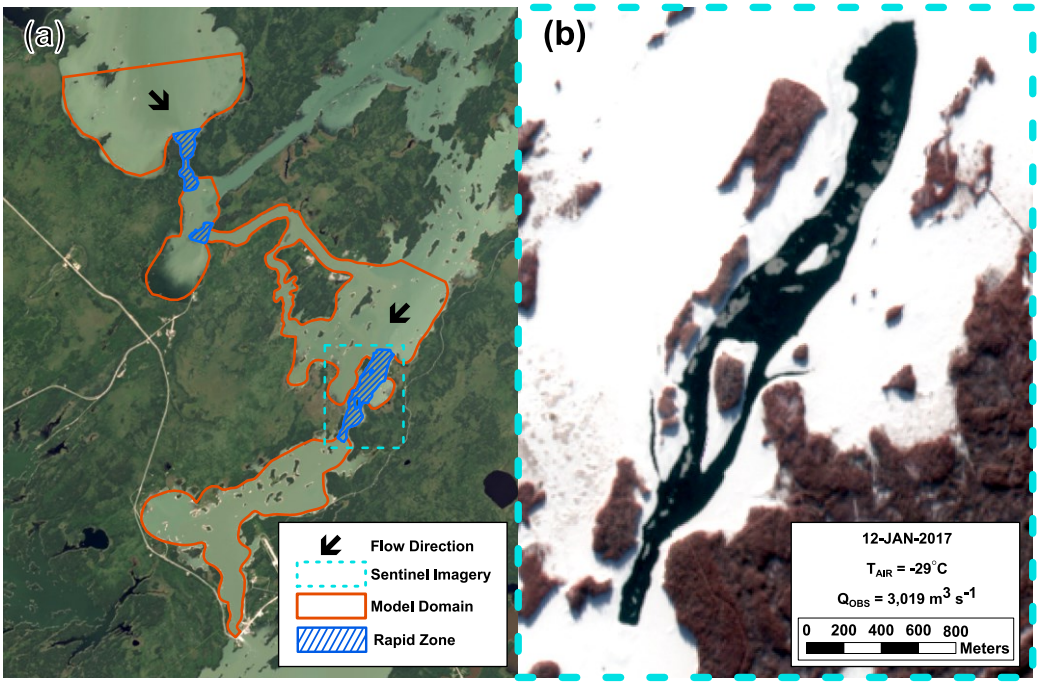

Fig. 4.8 - Designated rapid zones in model domain, and (b) visible skim ice run in the largest open-water area (Manitou Rapids). Note the large (hundreds of metres wide) skim ice floes in the open water section. [Base map in (a) from from ArcGIS World Imagery, Surface Layer Credits: Source: Esri, DigitalGlobe, GeoEye, Earthstar Geographics, CNES/Airbus DS, USDA, AeroGRID, IGN, and the GIS User Community; Sentinel-2 (ESA) image courtesy of the U.S. Geological Survey]

4.4.3.2 Stage 3 and 4: Forebay Drawdown and Discharge Decline

Following stable ice cover formation in Stage 2, dynamic ice jam calculations were disabled in the model prior to Stage 3 and 4 simulations. This simplification reduced computation time but inhibited further consolidation and mechanical thickening of the ice cover. This trade-off was considered suitable for the OLA, as mid-winter consolidation and recession of the ice cover is not a common occurrence due to the hydraulic characteristics of the reach (i.e., very mild bed slope and discharge regulation).

Following stable ice cover formation, ice resistance in the OLA evolves primarily because of thermal growth of the ice cover, and under cover transport and deposition of ice. Increase in ice cover thickness (h_i) due to thermal growth was simulated using Eq 4-6:

$$\frac{dh_i}{dt} = \frac{H_{IA}(T_m - T_{AIR}) - \emptyset_R + \beta}{\rho_i \lambda H_{IA}\left(\frac{h_i}{k_i} + \frac{h_s}{k_s} + \frac{1}{H_{IA}}\right)} \quad \text{Eq 4-6}$$

$$\text{if } [H_{IA}(T_m - T_{AIR}) - \emptyset_R + \beta] > 0 \frac{W}{m^2}$$

where T_{AIR} and T_m are the temperatures of air and the temperature at the ice/water interface [℃], respectively; H_{IA} is the ice-air heat transfer coefficient [W m^{-2} ℃$^{-1}$]; ρ_i is the density of ice [kg m^{-3}]; λ is the latent heat of fusion of ice [J kg^{-1}]; $\emptyset_R$ is the net solar radiation [W m^{-2}]; and β is an empirical heat flux coefficient [W m^{-2}]. The thermal resistances of snow ($h_s\ k_s^{-1}$) and ice ($h_i\ k_i^{-1}$) are included.

Model updates were required to include a snow cover during Stage 3 and 4 simulations, as this feature is typically excluded from short-term simulations in CRISSP2D. Snow-on-ground measurements from Thompson Airport (approximately 140 km from Jenpeg) were applied, after adjustments were made to account for the timing of freeze-up. Considering that strength of the ice cover limits the accumulation of snow on a reservoir (Ashton, 2011; Singh and Comfort, 1998), snow depths (h_s) were also adjusted to not exceed maximum permitted snow depth ($h_{s_{max}}$) calculated during simulations to more accurately reflect snow depth on the river (Eq 4-7).

$$h_{s_{max}} = \left(\frac{\rho_w}{\rho_s}\right)\left(1 - \frac{\rho_i}{\rho_w}\right) h_i \quad \text{Eq 4-7}$$

where h_i is simulated ice thickness, while ρ_w and ρ_s densities of water and snow [kg m^{-3}], respectively. In the case that the snow-on-ground record exceeded $h_{s_{max}}$ for a particular day, h_s was set to $h_{s_{max}}$. While this approach simplifies the complex evolution of snow on an ice cover, it does account for the role of ice thickness in limiting snow accumulation. As treatment of snow was not the primary focus of this study, more complex details such as re-distribution of snow by wind, varying snow

densities and snow ice layer formation were not included. The default CRISSP2D formulations for decay at the ice cover bottom (Eq 4-8) and ice cover surface (Eq 4-9) were applied, which are similar to Eq 4-6, although the thermal resistance of both ice and snow are excluded.

$$\frac{dh_i}{dt} = \frac{H_{WI}(T_m - T_W)}{\rho_i \lambda} \quad \text{if } T_w > T_m \qquad \text{Eq 4-8}$$

$$\frac{dh_i}{dt} = \frac{H_{IA}(T_{AIR} - T_m) - \emptyset_R + \beta}{\rho_i \lambda} \quad \text{if } [H_{IA}(T_{AIR} - T_m) - \emptyset_R + \beta] > 0 \frac{W}{m^2} \qquad \text{Eq 4-9}$$

where T_W is water temperature [°C], and H_{WI} is the water-ice heat transfer coefficient [W m^{-2} °C^{-1}].

In addition to thermal growth and decay, treatment of skim ice runs generated in rapid zones was included. An example of a mid-winter skim ice run event is observed in satellite imagery of Manitou Rapids on Fig. 4.8. These large (in the order of ten to hundreds of metres wide) skim ice floes form in response to supercooled conditions near the water surface, despite the limited streamwise distance available for development of the zero-degree isotherm. As these ice floes approach the leading edge of the downstream stable ice cover, they become crushed and eventually flow-entrained. Entrained ice particles are subject to erosion and depositional processes at the underside of the ice cover, in accordance with the ice supply and carrying capacity of the river (Shen and Wang, 1995).

Under cover ice processes were simulated by adapting an existing treatment in CRISSP2D (Shen et al., 1995). This treatment applies an empirical means of assessing potential for erosion and deposition of the modelled ice supply, as informed by laboratory experiments (Eq 4-10 from Shen et al., 1995a):

$$\vec{q}_{uc} = \begin{cases} 5.487(\theta - \theta_c)^{1.5} d_n \omega & if\ \theta > \theta_c \\ 0 & if\ \theta \leq \theta_c \end{cases} \qquad \text{Eq 4-10}$$

where d_n is the nominal diameter of the ice particles [m], ω is the buoyant velocity [m s^{-1}], and θ_c and θ are the dimensionless critical flow strength (adapted from van Rijn (1984)) and dimensionless local flow strength, respectively. If $\theta > \theta_c$, erosion of the under cover ice deposits will occur according to the ice discharge capacity ($\vec{q}_{uc}$) of the flow.

Considering the under cover ice particles in the OLA form from competent skim ice floes, either *fragmented ice* or *brash ice* are suitable descriptors for these particles (USACE, 2006). Direct observations of these particles are not available, although surface observations of brash ice near the Jenpeg forebay are likely analogous (Fig. 4.9).

Fig. 4.9 - Brash ice formed at the Jenpeg ice boom during early stages of ice cover formation. [Images courtesy of Manitoba Hydro.]

Similar to slush ice deposits that form via flocculation of suspended frazil ice, brash ice deposits can lead to considerably rough under ice conditions (Nezhikhovskiy, 1964). It is hypothesized that a continual supply of brash ice serves to increase the local roughness of the ice cover over winter. This effect counteracts the various mechanisms that decrease the roughness of the ice over winter, including freezing of interstitial water in the ice jam and thermal erosion of the underside of the cover (Ashton and Nufelt, 1991; Beltaos, 2011). A logarithmic relationship derived by Nezhikhovskiy (1964) relating ice thickness and ice cover roughness was applied to areas with simulated brash ice deposits. In ice cover areas where thickening occurred due to thermal growth alone, ice cover roughness over winter was assumed to remain unchanged following freeze-up. Further discussion on under ice roughness in the

OLA is provided by Lees et al. (2021a). Further information on roughness calculations for the OLA are provided in Appendix B.

4.4.3.3 Summary of Model Parameters

Relevant parameter values for model simulations were selected through a combination of field data sources, pertinent literature and preliminary model tests that yielded satisfactory performance. A summary of these values is provided in Table 4.3, while parameters not listed were generally assigned default values.

Table 4.3 - Summary of values selected for relevant parameters in the numerical model.

Simulated Ice Process	Parameter	Description	Value	Related Reference(s)
Freeze-Up Jamming	$t_{i_{min}}$	Minimum ice thickness for freezing	0.2 m	(Lees et al., 2021c)
	$\vec{v}_{crit}$	Critical freezing velocity	0.05 m s^{-1}	(Shen et al., 2000a)
	h_{crit}	Critical sheet ice thickness	0.01 m	(Wazney et al., 2019b)
	$\emptyset$	Internal friction angle of ice rubble	46º	
	T_{CR}	Threshold surface water temperature for border ice formation	-0.4℃	(Huang et al., 2012) (Newbury, 1968)
	$\vec{v}_{CR}$	Threshold velocity for border ice formation	0.15 - 0.25 m s^{-1}	
Thermal Ice Growth and Decay	R_t	Albedo of ice and snow	0.4	(Andreas and Jordan, 2004)
	ρ_s	Density of snow	170 kg m^{-3}	(Ashton, 2013)
	k_s	Thermal conductivity of ice	2.24 W m^{-1} ℃$^{-1}$	(Gray and Prowse, 1993)
	k_i	Thermal conductivity of snow	0.3 W m^{-1} ℃$^{-1}$	
Under Cover Ice Deposition and Transport	n_i	Manning's coefficient for ice (no under cover deposition of brash ice)	0.01	(Mann and Vogel, 1973) (Nezhikhovskiy, 1964)
		Manning's coefficient for ice (with under cover deposits of brash ice)	Minimum of: $(0.0192\, ln(h_i) + 0.0288, 0.1)$ where h_i = ice thickness	
	d_n	Nominal diameter of ice particles	0.01 m	(Shen et al., 1995)
	θ_c	Dimensionless critical flow strength	0.041	(Shen and Wang, 1995)
	ω	Buoyant velocity of under cover ice particles	$\sqrt{g d_n \left(\frac{\rho_w - \rho_i}{\rho_w}\right)}$ or 0.093 m s^{-1}	

4.4.4 Simulation Years and Performance Metrics

A study period encompassing winters 1996-1997 to 2020-2021 was selected. Winter 2003-2004 was excluded due to significant drought conditions in the Churchill/Nelson River Basin (Province of Manitoba, 2021b). Data from winters 2019-2020 and 2020-2021 were excluded from development of the hydraulic curves in this study (Fig. 4.4d-e), thus simulation results from these years were considered as a verification of the approach.

Performance metrics selected to assess results include error in various forms, including mean absolute error (*MAE*). Absolute error (*AE*) and relative error (*Err.*) were also included, in both standard and normalized form. These metrics were selected to assess both the simulated magnitude and rates of change of relevant hydraulic quantities. A summary of time-variables denoting the start and end of each stage (Fig. 4.10a-b), along with a definitions of performance metrics (Fig. 4.10c), is shown on Fig. 4.10.

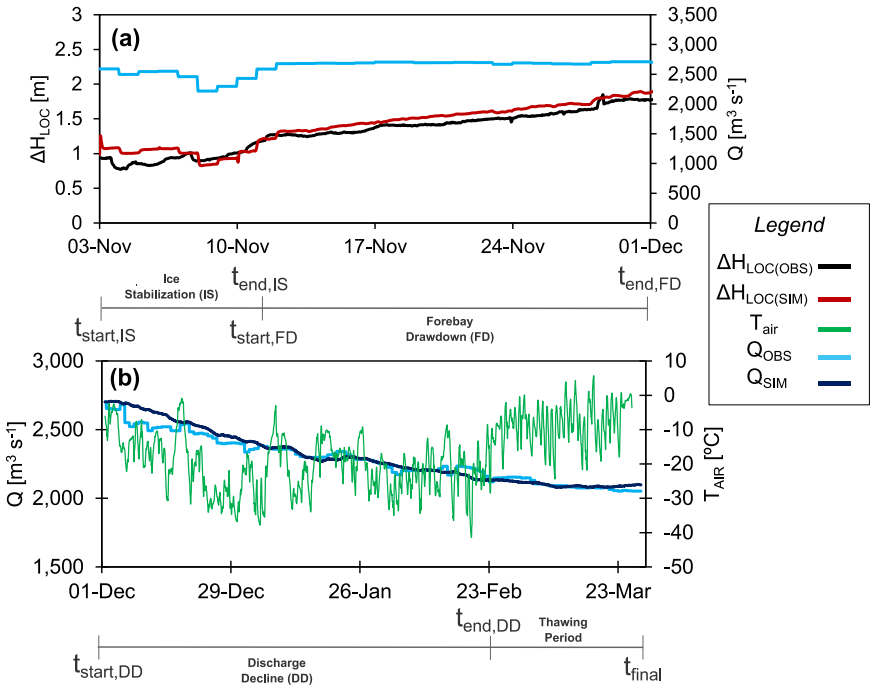

(c)

Model Output of Interest	Stage	Time Period	Performance Metric[1,2,3,4]
ΔH_{LOC}	Ice Stabilization (IS)	$t_{start,IS}$ - $t_{end,IS}$	MAE
		$t_{end,IS}$	AE AE / OBS
	Forebay Drawdown (FD)	$t_{start,FD}$ - $t_{end,FD}$	MAE
		$t_{end,FD}$	AE AE / OBS
Q	Discharge Decline (DD)	$t_{start,DD}$ - $t_{end,DD}$	mean(AE / OBS) max(AE / OBS)
		$t_{end,DD}$	Err. / OBS

Notes:

[1] $MAE = \frac{\sum_{i=2}^{n} |y_{SIM_i} - y_{OBS_i}|}{n}$ [2] $AE = |y_{SIM_i} - y_{OBS_i}|$

[3] $AE / OBS = |y_{SIM_i} - y_{OBS_i}| / |y_{OBS_i}|$ [4] $Err. = y_{SIM_i} - y_{OBS_i}$

*Where y is either ΔH_{LOC} or Q

Fig. 4.10 - Definitions of time variables applied to evaluate model performance during: (a) Stage 3, and (b) and Stage 4; (c) definitions of performance metrics applied to compare simulated and observed hydraulic variables.

4.5 Results

A graphical summary of model results from winters 1996 to 2020 is shown on Fig. 4.11.

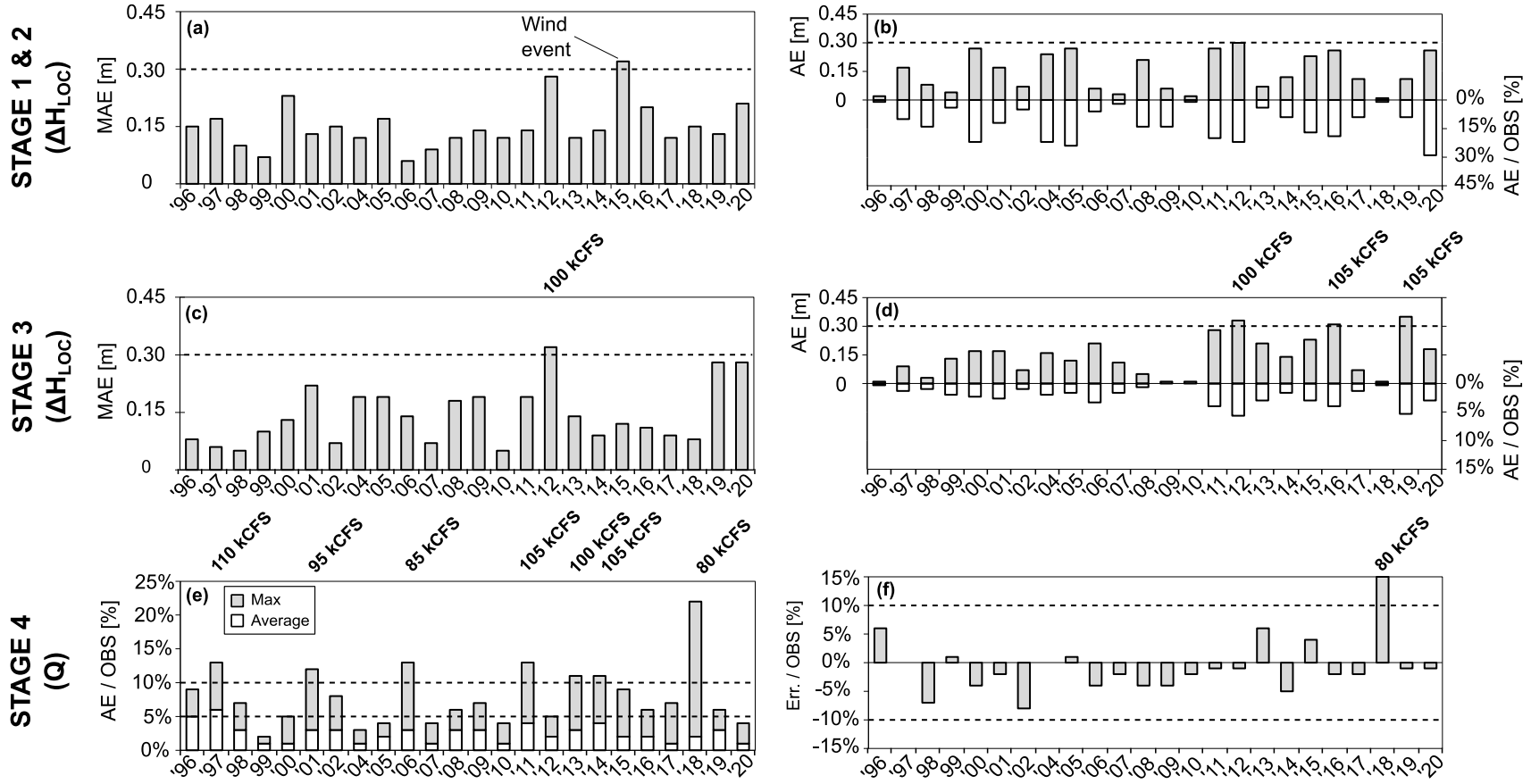

Fig. 4.11 - 1996-2020 performance statistics for simulations of: (a,b) Stage 1 and 2; (c,d) Stage 3; and (e,f) Stage 4. Discharge [k-ft^3 s^{-1} or kCFS] above chart indicates a year where error exceeds the accepted threshold (see Section 4.6.1).

In addition to acceptable error ranges indicated by dashed lines, discharge targets are included for years where errors exceed accepted thresholds. An illustration of the effect of wind set-down on model performance for 2015-2016 is shown on Fig. 4.12, resulting in considerable short-term error during simulation of Stage 2.

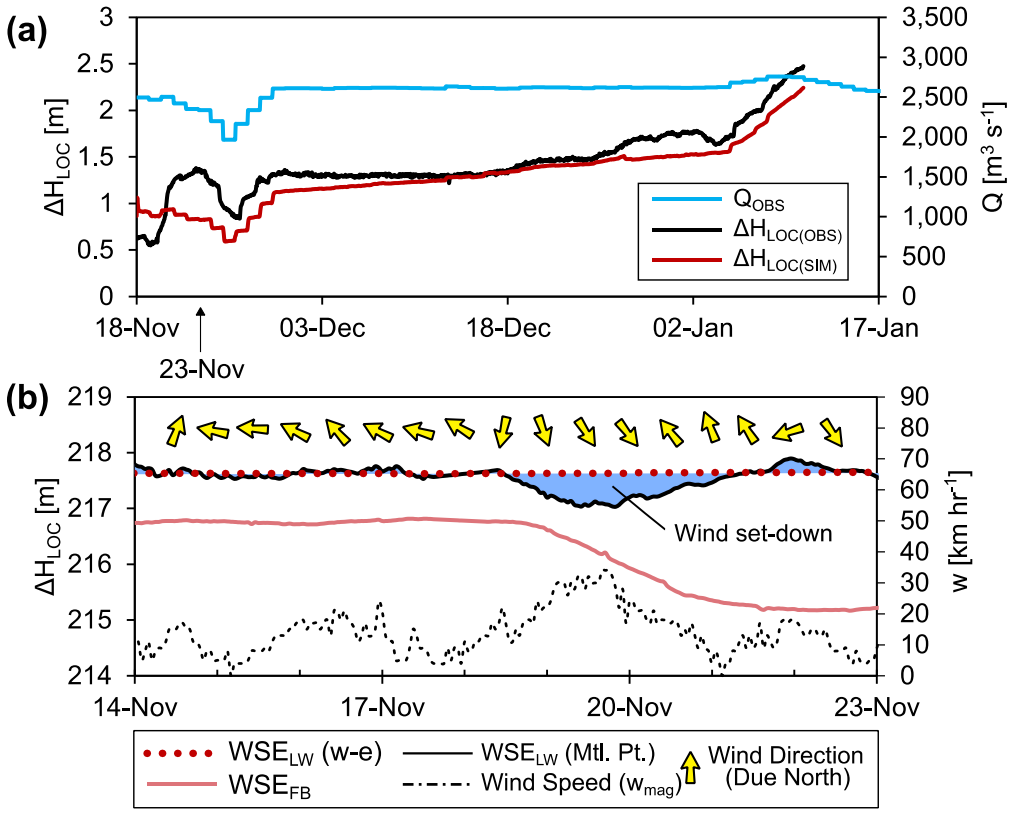

Fig. 4.12 - (a) Effect of wind on model performance during Stage 2 in 2015; and, (b) visualization of wind set-down (shaded blue) at the start of ice stabilization by comparing wind-eliminated (w-e) and northern Lake Winnipeg (Montreal Point; Mtl. Pt.) levels over a shorter duration.

Simulation results for years with Stage 3 error exceedances are shown on Fig. 4.13, with discrepancies mainly attributed to uncertainties associated with high discharge conditions.

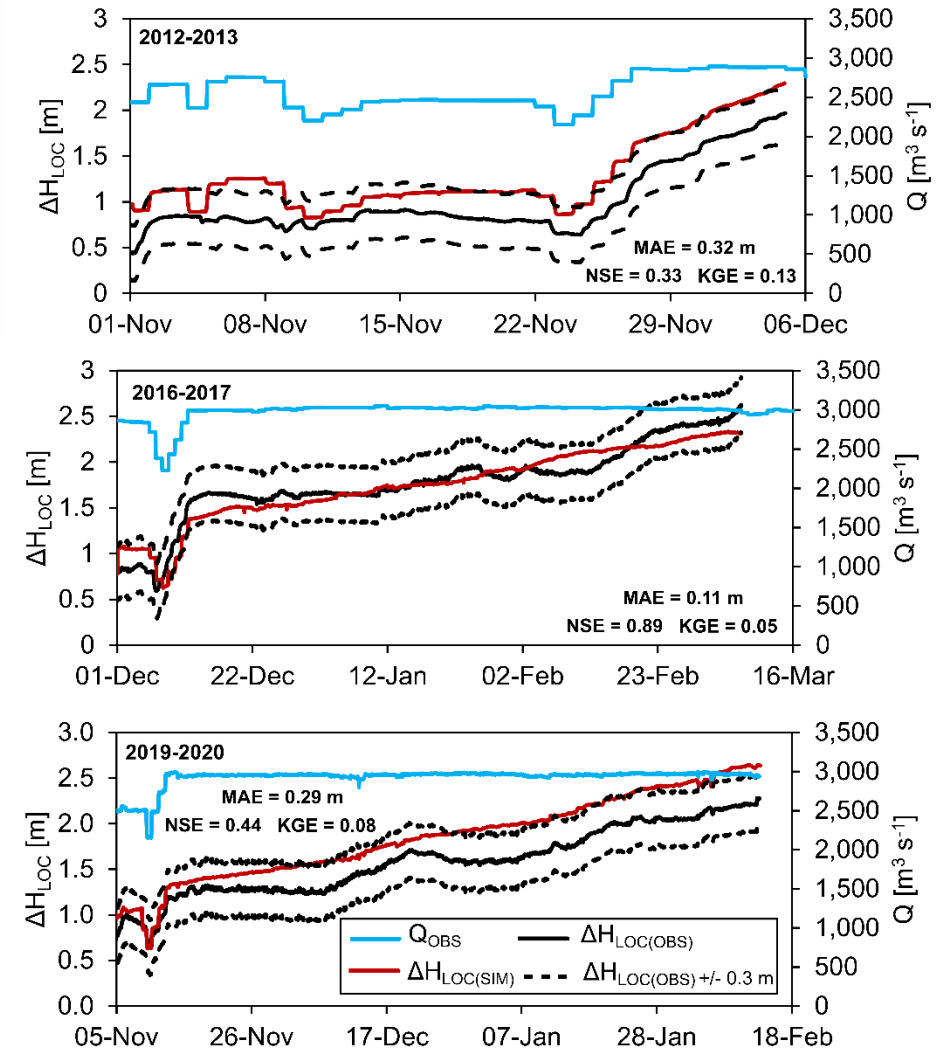

Fig. 4.13 - Simulation years where MAE or AE exceeds 0.3 m during Stage 3.

The hydraulic state of the model at the end of Stage 3, with regards to simulated flow proportions at upstream model boundary UB2 (Y_Q), are shown in contrast to open-water conditions on Fig. 4.14.

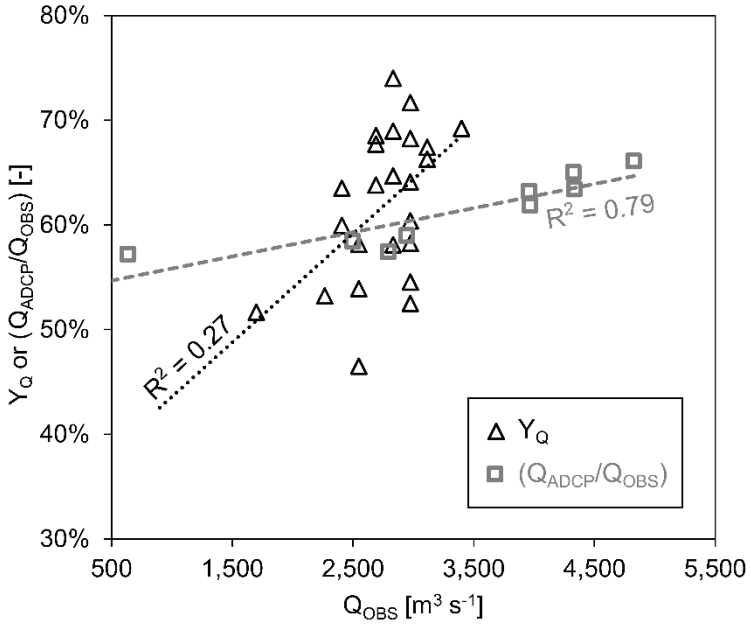

Fig. 4.14 - Observed open-water (Q_{ADCP}/Q_{OBS}) and simulated flow proportion at UB2 (Y_Q) under a range of discharges. A +12% adjustment (Bijeljanin, 2013) was applied to (Q_{ADCP}/Q_{OBS}) where needed to account for channel flow missing from Q_{ADCP} measurements.

Simulation results for years with Stage 4 error exceedances are shown on Fig. 4.15, with discrepancies mainly attributed to intermittent discharge changes resulting from mid-winter forebay operations. A visualization of under ice deposits and simulated hydraulics is shown on Fig. 4.16 relative to conditions observed in satellite imagery.

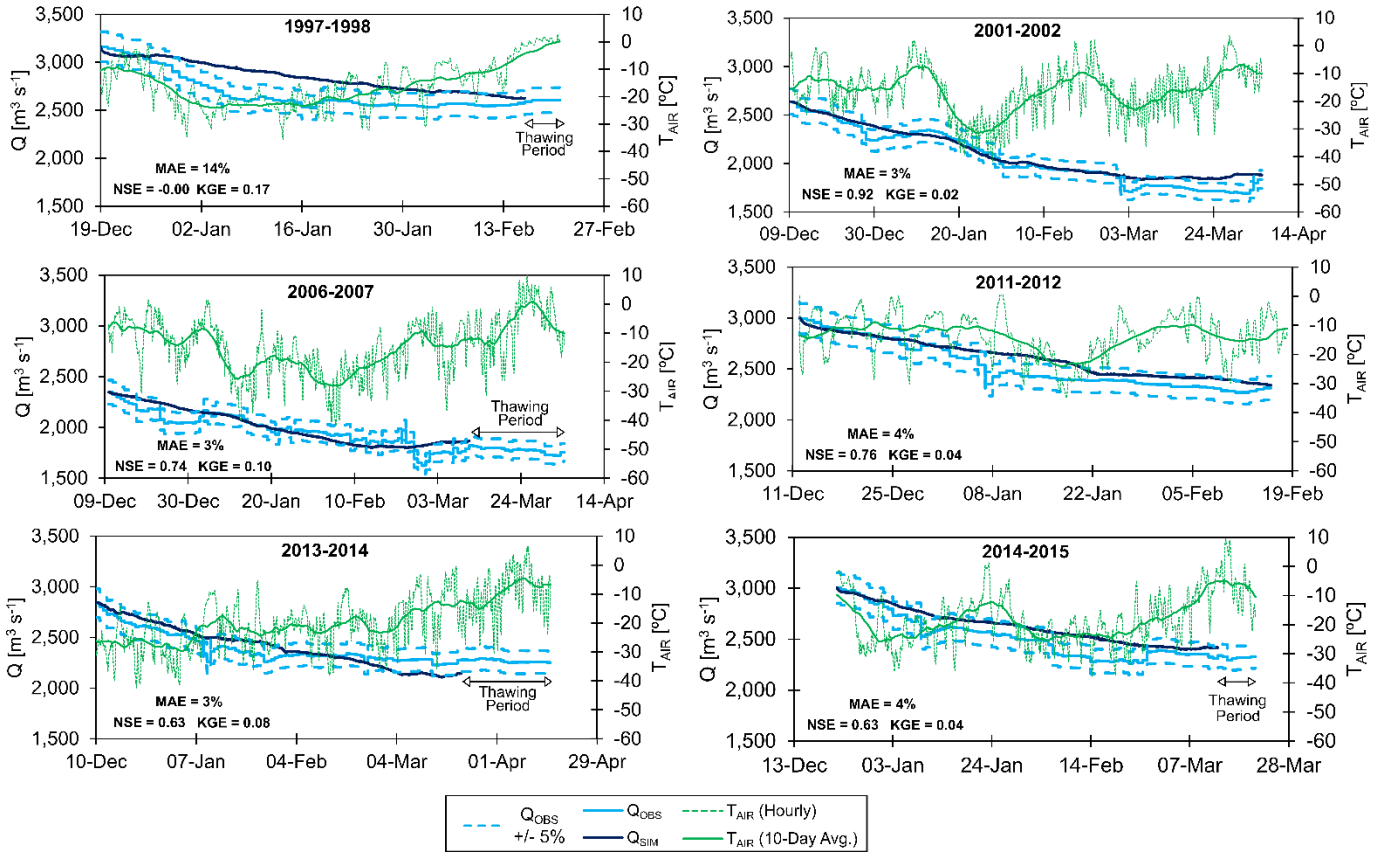

Fig. 4.15 - Mid-winter forebay changes contributing to maximum normalized AE exceeding 10% during Stage 4 simulations (thawing period excluded).

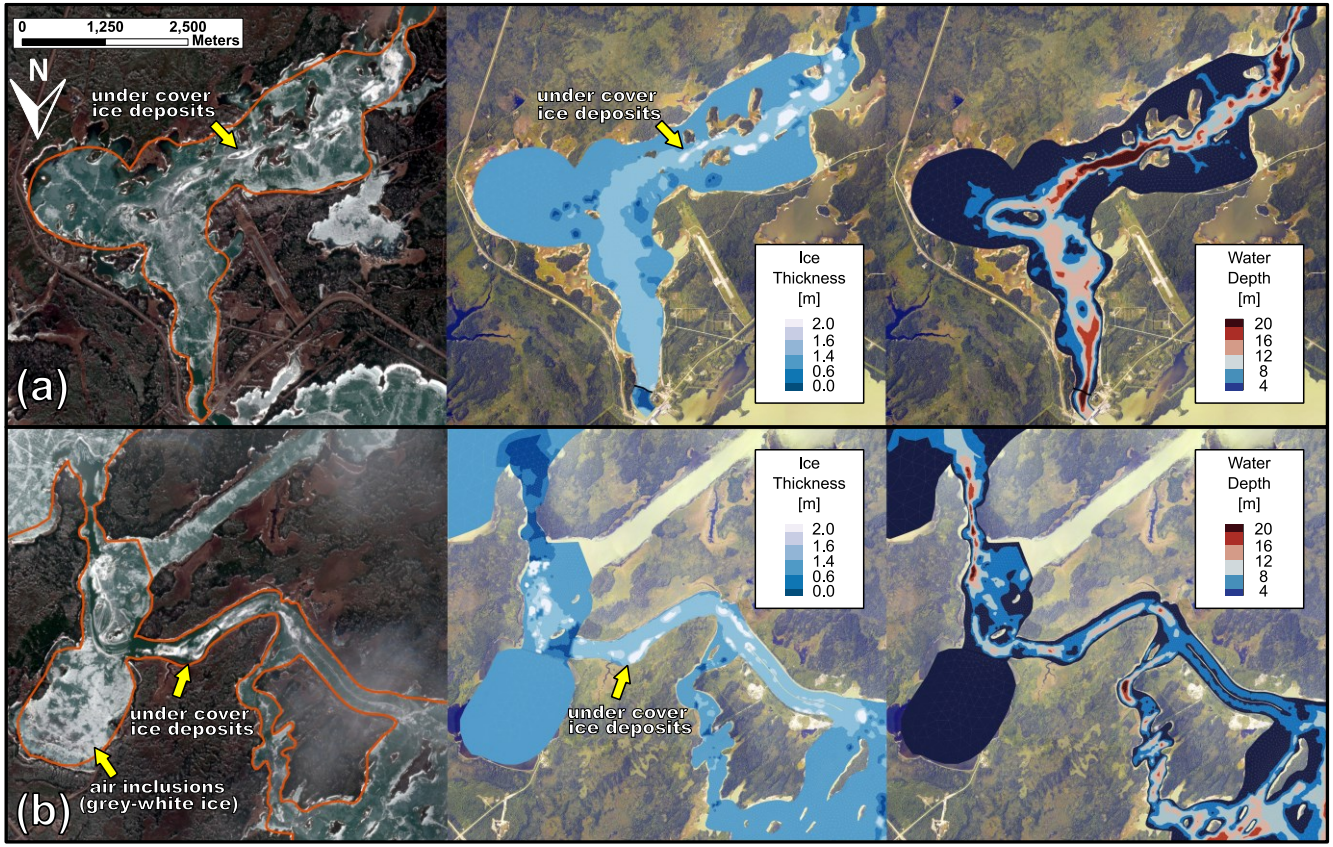

Fig. 4.16 - Comparison of under cover ice deposits (bright white) visible in satellite imagery (29-APR-2018; Sentinel-2 (ESA) image courtesy of the U.S. Geological Survey) with model outputs of ice thickness and water depth for (a) Reach 1 and (b) Reach 2 at $t_{final.}$ [Satellite imagery underlying model outputs provided courtesy of Manitoba Hydro.]

0

Using winter 2010-2011 as a base case (using meteorological data from Norway House), an evaluation of model sensitivity to WSE_{LW} (wind-eliminated) and heat flux conditions is shown on Fig. 4.17.

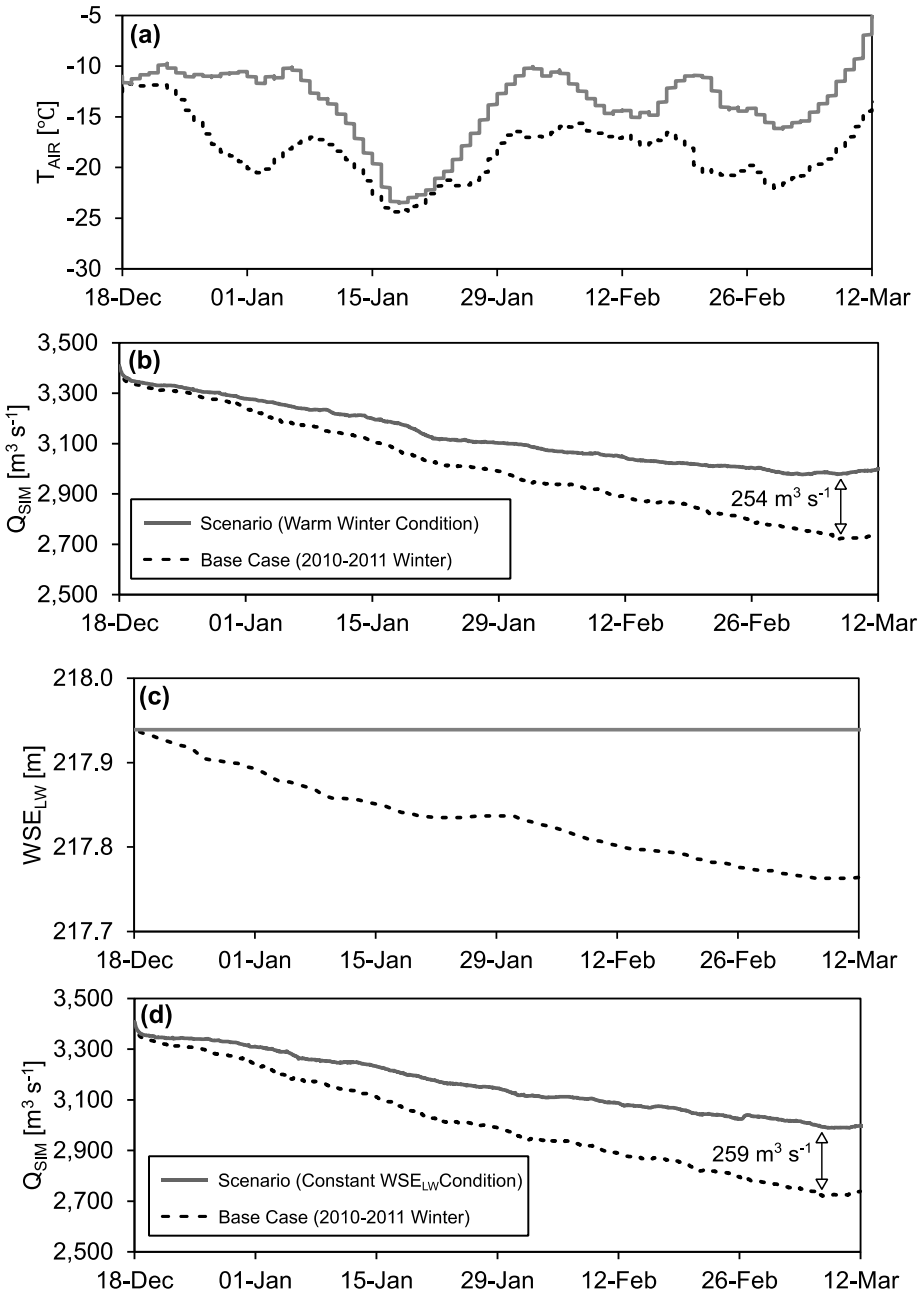

Fig. 4.17 - Evaluation of model sensitivity to (a,b) meteorological conditions; and (c,d) WSE_{LW} decline over winter.

4.6 Discussion

4.6.1 Estimated Range of Model Uncertainty

Results presented on Fig. 4.11 can be assessed by considering various factors that contribute to model uncertainty, including two that can be reasonably quantified. Firstly, the inherent error introduced by 3D open-water rating curves (Fig. 4.4b). This error is estimated to be up to 0.15 m of hydraulic head, as determined by a desktop analysis comparing rating curve outputs to historical data during steady conditions prior to freeze-up. Secondly, the error introduced through inaccuracies in discharge estimation at Jenpeg. It is hypothesized by Manitoba Hydro that historical discharge at Jenpeg may be slightly underestimated due to various sources of error (P. Slota, personal communication, November 26, 2020). It is also noted that these errors are most prominent under conditions of high spillway flow, which generally occur at higher discharges. While this study applies the most up-to-date adjusted discharge record for Jenpeg, some error in the record likely persists. Therefore, it is assumed that the adjusted discharge record is within +/- 5% of true values, which corresponds to an average additional error of 0.15 m of hydraulic head (for a total of 0.3 m of acceptable error). Additional details describing this estimation of acceptable error is provided in Appendix C.

Other sources of error are numerous (e.g., effects of ice on hydrometric measurements, accuracy of heat flux calculations, simplification in numerical simulations of ice processes, etc.), however attempts to quantify these sources of error is beyond the scope of this study.

4.6.2 Impact of Wind Set-Up/Set-Down on Simulation Error

For Stage 2 simulations, ΔH_{LOC} MAE exceeded 0.3 m during 2015-2016 (Fig. 4.12). A visualization of wind speed and direction prior relative to the date of maximum error (23-Nov; Fig. 4.12) highlights a strong north-westerly wind at the north end of Lake Winnipeg. This wind event forced a set-down event resulting in a dramatic decline in WSE_{FB} and proportional rise in $\Delta H_{LOC(OBS)}$. Considering that a wind-eliminated record for WSE_{LW} was applied during modelling, such dynamic wind-events are not captured in simulations. This obvious discrepancy is dissipative once the OLA becomes ice-covered. While wind-events can result in wave action and

subsequent ice cover failure at some sites (Sodhi et al., 1982), effects of wind on winter hydraulics in the OLA are minor due to expansive ice covers that greatly reduce potential for wave generation (Manitoba Conservation, 2001).

4.6.3 Simulation of Hydraulic Head, Upstream Flow Split and Discharge Decline

For Stage 3, ΔH_{LOC} MAE is within the acceptable range for all years except 2012-2013. At the end of forebay drawdown, ΔH_{LOC} was over-simulated during three years (Fig. 4.13). From visual inspection, error during these years is primarily in the form of uniform offset from observations, as trends of ΔH_{LOC} are generally well-simulated. High discharge ($\geq$ 100 k-ft^3 s^{-1}) is a common characteristic between most of these years, which may explain the simulated offset observed, as higher discharges are associated with greater uncertainty in observed discharge estimation and flow split estimation. Additional statistics of Kling-Gupta Efficiency (KGE; Guptaet al., 2009) and Nash-Sutcliffe Efficiency (NSE; Nash and Sutcliffe, 1970) were also included for these plots. These values provide additional insight into model performance during these simulations, especially with regards timing and trends of the simulated time-series where values less than zero for both NSE (Schaefli and Gupta, 2007) and KGE (Schonfelder et al., 2017) are considered unsatisfactory. Values closest to one are considered an optimal agreement between dataset.

Winter 2016-2017 is particularly notable, as observed forebay drawdown patterns are less than uniform relative to other years. Upon closer analysis, WSE_{LW} in 2016-2017 was exceptionally high (upper quartile of historical record) and steady. With WSE_{LW} close to the upper operating range limit for Lake Winnipeg regulation (715 ft.; Manitoba Hydro, 2014), the counteracting effect of higher lake levels against increasing ice resistance results in irregular forebay drawdown patterns that are difficult to simulate with accuracy with the current modelling approach.

During open-water conditions, a strong positive correlation is observed between Q_{OBS} and observed proportion of Q_{OBS} flowing through boundary UB2 (Q_{ADCP}/Q_{OBS}); Fig. 4.14). These discharge proportions are compared to simulated discharge proportions through UB2 (Y_Q) at the start of Stage 4 simulations. Compared to open-

water conditions, the range of discharges during winter in the OLA is much narrower. Further, simulated discharge proportions are highly variable between years. This variability is attributed to differing ice conditions and WSE_{LW} between years. Verification of these flow proportions would require strategic field measurements of under-ice discharge or velocity.

During Stage 4, average normalized AE for most years was ≤ 5%, which is within the accepted error range. Maximum normalized AE was evaluated separately and with a higher accepted error range (≤ 10%). Exceedances during six of seven years with high maximum normalized AE could be attributed to mid-winter changes to forebay levels (Fig. 4.11). As with Fig. 4.13, statistics of KGE and NSE are included for each plot. The effect of these minor forebay adjustments was a temporary reduction and rebound in Q_{OBS}, which could not be simulated by the numerical model due to the boundary configuration. Despite these intermittent discrepancies, overall discharge simulation during these years is satisfactory.

In the seventh year (2018-2019) with high maximum normalized AE, no mid-winter forebay adjustments occurred. Performance during this year is attributed to a 14 cm rise in WSE_{LW} which occurred between January and March 2019. The effect of this rise in water level is visible on Fig. 4.15, where the 2018-2019 decline in discharge is approximately one-third that of the derived trend from other years. As with Stage 2 results for 2016-2017 and 2019-2020, higher lake levels serve to compensate for increasing ice resistance by providing more hydraulic head. This may be especially apparent for lower discharges, such as those in 2018-2019 (80 k-ft^3 s^{-1} or kCFS). These results indicate that the methodology may perform poorly when applied during the exceptional conditions of rising Lake Winnipeg water levels over winter.

4.6.4 Extent and Location of Under Cover Ice Deposits

Simulated areas of brash ice deposits, as indicated by areas of exceptionally thick ice (> 2 m), are visible in both Reach 1 and Reach 2 (Fig. 4.16). Observed under ice deposits are visible in mostly snow-free Sentinel-2 satellite imagery from spring 2018 in the form of white patches that are distinct from the rest of the ice cover, including ice that is grey-white from air inclusions. A comparison of model results and satellite observations shows good agreement with respect to both extent and

location of deposits, adding to confidence that under ice processes were simulated as intended. Deposition patterns in Reach 2 (Fig. 4.16b) are also consistent with field measurements of a hanging dam in winter 1979-1980 (Hopper and Raban, 1980). Simulated water depth is included on Figure 8, to illustrate highly variable bathymetry that influences the local hydraulics that govern under ice processes.

4.6.5 Model Performance During Pre-Breakup (Thawing) Period

Despite promising performance during the freeze-up and mid-winter period, model limitations were identified during the pre-breakup (or 'thawing') period. The thawing period is characterized as the transition between a state of ice cover stability and breakup (defined by timestamps $t_{end,DD}$ and t_{final} on Fig. 4.10). Characteristics of the thaw include increasing magnitude of incoming solar radiation, greater number of daylight hours, warmer daytime temperatures, and a gradual melt of the ice cover's snow layer.

Model behavior during the thaw in most years tended to be a simulated plateau or rise in Q_{SIM}, despite the continual decline of Q_{OBS}. This behavior is attributed to the formulation of the ice decay equations in the numerical model. While the equations describing ice cover growth are well established and widely applied (Eq 4-6), thermal ice decay is more difficult to quantify due to the complex partitioning of energy gains by the snow and ice layers (Ashton, 2011). Using field data, Bilello (1980) applied empirical methods to characterize the thawing period using degree-days of thawing (*CDDT*), which accounted for the effect of snow in slowing thermal ice cover decay. Similarly, Shen and Yapa (1984) proposed an empirical unified degree-day method to estimate thermal growth and decay of an ice cover. In other cases, the snow layer is excluded altogether due to the short duration of the thawing period relative to the rest of winter.

In CRISSP2D, snow cover albedo is accounted for to reflect incoming radiation, however any thermal resistance provided by the snow cover to slow ice decay is absent. Thermal resistance of snow (0.04 to 1.0 W m^{-1} °C^{-1}; Arenson et al., 2014) is considerably less than that of thermal ice (2.7 W m^{-1} °C^{-1}; Arenson et al., 2014). As a result, in the absence of a snow layer the ice cover decays quickly in response to

positive heat fluxes (heat gain). This can lead to premature decline in ice resistance, and subsequent rise in Q_{SIM}.

Of the 24 simulation years in this study, the thawing period accounted for less than 10% of the total discharge decline during 21 of these years. Of the remaining three years, the thawing period period only exceeded 20% of the total discharge decline for one year (2005-2006) due to early spring conditions. While the thawing period is of short duration with low consequence for most simulation years, incorporating thermal resistance into decay equations yields improved results for 2005-2006. Ice surface decay Eq 4-9 was replaced with an adapted version of Eq 4-6 to ensure decay rates had the appropriate sign. The effect of thermal resistance on reducing ice decay rates, thus preventing premature rise in Q_{SIM} leading to improved simulation, is shown on Fig. 4.18.

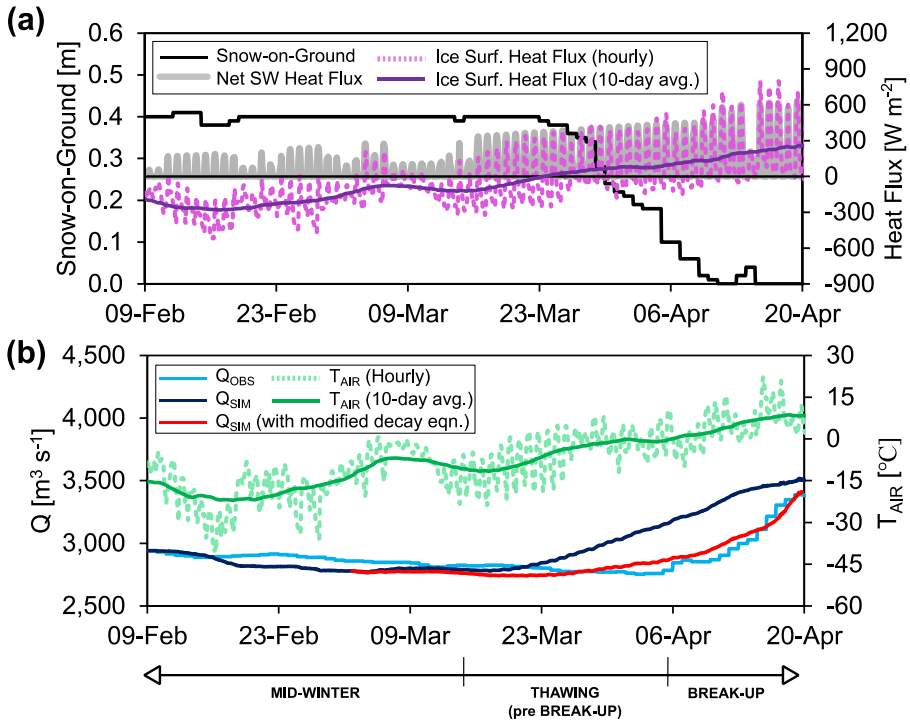

Fig. 4.18 - Discharge simulation during thawing period for 2005-2006 winter using default (dark blue) and modified decay (red) equations. Includes datasets of simulated ice surface heat flux (i.e., numerator of Eq 4-6), simulated net short-wave (SW) heat flux, observed snow-on-ground and observed air temperature.

4.6.6 Model Sensitivity to Heat Flux and Lake Winnipeg Decline

The methodology in this paper was designed, in part, for future application to assess the effects of climate variability in the OLA. Using winter 2010-2011 as a base case, model sensitivity was evaluated through two scenarios: (1) replacing 2010-2011 weather with that of a warmer winter (2011-2012), and (2) revising the downstream boundary (Eq 4-5) to reflect a constant WSE_{LW} over winter. The difference in 'discharge potential' (Fig. 4.17) at $t_{end,DD}$ for scenarios one and two were 254 m^3 s^{-1} and 259 m^3 s^{-1}, respectively, when compared to 2010-2011 base case. These differences each reflect a 9% increase in discharge potential above the base case. Physically-based metrics such as 'discharge potential' can provide relevant and quantitative descriptions of future impacts to river ice conditions as a result of climate change.

4.6.7 Evaluating Sensitivity of Model Parameters

A sensitivity analysis was performed on key parameters using the same evaluation period shown on Fig. 4.17. Parameters chosen reflect those with uncertain values, or those that have a high impact on ice-affected hydraulic calculations. These include wind speed (w_{dir}), albedo (R_t), an empirical heat flux coefficient (β), ice roughness (n_i), ice-air heat transfer coefficient (H_{IA}), and water-air heat transfer coefficient (H_{WA}). These results are shown on Fig. 4.19.

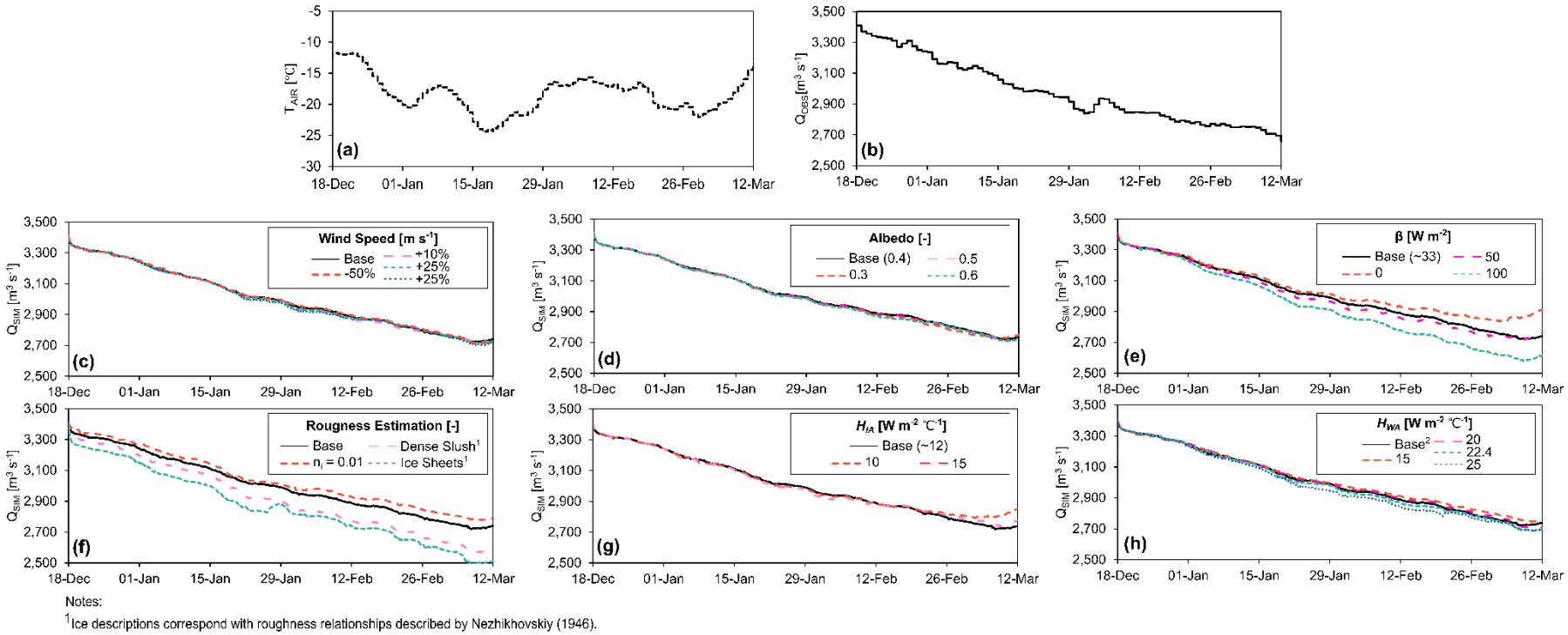

Fig. 4.19 – Model sensitivity to key model parameters under prescribed conditions (a,b). Parameters include: (c) wind speed (w_{dir}), (d) albedo (R_t), (e) β, (f) ice roughness (n_i), (g) H_{IA}, and (h) H_{WA}.

Considering the OLA is ice-covered during the simulation period, it is unsurprising that the effect of windspeed (Fig. 4.19c) on thermal and hydraulic processes is small. Considering the magnitude of mid-winter solar radiation is small, it is reasonable that the model also shows low sensitivity to albedo in this simulation (Fig. 4.19d).

In the event that a linear heat transfer method (Eq 1-2) is applied in lieu of a full energy budget method (Eq 1-1), model sensitivity to changes in H_{WA} is shown on Fig. 4.19h. This parameter mainly affects water temperature calculations, which subsequently impacts ice production as well as ice cover growth and decay. It is expected that higher H_{WA} values result in more ice production leading to greater discharge decline.

Other parameters impacting ice thickness calculations include H_{IA} (Eq 4-6 and Eq 4-9), which shows sensitivity during simulations mainly at the end of winter when air temperatures become warmer (Fig. 4.19g). Another parameter affecting ice thickness calculations is β (Fig. 4.19g), which shows high sensitivity. It is important to note that this parameter lacks a physical basis, and instead serves as a correction factor in Eq 4-6 and Eq 4-9.

The most sensitive model parameter with a physical-basis is ice roughness (Fig. 4.19f). While the selected ice thickness-roughness relationship for model simulations (described in Table 4.3) yielded adequate results, additional investigation of the roughness properties of under ice deposits in the OLA would provide further value. Other high-sensitivity parameters without a physical-basis (e.g., β) should be assigned a value in an informed manner, as these parameter adjustments may inadvertently result in compensation for model deficiencies or poor parameterization of other variables.

4.7 Conclusion

Efficient winter conveyance through the OLA is important for energy generation on the Nelson River hydropower system. Using a novel approach of coupled statistical and numerical modelling techniques, ice-affected hydraulics of the Nelson River's OLA were assessed across all stages of winter. Challenges with limited data availability and computational constraints were addressed using a truncated model domain and supplemental hydraulic relationships. An application of the approach

over many historical winters (1996-1997 to 2020-2021) yielded hydraulic quantities that, in most cases, were in good agreement with observations.

Numerical simulation of skim ice runs in open-water areas provided the ice supply required for evolution of ice restrictions throughout winter simulations. The quantity and roughness of under cover deposits were identified as important drivers of overall ice resistance. Simulated extent and location of these ice deposits was in good agreement with observations in satellite imagery. The numerical model was also adapted to account for the role of snow in slowing ice growth rates, while tests also show that snow can be applied to slow ice decay rates. Lastly, analysis of historical data illustrates the effect of both heat flux and WSE_{LW} on the hydraulic efficiency of the OLA.

Future expansion of the numerical model domain to the Lake Winnipeg outlet, while recommended to resolve the various assumptions in the methodology, is a data-intensive endeavour that may introduce new uncertainties. A brief model sensitivity scenario illustrates future application of the methodology to assess climate change impacts to winter hydraulics. Results from this study advance knowledge of ice-affected hydraulics in regulated river settings, in addition to enhancing local hydropower operations and related water resources research.

4.8 Chapter Summary

This chapter presents a detailed coupled methodology to simulate the effects of ice on the hydraulics of the Lake Winnipeg outlet. This included dynamic processes such as the evolution of a snow-on-ice layer, as well as under cover deposition and transport of entrained ice particles. The utility of the model in a climate change assessment scenario was demonstrated by evaluating model response to changes in both air temperatures and variations in Lake Winnipeg water levels. This application of the Chapter 4 model methodology to evaluate impacts of climate change is extended further by the research presented in Chapter 5.

Chapter 5: Quantifying future changes to winter discharge potential in a northern regulated river

5.1 Abstract

Shifts in climate conditions resulting from elevated levels of greenhouse gases in the atmosphere present threats to many communities, ecosystems and industries. For hydropower systems operating in cold regions, changes to economic conditions resulting from climate change, watershed hydrology, river ice processes and other factors may lead to sector-specific vulnerabilities. Projecting the impacts of climate change requires both a strong baseline characterization and an informed understanding of how system components and the natural environment interact. In northern Manitoba, Canada, the complex Nelson River hydropower network is a system that will inevitably be affected by climate change. By utilizing Lake Winnipeg as a primary reservoir, this economically-significant network supplies 75% of Manitoba's electricity demand. While researchers have studied both the hydrologic and hydraulic processes that govern Lake Winnipeg discharge, there is a need to bridge these interconnected disciplines to more accurately estimate lake outflows in a future climate landscape.

The objective of this study was to quantify the effects on ice on Lake Winnipeg winter outflow, both historically and in a future climate context. The study approach employs hydraulics-based approach driven by an ensemble of climate simulations from the *Coupled Model Intercomparison Project 5th Assessment Report* (*CMIP5;* Taylor et al., 2012) and corresponding hydrologic model projections of lake storage derived from the *Hudson Bay HYdrologic Predictions for the Environment* (*H-HYPE;* Lindström et al., 2010; Tefs, 2018). This was done using both empirical and numerical approaches, with the former providing a complete ensemble dataset for rigorous statistical analysis. These approaches were developed by leveraging existing site characterizations and region-specific tools. Calculations relied on hydro-meteorological modelled datasets (air temperature, precipitation and Lake Winnipeg water level), which were sourced from the BaySys Freshwater System team. Analysis and results focused on winter variables of interest, including *winter duration* annual *winter discharge decline*. Comparing results from 30-year reference

(1981-2010), near future (2021-2050) and far future (2041-2070) periods, several statistically significant changes were identified. Findings indicate that a future shift towards shorter winters and greater cumulative Lake Winnipeg winter outflow is expected with moderate to high confidence. Accompanying these projections is considerable uncertainty regarding intra-period rates of change. Further, significant increases to inter-annual variability of both hydrologic (i.e., winter discharge decline) and climatic (e.g., winter duration, start and end dates of winter) variables is expected in future years. While disagreement among individual CMIP5 simulations is important to consider when evaluating reliability of any specific narrative of climate impacts, findings from this study yield valuable insight for both long-term hydropower planning and future research.

5.2 Introduction

The projected long-term impacts of global climate change on the cryosphere are numerous and far-reaching. Among these impacts are anticipated changes to river ice processes in cold regions, with implications for communities, ecosystems, and industries. In most cases, river ice impacts resulting from future changes in a single climatic variable can be reasonably projected. For instance, warmer air temperatures may delay freeze-up and initiate an earlier breakup. However, concurrent changes to multiple variables may result in unexpected and counterintuitive impacts to ice characteristics and processes (Beltaos, 2013; Burrell et al., 2021). River regulation contributes additional complexity, as site-specific ice processes are influenced by the presence and operation of hydraulic structures.

In northern Manitoba, hydropower operations on the Nelson River are challenged with seasonal river ice conditions. Power generation at six locations relies on outflow from Lake Winnipeg, which is a large natural reservoir located in the *Nelson River Basin* (*NRB*). As with other regulated systems, this network is operated to control the annual discharge hydrograph, thus allowing for adequate flow volumes during winter months when electricity demand is high (Minville et al., 2009). Studies focused on quantifying Nelson River discharge have primarily relied on hydrologic modelling (MacDonald et al., 2018; Stadnyk et al., 2020), with recent efforts focused on improving representation of regulation routines, and hydropower-hydrology interactions (Beihagdar, 2019; Kim et al., 2022.; Tefs et al., 2021). While

these hydrologic models provide important variables that govern river ice processes (e.g., stage and discharge) in both historical and future climate settings, river ice processes are not explicitly represented in these models and are instead approximated by rudimentary treatments. These treatments aim to account the properties and behaviours of ice that impact river hydraulics.

While these river ice treatments may adequately account for ice effects in some locations, this is not the case for parts of the Nelson River due to the complexity of ice processes in these areas (Lees et al., 2021b, submitted.). Effects of river ice on Lake Winnipeg outflow (which supplies the Nelson River) are of particular concern at the immediate outlet of the lake, where an interconnected series of lakes and channels facilitates ice formations that restrict flow to varying degrees throughout winter. In an ideal case, the two-way coupling of hydrologic and hydraulic models would allow for comprehensive simulations that account for these river ice impacts (Das and Lindenschmidt, 2021). However, this endeavour is computationally infeasible resulting from a lack of parallelized code that would allow for simulation of the spatial and temporal scales demanded by climate change runs. In the interim, the use of one-way model coupling may improve representation of ice effects on simulated winter discharge.

Availability of baseline data assists in the characterization of present-day conditions, which is a fundamental step to navigating the uncertainty associated with a changing ice regime. Hydraulic research efforts in the Lake Winnipeg outlet region have yielded a detailed ice regime characterization (Lees et al., 2021b) and a rigorous river ice hydraulic modelling approach (Lees et al., submitted) that can be leveraged for discharge estimation and climate change assessment. The overall objective of this study is to quantify the effects on ice on Lake Winnipeg winter outflow, both historically and in a future climate context. This includes application of two approaches (i.e., empirical and numerical) to quantify the influence of river ice on flow conditions. Through one-way model coupling, these approaches are combined with hydrologic model projections of Lake Winnipeg storage levels to yield discharge estimates. This study presents one of the first detailed efforts to link site-specific river ice knowledge and large-scale hydrologic modelling in the NRB.

5.3 Background

5.3.1 Climate Change and River Ice

The regional dependence of watershed and riverine responses to changing hydro-meteorology contributes to challenges in projecting climate change impacts (Schleussnesr et al., 2016). In winter, this complexity is compounded by the non-linear relationship that is typical of river ice processes and the climatic variables that drive them (Beltaos, 2013). It is generally projected that future climatic conditions will lead to changes in ice-on duration, as well as the composition and extent of ice cover formations (Burrell et al., 2021).

Climate change in cold regions may lead to specific vulnerabilities for regulated rivers. In the event of higher discharge, increases to local flow velocities can inhibit surface ice cover formation, thus leading to increased frazil ice production (Timalsina & Alfredsen, 2015). Reduced duration of the stable ice cover period may also increase the risk of frazil ice events (Beltaos and Prowse, 2009; Huokuna et al., 2020a), which could lead to ice blockages of hydropower intake structures (Ettema et al., 2009; Gebre et al., 2014a). Delayed freeze-up and more dynamic mid-winter conditions may affect flow control practices, which are site-specific measures to promote stable ice cover formation, maintain mid-winter flow conveyance, and minimize adverse effects of breakup events (Tuthill, 1999).

Few studies have investigated the future impacts of climate change on freeze-up ice jam processes, although these processes will inevitably be influenced by changing discharge patterns and delays to winter onset. The lack of research is likely attributed to the numerical complexity involved in simulating these processes. During the ice-on period, climate change may lead to an increased frequency of mid-winter breakup events, resulting from a decline in ice cover stability caused by warmer air temperatures and more frequent rain-on-snow events (Beltaos, 2013). Extensive research has focused on breakup processes, as these events are most consequential for public safety and infrastructure. As outlined by Beltaos and Prowse (2009) and Turcotte et al. (2019), key factors that govern breakup processes include: timing of thaw onset, flow magnitude, ice jam volume, ice jam strength, and characteristics of

the preceding freeze-up. Future changes to hydro-meteorological conditions will inevitably influence most, if not all, of these factors.

Efforts to quantify effects of climate change on river ice have included analyses of satellite imagery and historical datasets (Yang et al., 2020; Chen and She, 2020), as well as applications of empirical equations and numerical models. Empirical and numerical approaches are developed pending data availability and in consideration of site-specific ice processes. Examples of river ice quantities that have been the focus of these studies include changes to:

- duration of ice cover season (Andrishak & Hicks, 2008; Gebre et al., 2014a);
- ice front position (Andrishak & Hicks, 2008; Jasek & Pryse-Phillips, 2015);
- ice thickness (Beltaos and Bonsal, 2021; Gebre et al., 2014a; Jasek & Pryse-Phillips, 2015);
- quantity of frazil ice production (Huokuna et al., 2009; Timalsina & Alfredsen, 2015);
- duration of freeze-up (Timalsina & Alfredsen, 2015); and,
- water quality and ecological impacts of ice conditions (Shakibaeinia et al., 2016).

River ice variables that are complex and/or stochastic by nature, such as the timing and location of ice bridge formation during ice jamming, are difficult to project with certainty in a future climate context. These variables can be assessed by extrapolating baseline data, which may yield insight into the sensitivity of certain processes to changing site conditions (Andrishak & Hicks, 2008). Analytical approaches may also be relied on, however, these can lead to exclusion or over-simplification of the interactions between processes (Huokuna et al., 2009). Analytical approaches may also have limited applicability in climate change assessments, as the equations involved are generally developed under assumptions of stationarity.

Drivers of river ice simulations assessing climate impacts typically include variables of precipitation and air temperature, as these important datasets are readily available from *Global Climate Models* (*GCMs*). Supplementary models are often required to provide hydrologic quantities (e.g., reservoir storage and discharge), examples of

which have included HBV (Gebre et al., 2014a) and WATLOOD (Prowse et al., 2006). Climatic variables such as windspeed, cloud cover, water temperature, and solar radiation may be sourced from supplementary equations (Timalsina & Alfredsen, 2015; Gebre et al., 2014a) and simplifying assumptions, or they may be excluded altogether if sufficient data are not available (Andrishak & Hicks, 2008). For hydropower applications, regulation routines are generally either constrained by applying current rules (Timalsina & Alfredsen, 2015) or by determining best practices through optimization.

Preparing climate data for river ice simulations typically includes a *delta change* or perturbation approach, which is the adjustment of input data using change factors calculated from GCM datasets (Navarro-Racines et al., 2020). It is less common for numerical studies to directly apply daily climate data for future periods, due to the computational constraints involved with these long-term simulations. For regulated rivers, few studies have coupled (in some form) hydraulic, hydrologic and hydropower models. Research by Gebre et al. (2014) is one exception to this with their combined use of the HBV hydrologic model, MIKE-ICE river ice model, and MyLake reservoir operations model. In Canada, Jasek and Pryse-Phillips (2015) applied CRISSP1D, the Peace River Thermal Ice Growth Model (PRTIGM), and data from the Pacific Climate Impacts Consortium to assess future river ice conditions on the regulated Peace River near the Site C dam.

The Nelson River region near Lake Winnipeg provides a challenging setting for investigating the interactions between watershed hydrology, hydropower regulation and river ice processes. This region will surely be impacted climate change for numerous reasons, including that flow is received from a large upstream watershed that encompasses drought prone prairies. Further, there is limited storage availability at run-of-the-river stations which may limit options for adaptation. By applying site-specific knowledge and hydraulic modelling techniques, this study serves as an important initial step towards improving how seasonal ice effects are accounted for in the hydrologic and hydropower models designed for this major system.

5.3.2 Study Area

The Nelson River (455 km long) features six power stations, which represent most of the hydropower generation potential in Manitoba, Canada (Fig. 5.1).

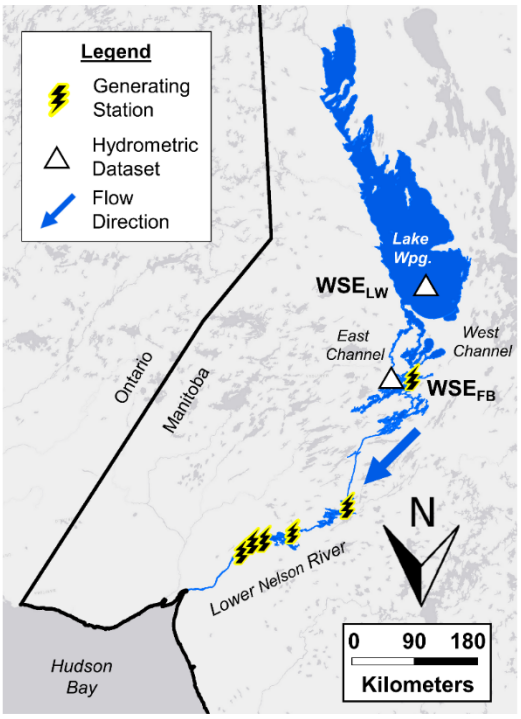

Fig. 5.1 - Study area and surrounding hydrologic features in northern Manitoba, Canada. [Base map from Esri, HERE, Garmin, © OpenStreetMap contributors, and the GIS User Community; water body and provincial boundary vector data from Government of Manitoba, 2001, Government of Canada, 2017]

The primary reservoir of the Nelson River, Lake Winnipeg, receives inflow from a drainage area of almost 1,000,000 km^2 (Province of Manitoba, 2021a). Further downstream, the Nelson River also receives inflows from the Burntwood and Grass rivers. Immediately downstream of the Lake Winnipeg outlet, the Nelson River's *West Channel* is characterized by a series of inter-connected lakes and channels that span approximately 100 km to Jenpeg Generating Station (Jenpeg). Also known as the *Outlet Lakes Area* (*OLA*), this region conveys 85% of total Lake Winnipeg outflow, while the remaining 15% (on average) flows through the Nelson River's *East Channel*. The area of interest for this study is the OLA, as this region is the most heavily monitored and conveys the majority of Lake Winnipeg's outflow.

In open-water conditions, discharge through the OLA is influenced by two primary controls: (a) the Jenpeg forebay water level (WSE_{FB}) and (b) Lake Winnipeg's water level (WSE_{LW}). WSE_{LW} is governed mainly by flow contributions from numerous rivers in the NRB (e.g. Winnipeg, Red, Assiniboine and Saskatchewan rivers), as well as operation of the Jenpeg. In ice-affected conditions, the presence of expansive river ice covers presents a third primary control that governs OLA discharge. Quantifying the effect of this ice control on discharge in a future climate setting is the primary contribution of this research.

5.3.3 Climate Data and H-HYPE Hydrologic Simulations

A *climate ensemble* refers to a collection of plausible future climate simulations, which can be presented together to account for the uncertainty of GCMs and their parameterizations (Falloon et al., 2014). A *climate simulation* refers to a GCM paired with a specific greenhouse gas concentration trajectory referred to as a *representative concentration pathway* (*RCP*). Climate simulations are typically selected to represent a range of climate variability from a larger suite of projections. Climate simulation data for this study were leveraged from the BaySys research project (Braun et al., 2021), which is focused on investigating effects of climate change and freshwater regulation on conditions in Hudson Bay (Barber, 2014). From a total of 54 GCMs among various RCPs available for BaySys from the CMIP5 (Taylor et al., 2012), 19 climate simulations were selected. This ensemble of 19 climate simulations explains roughly 90% of the variance of the complete 54 simulation ensemble (Braun et al., 2021). Climate simulation selection was based on annual averages and seasonal averages and is not specific to the NRB but rather is representative of the much larger HBDB. A summary of these 19 climate simulations is provided in Table 5.1.

Table 5.1 - CMIP5 climate simulations applied in this study.

Complete Identifier[1]	GCM	RCP	Shorthand Identifier[2]
ACCESS1-0_rcp45_r1i1p1	ACCESS1-0	4.5	A10r41
ACCESS1-0_rcp85_r1i1p1		8.5	A10r81
ACCESS1-3_rcp45_r1i1p1	ACCESS1-3	4.5	A10r41
ACCESS1-3_rcp85_r1i1p1		8.5	A10r81
CMCC-CM_rcp45_r1i1p1	CMCC-CM	4.5	CMMr41
CMCC-CMS_rcp85_r1i1p1	CMCC-CMS	8.5	CM5r81
CNRM-CM5-rcp45_r1i1p1	CNRM-CM5	4.5	CN5r41
CanESM2_rcp45_r1i1p1	CanESM2	4.5	CE2r41
GFDL-CM3_rcp45_r1i1p1	GFDL-CM3	4.5	GF3r41
INMCM4_rcp45_r1i1p1	INMCM4	4.5	INMr41
IPSL-CM5A-LR_rcp45_r1i1p1	IPSL-CM5A-LR	4.5	IALr41
IPSL-CM5A-LR_rcp85_r1i1p1		8.5	IALr81
MIROC-ESM_rcp85_r1i1p1	MIROC	8.5	MIEr81
MIROC-ESM-CHEM_rcp85_r1i1p1	MIROC-ESM-CHEM	8.5	MICr81
MIROC5_rcp45_r1i1p1	MIROC5	4.5	MI5r41
MIROC5_rcp85_r1i1p1		8.5	MI5r81
MRI-CGCM3_rcp45_r1i1p1	MRI-CGCM3	4.5	MR3r41
MRI-CGCM3_rcp85_r1i1p1		8.5	MR3r81
NorESM1-M_rcp45_r1i1p1	NorESM1-M	4.5	NOEr41

Notes:
[1](Braun et al., 2021)
[2](Kim, 2020)

Unless otherwise mentioned, climate simulation data were applied as provided without adjustment. Hydrologic modelling provides a means of simulating the water balance of a basin, which includes quantities of streamflow and reservoir storage. As part of BaySys, hydrologic modelling was performed using a modified version of Hydrologic Predictions for the Environment (HYPE), a semi-distributed catchment model developed by the Swedish Meteorological and Hydrologic Institute (Lindström et al., 2010). More specifically, a refined version of HYPE was developed to better represent lakes, effective drainage areas, and regulation routines of the rivers within the HBDB. This refined version is referred to as H-HYPE (Stadnyk et al. 2020; Tefs et al. 2021). In H-HYPE, WSE_{LW} is estimated as a function of inflow to Lake Winnipeg and outflow to the Nelson River. Using historical

records and expertise at Manitoba Hydro, an operating range of WSE_{LW} was assigned in H-HYPE for each day of the year. Based on H-HYPE simulated WSE_{LW} (i.e., $WSE_{LW(HYPE)}$) and the assigned operating range, H-HYPE Lake Winnipeg outflow (Q_{HYPE}) is calculated through the regulation rules summarized in Table 5.2.

Table 5.2 - Rules for Lake Winnipeg outflow determination (adapted from Tefs et al. 2021).

H-HYPE Zone-Option	Lake Winnipeg Outflow Assignment Rule	Description
Drought Option	Fixed Value	Minimum outflow
Low Option	Monthly	Outflow calculated using month-specific coefficients
Operations Option		
High Option	Fixed Curve	Outflow calculated with fixed coefficients
Flood Option	Fixed Value	Maximum outflow

While river ice is not explicitly represented in H-HYPE, the use of a daily WSE_{LW} operating ranges accounts for seasonal differences between open-water and ice-impacted conditions. Comparing the ensemble of Q_{HYPE} results across all 19 climate simulations for years 1981-2010 with observed conditions (Q_{OBS}) during the same time-period shows good agreement. When results for the winter period are isolated (November to March), more significant differences between Q_{HYPE} and Q_{OBS} emerge (see Fig. 5.2).

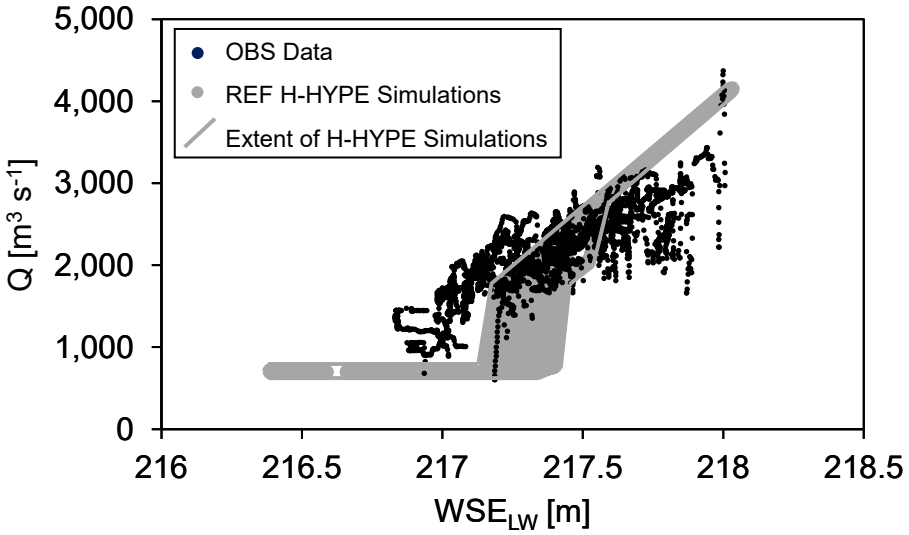

Fig. 5.2 - Comparison of OBS and simulated H-HYPE REF ensemble of WSE_{LW} and Q for 1981-2010 (November - March).

This noticeable difference between Q_{HYPE} and Q_{OBS} is attributed mainly to how the hydraulic characteristics of the Lake Winnipeg outlet are represented in H-HYPE. Firstly, in the real-world system, the WSE_{FB} at Jenpeg can be gradually drawn down during winter. This increases the hydraulic head between Lake Winnipeg and the Jenpeg forebay to compensate for ice-induced head losses. As a result, Q_{OBS} can be maintained at a higher rate for longer before eventually declining once WSE_{FB} reaches a minimum operating level. Secondly, once the forebay is fully drawn down, Q_{OBS} is constrained by WSE_{LW} and the severity of ice restrictions in the OLA. This system behaviour is not represented using seasonal operating ranges.

In an ideal scenario, a robust improvement to H-HYPE simulations for the Lake Winnipeg outlet would require *two-way model coupling* with a river ice hydraulic model, however this endeavour involves numerous complications related to information exchanges and model structures. However, future research into model coupling within a local area may be more feasible. At this time, Lake Winnipeg water levels projected by H-HYPE can serve as input to a river ice analysis methodology through *one-way model coupling*, which can then yield an alternate set of Lake Winnipeg outflows. One-way model coupling refers to individual models being run to completion in series, where output from one model serves as input to

next (Benra et al., 2011). The two types of river ice assessment methodologies developed for this study (numerical and empirical) are discussed further in Section 5.3.4.

The approach of one-way model coupling includes the key assumption that $WSE_{LW(HYPE)}$ datasets are applicable under an alternate dataset of Lake Winnipeg outflows. This approach is considered reasonable owing to the large storage size of Lake Winnipeg, which limits stage fluctuations over winter. Further, because hydraulic equations and regressions were developed based historical operating conditions, this also supports the justification that discharge projections are feasible. While there is uncertainty in the approach, the assumption that one-way coupling is applicable is necessary at this stage and represents a first step in a new research area for this location.

5.3.4 Numerical and Empirical River Ice Approaches

To generate new datasets of Lake Winnipeg outflows, two river ice modelling approaches are employed. The first approach was designed by Lees et al. (submitted) and uses a numerical model with supplementary hydraulic equations specifically derived for the OLA. This approach leverages a previously-developed OLA specific 2D river ice model designed using CRISSP2D (Lees et al., 2019; Shen et al., 1995a). Selection of a 2D model is warranted for the Outlet Lakes Area, due to role of transverse flow distribution during freeze-up jamming and under cover deposition and transport of ice calculations. The presence of extensive meanders, islands, and flow splits/confluences all contribute to variation in transfer flow distribution throughout the model domain. It is important to simulate these ice processes accurately to achieve strong model performance in estimating ice resistance, especially during unsteady hydro-meteorological conditions.

CRISSP2D was selected specifically for its comprehensive simulation capabilities of thermal and dynamic ice processes. This first approach is referred to as the *Coupled River Ice Methodology* (*CRIM*) and is discussed further in Section 5.4.4.

While CRIM shows strong performance in simulating ice-affected hydraulics for historical years, the approach is constrained by considerable computational requirements. The ratio of run-time (i.e., physical time for the model to run) to

simulation-time (i.e., time-period simulated by model) varies based on a variety of factors, including computer hardware specifics and simulation settings. However, the approximate range of this ratio for typical simulations is 0.08 to 0.17, meaning a simulation-time of five months (i.e., a typical winter) may take two to four weeks of run-time. Considering there are 80 years of data for each of the 19 climate scenarios, applying CRIM to every winter would take a minimum of 1.3 years per climate simulation given the non-parallel structure of the model and the limitations of computational resources for series computing.

It is well-established that discussions of changing climate conditions benefit from both simulation-specific and ensemble-based analyses. Considering CRIM cannot yield a complete ensemble of results, an alternate approach is required. This motivated development of the *Empirical River Ice Approach* (*ERIA*), which is based on the CRIM hydraulic equations and use of supplementary equations to compensate for the exclusion of the numerical model. Details of ERIA's MATLAB-based calculations are discussed further in Section 5.4.2. While results from ERIA are considered an approximation of an ensemble result that CRIM simulations would provide, it is suspected that the bias between CRIM and ERIA calculations will be reflected similarly amongst all climate simulation winters. This justifies the use of ERIA as a tool for assessing relative changes across ensemble datasets.

While CRIM cannot be applied to every simulation winter due to computational constraints, there is merit of applying this approach to a strategically selected subset of winters, as these results can shed light on the reliability of ERIA calculations. Further, a detailed explanation of the CRIM methodology can provide the basis for future climate change research. Concurrent development of both ERIA and CRIM is valuable for related studies in the OLA region, as the practical nature of ERIA may be better suited for hydrologic or hydropower operations models that cannot be easily coupled with a complex 2D river ice model.

5.4 Methodology

5.4.1 Hydro-Meteorological Data Inputs

This study applied data from both historical observations and climate simulations. Historical datasets used in this study are summarized in Table 5.3.

Table 5.3 - Availability of relevant historical datasets in and around the OLA

Time Period	Regional Monitoring Locations			
	Lake Winnipeg	Norway House	Thompson	Jenpeg GS
1977-1996	○	⊙	□	○●
1996-1998	○	⊙	□	○●
1998-2008[1]	○	⊙	□	○●
2008-present[2]	○	⊙	□	○●

Notes:

○Water Surface Elevation (Manitoba Hydro)

●Discharge (Manitoba Hydro)

⊙Air Temperature, Wind Speed and Direction (Environment Canada, 2021)

□Precipitation, Snow-on-Ground (Environment Canada, 2021)

Datasets from different regional monitoring (Table 5.3) locations were selected based on availability and proximity to the OLA (furthest station being Thompson located 130 km north of Jenpeg). Historical observations were utilized for comparison with climate simulation data and were necessary to generate inputs for CRIM simulations (see Section 5.4.4).

Climate simulations consisted of 19 bias-corrected datasets shared by Ouranos consortium via the BaySys research group (see Section 5.3.3) in the form of gridded datasets at a 0.5 degree resolution. Using the grid cell closest to Jenpeg, time-series of daily precipitation [mm], daily maximum air temperature [°C], and daily minimum air temperature [°C] were extracted. Considering that the ensemble features some climate simulations where leap years are included, leap days were removed where required for consistency throughout all datasets. Removal of leap

days is a common approach employed in other climate studies (e.g. Pradhananga et al., 2020)

Hydrologic datasets of $WSE_{LW(HYPE)}$ and Q_{HYPE} were sourced from H-HYPE model simulations (Tefs, 2018). As discussed in Section 5.4.4, Q_{HYPE} records were not directly used for analyses in this study. Three time-periods were established (Table 5.4) to allow for comparison of 30-year datasets for statistical trend detection.

Table 5.4 - Time periods for analysis using climate simulation and H-HYPE data.

Years	Time-Period	Acronym
1981-2010	Reference	REF
2021-2050	near-Future	n-FUT
2041-2070	far-Future	f-FUT

5.4.2 Empirical Discharge Estimation

As discussed in Section 5.3.4, the ERIA approach was developed in response to the significant computational time associated with numerical simulations. ERIA applies several empirical equations derived from site-specific data, a process facilitated using MATLAB. ERIA was developed from the basis of a previous description of winter flow stages in the OLA (Lees et al., submitted). These stages are simplified in the graphical summary provided on Fig. 5.3(a-e), which is referenced in later sections.

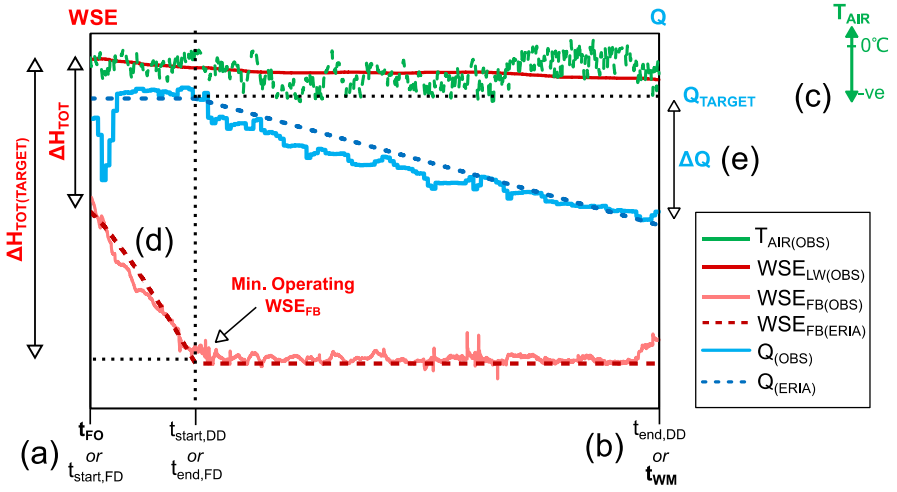

Fig. 5.3 - Definition of winter stage and relevant variables for ERIA calculation, including: (a) freeze-up onset (t_{FO}), (b) warming onset (t_{WM}), (c) winter discharge target (Q_{TARGET}), (d) forebay drawdown (FD) until ΔH_{TOT} equals $\Delta H_{TOT(TARGET)}$, and (e) discharge decline (DD) represented by ΔQ.

Fig. 5.3 includes time identifiers for freeze-up onset (Fig. 5.3a) and warming onset (Fig. 5.3b). The period of forebay drawdown ($t_{START,FD}$ to $t_{END,FD}$) represents a case of complete forebay drawdown (i.e., when ΔH_{TOT} reaches $\Delta H_{TOT(TARGET)}$; Fig. 5.3d) to maintain the flow target (Q_{TARGET}; Fig. 5.3c). Following complete forebay drawdown, discharge will decline over the subsequent period ($t_{START,DD}$ to $t_{END,DD}$; Fig. 5.3e). Note that depending on Lake Winnipeg conditions and ice restriction severity, there can be winters where the forebay is not completely drawn down (i.e., ΔH_{TOT} does not reach $\Delta H_{TOT(TARGET)}$). In these cases, Q_{TARGET} is maintained throughout the entire winter without decline. The four stages of winter – freeze-up onset, ice stabilization, forebay drawdown, and discharge decline – are described in Lees et al. (submitted).

5.4.2.1 Step (a) and (b): Start and End of Winter

At the early stages of winter, the first appearance of ice in the OLA occurs at shorelines (border ice) and within shallow back bays. Operational experience suggests that significant ice formation occurs at about 50 cumulative degree-days of freezing (*CDDF*) (Lees et al., 2021b), after which point significant impacts to OLA hydraulics are observed. This *CDDF* threshold was selected to indicate the start of

winter (i.e., t_{FO}). *CDDF* was calculated as a measure of departure of air temperature (T_{AIR}) from a base temperature (selected as 0°C) (Boyd, 1979). As shown in Eq 5-1, T_{AIR} was subtracted from *CDDF* in the case that T_{AIR} was greater than 0°C:

$$CDDF = \sum_{i=1} \left(0℃ - T_{AIR_i}\right)^+ \qquad \text{Eq 5-1}$$

$$\textit{where for each day } X^+ = max\ (X, 0)$$

While the *CDDF* threshold has been operationally reliable for predicting the onset of freeze-up, there is no established threshold for breakup in the OLA. Further, there are limited data available to characterize the timing and nature of this breakup. Using observed hydrometric records (Q_{OBS}, $WSE_{FB(OBS)}$, and $WSE_{LW(OBS)}$) for select winters from 1977 to 2018, an end-of-winter date was established by visual inspection to identify the timing when OLA ice resistance starts to diminish significantly. This time is characterized as the *warming onset* and is represented by t_{WM}. To facilitate a threshold approach to calculating t_{WM}, cumulative degree-days of warming (*CDDW*) was selected as a predictor variable as *CDDW* is a surrogate measure of heat gain for both ice-covered and open-water sections of a water body (Eq 5-2):

$$CDDW = \sum_{i=1} \begin{cases} -\left|T_{AIR_i}\right| & if\ (T_{AIR_i} \leq T_{WM}) \\ \left|T_{AIR_i}\right| & if\ (T_{AIR_i} > T_{WM}) \end{cases}^+ \qquad \text{Eq 5-2}$$

$$\textit{where for each day } X^+ = max\ (X, 0℃)$$

where T_{WM} is the base temperature for warming [°C]. An example of the identification of t_{WM} is shown on Fig. 5.4 for observed winter conditions in 2008-2009.

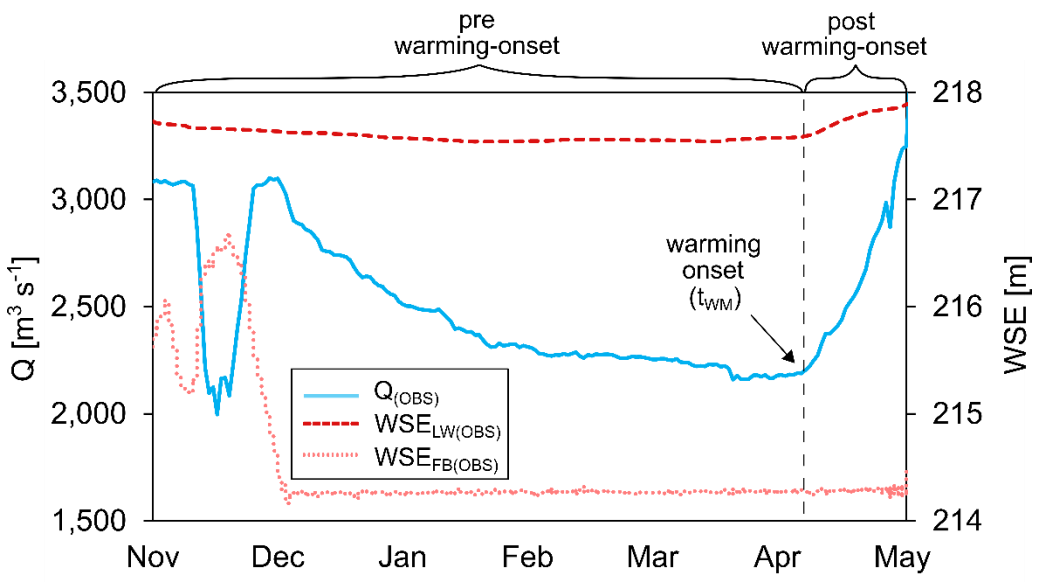

Fig. 5.4 - Example of the identification of the warming onset (2008-2009 winter) using observed hydrometric data.

Calibration was required to determine: (1) the minimum $CDDW$ required for the warming onset ($CDDW_{MIN}$), and (2) the base temperature for warming (T_{WM}). Using the dataset of observed t_{WM} dates from 1977 to 2018 and Eq 5-2, calibration was performed by adjusting T_{WM} and $CDDW_{MIN}$, while minimizing the objective function *sum of absolute error* (*SAE*). Result of this calibration was an annual *mean absolute error* (*MAE*) of 9 days and an annual maximum *absolute error* (Max. *AE*) of 23 days, as shown on Fig. 5.5.

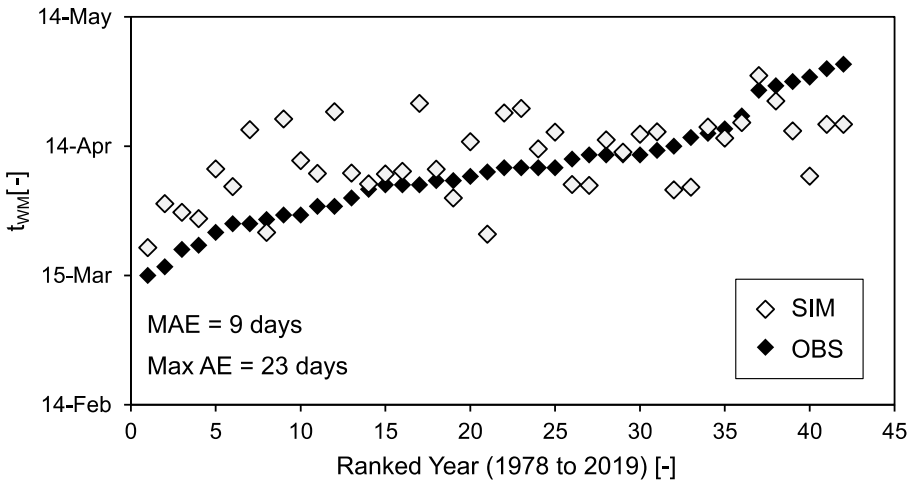

Fig. 5.5 - Result of calibrating t_{TH} by adjusting $CDDW_{MIN}$ (50°C-days) and T_{WM} (-12°C).

Calibrated values for $CDDW_{MIN}$ and T_{WM} were found to be 50°C-days and -12°C, respectively. A widely-cited report on ice decay (Bilello, 1980) suggests that T_{WM} less than 0°C to calculate $CDDW$ is appropriate for river ice environments. Bilello (1980) also notes a typical range of values for T_{WM} being -10°C to -5°C, which is comparable to the calibration result. Correspondence with Manitoba Hydro indicates that a warming threshold of 50°C-day on average is consistent with their analyses which used air temperature data from Thompson, although uncertainty remains in the reliability of this threshold (S. Wang, personal communication, September 16, 2021).

Interestingly, 50°C-day serves as a threshold for both freeze-up and warming onsets. Using these thresholds, histograms of t_{FO} and t_{WM} dates for REF, n-FUT and f-FUT ensemble winters are shown on Fig. 5.6.

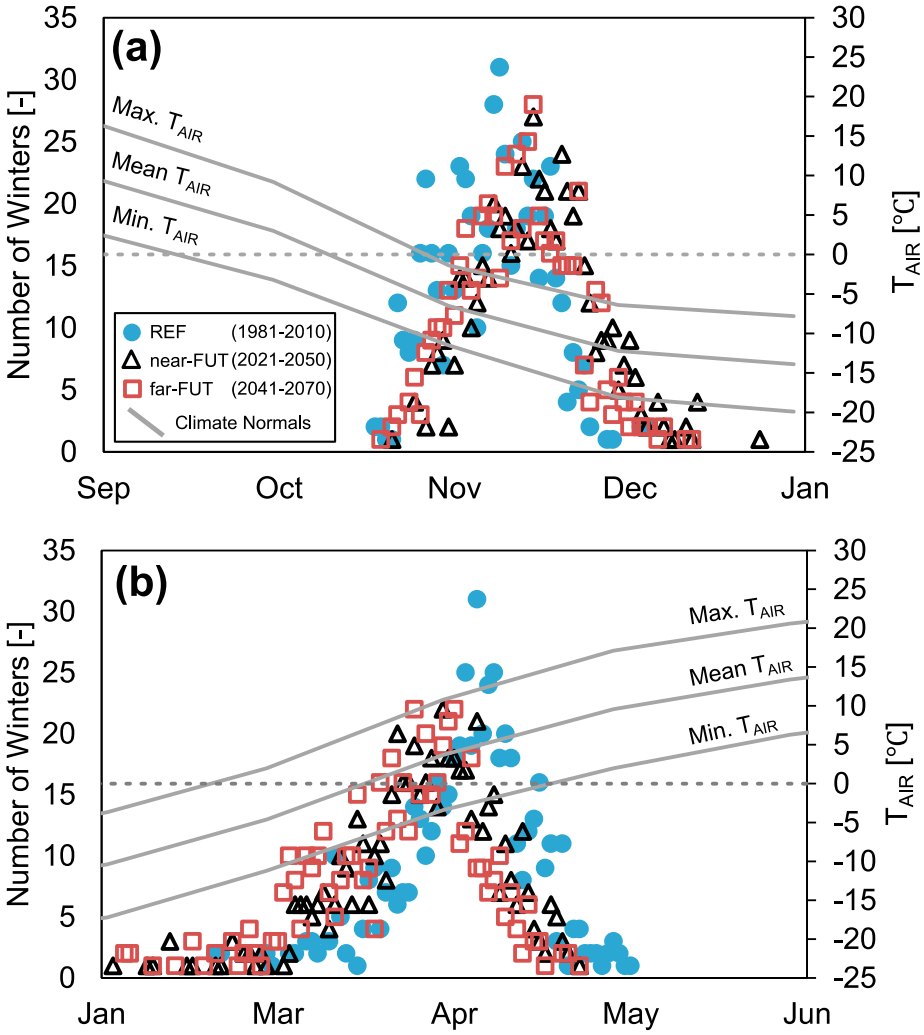

Fig. 5.6 - Histogram of (a) freeze-up and (b) break-up dates for REF, n-FUT and f-FUT winters; ECCC T_{AIR} Climate Normals (years 1981-2010) sourced from Norway House A [ECCC station ID: 506B047] are included.

A shift is visible in histograms for both the start-of-winter (Fig. 5.6a) and end-of-winter (Fig. 5.6b), with the general trend being later freeze-up and earlier warming onset in future winters.

5.4.2.2 Step (c): Winter discharge target

At the onset of winter, freeze-up in the OLA features a brief ice stabilization (IS) period, which is characterized by temporary flow reductions (which are typically in increments 140 ft^3 s^{-1} for several days in duration) to facilitate formation of a smooth and stable ice cover upstream of Jenpeg (Zbigniewicz, 1997). The IS period is

typically 1 to 3 weeks on average, representing a small fraction of the total winter. As a result of its short duration and highly dynamic nature, the IS period was not explicitly represented in ERIA calculations.

Alternatively, ERIA calculations assume a steady discharge over the IS period, where the steady discharge is established according to the *winter discharge target* (Q_{TARGET}). According to Manitoba Hydro, Q_{TARGET} depends on observed hydraulic conditions and energy system requirements, and is set based on two primary factors (K. Gawne, personal communication, May 5, 2021):

1) Overall water condition – sustaining a specified Q_{TARGET} over winter depends on storage availability in Lake Winnipeg, with higher lake levels corresponding with higher possible discharge targets.
2) Pre-IS flows – setting Q_{TARGET} well-above the pre-IS flowrate may result in excess staging on Cross Lake (downstream of Jenpeg), possibly leading to slush-ice conditions and stakeholder concerns.

The factors involved in establishing Q_{TARGET} are numerous, both qualitative and quantitative, and are often specific to the conditions of a particular year. To simplify this decision process, this target was established in ERIA using a stage-discharge relationship of freeze-up WSE_{LW} and Q_{TARGET} derived from historical data (Fig. 5.7).

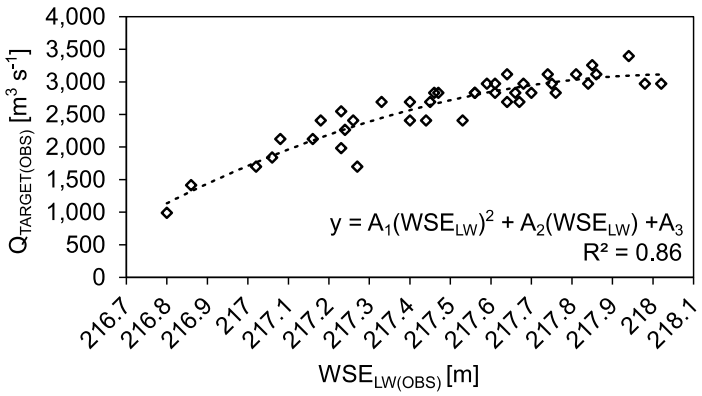

Fig. 5.7 - Historical WSE-Q_{TARGET} curve derived from mean conditions during the forebay drawdown period. Data comprises select years from 1984 to 2018, where 2003 was excluded as Q_{TARGET} could not be identified with a high degree of confidence.

The non-linear *WSE-Q_{TARGET}* curve on Fig. 5.7 represents the flow rate that can be sustained over winter, based on historical operations and conditions in Lake Winnipeg. The asymptotic nature of this curve suggests that there is an upper limit to the maximum discharge that can be sustained during winter, even at the high-end range of Lake Winnipeg regulation (i.e., 217.93 m).

5.4.2.3 Step (d): Forebay drawdown

Given an open-water scenario with a constant WSE_{LW}, WSE_{FB} remains constant under steady discharge conditions. In contrast, the presence of an ice cover requires the continual drawdown of WSE_{FB} to compensate for increasing ice-induced head losses. As described by Lees et al. (submitted), the rate of forebay drawdown (DD_R [m day^{-1}]) can be reasonably approximated using WSE_{LW} and Q_{TARGET}, as summarized in OLA-specific regression functions (years 1984-2018, excluding 2003) (Eq 5-3).

$$DD_R = \begin{cases} 0.03, & Q_{TARGET} \leq 1{,}982\ m^3\ s^{-1} \\ 0.28WSE_{LW}^{\ 2} - 120.47WSE_{LW} + 13113.00, & Q_{TARGET} = 2{,}265\ m^3\ s^{-1} \\ 0.56WSE_{LW}^{\ 2} - 245.23WSE_{LW} + 26693.87, & Q_{TARGET} = 2{,}549\ m^3\ s^{-1} \\ 0.61WSE_{LW}^{\ 2} - 264.41WSE_{LW} + 28818.69, & Q_{TARGET} = 2{,}832\ m^3\ s^{-1} \\ 0.92WSE_{LW}^{\ 2} - 402.10WSE_{LW} + 43836.17, & Q_{TARGET} = 3{,}114\ m^3\ s^{-1} \\ 222.57 - WSE_{LW}, & Q_{TARGET} > 3{,}114\ m^3\ s^{-1} \end{cases} \quad \text{Eq 5-3}$$

Note that coefficients in Eq 5-3 were shortened to two decimal places for brevity. DD_R was used to adjust WSE_{FB} until ΔH_{TOT} (i.e., hydraulic head from Lake Winnipeg to Jenpeg) reached ΔH_{TARGET}, from which point onward the forebay level was considered steady at a minimum operating level. It is noted that in some cases the forebay may never reach its minimum operating level, due to high lake levels and/or low ice impacts, and in these cases the flow target will be sustained throughout winter without decline.

5.4.2.4 Step (e): Discharge decline

Once WSE_{FB} reaches a minimum operating level, Jenpeg operators can no longer compensate for increasing head losses to encourage outflow from Lake Winnipeg. From this point onwards, Lake Winnipeg outflow begins to decline. For years with high WSE_{LW} and modest ice restrictions, discharge decline will be small, compared to

higher rates of discharge decline that will be experienced with lower WSE_{LW} and severe ice restrictions. To make up for the lack of a numerical model to calculate the cumulative effects of WSE_{LW} and ice restrictions on discharge decline, a multiple linear regression (MLR) was employed for ERIA.

MLR is justified as a suitable technique for this task, as it allows for use of multiple independent predictor variables. Predictor variables selected and a brief justification for their inclusion are summarized as follows:

1) **X_1** or **$|\Delta WSE_{LW}|$ [m]:** X_1 represents the net change in lake level over the discharge decline period (i.e., $t_{start,DD}$ to t_{WM}). This reflects changes in Lake Winnipeg storage and subsequent effect on hydraulic head across the OLA, as this energy gradient drives Lake Winnipeg outflow. Historical observations indicate significantly less discharge decline in the case of a net Lake Winnipeg level increase (i.e., net rise in lake level over winter), compared to the case of a net Lake Winnipeg level decrease (i.e., net fall in lake level over winter).
2) **X_2** or **Number of days where $T_{MIN} \leq$ -15°C [-]:** Following ice cover formation at freeze-up, the open-water areas that remain in the OLA are characterized by high flow velocities ($\geq$ 1 m s^{-1}). These rapid sections are located mainly at channel confluences and constrictions; regions that have a strong influence on river hydraulics. Ice volumes generated in these open-water sections result in formation of under-ice obstructions that increase head losses through winter. As flow velocities increase, greater heat loss is required to generate supercooled conditions at the river surface for skim ice floe formation (Lees et al., 2021b; Matoušek, 1984b). A visual assessment of hydrometric records and mid-winter satellite imagery indicates that skim ice floes comprise a significant portion of the total ice volume that supplies under-ice obstructions. Further comparison of these images with air temperature records shows that the presence of skim ice floes (also termed as a *skim ice run*) is coincident with sufficiently cold temperatures ($T_{MIN} \leq$ -15°C; as determined by calibration of X_2). While thermal thickening of surface ice covers can still occur when $T_{MIN} >$ -15°C, effect of this thicker ice

on hydraulics is less significant than that of under-ice deposits near rapid areas.

3) X_3 or WSE_{LW} **at** t_{FO} **[-]:** WSE_{LW} at the onset of freeze-up, and the associated Q_{TARGET}, also has some influence on the magnitude of discharge decline.

Historical observations selected for MLR are shown on Fig. 5.8, including partition between groups where net WSE_{LW} rise and net WSE_{LW} fall were observed.

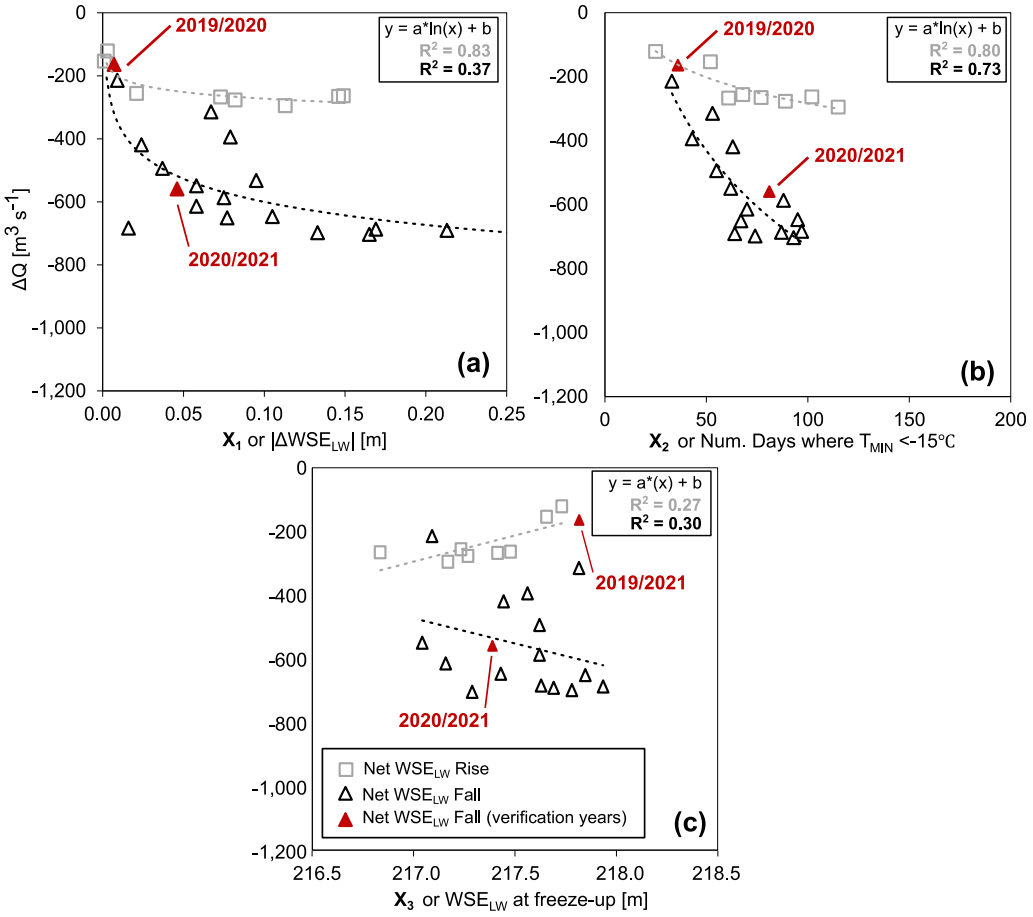

Fig. 5.8 - Hydro-meteorological variables: (a) X_1, (b) X_2, (c) X_3 selected for MLR to predict ΔQ. Datasets comprise select years from 1984 to 2018.

Years were excluded from MLR shown on Fig. 5.8 include: 1997, 1998, 1999, 2003, 2006, 2011, 2012, 2013 and 2016. The reason for these exclusions was either that the period of flow decline was too short, or manipulations of mid-winter forebay water levels affected the accuracy of flow decline estimates. As a result, these select observations were not considered to be comparable to other years. Resulting MLR equations for net WSE_{LW} rise and fall cases are shown in Eq 5-4 and Eq 5-5, respectively (limited to two decimal places for brevity).

$$\Delta Q = 111.956X_1 - 2.21X_2 + 70.93X_3 - 15499.37 \quad \text{Eq 5-4}$$

$$for\ net\ WSE_{LW}\ rise\ (R^2 = 0.79)$$

$$\Delta Q = -1168.12X_1 - 4.25X_2 + 3.84X_3 - 1000.18 \quad \text{Eq 5-5}$$

$$for\ net\ WSE_{LW}\ fall\ (R^2 = 0.73)$$

5.4.2.5 Approach Verification

To evaluate the predictive strength of the ERIA methodology, ERIA results were compared to winter flows calculated using the *historical ice-factor* (IF_{HIST}), which is effectively the current benchmark for ice forecasting in the OLA. The OLA ice-factor is defined as the ratio of equivalent discharge calculated using open-water rating curves and ice-impacted water levels (Q_{O-W}), to observed ice-affected discharge (Q_{OBS}):

$$IF_{OBS} = \frac{Q_{O-W}}{Q_{OBS}} \qquad \text{Eq 5-6}$$

In plain language, the IF can be interpreted as a unitless measure of the severity of ice impacts on Lake Winnipeg outflow conveyance, with a higher ice factor indicating more severe ice impacts. IF_{HIST} represents typical ice conditions based on observed data (1984-2018) and takes the form of a daily time-series that relies on a single independent variable (i.e., day-of-year). To properly evaluate performance of ERIA, the methodology was applied to produce a discharge and ice factor time-series (Q_{ERIA} and IF_{ERIA}, respectively) for each historical year (1984-2020) using Eq 5-7.

$$IF_{ERIA} = \frac{Q_{O-W}}{Q_{ERIA}} \qquad \text{Eq 5-7}$$

As shown on Fig. 5.8, hydro-meteorological conditions in winter 2019/2020 were almost outside the range of data used for MLR, while conditions in winter 2020/2021 were closer to the middle of the range of regression data. IF_{HIST} and IF_{ERIA} were compared to IF_{OBS} using three performance metrics: percent bias (PBIAS), Nash-Sutcliffe efficiency (NSE), and mean absolute error (MAE), as shown in Eq 5-8(a-c).

$$PBIAS = \frac{\sum_{i=1}^{n}\left(IF_{OBS}^{i} - X\right)}{\sum_{i=1}^{n}\left(IF_{OBS}^{i}\right)} \qquad \text{(a)} \qquad \text{Eq 5-8}$$

$$NSE = 1 - \frac{\sum_{i=1}^{n}\left(IF_{OBS}^{i} - X\right)^2}{\sum_{i=1}^{n}\left(IF_{OBS}^{i} - \bar{Y}\right)^2} \quad \text{(b)}$$

$$MAE = \frac{\sum_{i=1}^{n} |IF_{OBS}^{i} - X|}{n} \quad \text{(c)}$$

where X = *either* IF_{ERIA}^{i} *or* IF_{HIST}^{i}

and Y = *either* IF_{ERIA} *or* IF_{HIST}

These metrics were chosen based on their suitability for evaluating the performance of water resources models (Moriasi et al., 2007). PBIAS (Eq 5-8a) is a measure of the tendency of simulated data to be larger or smaller than observed data (Moriasi et al., 2007). A perfect value for PBIAS is 0% with a recommended acceptable range of ±25% (2007). NSE (Eq 5-8b) is a normalized statistic that compares relative magnitudes of residual variance to measured data variance, and indicates how well simulated and observed data fit a 1:1 line (2007). A perfect value of NSE is 1, with a recommended range of > 0.5 (2007). Lastly, MAE (Eq 5-8c) is a widely-applied metric for model evaluation that indicates average absolute deviation of simulations from observed data. The recommended range for MAE will vary between variables.

By comparing the predictive power of IF_{ERIA} and IF_{HIST} using PBIAS, NSE and MAE, IF_{ERIA} outperforms IF_{HIST} for 72%, 67% and 69% of historical years, respectively (Fig. 5.9).

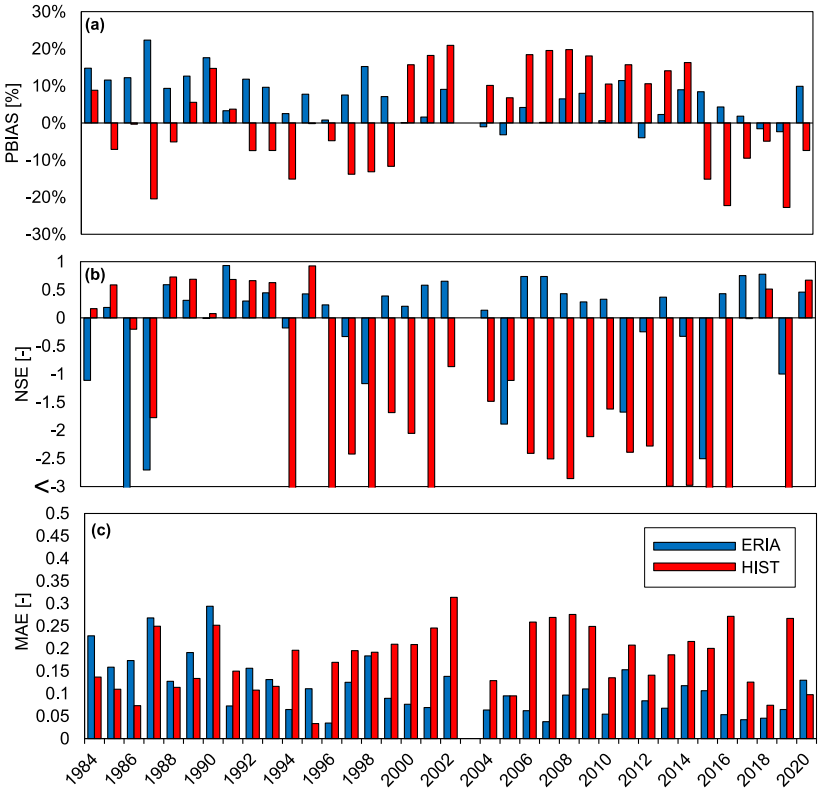

Fig. 5.9 - Comparison of IF_{ERIA} and IF_{HIST} to IF_{OBS} using (a) PBIAS, (b) NSE and (c) MAE.

While this majority result weighs in favour for selection of ERIA over IF_{HIST}, even stronger performance is hindered by uncertainty in the *WSE*-Q_{TARGET} curve (see Fig. 5.7). This is especially apparent for older historical years (pre-2000s), where a high positive PBIAS (Fig. 5.9a) indicates that ERIA underpredicts the ice factor, which can be traced back to an overestimation of the discharge target using the *WSE*-Q_{TARGET} curve. To quantify the bias that the *WSE*-Q_{TARGET} curve contributes, ERIA calculations were repeated without this curve, and instead Q_{TARGET} was assigned based on observed values for each historical year. Effectively, this approach accounts for the numerous year-specific conditions that inform selection of Q_{TARGET} that cannot be represented by a single curve. The improved performance of ERIA by manually assigning Q_{TARGET} is shown on Fig. 5.10.

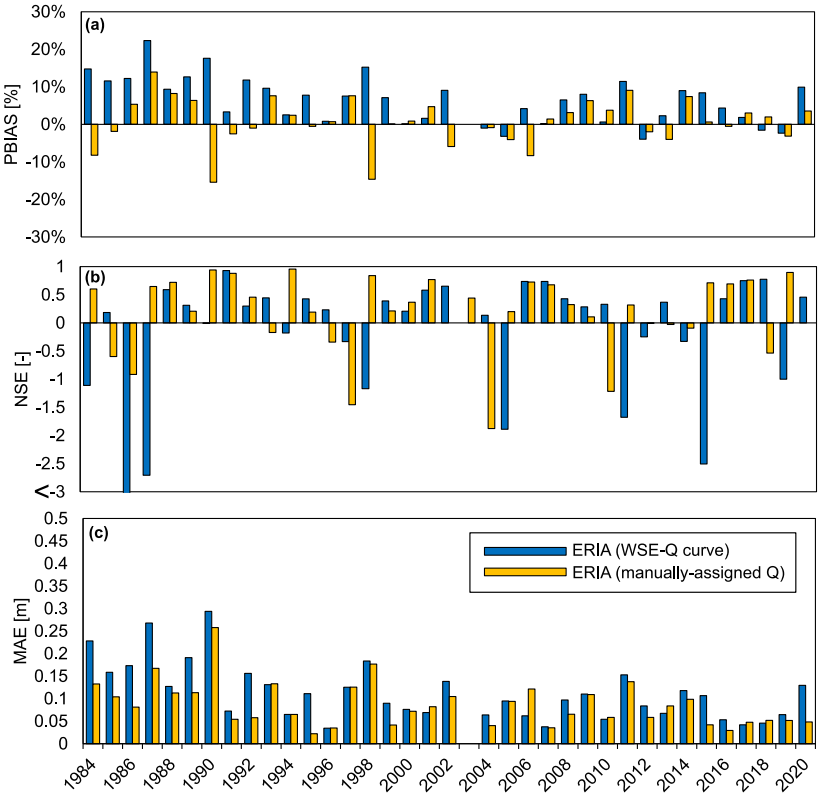

Fig. 5.10 - Comparison of ERIA using different discharge target approaches for (a) PBIAS, (b) NSE and (c) MAE.

After applying ERIA results using a manually assigned Q_{TARGET} to update MAE, NSE and PBIAS statistics, IF_{ERIA} outperforms IF_{HIST} for 94%, 86% and 83% of years, respectively. This suggests that by improving the means of Q_{TARGET} estimation, ERIA performance could be improved. Regardless, considering that the same $WSE\text{-}Q_{TARGET}$ curve is applied for all REF, n-FUT and f-FUT winters, the approach is appropriate for evaluating relative changes despite its limitations in reflecting observed conditions.

5.4.3 Post-Processing and Statistical Analysis

By combining steps (a) through (e) in Section 5.4.2, ERIA was applied to calculate the following hydraulic variables:

1) *Winter discharge decline* (ΔQ), which represents a change in Lake Winnipeg outflow over winter from t_{FO} to t_{WM}.

2) *Normalized winter discharge decline* ($\Delta Q/\Delta t$), which represents the change in Lake Winnipeg outflow standardized by *winter duration* (Δt).

These two variables represent a primary contribution of this study, as they reflect the cumulative effect of ice severity and hydraulic system operations on flow conveyance. Additional winter-specific variables (Table 5.5) were selected for inter- and intra-period evaluation of REF, n-FUT and f-FUT years.

Table 5.5 - Study variables of interest

Variable	Equation (if applicable)	Equation Reference (if applicable)	Units	Description
ΔQ	$Q_{FINAL} - Q_{TARGET}$	(1)	[$m^3 s^{-1}$]	winter discharge decline
Δt	$\lvert t_{WM} - t_{FO} \rvert$	(2)	[day]	winter duration
$\Delta Q/\Delta t$	$\frac{Q_{FINAL} - Q_{TARGET}}{\lvert t_{WM} - t_{FO} \rvert}$	(3)	[$m^3 s^{-1}$ day^{-1}]	normalized winter discharge decline
$CDDF_{TOT}$	$\sum_{DOY=DOY_{FO}}^{DOY_{WM}} (0℃ - T_{AIR}^{DOY})^{+}$ $where\ X^{+} = MAX(X, 0)$	(4)	[℃-day]	total CDDF over winter
DY_{WM}	$\frac{1}{\Delta t} \sum_{DOY=93}^{DOY_{WM}} \lvert T_{AIR}^{DOY} \rvert\ if\ (T_{AIR} > T_{WM})$	(5)	[℃-day]	number of mid-winter warming days (January 1st to DOY_{WM})
$T_{AIR_{JAN}}$	$\frac{1}{31} \sum_{DOY=1}^{31} T_{AIR}^{DOY}$	(6)	[℃]	average January air temperature
$h_{SOG\,mean}$	$\frac{1}{\Delta t} \sum_{DOY=DOY_{FO}}^{DOY_{WM}} h_{SOG}^{DOY}$	(7)	[m]	average snow-on-ground
$h_{SOG\,max}$	$max(h_{SOG}^{DOY_{FO}}, \dots, h_{SOG}^{DOY_{WM}})$	(8)	[m]	maximum snow-on-ground
DOY_{FO}	N/A	N/A	[-]	nth day of freeze-up onset relative to October 1st
DOY_{BO}	N/A	N/A	[-]	nth day of warming onset relative to October 1st

Notes:
N/A = not applicable

5.4.3.1 Statistical Tests and Techniques

Several statistical tests and techniques were selected for inter- and intra-period comparison of REF, n-FUT and f-FUT datasets. This study focuses exclusively on non-parametric tests and techniques, which have high utility considering they do not require knowledge of the data's parent distribution (Totaro et al., 2020). The Mann-Whitney-Wilcoxon U (MWW) test (Mann and Whitney, 1947) was chosen to identify statistically significant changes in n-FUT and f-FUT populations relative to REF populations. A comparison of n-FUT and f-FUT populations was excluded because one-third of these datasets overlap (Table 5.4). The assumptions of the MWW test are that the datasets are both independently sampled and unbiased, which are assumptions satisfied for the variables in Table 5.5. The Mann-Kendall (M-K) test (Kendall, 1975; Mann, 1945) was selected to identify statistically significant trends within REF, n-FUT and f-FUT populations. To accompany the M-K test, the Theil-Sen estimator of Sen's slope (*SS*; Sen, 1968) was selected to quantify the magnitude and direction of non-parametric trends. Unless otherwise stated, MWW and M-K tests were performed using a two-sided approach with a 5% significance level (95% confidence interval).

The aforementioned non-parametric tests were conducted through both *simulation-specific* and *ensemble-based* analyses. Simulation-specific analyses were performed for each of the 19 climate scenarios individually, while an ensemble-based analysis applied data from all climate simulations together. Statistical significance in ensemble-based calculations was determined through hypothesis testing using a *probability value* ($p_{ensemble}$). Similarly, hypothesis testing was applied to identify statistical significance in simulation-specific calculations, with the additional calculation of a *significance proportion* (P_{sig}). P_{sig} represents the proportion of climate simulations that yielded a statistically significant result, which quantifies the degree to which climate simulations are in agreement on a particular projection. Two additional statistical metrics were added to quantify variability within study datasets. The metric a*verage absolute deviation* (*AAD*; Eq 5-9), which serves as a non-parametric alternative to standard deviation, was chosen to evaluate variability:

$$AAD = \frac{1}{n}\sum_{i=1}^{n} |y_i - (SS_Y x_i + b_Y)| \quad \text{Eq 5-9}$$

where Y is the response variable data of interest, y_i is the value of Y at index i, and SS_Y and b_Y are the Sen's slope and estimated intercept of Y, respectively. Note that Eq 5-9 incorporates de-trending of datasets to exclude influence of inter-annual trends on quantities of variability. Considering the Theil-Sen estimator does not provide a y-intercept (b), this was estimated using Eq 5-10 (Granato 2006; Conover 1980).

$$b_Y = Y_{MED} - (SS_Y)(X_{MED}) \quad \text{Eq 5-10}$$

where Y_{MED} is the median value of the response variable, and X_{MED} is the median value of the explanatory variable (i.e., year). The metric *interquartile range* (*IQR*) was selected as a robust metric to quantify variability within each year of ensemble-based calculations, based on the 75th and 25th percentile values of the response variable (Y) (Eq 5-11).

$$IQR = Y_{75th} - Y_{25th} \quad \text{Eq 5-11}$$

Results from ensemble-based analyses were assessed as an indication of statistically significant shifts and trends, while P_{sig} values were translated to a measure of likelihood. Using categories defined by the Intergovernmental Panel on Climate Change (Bush and Lemmen, 2019; IPCC, 2013) , likelihood categories were defined as follows: *virtually certain*: $P_{sig} \geq 99\%$; *very likely:* $99\% > P_{sig} \geq 90\%$; *likely:* $90\% > P_{sig} \geq 50\%$; *about as likely as not*: $50\% > P_{sig} \geq 33\%$; and *unlikely*: $P_{sig} < 33\%$. By combining statistical significance and likelihood, confidence colour coding was applied (Table 5.6) to categorize outcomes from not statistically significant (white) to statistically significant with a large degree of likelihood (green).

Table 5.6 - Confidence criteria (green through red) for trend and difference results based on ensemble statistical significance and likelihood classification.

Ensemble-Based Criteria	Simulation-Specific Criteria	Statistical Significance	Likelihood	Projection Confidence
$p_{ensemble} < 0.05$	$P_{sig} > 50\%$	statistically significant	more likely than not' to 'virtually certain	High (green)
$p_{ensemble} < 0.05$	$33\% < P_{sig} \leq 50\%$	statistically significant	about as likely as not	Moderate (yellow)
$p_{ensemble} < 0.05$	$0\% < P_{sig} \leq 33\%$	statistically significant	unlikely	Low (orange)
$p_{ensemble} \geq 0.05$	N/A	not statistically significant	N/A	N/A (white)

Notes:

N/A = not applicable

5.4.3.2 Ellipse Calculations

In addition to the statistical tests described in Section 5.4.3.1, confidence ellipses were employed as a visualization of shifts in $\Delta Q/\Delta t$. Formal definitions of these shapes vary in the literature, however, they are generally described as an oval region developed for two-variable datasets that encompasses approximately 95% of the data (Alexandersson, 2004). The size and skew of these ellipses provides a visualization of variability. An example of ellipse calculation and plotting is shown on Fig. 5.11.

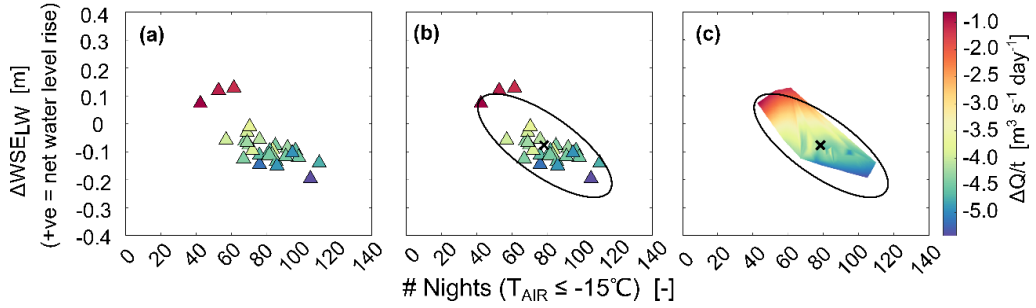

Fig. 5.11 - Derivation of a 95% confidence ellipse using the two dominant variables from MLR (Fig. 5.8). Steps include (a) calculation of $\Delta Q/\Delta t$, (b) ellipse bound and centroid definition, and (c) $\Delta Q/\Delta t$ interpolation and data extraction.

The two parameters selected for ellipses calculations are those with strong correlation to ΔQ (X_1 and X_2 on Fig. 5.8). Following calculation of these oval bounds and centroids (Fig. 5.11b), a thin-plate spline interpolation was applied to generate a surface for extraction of a centroid value. This procedure was repeated using REF, n-FUT and f-FUT winters from each climate simulations. The confidence ellipse technique is complementary to more rigorous statistical tests and provides qualitative descriptions to accompany quantitative discussions of significance.

5.4.3.3 Box-Whisker Plots

Box-whisker plots are a useful tool to visualize the spread and centres of a dataset. Unless otherwise stated, the centre value of the box-whisker plots represents the median value of the dataset. The bounds of the box represent the 25th and 75th percentiles, while the ends of the whiskers represent the minimum and maximum value. Outliers are included within these box-whisker plots.

5.4.4 Numerical Discharge Simulation

In Section 5.4.2, an empirical approach is described that allows for computationally efficient calculations that yield expansive datasets for ensemble-based analyses. In addition to ERIA, winter flow conveyance can also be quantified using a numerical modelling approach. This approach involves adapting a previously-developed tool to quantify the impacts of ice on OLA hydraulics using a combination of numerical and

statistical tools (described in Section 5.3.4 and by Lees et al. submitted). This adapted approach is referred to hereon as CRIM.

5.4.4.1 Representative Winter Selection

In lieu of applying CRIM to all REF, n-FUT and f-FUT winters, a subset of winters were selected for evaluation. These winters were selected by creating a histogram of freeze-up WSE_{LW} for all REF (1981-2010) and FUT (2021-2070) winters in bin increments of 10 cm (Fig. 5.12).

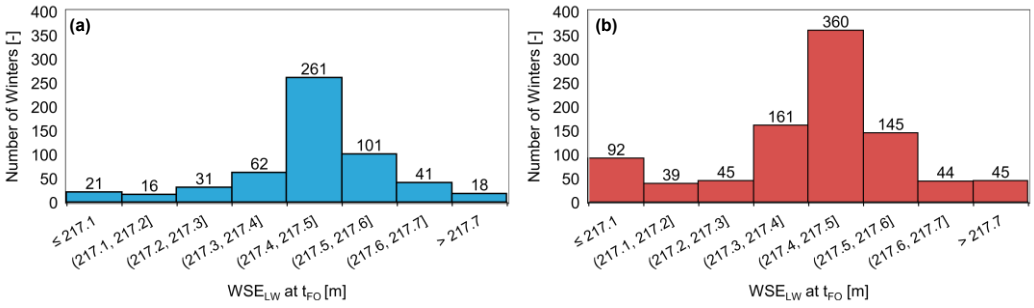

Fig. 5.12 - Histograms of WSE_{LW} at freeze-up (t_{FO}) for (a) REF (1981-2010) winters and (b) FUT (2021-2070) winters.

The upper (UB) and lower bounds (LB) of the histogram (217.1 m and 217.7 m, respectively) were selected such that approximately 90% of winters were accounted for in both REF and FUT periods. Using ERIA calculated values of ΔQ, three representative winters were selected within each bin for a total of 36 winters. These 36 winters (see *Strategic CRIM Runs* on Fig. 5.13) represent 'large', 'moderate' and 'small' ΔQ cases, as shown relative to the box-whisker plots on Fig. 5.13.

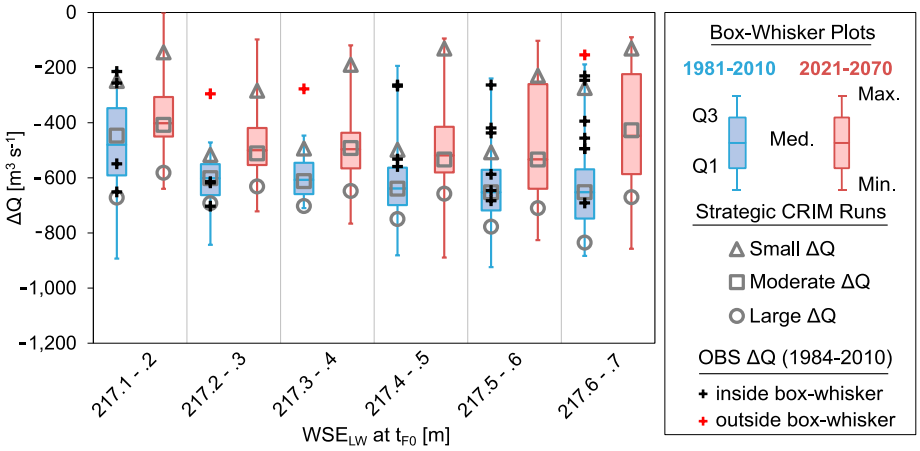

Fig. 5.13 - Comparison of ERIA ΔQ box-whisker plots and observed ΔQ. Winters selected for CRIM simulation ('small', 'moderate' and 'large') based on ERIA ΔQ results are shown.

Note that OBS markers are also included for ground-truthing purposes. Winters selected for CRIM runs represent 2.4% of the total 1520 winters that comprise REF and FUT ensembles. As summarized in the testing matrix (Table 5.7), CRIM runs represent winters from all but one climate simulation (A13r41).

Table 5.7 - Testing matrix of CRIM runs. 'Small', 'moderate', and 'large' ΔQ runs are represented by triangles, squares and circles, respectively for REF (blue) and FUT (red) periods.

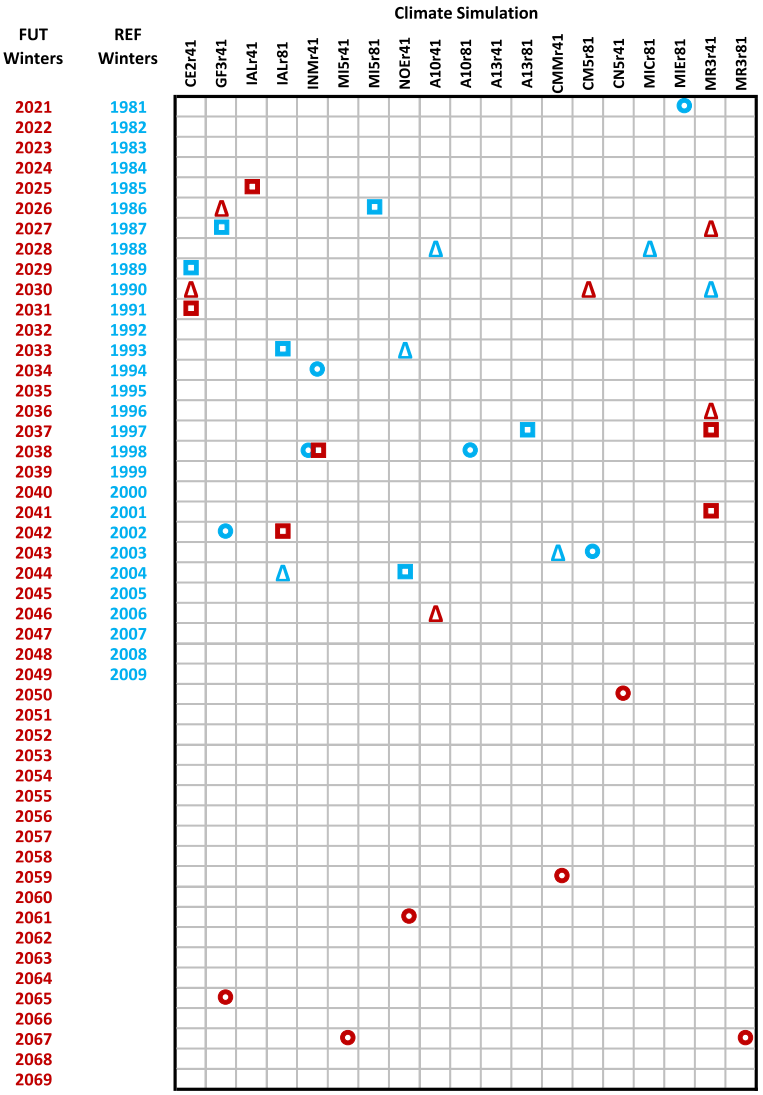

As shown on Fig. 5.14, contributions of cold conditions (predictor variable X_2 on Fig. 5.8) and WSE_{LW} variation (predictor variable X_1 on Fig. 5.8) to discharge decline vary between selected REF and FUT winters.

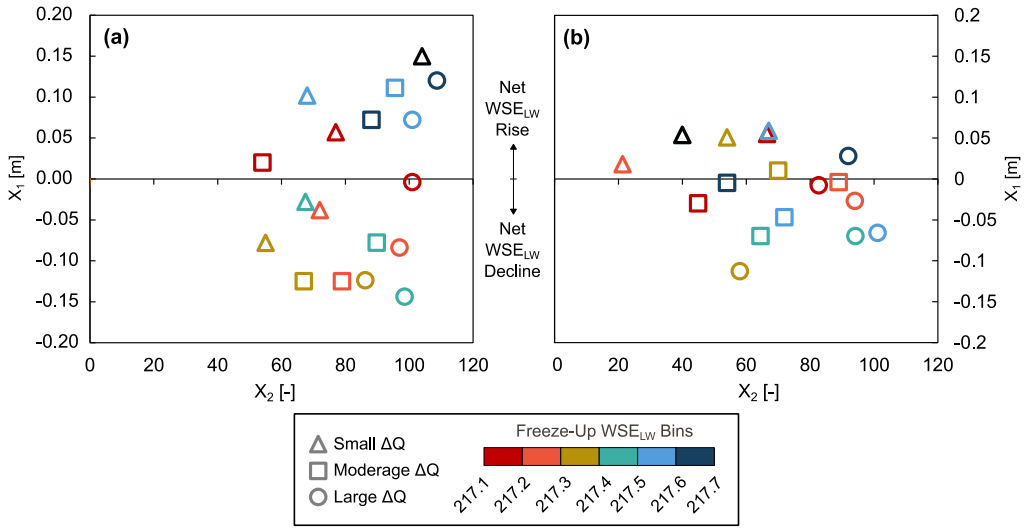

Fig. 5.14 - Contributions of X_1 and X_2 to ΔQ for CRIM runs within each WSE_{LW} bin for (a) REF and (b) FUT periods.

While the range of anticipated discharge decline is appropriate using the selected 36 climate simulations, the dominance of variables X_1 and X_2 should be considered when evaluating results. While a complete ensemble of CRIM runs would be optimal, this strategic approach allows for a narrowing of the number of runs, while still providing data for comparison between ERIA and CRIM.

5.4.4.2 Model Configuration

Conversion of data sources to input files and configuration of the numerical model were pre-requisite steps for CRIM runs. A schematic of these pre-processing steps is shown on Fig. 5.15, and is discussed in detail throughout later sections.

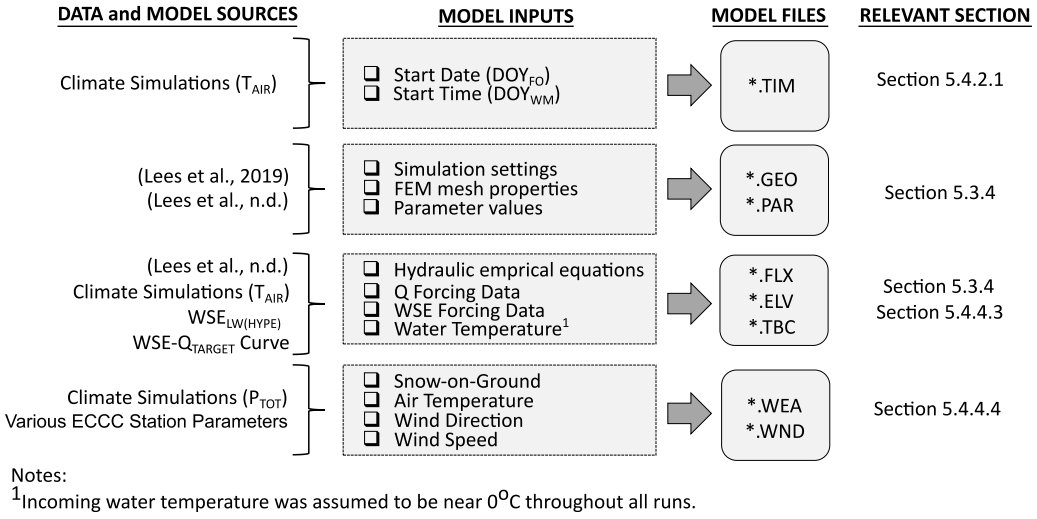

Fig. 5.15 - Creation of model input files for CRIM runs.

The duration of each simulation (specified in the *.TIM file) was determined by the start date (DOY_{FO}) and end date (DOY_{WM}) of winter. Properties describing the model domain, parameter values, and other settings (specified in *.GEO and *.PAR files) are described in previous works (Lees et al. 2019; submitted). Procedures followed to generate hydro-meteorological forcing datasets for each winter are described in Sections 5.4.4.3 and 5.4.4.4.

5.4.4.3 Hydrologic Model Inputs

CRIM simulations required assignment of discharge (*.FLX file), water level (*.ELV file) and water temperature datasets (*.TBC). The detailed configuration of these boundaries with accompanying justifications is discussed in detail by Lees et al. (submitted). Discharge values were assigned based on Q_{TARGET}, which was calculated using the $WSE\text{-}Q_{TARGET}$ curve on Fig. 5.7. $WSE_{LW(HYPE)}$ at t_{FO} was sourced as input to this curve and was applied without adjustment. Local WSE datasets for model forcing were generated using the methodology described in Lees et al. (submitted), which employed a combination of backwater algorithms and site-specific rating curves. Water temperature assigned at upstream boundaries was assumed to be slightly above zero (0.05°C) for the duration of all simulations, as unsteady water temperature data were unavailable. This assumption is justified based

on historical water temperature records, which indicates that mid-winter water temperatures throughout the OLA are close to 0°C.

5.4.4.4 Meteorological Data Inputs

In the absence of complete weather datasets, CRIM's thermal calculations were performed using four meteorological inputs variable: T_{AIR}, snow-on-ground (h_{SOG}), wind direction (w_{dir}), and wind magnitude (w_{mag}).

As discussed in Section 5.3.3, T_{AIR} was available for all climate simulations in the form of daily maximum and daily minimum time-series. Instead of applying an average daily time-series of T_{AIR}, which would be an oversimplification of hourly conditions, an hourly time-series of T_{AIR} was derived for each winter to better reflect the diurnal patterns of this variable. An adapted version of the *WAVE* algorithm described by Reicosky et al. (1989) was selected for this task, based on *WAVE*'s performance relative to other T_{AIR} conversion approaches. An example of this conversion is shown on Fig. 5.16 for the early winter period.

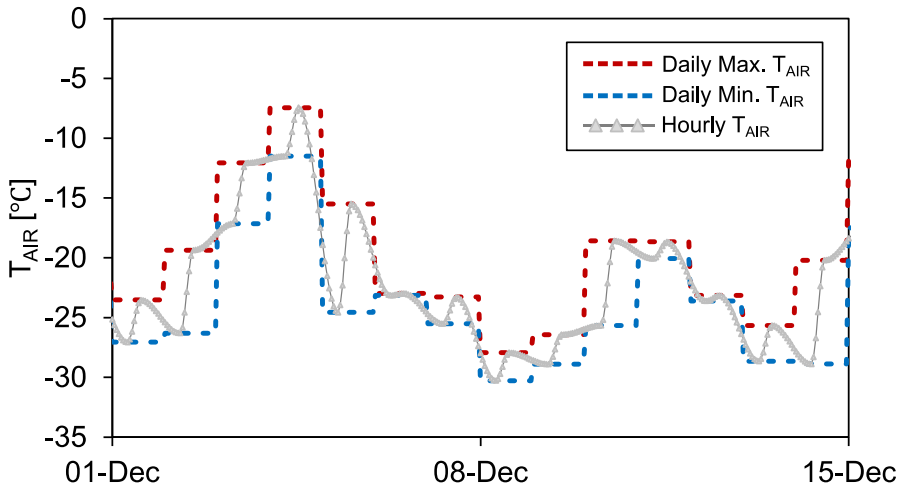

Fig. 5.16 - Visualization of hourly air temperature derived from daily max. and min. air temperature. Conversion algorithm adapted from the *WAVE* method (Reicosky et al., 1989).

The *WAVE* approach requires a complete maximum and minimum T_{AIR} time-series for conversion, as the minimum T_{AIR} for day *n* is required for day *n-1* calculations. Key assumptions of the approach include that maximum T_{AIR} occurs at 14:00 and

minimum T_{AIR} occurs at sunrise. Sunrise hours were calculated using the solar radiation equations described in CRISSP2D documentation (Liu and Shen, 2011).

Also mentioned in Section 5.3.3 is the availability of daily precipitation (P_{TOT}) from climate simulations, which requires conversion before application in CRIM. Numerical model calculations over winter require a time-series of h_{SOG}, which is adjusted during simulations based on the weight-bearing capacity of the ice cover. This snow-on-ground layer, or more accurately snow-on-ice layer, serves to attenuate thermal growth and decay of the cover. Considering that P_{TOT} was not partitioned into snow and rain amounts, conversion of P_{TOT} to h_{SOG} required conversion using multiple equations and accompanying calibrated coefficients. By expressing P_{TOT} in units of [kg m^{-2}], P_{TOT} is converted to cumulative snow (P_{SNOW}) using Eq 5-12 (Beltaos, 2013):

$$P_{SNOW} = \frac{100 P_{TOT}}{\rho_s} \qquad \text{Eq 5-12}$$

where ρ_s is snow density [kg m^{-3}]. P_{SNOW} was converted to h_{SOG} with additional adjustments to account for changing snow density and melt. As snow depth increases, so does the density of the snowpack, which is accounted for using the adjustment in Eq 5-13 (Beltaos, 2013):

$$\rho_s = R_{SNOW} - \frac{204.7}{h_{SOG}}\left[1 - e^{-\frac{h_{SOG}}{0.67}}\right] \qquad \text{Eq 5-13}$$

where R_{SNOW} is a regional snow coefficient [mm]. The other correction is to account for daily melt (M), which is estimated using a measure of deviation from the melting point of snow (T_M) and a melt coefficient (C_m). This daily melt was calculated using Eq 5-14 (United States Department of Agriculture, 2004).

$$M = C_m[T_{AIR} - T_M] \qquad \text{Eq 5-14}$$

Parameters T_M and C_m were calibrated using a historical time-series (1980-2010) of $P_{TOT(OBS)}$ and $h_{SOG(OBS)}$ obtained from ECCC station Thompson Airport [ID: 5062922]. This calibration process involved Eq 5-12 through Eq 5-14, whereby

parameters T_M and C_m were adjusted while converting $P_{TOT(OBS)}$ to $h_{SOG(CALC)}$, and minimizing the objective function SAE through comparison with $h_{SOG(OBS)}$. An example of the final calibration of a typical winter is shown on Fig. 5.17.

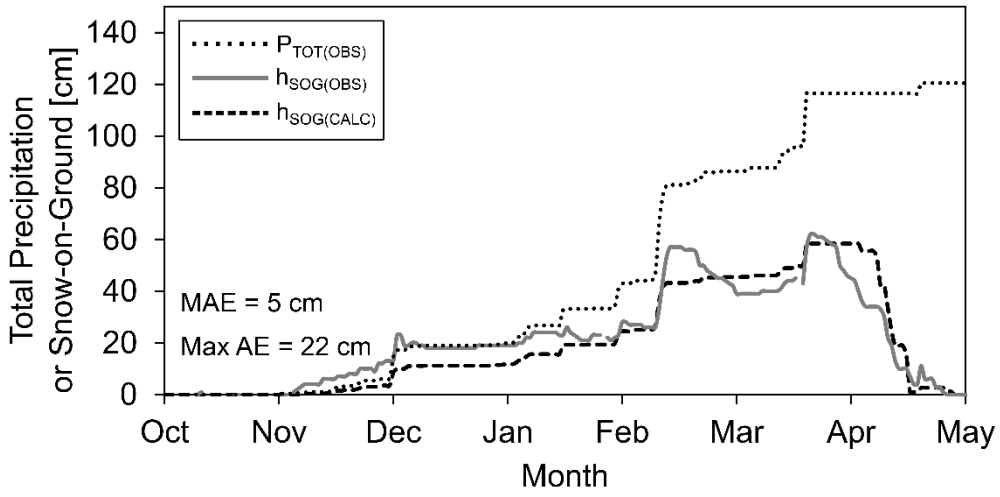

Fig. 5.17 - Comparison of $h_{SOG(OBS)}$ with $h_{SOG(CALC)}$ calculated using $P_{TOT(OBS)}$.

Calibrated values for T_M and C_m were found to be 0°C and 7 mm °C^{-1}, respectively. This calibrated value for C_m is close to the typical range of 1.6 to 6 mm °C^{-1} (United States Department of Agriculture, 2004), while 0°C is a reasonable value for a base temperature. It is noted that many of these snow equation variables (particularly C_m) will vary spatially and temporally, thus these values are site-averaged seasonal values.

Lastly, wind direction (w_{dir}) and magnitude (w_{mag}) were required for numerical simulations. Considering these datasets are not available for the 19 climate simulations, historical averaged daily values were applied. Using a historical time-series (1980-2010) of wind data from ECCC station Norway House A [ID: 506B047], a dataset was developed to assign daily w_{dir} and w_{mag} values during simulations (Fig. 5.18).

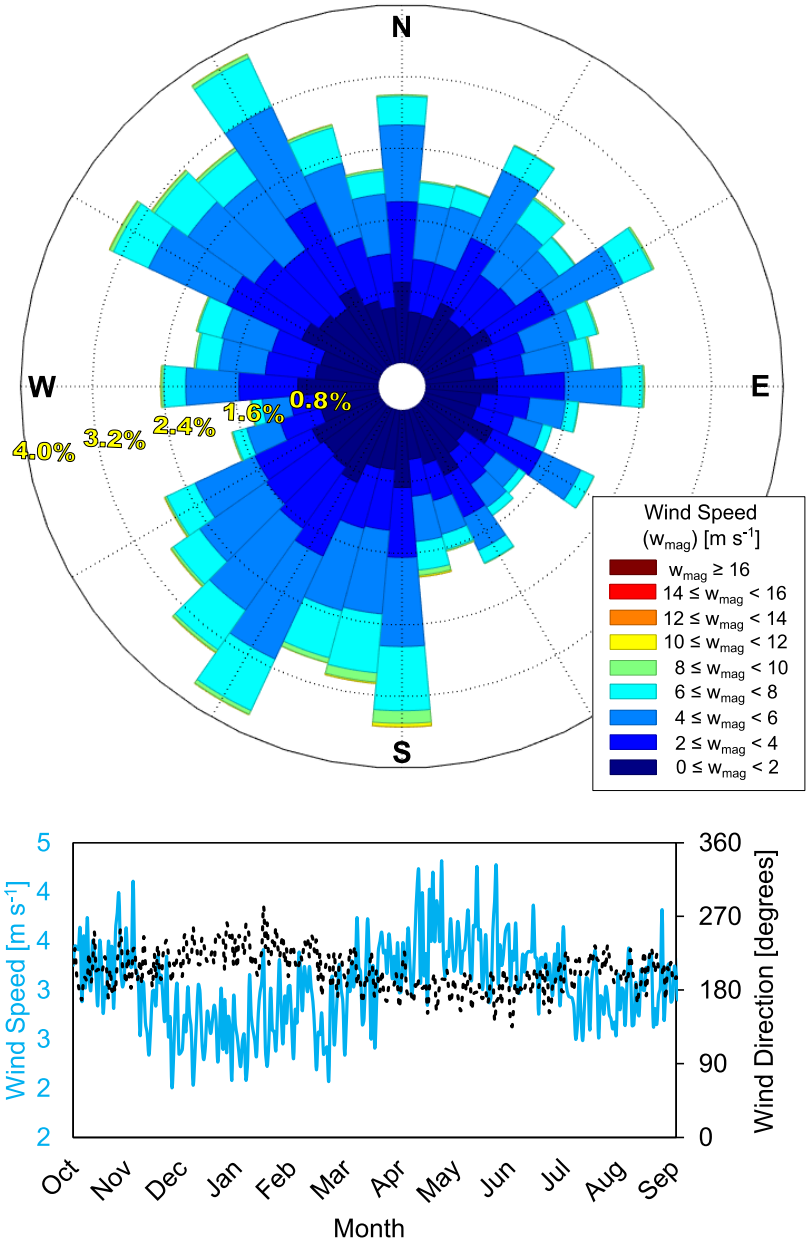

Fig. 5.18 - Wind rose and day-of-year time-series of wind speed (w_{mag}) and wind direction (w_{dir}) using data from ECCC station Norway House A [ID: 506B047].

While w_{dir} and w_{mag} are required inputs for model simulations, the effect of wind on hydraulics during the ice-on period is small. Similarly, the impact of wind uncertainty on thermal and ice dynamic processes is also small. As such, the simplified approach of day-of-year averaging is of low consequence for CRIM runs.

5.5 Results and Discussion

5.5.1 Influence of wet and dry conditions on winter discharge decline

The primary factors influencing winter discharge decline in the OLA include WSE_{LW} conditions and the severity of ice restrictions. These factors are represented by predictor variables X_1 and X_2 in the form of confidence ellipses on Fig. 5.19.

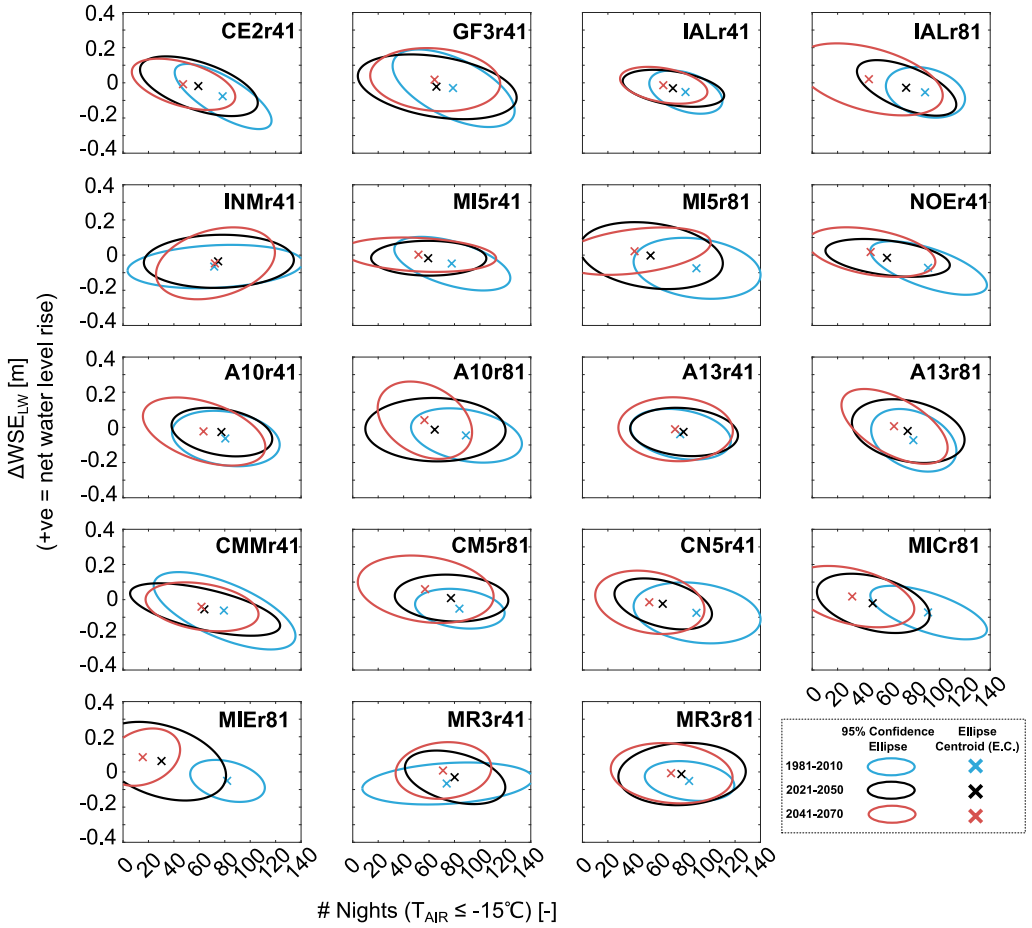

Climate Scenario	1981-2010 vs. 2021-2050		1981-2010 vs. 2041-2070	
	% $\Delta X_{E.C.}$	% $\Delta Y_{E.C.}$	% $\Delta X_{E.C.}$	% $\Delta Y_{E.C.}$
CE2r41	24%	76%	40%	90%
GF3r41	17%	26%	18%	161%
IALr41	12%	41%	22%	74%
IALr81	17%	48%	50%	138%
INMr41	-4%	46%	-1%	28%
MI5r41	24%	63%	34%	105%
MI5r81	40%	97%	54%	129%
NOEr41	35%	79%	50%	124%
A10r41	4%	58%	21%	64%
A10r81	28%	72%	37%	191%
A13r41	-3%	34%	5%	73%
A13r81	6%	72%	19%	109%
CMMr41	19%	11%	22%	35%
CM5r81	8%	118%	32%	217%
CN5r41	30%	69%	41%	80%
MICr81	48%	72%	65%	125%
MIEr81	63%	223%	81%	266%
MR3r41	-8%	54%	4%	112%
MR3r81	7%	77%	17%	86%

Fig. 5.19 - Comparison of 95% confidence ellipses for REF, n-FUT and f-FUT periods. Includes percentage-change of ellipse centroid in both the x- (predictor variable X_2) and y- (predictor variable X_1) directions.

Also included on Fig. 5.19 is an accompanying table with colour gradients indicating the contributions of predictor variables to shifts in ellipse centroids (EC). By projecting an ellipse using these two variables, a graphical shift in EC upwards and to the left represents an inter-period change towards greater Lake Winnipeg storage levels and warmer winter conditions. This shift is apparent across most of the 19 climate simulations, although some simulations project a greater magnitude change relative to others.

Analysis by Kim (2020) highlighted six climate simulations within the ensemble that project the greatest shifts in discharge over time, thus representing the extreme ends of the ensemble range. Kim identified that IALr81, MICr81 and MIEr81 project the greatest future shifts towards lower flows ('dry'), while simulations INRr4, MR3r41 and MR3r81 project the greatest shifts towards higher flows ('wet'). Average annual precipitation and temperature conditions of these 'dry' and 'wet' simulations are shown relative to the complete ensemble on Fig. 5.20.

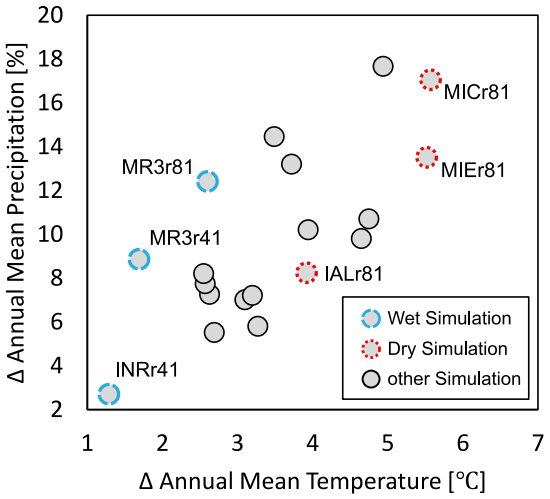

Fig. 5.20 - Identification of 'dry' and 'wet' simulations (from Kim (2020)) in contrast to other simulations in the climate ensemble (figure adapted and modified from Braun et al. 2021).

Further discussion is required to interpret wet and dry simulations in the context of river ice restrictions. As shown on Fig. 5.19, dry simulations are associated with the greatest shift in ellipse centroid, which is reasonable considering that these

simulations project strong increases to average air temperatures. In contrast, a more modest delta-change in air temperature is projected for wet simulations. It is important to note that projections of wet and dry conditions are not a function of precipitation and air temperature alone. Instead, wet and dry conditions are also a function of other hydrologic processes (e.g., evapotranspiration) and the watershed response during hydrologic simulations in the Lake Winnipeg basin.

Further insight is gained from assessing Q_{TARGET} (Fig. 5.21) for wet and dry simulation years (Fig. 5.20), as calculated using the *WSE*-Q_{TARGET} cuve.

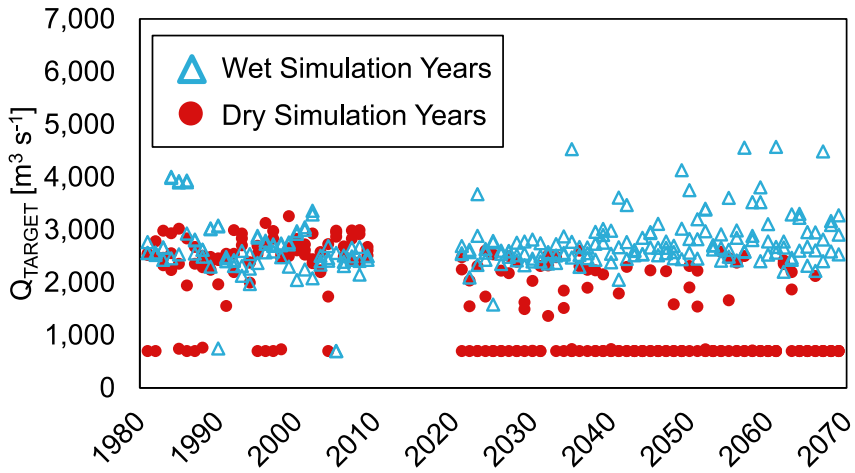

Fig. 5.21 - REF and FUT Q_{TARGET} for wet (INRr4, MR3r41 and MR3r81) and dry (IALr81, MICr81 and MIEr81) simulation years.

There is an evident downward shift in Q_{TARGET} for dry simulations, with an increasing frequency of winters where Lake Winnipeg outflow is at a minimum. MWW test results support this observation, as a statistically significant shift was identified for all three dry simulations (see Section 5.5.2). While an upward shift in Q_{TARGET} is observed for wet simulation years, this shift is more subtle due to the asymptotic nature of the *WSE*-Q_{TARGET} curve at higher lake levels resulting in diminishing increases to Lake Winnipeg outflows. A statistically significant MWW result was identified for only one of three wet simulations (see Section 5.5.2).

When considering changing WSE_{LW} over winter, classifications of 'wet' and 'dry' can lead to counterintuitive conclusions. In the case of dry simulation years, H-

HYPE's discharge equations reduce Lake Winnipeg's outflow to promote storage increase (and subsequent rise in WSE_{LW}) to an acceptable operating range. This rise in WSE_{LW} helps to counteract the hydraulic resistance of OLA ice obstructions, resulting in a smaller $\Delta Q/\Delta t$. In the case of wet simulation years, WSE_{LW} values are generally high and consistent (i.e., minimal net rise or decline), meaning that lake levels have very little influence on $\Delta Q/\Delta t$ in wet years according to ERIA predictor variables (see Fig. 5.8).

By assessing the box-whisker plots on Fig. 5.22, it is evident that dry simulations project larger positive changes to $\Delta Q/\Delta t$ in the future (i.e., less discharge decline).

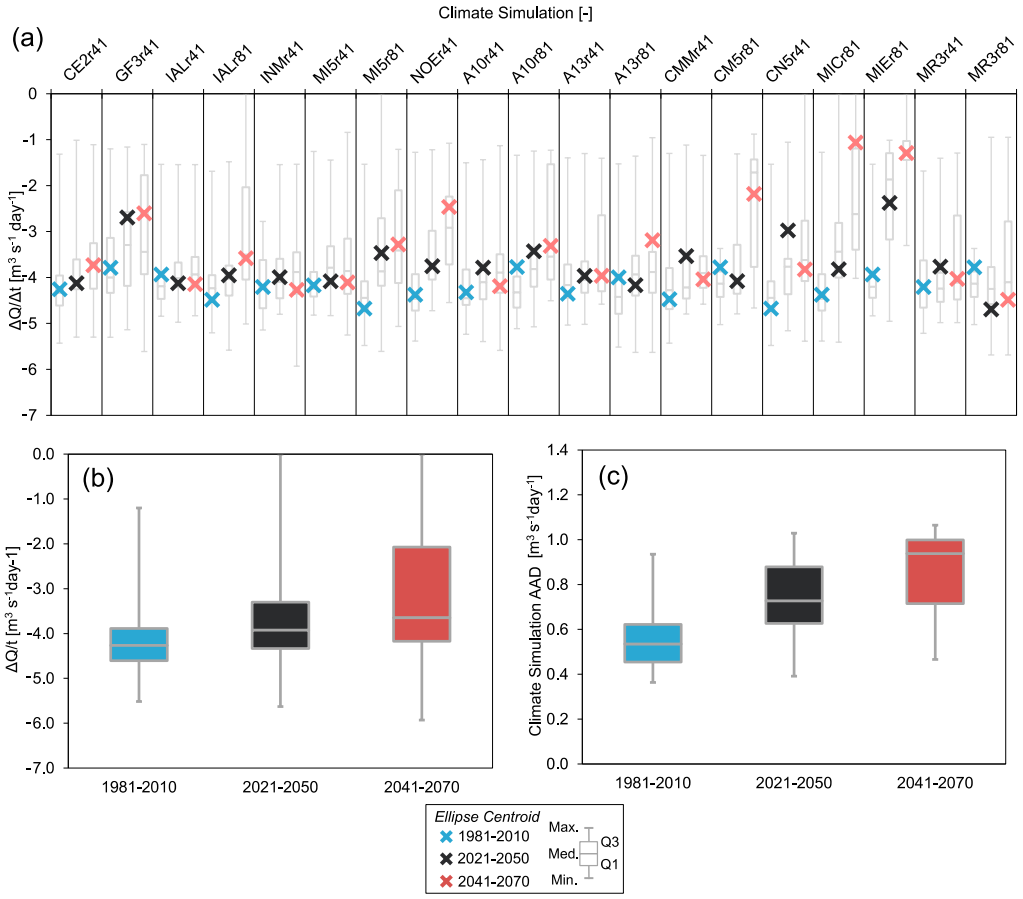

Fig. 5.22 – (a) Climate simulation box-plots (with ellipse centroids); (b) ensemble comparisons of $\Delta Q/\Delta t$ for REF, n-FUT and f-FUT periods; and (c) ensemble comparisons of AAD for REF, n-FUT and f-FUT periods.

On the contrary, wet simulations project more modest changes to $\Delta Q/\Delta t$. It is necessary to note that despite modest projections to changing $\Delta Q/\Delta t$, should wet simulation projections become reality the hydraulic head provided by consistently high lake levels will greatly help to offset ice restriction severity. Results shown on Fig. 5.22 are discussed further in later sections.

5.5.2 Confidence in and likelihood of changing discharge decline in future winters

This study included application of climate simulations selected to represent a wide-range of conditions over the HBDB, although the specific application here is localized to within the NRB. As noted by previous authors (i.e. MacDonald et al., 2018), there is considerable variability among simulation projections. With regards to assessing future changes to $\Delta Q/\Delta t$, this variability is evident by the diversity amongst the 19 sets of $\Delta Q/\Delta t$ box-whisker plots on Fig. 5.22.

An ensemble-analysis of $\Delta Q/\Delta t$ conditions on Fig. 5.22b illustrates statistically significant shifts between REF and both n-FUT ($p < 0.001$) and f-FUT periods ($p < 0.001$). These positive shifts suggest that for the same Q_{TARGET}, cumulative winter discharge will be greater in n-FUT and f-FUT periods relative to the REF period. Using median values from the box-whisker plots on Fig. 5.22b, projected shifts in $\Delta Q/\Delta t$ are +0.3 $m^3\ s^{-1}\ day^{-1}$ and +0.6 $m^3\ s^{-1}\ day^{-1}$ for n-FUT and f-FUT, respectively. Based on P_{sig} values (Table 5.8), these shifts are *about as likely as not* (P_{sig} = 47%) and *likely* (P_{sig} = 68%), for n-FUT and f-FUT periods, respectively.

Table 5.8 - Climate scenario MWW test results for inter-period comparisons of $\Delta Q/\Delta t$.

Climate Simulation	p-value[1]	
	REF vs. n-FUT	REF vs. f-FUT
CE2r41	0.014	<0.001
GF3r41	0.19	0.086
IALr41	0.17	0.04
IALr81	0.15	<0.001
INMr41	0.42	0.24
MI5r41	0.0096	0.12
MI5r81	<0.001	<0.001
NOEr41	<0.001	<0.001
A10r41	0.19	0.032
A10r81	0.0029	<0.001
A13r41	0.41	0.10
A13r81	0.029	0.0051
CMMr41	0.34	0.051
CM5r81	0.27	<0.001
CN5r41	<0.001	<0.001
MICr81	<0.001	<0.001
MIEr81	<0.001	<0.001
MR3r41	0.92	0.24
MR3r81	0.78	0.54
P_{SIG}[2]	**9 / 19 (47 %)**	**13 / 19 (68 %)**

Notes:
[1]Dark grey shading signifies statistically significant results (two-sided; 5% significance level)
[2]See Table 5.6 for the criteria outlined for colour shading.

Shifts in winter discharge can also be assessed using ΔQ data for specific WSE_{LW} bins (Fig. 5.23), which gives an appreciation for the absolute magnitudes of discharge that are being discussed.

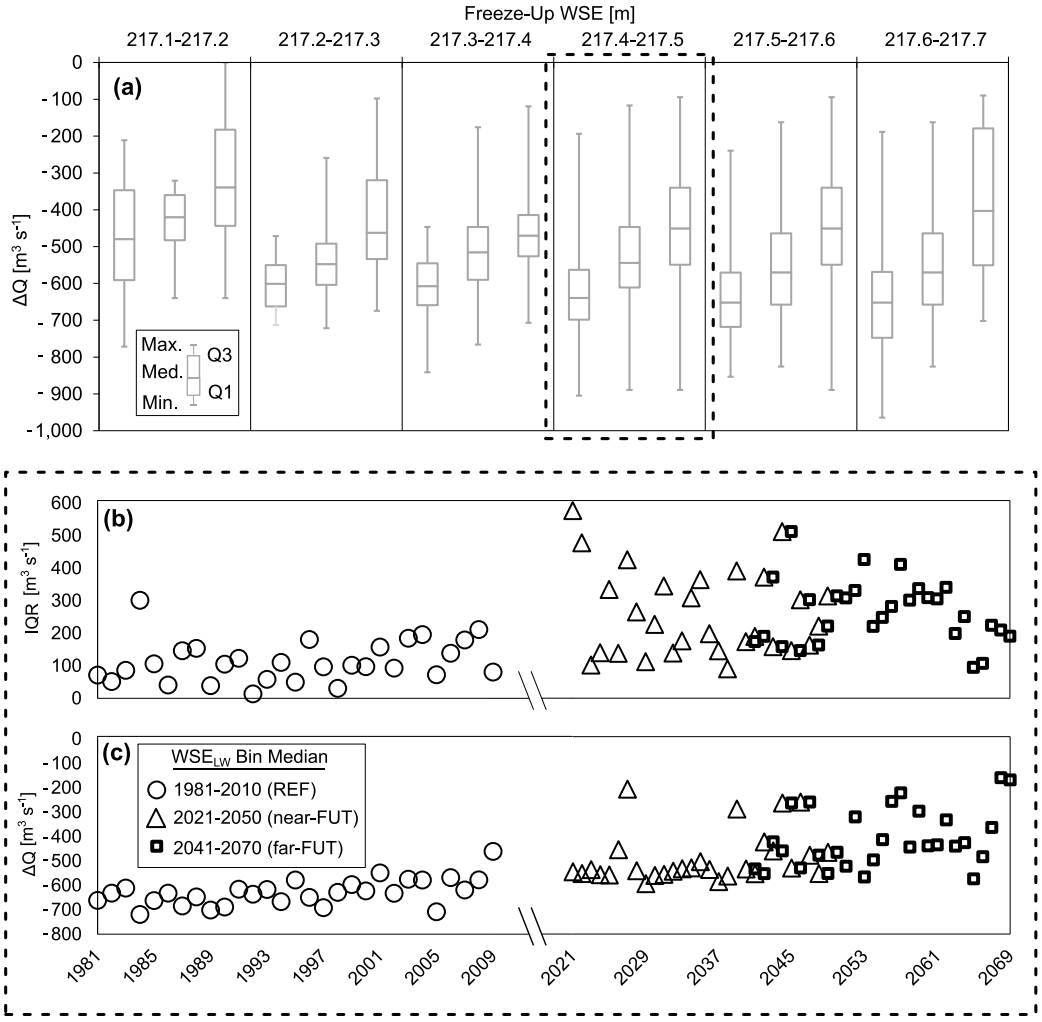

Fig. 5.23 - (a) Box-plot comparisons of ΔQ for REF, n-FUT and f-FUT periods; (b,c) *IQR* and median ΔQ included for a specific WSE_{LW} bin (217.4-217.5 m).

Using ΔQ instead of $\Delta Q/\Delta t$, likelihoods of positive shifts in discharge decline from REF to n-FUT and f-FUT periods are increased to likely (P_{sig} = 83%) and virtually certain (P_{sig} = 100%), respectively.

Ensemble trends of $\Delta Q/\Delta t$ (Table 5.9) are shown to be statistically significant and positive for both n-FUT and f-FUT periods, while no significant trend is observed for the REF period.

Table 5.9 - Intra-period trend results for relevant winter variables (see Table 5.6 for description of background shading).

Metric	Units	REF (1981-2010)			n-FUT (2021-2050)			f-FUT (2041-2070))		
		P_{sig}	$p_{ensemble}$	SS	P_{sig}	$p_{ensemble}$	SS	P_{sig}	$p_{ensemble}$	SS
$\Delta Q/\Delta t$	[$m^3\ s^{-1}\ day^{-1}$]	11%	0.59	0.001470	16%	0.049	-0.01079	21%	<0.001	-0.02785
DOY_{FO}	[-]	37%	0.0041	0.1884	26%	0.0069	0.1358	21%	0.0091	0.1913
DOY_{TH}	[-]	37%	0.15	-0.1296	26%	0.0014	-0.2547	26%	0.0037	-0.2406
Δt	[day]	16%	0.016	-0.2945	16%	<0.001	-0.3565	21%	<0.001	-0.4586
$CDDF_{TOT}$	[°C-day]	16%	<0.001	-10.8472	26%	<0.001	-13.1083	37%	<0.001	-11.4283
DY_{WM}	[°C-day]	0%	0.34	0.4265	16%	0.053	0.6806	5%	1.00	<0.001
$T_{AIR_{JAN}}$	[°C]	21%	0.12	-0.0352	26%	<0.001	-0.0995	21%	<0.001	-0.0869
$h_{SOG\,mean}$	[m]	0%	0.89	<0.001	0%	0.59	<0.001	0%	0.51	<0.001
$h_{SOG\,max}$	[m]	0%	0.49	<0.001	5%	0.28	<0.001	5%	0.77	<0.001

In contrast to MWW tests, P_{sig} values for M-K tests (Table 5.9) for n-FUT and f-FUT periods are shown to be low (P_{sig} = 16% and P_{sig} = 21%, respectively), indicating that these ensemble trends in $\Delta Q/\Delta t$ are *unlikely*. It is notable that confidence in trends is greater in n-FUT and f-FUT periods relative to the REF period for most winter variables, however there is low confidence in any projected future trend.

M-K tests using ΔQ instead of $\Delta Q/\Delta t$ on Fig. 5.24 show agreement amongst simulations, where likelihood is upgraded to *about as likely as not* (P_{sig} = 33%) and *likely* (P_{sig} = 67%) for n-FUT and f-FUT, respectively.

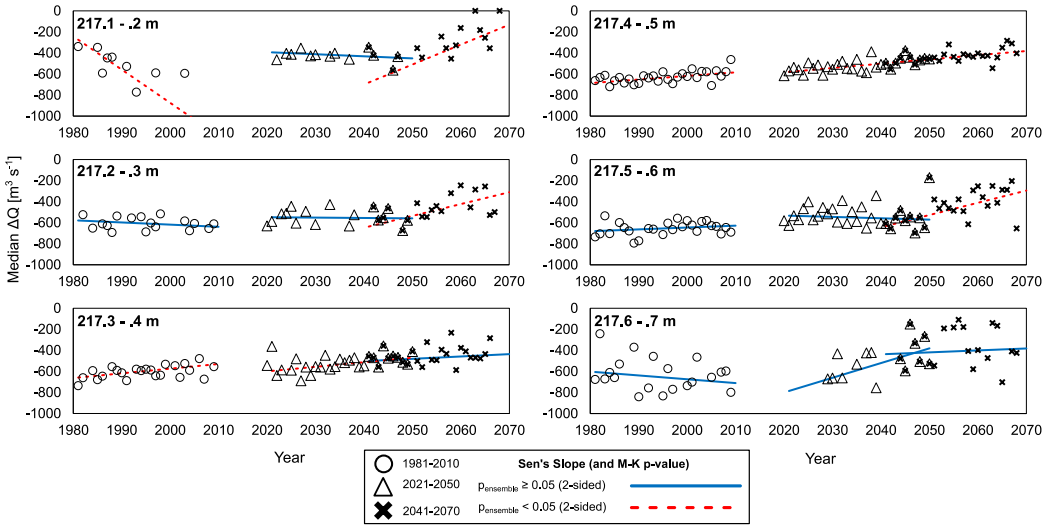

Fig. 5.24 - Ensemble trend for median ΔQ values of different WSE_{LW} ranges (Fig. 5.23). M-K test result is indicated by line type and colour.

From assessing changes in ΔQ and $\Delta Q/\Delta t$, there is moderate to high confidence in the assertion that cumulative winter discharge will increase in future years. These results are consistent with findings from MacDonald et al. (2018), who project a likely increase in streamflow for Manitoba Hydro operations. It is notable that MacDonald et al. (2018) focused on watershed hydrology and not particularly on the ice impacts at the Lake Winnipeg outlet.

The resulting increases in cumulative flow volumes will likely translate to seasonal increases in power generation along the Nelson River. Projections of ΔQ can be

further analysed to approximate what these generation increases might be. For instance, for the WSE_{LW} bin 217.4 – 217.5 m on Fig. 5.23, a positive shift of 188 m^3 s^{-1} is projected between REF and f-FUT periods (using median values). To translate this discharge to energy (E; [kWh]) generation at Jenpeg, Eq 5-15 can be applied.

$$E = \frac{\eta H g \rho_w Q}{1000} * t \qquad \text{Eq 5-15}$$

Application of Eq 5-15 requires additional assumptions and approximations: efficiency (η [-]) is 0.7, operating head at Jenpeg (H [m]) is 6.7 m; the 188 m^3 s^{-1} increase in discharge is achieved for the entire winter; and t is 5824 hours (i.e., 5 month winter duration). Under these assumptions, Eq 5-15 yields 5.04E7 kWh, which would represent a 0.14% increase to the 36.9 tWh of total energy generation previously reported by Manitoba Hydro (Canadian Energy Regulator, 2021). At the current residential energy charge of 9.324¢ per kWh, this 0.14% increase translates to $4.7 million. This approximate change in energy generation becomes even greater when generation at other Nelson River stations is also considered. While these power and revenue amounts are merely approximations, they do provide a sense of the economic benefits that could be obtained from increased flow quantities.

While *SS* (Table 5.9 and Fig. 5.24) generally shows increases using both ΔQ and $\Delta Q/\Delta t$, there is only low to moderate confidence in these projections. This confidence reflects high inter-annual variability and a lack of agreement amongst the climate simulations. This means that although there is reasonable confidence that ice restrictions will have less effect on discharge in the future, the rate at which this change will occur remains uncertain.

5.5.3 Ensemble spread and inter-annual variability

Variation between climate simulations can be quantified by assessing ensemble spread, which is a measure of the *IQR* amongst climate simulations (Chegwidden et al., 2019). A time-series of *IQR* for $\Delta Q/\Delta t$ (Fig. 5.25b) shows a statistically significant shift from REF to n-FUT and f-FUT winters.

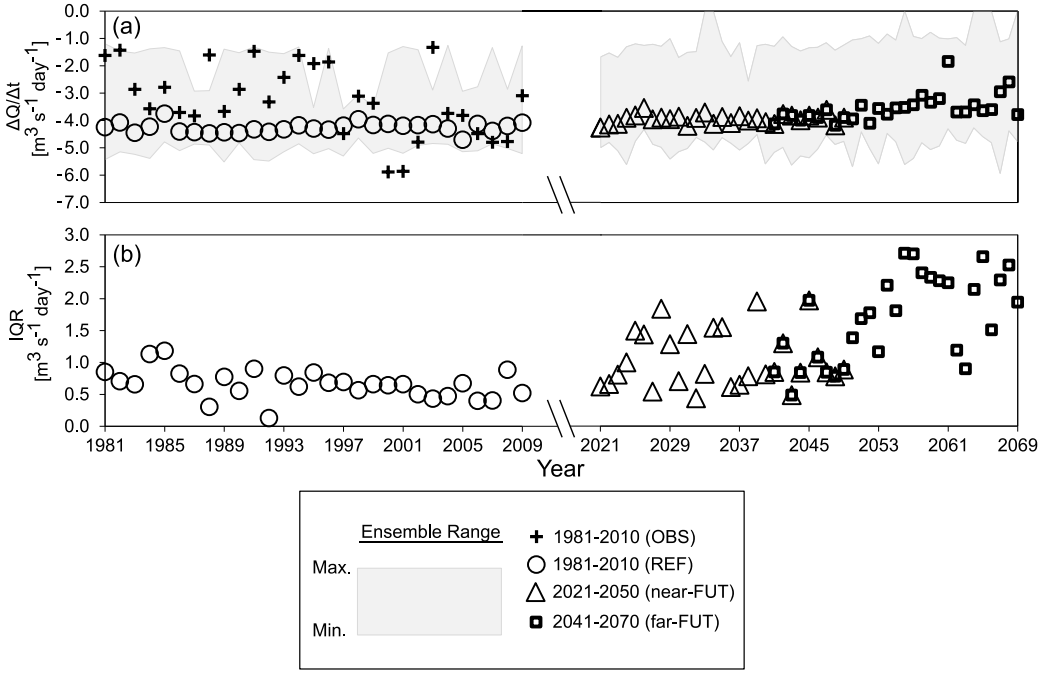

Fig. 5.25 - *ΔQ/Δt* ensemble range and median for REF, near-FUT and far-FUT periods (including OBS data). Ensemble *IQR* (25/75) included to illustrate model divergence over time.

An increasing trend in ensemble spread is visible, with *IQR* nearly tripling between REF and f-FUT periods. Similar trends are observed in the time-series of IQR for *ΔQ* (Fig. 5.23b). Sources contributing to this ensemble spread are numerous, but primarily include hydrologic model representation of physical processes (Sheffield and Wood, 2007), GCMs and RCP scenario assumptions (Lemaitre-Basset et al., 2021), and the internal variability of climate models (Olonscheck and Notz, 2017). Relative to a narrow ensemble spread, greater spread indicates divergence in agreement amongst simulations. It is also noted that the degree of ensemble divergence may vary between individual winter variables, although such analysis is not pursued in this study.

Inter-annual variability within each climate simulation, which is a measure of year-to-year fluctuations relative to an ensemble mean (Lüthi et al., 1996), is another measure of interest. *AAD* on de-trended data serves as a robust measure of inter-annual variability. An ensemble box-whisker plot of *AAD* is shown on Fig. 5.22c, which illustrates statistically significant shifts from REF to both n-FUT and f-FUT

periods. Further, Table 5.10 indicates that increases in inter-annual variability of $\Delta Q/\Delta t$ are *likely* (P_{sig} = 79%) and *highly likely* (P_{sig} = 95%) for n-FUT and f-FUT periods, respectively.

Table 5.10 - Significance proportion of climate simulations indicating increasing shifts in AAD (using detrended data) between REF and n-FUT or f-FUT periods (see Table 5.6 for description of background shading).

Metric	Units	P_{sig}	
		REF to n-FUT	REF to f-FUT
$\Delta Q/\Delta t$	[m^3 s^{-1} day^{-1}]	79%	95%
DOY_{FO}	[-]	63%	53%
DOY_{TH}	[-]	63%	68%
Δt	[day]	68%	68%
$CDDF_{TOT}$	[°C-day]	63%	47%
DY_{WM}	[°C-day]	47%	58%
$T_{AIR_{JAN}}$	[°C]	32%	32%
$h_{SOG\,mean}$	[m]	58%	63%
$h_{SOG\,max}$	[m]	63%	68%

Interestingly, almost all variables analysed show moderate to high confidence of increases to inter-annual variability, which reflects a general projection of less consistent future winter conditions. Variable $\Delta Q/\Delta t$ shows the highest likelihood of increasing inter-annual variability relative to other variables in Table 5.10, which is reasonable considering that $\Delta Q/\Delta t$ reflects the cumulative effect of multiple other variables.

Implications of greater inter-annual variability are that winter conditions will become less consistent year-to-year, which will inevitably impact hydropower

operations. With more variable conditions, anticipating cause-and-effect relationships of operational procedures and river ice conditions becomes more challenging. Further, increased inter-annual variability presents uncertainty to decision-makers responsible for long-term flow forecasting and waterway management.

5.5.4 Changing winter landscape and OLA hydraulics

As highlighted in Table 5.9, even in the case where a statistically significant ensemble trend was identified for a winter variable, there is low confidence in these projections. This low confidence is not surprising considering the variability amongst the 19 climate simulations, which underpins the methodology used to select these climate simulations (i.e., climate simulations were selected to encompass a wide-range of variability across the HBDB). Despite uncertainty in intra-period trends, there is moderate to strong confidence that shifts in key winter variables will occur (Table 5.11).

Table 5.11 - Climate scenario MWW test results for inter-period comparisons of relevant winter variables.

Metric	Units	n-FUT (2021-2050)			f-FUT (2021-2070)		
		P_{sig}	$p_{ensemble}$	Direction of Median Shift[1]	P_{sig}	$p_{ensemble}$	Direction of Median Shift[1]
$\Delta Q/\Delta t$	[m^3 s^{-1} day^{-1}]	47%	<0.001	↑	68%	<0.001	↑
DOY_{FO}	[-]	37%	<0.001	↑	53%	<0.001	↑
DOY_{TH}	[-]	53%	<0.001	↓	63%	<0.001	↓
Δt	[day]	68%	<0.001	↓	84%	<0.001	↓
$CDDF_{TOT}$	[°C-day]	74%	<0.001	↓	84%	<0.001	↓
DY_{WM}	[°C-day]	N/A	0.68	↓	11%	<0.001	↑
$T_{AIR_{JAN}}$	[°C]	N/A	0.42	↓	58%	<0.001	↑
$h_{SOG_{mean}}$	[m]	11%	0.010	↓	26%	0.015	↑
$h_{SOG_{max}}$	[m]	11%	0.0055	↓	26%	0.019	↓

Notes:

[1]Up arrow = more positive; down arrow = more negative

MWW test results suggest future shifts towards later freeze-up dates (DOY_{FO}) and earlier warming onset dates (DOY_{WM}), both of which contribute to shorter winter. By comparing the shift in histogram centroid between REF and f-FUT ensembles on Fig. 5.6, a 6-day shift towards later freeze-up is projected (10-NOV to 16-NOV). Using this same figure, a 12-day shift towards earlier breakup is projected (7-APR to 27-MAR). This is consistent with projections by the Government of Canada (Bush

and Lemmen, 2019), who projects 7-day and 10-day shifts in lake freeze-up and break-up dates for the OLA, respectively. Also shown in Table 5.11 is a shift towards lower $CDDF_{TOT}$, which indicates lower cumulative heat loss (and subsequent ice production) in future winters. This is an intuitive finding that indicates that future winters will generally be warmer as a result of climate change.

Lengths of future winters (Δt) are likely to become more variable year-to-year in n-FUT and f-FUT periods (Table 5.10). This inter-annual variability impacts both the seasonality of river and lake ice (Sharma et al., 2016) and the reliability of current forecasting methods for projecting break-up and freeze-up dates. While the frequency and severity of ice jams and mid-winter breakup processes will also be affected by climate change (Prowse et al., 2011), these impacts will vary based on site-specific conditions (i.e. regulation and channel characteristics) and the interactions between changing atmospheric (e.g., air temperature) and cryosphere conditions (e.g., snow cover and river ice properties).

5.5.5 Evaluation of CRIM run results

Prior to analysing CRIM results, a post-simulation correction was required. CRIM performance during the late-winter period has been previously identified as challenging; a characterization that is attributed to both the representation of the ice cover's snow-layer in the model and the formulation of thermal ice decay equations in CRISSP2D (Lees et al., submitted). These two factors contribute to a premature simulated plateau or rise in simulated discharge as a result of ice cover thinning, resulting in considerable deviation from expected model performance.

To address this performance issue, data were removed from the end of CRIM simulations according to a thermal threshold. For CRIM simulations using full energy-budget calculations (Lees et al., submitted), a threshold of a 10-day T_{AIR} average of -10°C was found to be a suitable. Using linear energy-budget calculations in this study, a modified threshold of a 10-day T_{AIR} average of 0°C was found to be appropriate. As shown on Fig. 5.26, filtering of more than 10% of winter was only required for two of the 36 simulated winters (217.3 to 217.4 m; *large* and *small* ΔQ runs), meaning that in most cases only a small fraction of winter (t_{end_sim} to t_{WM}) was impacted by the above-mentioned performance deficit.

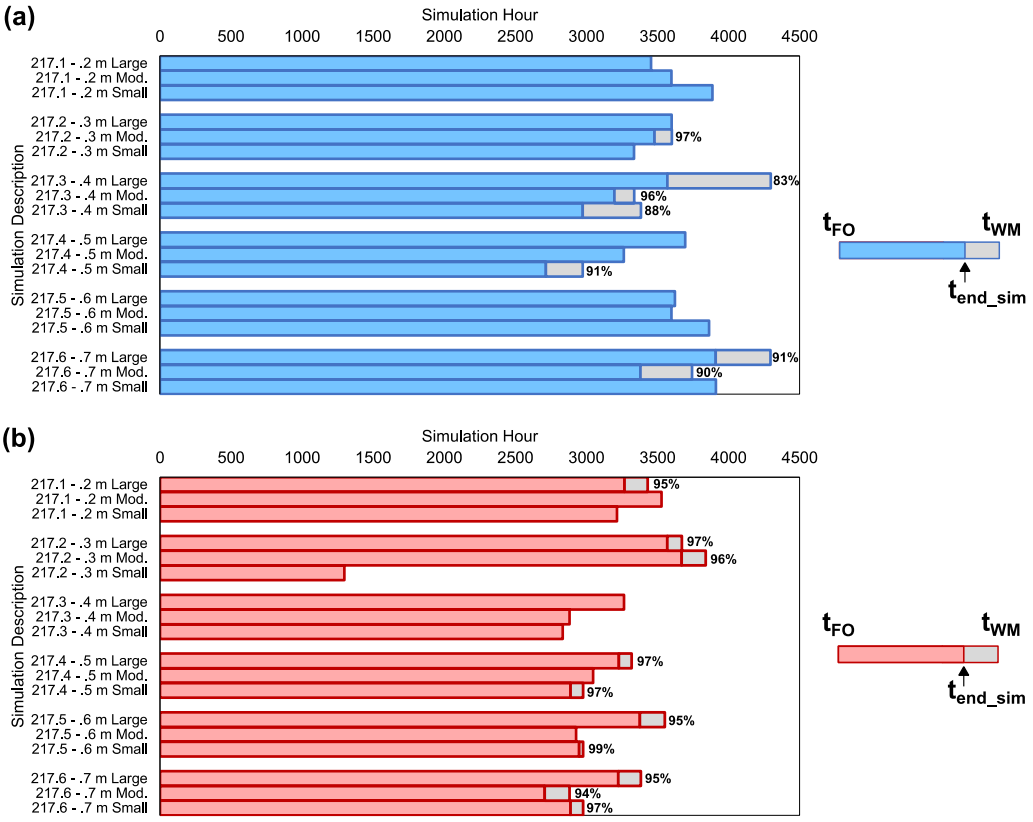

Fig. 5.26 - Magnitude of the thawing period (t_{end_sim} to t_{WM}) removed from CRIM run results for comparison with ERIA results.

As discussed in Section 5.4.4.1, the selection of winters for each WSE_{LW} bin was based on the ΔQ quantities projected by ERIA. A comparison of ΔQ calculated using CRIM relative to the ERIA box-whisker plots (Fig. 5.27) is informative for multiple reasons.

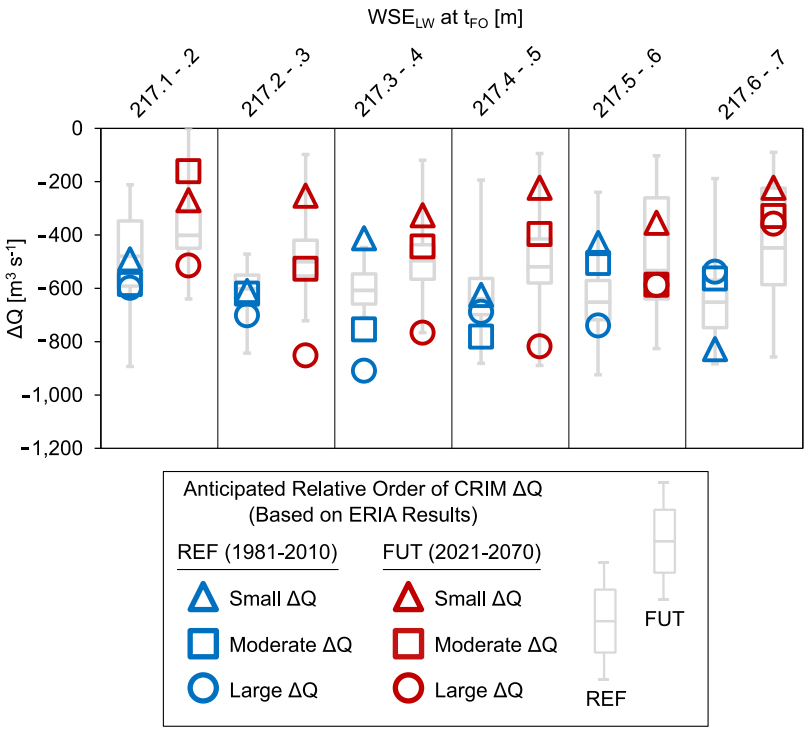

Fig. 5.27 - CRIM simulated ΔQ (markers) relative to ERIA ΔQ box-whisker plots. Marker types indicate expected relative magnitudes based on ERIA ΔQ results.

Firstly, CRIM calculated ΔQ falls within the bounds of ERIA box-whisker plots for 89% of simulated winters. This supports the argument for consistency between CRIM and ERIA projections. A second insight from Fig. 5.27 is identified by comparing the hierarchy of CRIM simulated ΔQ (i.e., *small*, *moderate*, and *large*) relative to what was expected based on ERIA results. For 9 of 12 (75%) groups, the relative order of ΔQ is consistent between CRIM and ERIA. This consistency supports the argument that variables X_1 and X_2 are suitable predictors for quantifying ΔQ using an empirical approach.

While differences in ΔQ values for specific winters between CRIM and ERIA were observed (Fig. 5.28), this is very reasonable considering the numerous differences between the two approaches.

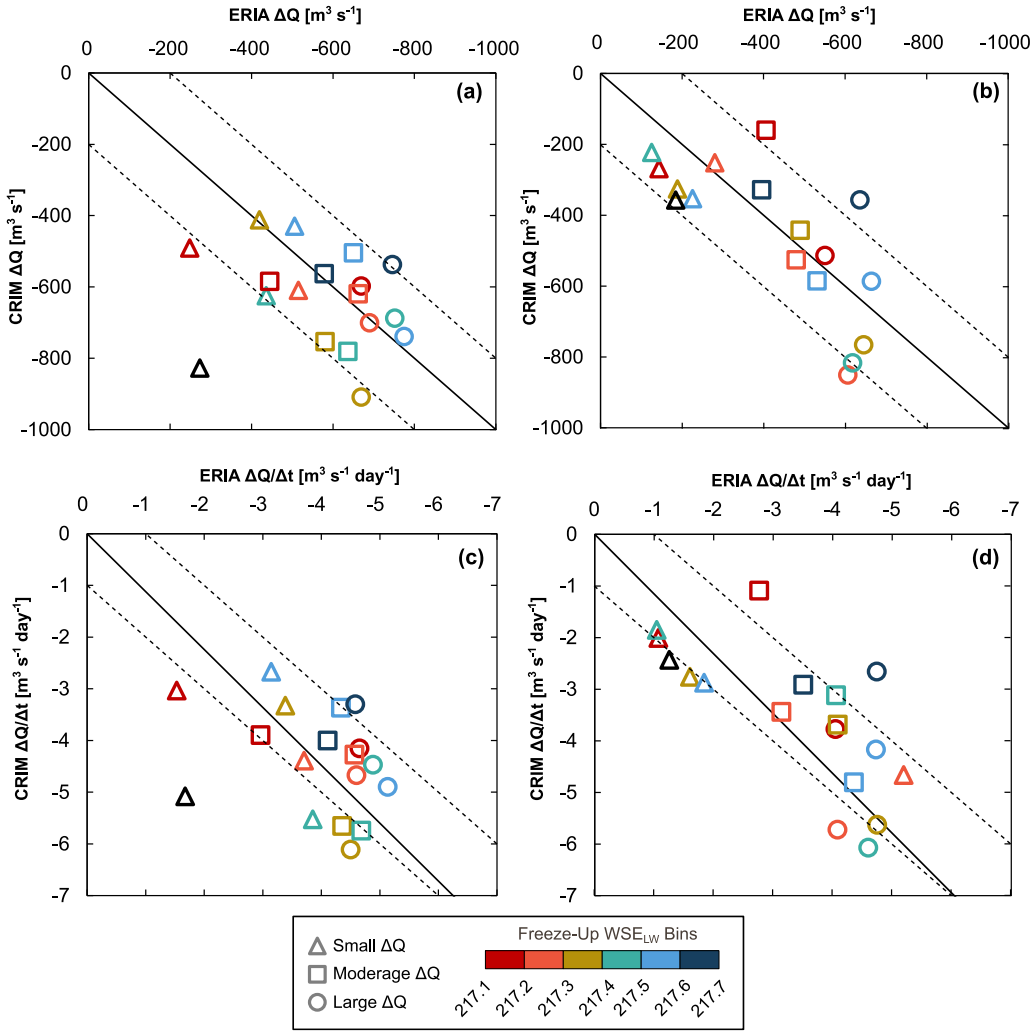

Fig. 5.28 - Comparison of ΔQ (and $\Delta Q/\Delta t$) calculated using ERIA and CRIM methodologies for REF (a,c) and FUT (b,d) simulations.

CRIM includes much more detailed calculations, use of hourly forcing data, and additional datasets (e.g., snow cover). As shown on Fig. 5.28, there appears to be a slight bias towards higher magnitude ΔQ projected by CRIM relative to ERIA, although bias in the other direction is observed for numerous winters. Comparing CRIM and ERIA for both REF and FUT populations, MAE is 136 m^3 s^{-1} and 119 m^3 s^{-1}, respectively. This shows comparable agreement between CRIM and ERIA winters for both REF and FUT periods. The slight discrepancy in MAE is attributed to a few cases of exceptional WSE_{LW} rise in REF winters (see Fig. 5.14 where $X_2 >$ 0.1 m), which presents a challenging condition to simulate in CRIM (Lees et al., submitted). While it's acknowledged that ERIA results are approximations, when

applied identically across all winters this approach is sufficient to yield insight into relative shifts and inter-annual trends in future conditions.

5.6 Conclusion

Among the anticipated impacts of climate changes in cold regions are changes to the characteristics of river ice processes. For hydropower operations, these impacts will vary and may present both opportunities and potential risks. In the NRB, winter outflow from Lake Winnipeg that supplies the Nelson River is governed primarily by ice restrictions and storage in the lake. Using both empirical and numerical model assessment approaches in this study, the cumulative effects of ice and lake levels were quantified through calculation of winter discharge decline (standard and normalized). When combined with assessments of other variables, a thorough characterization of future winter conditions starts to emerge.

The following are the major conclusions of this study:

- Changes in winter discharge decline were found to be most significant for 'dry' compared to 'wet' climate scenarios (Kim, 2020), which is a reflection of the predictor variables selected to quantify ice impacts on discharge. Ensemble and simulation-specific analyses yielded statistically significant decreases in winter discharge decline, with moderate to high confidence. Using median ensemble values, these shifts in $\Delta Q/\Delta t$ are projected to be +0.3 $m^3\ s^{-1}\ day^{-1}$ and +0.6 $m^3\ s^{-1}\ day^{-1}$ for n-FUT and f-FUT periods, respectively. This cumulative discharge volume increase in future winters translates to increases in power generation potential.
- Shifts in start- and end-of-winter dates are expected with high confidence, resulting in future winters having a shorter duration. On average, projected shifts in freeze-up onset and warming onset dates are 6-days earlier and 12-days later, respectively. These findings consistent with Government of Canada (Bush and Lemmen, 2019) projections of changes in lake ice cover dates for the OLA. Further, shifts towards lower heat loss are also projected, meaning that future winters will also be warmer relative to present-day conditions.

- While shifts in hydro-climatic conditions were identified with moderate to high confidence using MWW tests, M-K tests yield only low to moderate confidence on any trend. This result is owed to a lack of agreement amongst climate simulations, and high inter-annual variability within climate simulations. As a result, rates of intra-period change of winter conditions remain uncertain.
- Statistically significant increases in *AAD* were identified with moderate to high confidence for almost every winter variable, which translates to increased variability of winter conditions year-to-year. This finding presents a risk to the reliability of long-term flow forecasting and waterway management, which are both important for hydropower operations.
- The advantages of ERIA are numerous and include high computational efficiency and ease of implementation. When ERIA is compared to the current benchmark of river ice forecasting (i.e., historical ice-factor), ERIA shows superior performance. ERIA can be adapted as a whole or in parts to improve representation of Lake Winnipeg outlet ice-affected hydraulics in hydrology and hydropower models.
- CRIM runs of a subset of reference and future winters required strategic adaptation of a previously developed methodology to quantify OLA hydraulics. While the limited set of CRIM results did not allow for ensemble analysis, a comparison of CRIM and ERIA projections helped to support the validity of the ERIA approach. This study underlines the importance of continued improvement of CRISSP2D computational efficiency, which in part can be achieved through implementing parallel coding.

Findings from this study indicate potential opportunity for increased power generation on the Nelson River in future winters. However, this projection is accompanied with increases to inter-annual variability, which could have adverse effects on system operations. While the developed methodology is specific to the OLA, the approach can be adapted for other rivers where there is interest in quantify the effects of climate change on local river ice conditions.

5.7 Chapter Summary

Chapter 5 presents two methodologies (empirical and numerical) to evaluate the impacts of climate change on the OLA ice regime and Lake Winnipeg outflows. By leveraging one-way model coupling with a hydrologic model, an ensemble-based assessment yielded a moderate to high confidence prediction that future cumulative Lake Winnipeg winter outflows will be higher relative to baseline conditions. This is owed to future winters becoming less severe and of a shorter duration. Further, a predicted increase in inter-annual winter variability will likely pose challenges to managing waterway conditions in the future, potentially presenting risks to hydropower operations.

Chapter 6: Conclusions and Future Work

This chapter concludes this thesis by providing a summary of key findings and contributions related to the research objectives. Study limitations and proposed opportunities for future work are also discussed.

6.1 Summary and Conclusions

The overall aim of this study was to investigate and simulate the effects ice processes, hydropower operations and climate variability on the hydraulics of the OLA. The specific objectives of this study were to characterize the local ice regime using historical data and a site-specific monitoring program, simulate winter hydraulics and river ice processes using a numerical model, and quantify impacts of climate change on ice conditions and Lake Winnipeg outflows.

In Chapter 2, a detailed characterization of historical ice conditions is presented. Using a dataset of observations derived from helicopter photos and satellite imagery, a 2D hydraulic model, and analytical estimates of ice production, frontal progression patterns in two dynamic reaches were quantified. Model development included consolidation of field-collected and historical bathymetry, and hydrodynamic calibration of a diverse series of reaches.

Chapter 2 findings contribute directly to research Objectives 2 and 3. This work marks the first peer-reviewed journal publication to provide a detailed characterization of the OLA's ice regime. Through quantification and visualization of the cause-and-effect relationships between ice processes and flow control practices, a primary finding of this study was evidence that flow cutbacks are most effective at accelerating frontal progression during periods of high ice production. Further, efficacy of flow cutbacks was shown to be most uncertain during periods of low heat loss. This characterization of frontal progression events serves as a baseline description of freeze-up ice conditions for the region. Additional contributions of this chapter are as follows:

1) Development of one of the largest known datasets of observed skim ice run events on any regulated river. The high flow rates, very mild bed slopes, and

subarctic climate conditions of the Nelson River region contribute to the novelty of this dataset.

2) Comparison of skim ice run observations with a well-established and frequently cited framework designed to classify ice floe formation (Matoušek, 1984b). Observations show good agreement with the framework, but also yield insight into how the framework can be incompatible with ice floe conditions on large rivers.
3) Presentation of evidence reinforcing the importance of considering channel morphology when selecting a suitable ice formation metric (i.e., Froude number or velocity). In the case of deep flow conditions and thin ice covers, velocity was found to be a more reliable metric.
4) Demonstration of the use of novel field measurement techniques, such as UAV imagery coupled with photogrammetry to estimate ice floe velocities for model verification.

In Chapter 3, a treatment of skim ice run during freeze-up jamming was developed for the CRISSP2D model. This chapter provides a detailed description of the base CRISSP2D model and the new treatment, along with demonstrated application in an ideal trapezoidal model. Research for this chapter was motivated by a field-data informed hypothesis that the strength of large skim ice floes is a key factor in the rapid frontal progression of an ice cover on very mild-sloped rivers. Chapter 4 also includes a detailed review summarizing the knowledgebase of skim ice runs, with relevant studies ranging from laboratory investigations to site-specific monitoring programs.

Chapter 3 findings contribute directly to research Objective 1. This work included collaboration with researchers at three institutions to finalize a peer-reviewed journal publication. The primary contribution of this chapter is development of a treatment that captures the dual roles of heat loss during ice jamming in a skim ice regime, which are: (1) to increase the overall quantity of ice generated, and (2) to considerably increase the strength and stability of individual skim ice floes. Additional contributions of this chapter are as follows:

1) Simulation of frontal progression rates in a trapezoidal channel that are consistent with those estimated from ice front observations in the Upper

Nelson River (0.01 to 0.05 m s^{-1}). As described in a conference proceeding based on this research (Lees et al., 2021a), when this treatment was applied the Jenpeg-specific CRISSP2D model, the accuracy of frontal progression simulations (i.e., RMSE) improved by 56-74% during freeze-up simulations.

2) Demonstration of a simulated flow control scenario using different air temperatures. Flow cutbacks were shown to increase ice floe strength because of increased travel time from formation to ice jamming, resulting in faster formation of a thinner ice cover.
3) Presentation of a sensitivity analysis which evaluated the effects of varying channel characteristics (i.e., sinuosity and bed slope) and model parameters on ice jam formations.

The treatment developed in Chapter 3 is important for winter-long simulations in the OLA, considering that by improving the timing and simulated thickness of the initial ice cover, the simulation of winter-long hydraulic conditions is also improved (see Chapter 4).

In Chapter 4, a novel methodology was developed to simulate ice processes and winter hydraulics (i.e., hydraulic head and discharge) within the OLA. In this chapter, a Jenpeg-specific CRISSP2D model was coupled with hydraulic equations to estimate ice impacts across a vast 100-km reach of inter-connected lakes and channels. Despite the limited model domain extent relative to the entire OLA study area, the methodology effectively addresses data gaps to yield strong performance over a wide range of winter conditions.

Chapter 4 findings contribute directly to research Objective 1 and 3. This work was submitted for publication and is currently under review. The primary contribution of this chapter is design of the most advanced river ice modelling tool available for the OLA, with utility for both Nelson River hydropower operators and other water resources researchers. Additional contributions of this chapter are as follows:

1) Adaptation of existing CRISSP2D subroutines to simulate under cover deposition and transport of ice particles (including a treatment for ice deposit roughness), yielding good agreement with observed hydrometric data and under ice conditions visible in Sentinel-2 satellite imagery. Simulation results

are also consistent with hanging dam observations by Manitoba Hydro (Hopper and Raban, 1980).

2) Inclusion of a snow-on-ground record during long-term simulations in CRISSP2D to account for snow-on-ice. CRISSP2D was also adapted to adjust snow-depths based on the weight bearing capacity of the ice cover.
3) Identification of numerical model under-performance during the 'warming' or pre-breakup period. Improvement to simulations was demonstrated by implementing a modified form of the CRISSP2D ice decay equation.
4) Estimation of the ice-affected flow splits in the OLA using model simulations, which complements the established open-water flow split relationship.
5) Articulation of the key factors that affect Lake Winnipeg outflows – water levels at the start of winter, change in water levels over winter, and severity of ice impacts – including evidence to support these claims.

In Chapter 5, an assessment of climate change impacts on OLA ice processes and Lake Winnipeg winter outflows is presented. Using both empirical and numerical assessment approaches, hydrologic and climate change data from the BaySys Freshwater System team were applied to predict future changes to winter conditions. This chapter serves as an important step in bridging hydraulic and hydrologic modelling tools, which is critical not only for simulations of Lake Winnipeg winter outflows, but also for the field of river ice engineering.

Chapter 5 findings contribute directly to research Objectives 2 and 4. The primary contribution of this research is the combination of both ensemble-based and simulation-specific analyses of Lake Winnipeg winter discharge conditions. The projection of statistically significant increases to winter discharge in the future is supported by related hydrology studies in the region. As a whole or in-part, the Chapter 5 methodology can improve how river ice processes are represented in hydrologic and hydropower models that include the NRB. Additional contributions of this chapter are as follows:

1) Identification of statistically significant changes to both inter-annual variability and shifts in winter variables between reference and future winters. These results indicate moderate to high confidence that there will be

a transition towards shorter and warmer winters; both factors which contribute to increases in cumulative winter discharge.

2) Establishment of thresholds to quantify shifts in start- and end-dates of winter, which yield good agreement with literature values (Bush and Lemmen, 2019) and site-specific knowledge of Manitoba Hydro engineers.
3) Demonstration of the performance advantage of the developed study approach over use of a *historical ice-factor*, which currently serves as the conventional standard for ice forecasting in the OLA.
4) Application of re-sampling algorithms and numerous regression equations to convert large scale CMIP5 climate simulation data into local scale inputs for river ice model simulations.

6.2 Future Work

Recommendations for future work are described in the following sections.

6.2.1 Field Studies and Monitoring

1. The local river ice monitoring program in the OLA should continue. This includes deployment of trail cameras, water temperature sensors, water pressures sensors, and a barologger. Additionally, the radiometer installed at the Jenpeg weather station should remain active. Measurements from this network are helpful to characterize the onset and nature of freeze-up and ice floe formation. The current state of the monitoring program as of winter 2021-2022 is shown on Fig. 6.1.

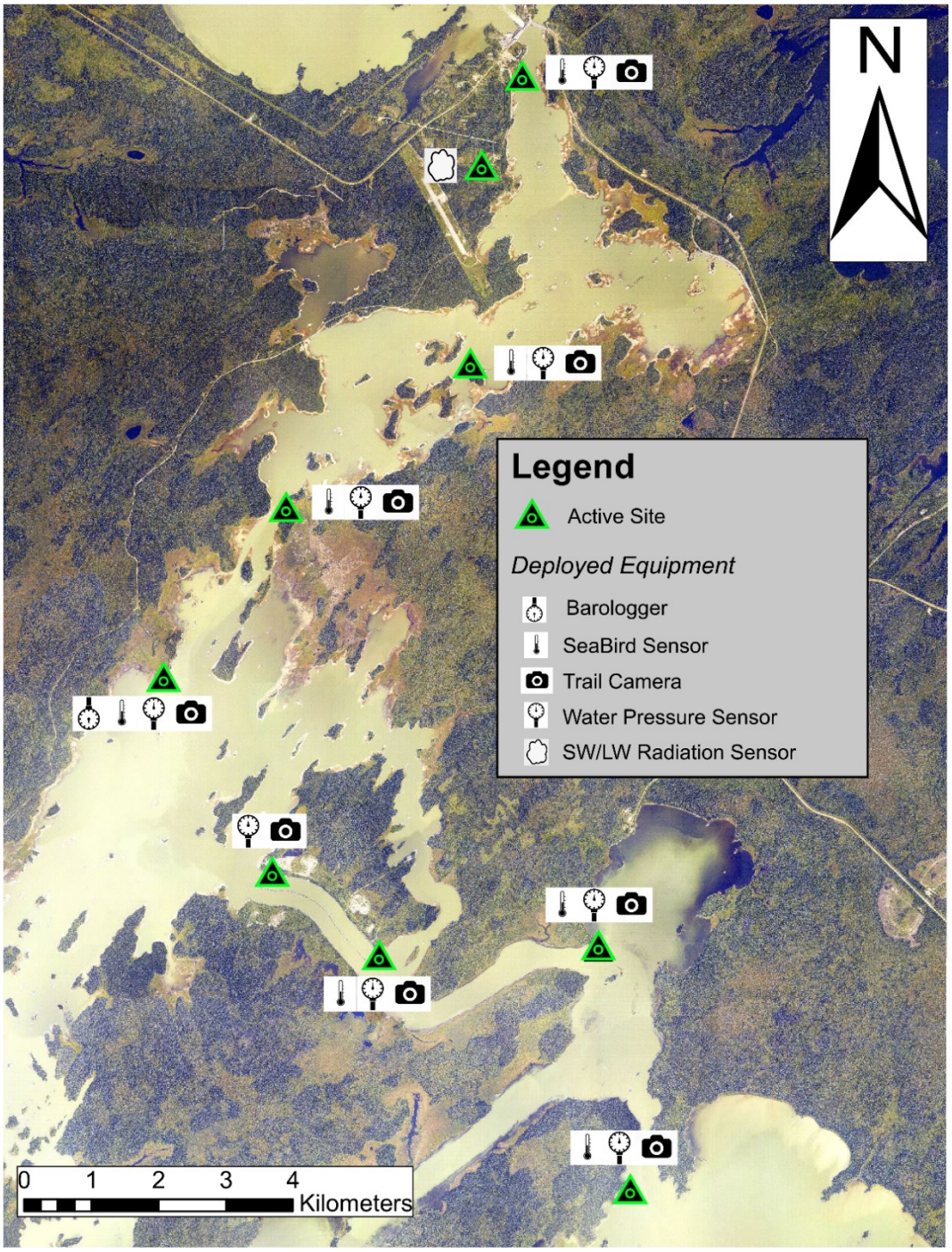

Fig. 6.1 – Current state of the OLA river ice monitoring network as of winter 2021-2022. [Background imagery courtesy of Manitoba Hydro]

2. Prior to the 2021-2022 freeze-up, additional pressure transducers were strategically deployed to support calculation of local water surface profiles in areas that are prone to significant under ice deposition. These measurements can yield insight into roughness of these deposits and the evolution of ice deposition and transport processes through winter.
3. Numerical simulations in Chapter 4 highlight differences in flow split quantities for open-water versus ice-affected conditions. However, it is noted that simulated ice affected flow split quantities are not verified. Field measurements of under-ice velocities when the Jenpeg forebay is at a minimum operating level would help to verify simulated ice-affected flow splits. If conditions do not allow for safe ice passage to conduct these measurements, winter-long deployment of an under-ice profiler or ADCP could be pursued.
4. To support improved representation of snow evolution on an ice cover (see *Numerical Modelling* future work section), a snow monitoring program should be implemented. This could include taking multiple snow and ice cores at strategically selected locations throughout winter. When paired with weather station measurements, specifically short- and long-wave radiation, these observations could contribute to knowledge of snow characteristics on reservoirs.
5. To support model expansion (see Section 6.2.2) additional bathymetric data collection should commence to fill data gaps. Given the expansive areas of the lakes where most data gaps are, alternative technologies beyond use of an ADCP should be explored, as boat trolling with an ADCP requires considerable time and logistical effort. To support simulations and model calibration in an expanded model domain, Manitoba Hydro should re-activate historical monitoring sites that were initially installed around the start of Lake Winnipeg Regulation. Conveniently, most of these sites (red triangles) align with optimal locations for future hydrometric monitoring (yellow triangles) (Fig. 6.2).

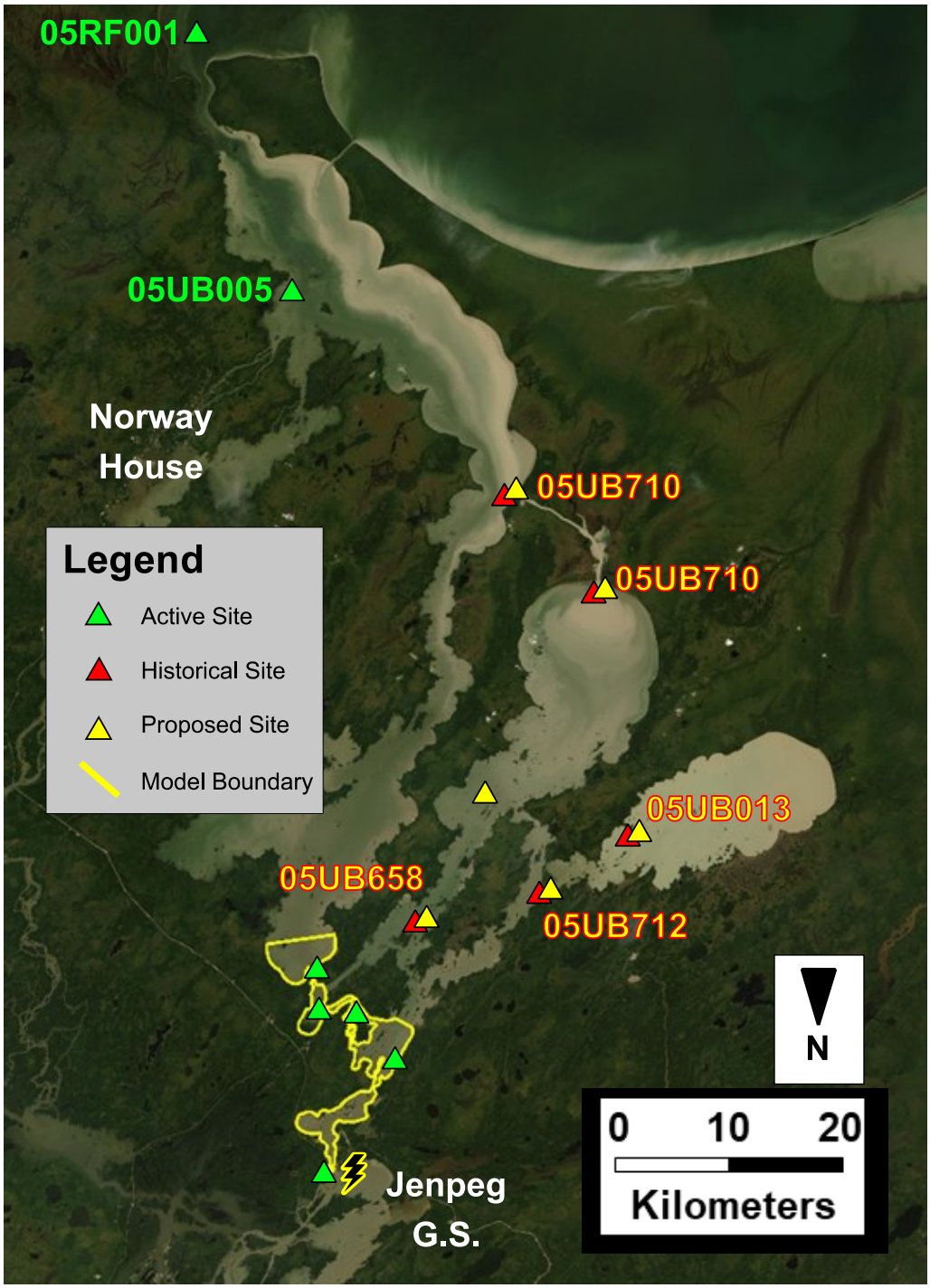

Fig. 6.2 – Manitoba Hydro's hydrometric monitoring network in the OLA (green triangles), along with recommendations for future monitoring sites (yellow triangles), which generally coincide with Manitoba Hydro legacy monitoring sites (red triangles). [Background imagery from ArcGIS World Imagery, Surface Layer Credits: Source: Esri, DigitalGlobe, GeoEye, Earthstar Geographics, CNES/Airbus DS, USDA, AeroGRID, IGN, and the GIS User Community]

6. The COVID-19 pandemic has been a disruptive event worldwide, with one consequence being interruptions to remote site accessibility. In coordination with Manitoba Hydro, researchers should continue to collaborate and build field monitoring capacity within the Cross Lake Boat Patrol crew. By actively participating in field work, crew members may be in a position to support data collection in the event that field accessibility becomes an issue in the future.

6.2.2 Numerical Modelling

7. While the methodology presented in Chapter 4 allowed for simulations of OLA hydraulics with a limited model domain, this approach included myriad assumptions with limited verification. Expansion of the numerical model domain up to Lake Winnipeg is recommended for future research, while it acknowledged that bathymetric data collection and additional hydrometric monitoring will be required to support this expansion (see Section 6.2.1).
8. As highlighted in Chapter 4, there is room for improvement in how snow is represented in long-term CRISSP2D simulations. Targeted areas of improvement include incorporating snow-ice layer formation, evaluation of model parameters related to snow, and verification of heat flux quantities during the warming period.
9. While success in simulation of undercover ice processes was achieved, there is opportunity for enhancing how these processes are simulated in CRISSP2D. For instance, model performance and stability in the case of grounded under cover ice should be checked, especially in areas with expansive border ice covers. The method for translating under cover parcels during transport should be improved to reduce the likelihood that parcels overrun the model domain and become 'lost'. These treatments should also be tested on other field sites and against laboratory data from controlled studies, as application has so-far been limited to very few regions.
10. CRISSP2D model performance in routing mobile parcels through a narrow open-water lead flanked by border ice should be revisited. These border ice areas provide a challenging modelling environment resulting in parcels being 'trapped' at border ice edges (i.e., parcel velocity becomes negligible or zero)

or lost all-together under border ice. This issue is not limited to OLA, as parcel and border ice interactions have been noted as a model limitation during application of CRISSP2D by Manitoba Hydro upstream of Keeyask Generating Station.

11. The treatment developed for freeze-up jamming in a skim ice regime should be applied to other rivers where substantial skim ice runs have been observed, including the Tanana River and Peace River. Further study should investigate simulation of mixed ice regime, where there are significant runs of both frazil ice pans and skim ice floes.
12. The computational efficiency of CRISSP2D could be greatly improved by implementing parallel computing capabilities. Additionally, the parcel search algorithm implemented in the SPH method used for ice dynamic calculations presents a computation bottleneck that could be improved.
13. It is recommended that the CRISSP2D model platform be translated for use in a Linux environment, which would allow for simulations on remote computing platforms where Linux is commonplace.
14. If through a combinations items (12) and (13) CRISSP2D computations become more efficient it is recommended that a complete ensemble of simulations is pursued using CRIM (see Chapter 5).

6.2.3 Interdisciplinary Collaboration

15. The ERIA methodology presented in Chapter 5 has considerable potential to improve how ice is represented in the hydrologic and hydropower models that rely on accurate estimates of Lake Winnipeg outflow. These hydraulic and ice equations developed could be adapted as a whole, or in part, within these other models.

References

Abdelnour, E., Abdelnour, R., Malenchak, J., 2012. Design, Fabrication and Deployment of an Ice Boom at Jenpeg Generating Station, in: Proc. from the CDA Annual Conference on Dam Safety. Saskatoon, Canada, pp. 1–14.

Adams, W.P., Prowse, T.D., 1981. Evolution and magnitude of spatial patterns in the winter cover of temperate lakes. Fennia 159, 343–359.

Alexandersson, A., 2004. Graphing Confidence Ellipses: An Update of Ellip for Stata 8. Strat. J. 4, 242–256. https://doi.org/10.1177/1536867x0400400302

Andreas, E.L., Jordan, R.E., 2004. Simulations of Snow, Ice and Near-Surface Atmospheric Processes on Ice Station Weddell. J. Hydrometeorlogy 5, 611–624.

Andreasson, P., Hammar, L., Shen, H.T., 1998. The influence of surface turbulence on the formation of ice pans. Ice Surf. Waters 69–76.

Andres, D., 1999. The Effects of Freezing on Stability of a Juxtaposed Ice Cover, in: Proc. from the Workshop on River Ice. Winnipeg, Canada, pp. 209–222.

Andrishak, R., Hicks, F., 2008. Simulating the effects of climate change on the ice regime of the Peace River. Can. J. Civ. Eng. 35, 461–472. https://doi.org/10.1139/L07-129

Arenson, L.U., Colgan, W., Marshall, H.P., 2014. Chapter 2: Physical, Thermal and Mechanical Properties of Snow, Ice, and Permafrost, in: Haeberli, W., Whiteman, C.A. (Eds.), Snow and Ice-Related Hazards, Risks and Disasters. pp. 35–76. https://doi.org/10.1016/B978-0-12-394849-6.00002-0

Ashton, G., 2013. Thermal Processes, in: Beltaos, S. (Ed.), River Ice Formation. Committee on River Ice Processes and the Environment; Canadian Geophysical Union, Hydrology Section, Edmonton, Alberta, pp. 77–106.

Ashton, G., 1986. River and Lake Ice Engineering. Water Resources Publications, Littleton, Colorado.

Ashton, G., 1974. Froude Criterion for Ice-Block Stability. J. Glaciol. 13, 307–313.

https://doi.org/10.1017/S0022143000023108

Ashton, G.D., 2011. River and lake ice thickening, thinning, and snow ice formation. Cold Reg. Sci. Technol. 68, 3–19. https://doi.org/10.1016/j.coldregions.2011.05.004

Ashton, G.D., 1989. Thin Ice Growth. Water Resour. Res. 25, 564–566.

Ashton, G.D., Nufelt, J., 1991. Evolution of ice cover roughness, in: Proc. from the International Speciality Conference on Cold Regions Engineering (ASCE). West Lebanon, USA, pp. 1603–1624.

Barber, D., 2014 BaySys - Contributions of climate change and hydroelectric regulation to the variablity and change of freshwater-marine coupling in the Hudson Bay System (proposal 174460). https://doi.org/10.1017/CBO9781107415324.004

Beihagdar, P., 2019. Developing an Integrated Water Management Model for Simulating the River-Reservoir System Operated by Manitoba Hydro. M.Sc. Thesis, University of Manitoba.

Beltaos, S., 2013. Ice Cover Formation, in: Beltaos, S. (Ed.), River Ice Formation. Committee on River Ice Processes and the Environment; Canadian Geophysical Union, Hydrology Section, Edmonton, pp. 181–251.

Beltaos, S., 2011. Developing Winter Flow Rating Relationships Using Slope-Area Hydraulics. River Res. Appl. 27, 1076–1089. https://doi.org/10.1002/rra.1404

Beltaos, S., 2008. Hydro-climatic impacts on the ice cover of the lower Peace River. Hydrol. Process. 22, 3252–3263. https://doi.org/10.1002/hyp.6911

Beltaos, S., 1995. Chapter 4: Theory, in: Beltaos, S. (Ed.), River Ice Jams. Water Resources Publications, LLC, Highlands Ranch, Colorado, pp. 105–146.

Beltaos, S., Bonsal, B., 2021. Climate change impacts on Peace River ice thickness and implications to ice-jam flooding of Peace-Athabasca Delta, Canada. Cold Reg. Sci. Technol. 186. https://doi.org/10.1016/j.coldregions.2021.103279

Beltaos, S., Dean, A.M., 1981. Field investigations of a hanging ice dam, in: Proc. International Association for Hydraulic Research Symposium on Ice. Quebec

City, Canada, pp. 457–488.

Beltaos, S., Prowse, T., 2009. River-ice hydrology in a shrinking cryosphere. Hydrol. Process. 23, 122–144. https://doi.org/10.1002/hyp.7165

Benra, F.K., Dohmen, H.J., Pei, J., Schuster, S., Wan, B., 2011. A comparison of one-way and two-way coupling methods for numerical analysis of fluid-structure interactions. J. Appl. Math. 2011. https://doi.org/10.1155/2011/853560

Bijeljanin, M., 2013. Application of CRISSP-2D Finite Element Modelling in Predicting Ice Formation Processes Upstream of the Jenpeg Generating Station. M.Sc. Thesis, University of Manitoba.

Bijeljanin, M., Clark, S.P., 2011. Application of Numerical Modelling Towards Prediction of River Ice Formation on the Upper Nelson River, in: Proc. from the Workshop on River Ice. Winnipeg, Canada, pp. 135–146.

Bilello, M.A., 1980. Maximum thickness and subsequent decay of lake, river and fast sea ice in Canada and Alaska (CRREL Report 80-6). Hanover, NH.

Blackburn, J., She, Y., 2019. A comprehensive public-domain river ice process model and its application to a complex natural river. Cold Reg. Sci. Technol. 163, 44–58. https://doi.org/10.1016/j.coldregions.2019.04.010

Bourban, S.E., Huang, F., Shen, H.T., Ata, R., 2018. Introducing K HIONE – (Eulerian) Part I of the ice modelling component of TELEMAC, in: Proc. from the Telemac & Mascaret User Club. Norwich U.K.

Boyd, D.W., 1979. Degree Days: The different types, NRC Publications Archive (1979-01). https://doi.org/10.4224/40000571

Braun, M., Thiombiano, A.N., Vieira, M.J.F., Stadnyk, T.A., 2021. Representing climate evolution in ensembles of GCM simulations for the Hudson Bay System. Elem. Sci. Anthr. 9, 1–19. https://doi.org/10.1525/elementa.2021.00011

Brayall, M., Hicks, F.E., 2012. Applicability of 2-D modelling for forecasting ice jam flood levels in the Hay River Delta, Canada. Can. J. Civ. Eng. 39, 701–712.

https://doi.org/10.1139/L2012-056

Brown, D., 2019. Tracker Video Analysis and Modelling Tool [WWW Document]. URL http://physlets.org/tracker/ (accessed 11.28.18).

Burrell, B.C., Beltaos, S., Turcotte, B., 2021. Effects of Climate Change on River-Ice Processes and Ice Jams. Int. J. River Basin Manag. 1–78. https://doi.org/10.1080/15715124.2021.2007936

Bush, E., Lemmen, D.S., 2019. Canada's Changing Climate Report. Ottawa, Canada.

Calkins, D.J., Gooch, G., 1982. Ottauquechee River - Analysis of Freeze-up Processes, in: Proc. from the Workshop on River Ice. Edmonton, Canada, pp. 2–37.

Canadian Energy Regulator, 2021. Provincial and Territorial Energy Profiles – Manitoba [WWW Document]. URL https://www.cer-rec.gc.ca/en/data-analysis/energy-markets/provincial-territorial-energy-profiles/provincial-territorial-energy-profiles-manitoba.html

Carson, R.W., Healy, D., Beltaos, S., Groeneveld, J., 2003. Tests of River Ice Jam Models – Phase 2, in: Proc. from the Workshop on River Ice. Edmonton, Canada.

Chegwidden, O.S., Nijssen, B., Rupp, D.E., Arnold, J.R., Clark, M.P., Hamman, J.J., Kao, S.C., Mao, Y., Mizukami, N., Mote, P.W., Pan, M., Pytlak, E., Xiao, M., 2019. How Do Modeling Decisions Affect the Spread Among Hydrologic Climate Change Projections? Exploring a Large Ensemble of Simulations Across a Diversity of Hydroclimates. Earth's Futur. 7, 623–637. https://doi.org/10.1029/2018EF001047

Chen, Y., She, Y., 2020. Long-term variations of river ice breakup timing across Canada and its response to climate change. Cold Reg. Sci. Technol. 176. https://doi.org/10.1016/j.coldregions.2020.103091

Cherry, J.E., Knapp, C., Trainor, S., Ray, A.J., Tedesche, M., Walker, S., 2017. Planning for climate change impacts on hydropower in the Far North. Hydrol. Earth Syst. Sci. 21, 133–151. https://doi.org/10.5194/hess-21-133-2017

Chow, V. Te, 1959. Open-channel hydraulics, Open-Channel Hydraulics. McGraw-Hill, New York.

Clark, S., 2013. Border and Skim Ice, in: Beltaos, S. (Ed.), River Ice Formation. Committee on River Ice Processes and the Environment; Canadian Geophysical Union, Hydrology Section, Edmonton, pp. 77–106.

Conover, W.J., 1980. Practical nonparametric statistics. Wiley, New York.

Countermash, B., McGilvary, R., 1994. Analyzing the Stability of Floating Ice Floes (CRREL Report 94-13). Hanover, USA.

Countermash, B.A., McGilvary, W.R., 1993. Static analysis of floating ice block stability. J. Hydraul. Res. 31, 147–160.

Daly, S., 2013. Frazil Ice, in: Beltaos, S. (Ed.), River Ice Formation. Committee on River Ice Processes and the Environment; Canadian Geophysical Union, Hydrology Section., Edmonton, Alberta, pp. 107–134.

Daly, S., 1984. Frazil ice dynamics (CRREL Monograph 84-1). Hanover, USA.

Daly, S.F., 1991. Frazil Blockage of Intake Trash Racks (CRREL Report 91-1). Hanover, USA.

Daly, S.F., Axelson, K.D., 1990. Stability of floating and submerged blocks. J. Hydraul. Res. 28, 737–752. https://doi.org/10.1080/00221689009499023

Das, A., Lindenschmidt, K.E., 2021. Modelling climatic impacts on ice-jamfloods: A review of current models, modelling capabilities, challenges, and future prospects. Environ. Rev. 29, 378–390. https://doi.org/10.1139/er-2020-0108

Derecki, J.A., Quinn, F.H., 1987. Record St. Clair River Ice Jam of 1984. J. Hydraul. Eng. 112, 1182–1193. https://doi.org/10.1061/(ASCE)0733-9429(1986)112:12(1182)

Dow Ambtman, K.E., Hicks, F.E., Steffler, P.M., 2011. Experimental Investigation of the Pressure Distribution beneath a Floating Ice Block. J. Hydraul. Eng. 137, 399–411. https://doi.org/10.1061/(ASCE)HY.1943-7900.0000315

Ettema, R., Kirkil, G., Daly, S., 2009. Frazil ice concerns for channels, pump-lines,

penstocks, siphons, and tunnels in mountainous regions. Cold Reg. Sci. Technol. 55, 202–211. https://doi.org/10.1016/j.coldregions.2008.04.008

Falloon, P., Challinor, A., Dessai, S., Hoang, L., Johnson, J., Koehler, A.K., 2014. Ensembles and uncertainty in climate change impacts. Front. Environ. Sci. 2, 1–7. https://doi.org/10.3389/fenvs.2014.00033

Gebre, S., Boissy, T., Alfredsen, K., 2014a. Sensitivity to climate change of the thermal structure and ice cover regime of three hydropower reservoirs. J. Hydrol. 510, 208–227. https://doi.org/10.1016/j.jhydrol.2013.12.023

Gebre, S., Timalsina, N., Alfredsen, K., 2014b. Some Aspects of Ice-Hydropower Interaction in a Changing Climate. Energies 7, 1641–1655. https://doi.org/10.3390/en7031641

Ghareh Aghaji Zare, S., Moore, S., Rennie, C., Seidou, O., Ahmari, H., Malenchak, J., 2016. Estimation of composite hydraulic resistance in ice-covered alluvial streams. Water Resour. Res. 52, 1306–1327. https://doi.org/10.1002/2015WR018096

Gherboudj, I., Bernier, M., Hicks, F., Leconte, R., 2007. Physical characterization of air inclusions in river ice. Cold Reg. Sci. Technol. 49, 179–194. https://doi.org/10.1016/j.coldregions.2007.02.008

Gupta, H. V., Kling, H., Yilmaz, K. K. and Martinez, G. F.: Decomposition of the mean squared error and NSE performance criteria: Implications for improving hydrological modelling, J. Hydrol., 377(1-2), 80–91, doi:10.1016/j.jhydrol.2009.08.003, 2009.

Granato, G.E., 2006. Kendall-Theil Robust Line (KTRLine—version 1.0)—A visual basic program for calculating and graphing robust nonparametric estimates of linear-regression coefficients between two continuous variables, in: Section A, Statistical Analysis, Book 4, Hydrologic Analysis and Interpretation. p. 31.

Gray, D.M., Prowse, T., 1993. Chapter 7: Snow and Floating Ice, in: Maidment, D. (Ed.), Handbook of Hydrology. McGraw-Hill, New York, pp. 7.1-7.58.

Groeneveld, J., Malenchak, J., Morris, M., 2017. Numerical Model Studies of Ice Conditions During the Design and Construction of the Keeyask Generating

Station, in: Proc. from the Workshop on River Ice. Whitehorse, Canada.

Hammar, L., Shen, H.T., Kolerski, T., Yuan, Y., Sobczak, L., 2002. A laboratory study on freezeup ice runs in river channel, in: Proc. from the IAHR Ice Symposium. Dunedin, New Zealand.

Hara, F., Kawai, T., Hanada, M., Nishihata, A., Saeki, H., 1996. Movement of ice blocks under an ice cover, in: Proc. from the IAHR Ice Symposium. Beijing, China, pp. 769–778.

Hirayama, K., 1986. Growth of ice cover in steep and small rivers, in: Proc. from the IAHR Ice Symposium. Iowa City, USA, pp. 451–464.

Hopper, H.R., Raban, R.R., 1980. Hanging dams in the Manitoba Hydro system, in: Proc. from the Workshop on River Ice. Burlington, Canada, pp. 195–208.

Huang, F., Shen, H.T., Knack, I., 2012. Modeling border ice formation and cover progression in rivers, in: Proc. from the IAHR Ice Symposium. Dalian, China, pp. 139–149.

Huokuna, M., Aaltonen, J., Veijalainen, N., 2009. Frazil ice problems in changing climate conditions, in: Proc. from the Workshop on River Ice. St. John's, Canada.

Huokuna, M., Morris, M., Beltaos, S., Burrell, B.C., 2020. Ice in reservoirs and regulated rivers. Int. J. River Basin Manag. 1–16. https://doi.org/10.1080/15715124.2020.1719120

IPCC, 2013. Climate Change 2013: The Physical Science Basis.

Jasek, M., Gauthier, Y., Poulin, J., Bernier, M., 2013. Monitoring of Freeze-up on the Peace River at the Vermilion Rapids using RADARSAT-2 SAR data, in: Proc. from the Workshop on River Ice. Edmonton, Canada.

Jasek, M., Pryse-Phillips, A., 2015. Influence of the proposed Site C hydroelectric project on the ice regime of the Peace River. Can. J. Civ. Eng. 42, 645–655. https://doi.org/10.1139/cjce-2014-0425

Katopodis, C., Ghamry, H.K., 2007. Hydrodynamic and physical assessment of ice-covered conditions for three reaches of the Athabasca River, Alberta, Canada.

Can. J. Civ. Eng. 34, 717–730. https://doi.org/10.1139/L07-026

Kendall, M.G., 1975. Rank Correlation Methods. Oxford University Press, New York.

Kennedy, R.E., 1944. Computation of daily isolation energy. Bulletin of the American Meteorlogical Society, V. 30.

Kim, S., Stadnyk, T.A., Asadzadeh, M., 2022 Climate change impact on water supply and hydropower generation potential in Northern Manitoba.

Kim, S.J., 2020. Climate Change Impact Analysis on Hydropower Operations in the Lower Nelson River Basin by. M.Sc. Thesis, University of Manitoba.

Kivisild, H.R., 1959. Hanging Ice Dams, in: Proc. International Association for Hydraulic Research Congress. Montreal, Canada.

Knack, I., Shen, H.S., 2018. A Numerical Model Study on Saint John River Ice Breakup. Can. J. Civ. Eng. 45, 817–826. https://doi.org/dx.doi.org/10.1139/cjce-2018-0012

Kolerski, T., 2021. Assessment of the ice jam potential on regulated rivers and reservoirs with the use of numerical model results. Cold Reg. Sci. Technol. 191. https://doi.org/10.1016/j.coldregions.2021.103372

Lal, A.M.W., Shen, H.T., 1989. A Mathematical Model for River Ice Processes (RICE), Report No. 89-4.

Larsen, P., 1975. Notes on the Stability of Floating Ice Blocks, in: Proc. from the IAHR Ice Symposium. Hanover, USA, pp. 305–403.

Lees, K., Clark, S., Malenchak, J., Chanel, P., 2021a. Numerical Simulation of Winter Conveyance through the Outlet Lakes Area (Upper Nelson River), in: Proc. from the Workshop on River Ice. Saskatoon, Canada (virtual).

Lees, K., Clark, S., Malenchak, J., Chanel, P., 2019. Two-Dimensional Modelling of Freeze-Up Conditions near Jenpeg Generating Station, in: Proc. from the Workshop on River Ice. Ottawa, Canada.

Lees, K., Clark, S.P., Malenchak, J., Chanel, P., 2021b. Characterizing ice cover

formation during freeze-up on the regulated Upper Nelson River, Manitoba. J. Cold Reg. Eng. 35. https://doi.org/10.1061/(ASCE)CR.1943-5495.0000254

Lees, K., Clark, S.P., Malenchak, J., Chanel, P., submitted A novel methodology to quantify hydraulic conveyance through an ice-impacted lake-outlet system.

Lees, K., Clark, S.P., Malenchak, J., Shen, H.T., Knack, I., 2021c. Numerical simulation of freeze-up jamming in a skim ice regime. Cold Reg. Sci. Technol. 191. https://doi.org/10.1016/j.coldregions.2021.103354

Lemaitre-Basset, T., Collet, L., Thirel, G., Parajka, J., Evin, G., Hingray, B., 2021. Climate change impact and uncertainty analysis on hydrological extremes in a French Mediterranean catchment. Hydrol. Sci. J. 66, 888–903. https://doi.org/10.1080/02626667.2021.1895437

Lindenschmidt, K.E., 2017. RIVICE—A Non-Proprietary, Open-Source, One-Dimensional River-Ice Model. https://doi.org/10.3390/w9050314

Lindström, G., Pers, C., Rosberg, J., Strömqvist, J., Arheimer, B., 2010. Development and testing of the HYPE (Hydrological Predictions for the Environment) water quality model for different spatial scales. Hydrol. Res. 41, 295–319. https://doi.org/10.2166/nh.2010.007

Liu, L., Shen, H.T., 2011. CRISSP2D Version 1.1 Programmer's Manual. CEATI Rep. T012700-0401.

Liu, L., Li, H., Shen, H.T., 2006. A Two-Dimensional Comprehensive River Ice Model, in: Proc. from the IAHR Ice Symposium. Sapporo, Japan, pp. 69–76.

Lüthi, D., Cress, A., Davies, H.C., Frei, C., Schär, C., 1996. Interannual variability and regional climate simulations. Theor. Appl. Climatol. 53, 185–209. https://doi.org/10.1007/bf00871736

MacDonald, M.K., Stadnyk, T.A., Déry, S.J., Braun, M., Gustafsson, D., Isberg, K., Arheimer, B., 2018. Impacts of 1.5°C and 2.0°C warming on pan-Arctic river discharge into the Hudson Bay Complex through 2070. Geophys. Res. Lett. 7561–7570. https://doi.org/10.1029/2018GL079147

Malenchak, J., Morris, M., Shen, H.T., Doering, J., 2006. Modeling anchor ice

growth at sundance rapids, in: Proc. from the IAHR Ice Symposium. Sapporo, Japan, pp. 253–260.

Malenchak, J.J., 2011. Numerical Modeling of River Ice Processes on the Lower Nelson River. Ph.D. Thesis, University of Manitoba.

Manitoba Conservation, 2001. Shoreline Management Handbook.

Manitoba Hydro, 2014. Lake Winnipeg Regulation - A document in support of Manitoba Hydro's Request for a Final License under the Manitoba Water Power Act. Winnipeg, Manitoba.

Mann, H., 1945. Nonparametric Tests Against Trend. Econometrica 13, 245–259.

Mann, H.B., Whitney, D.R., 1947. On a Test of Whether one of Two Random Variables is Stochastically Larger than the Other. Ann. Math. Stat. 18, 50–60. https://doi.org/10.1214/aoms/1177730491

Mann, W., Vogel, C., 1973. Lake Winnipeg Regulation Project, in: Canadian Electrical Association. Toronto, Canada.

Mann, W.K., 1971. Effect of varying ice roughness and channel roughness (Internal Manitoba Hydro memo: unpublished).

Marcotte, N., 1984a. Anchor Ice in Lachine Rapids - Results of Observations and Analysis, in: Proc. from the IAHR Ice Symposium. Hamburg, Germany, pp. 151–160.

Marcotte, N., 1984b. Recent Developments on Mathematical Modelling of Winter Thermal Regime of Rivers, in: Proc. from the IAHR Ice Symposium. Hamburg, Germany, pp. 201–210.

Marcotte, N., 1975. Heat transfer from open-water surfaces in winter (Technical Memorandum No. 114). Ottawa, Canada.

Martinson, K., Sydor, M., Marcotte, N., Beltaos, S., 1993. RIVICE model update, in: Proc. Workshop on Environmental Aspects of River Ice. Saskatoon, Canada, pp. 127–144.

Matoušek, V., 1992. Frazil and skim ice formation in rivers, in: Proc. from the IAHR

Ice Symposium. Banff, Canada, pp. 1–22.

Matoušek, V., 1984a. Regularity of the freezing-up of the water surface and heat exchange between water body and water surface, in: Proc. from the IAHR Ice Symposium. Hamburg, Germany, pp. 187–200.

Matoušek, V., 1984b. Types of Ice Run and Conditions for Their Formation, in: Proc. from the IAHR Ice Symposium. Hamburg, Germany, pp. 315–327.

McFarlane, V., Loewen, M., Hicks, F., 2014. Laboratory measurements of the rise velocity of frazil ice particles. Cold Reg. Sci. Technol. 106–107, 120–130. https://doi.org/10.1016/j.coldregions.2014.06.009

Merwade, V., Cook, A., Coonrod, J., 2008. GIS techniques for creating river terrain models for hydrodynamic modeling and flood inundation mapping. Environ. Model. Softw. 23, 1300–1311. https://doi.org/10.1016/j.envsoft.2008.03.005

Michel, B., 1984. Comparision of field data with theories on ice cover progression in large rivers. Can. J. Civ. Eng. 6–8.

Michel, B., 1978. Ice accumulation at freeze-up or breakup., in: Proc. IAHR Ice Symposium. Lulea, Sweden, pp. 301–317.

Michel, B., 1971. Winter Regime of Rivers and Lakes.

Michel, B., 1967. Morphology of Frazil Ice, in: Proc. from the Conference on Physics of Snow and Ice. Sapporo, Japan.

Michel, B., Marcotte, N., Fonseca, F., Rivard, G., 1982. Formation of Border Ice in the Ste. Anne River, in: Proc. from the Workshop on River Ice. Edmonton, Canada.

Miles, T., 1993. A Study of Border Ice Growth on the Burtwood River. M.Sc. Thesis, University of Manitoba.

Minville, M., Brissette, F., Krau, S., Leconte, R., 2009. Adaptation to Climate Change in the Management of a Canadian Water-Resources System Exploited for Hydropower 2965–2986. https://doi.org/10.1007/s11269-009-9418-1

Moriasi, D.N., Arnold, J.G., Van Liew, M.W., Binger, R.L., Harmel, R.D., Veith,

T.L., 2007. Model evaluation guidelines for systematic quantification of accuracy in watershed simulations. Trans. ASABE 50, 885–900. https://doi.org/10.13031/2013.23153

Morse, B., Richard, M., 2009. A field study of suspended frazil ice particles. Cold Reg. Sci. Technol. 55, 86–102. https://doi.org/10.1016/j.coldregions.2008.03.004

Mueller, J.E., 1968. An introduction to the hydraulic and topographic sinuosity indexes. Ann. Assoc. Am. Geogr. 58, 371–385. https://doi.org/10.1111/j.1467-8306.1968.tb00650.

Nash, J. E., & Sutcliffe, J. V. (1970). River flow forecasting through conceptual models part I—A discussion of principles. Journal of hydrology, 10(3), 282-290.

Navarro-Racines, C., Tarapues, J., Thornton, P., Jarvis, A., Ramirez-Villegas, J., 2020. High-resolution and bias-corrected CMIP5 projections for climate change impact assessments. Sci. Data 7, 1–14. https://doi.org/10.1038/s41597-019-0343-8

Newbury, R., 1968. A study of subarctic river processes. Ph.D. Thesis, Johns Hopkins University.

Nezhikhovskiy, R.A., 1964. Coefficients of Roughness of Bottom Surface of Slush-Ice Cover. Trans. State Hydrol. Inst. 54–82.

Olonscheck, D., Notz, D., 2017. Consistently estimating internal climate variability from climate model simulations. J. Clim. 30, 9555–9573. https://doi.org/10.1175/JCLI-D-16-0428.1

Osterkamp, T.E., Gosink, J.P., 1983. Frazil ice formation and ice cover development in interior Alaska streams. Cold Reg. Sci. Technol. 8, 43–56. https://doi.org/10.1016/0165-232X(83)90016-2

Pariset, E., Hausser, R., 1961. Formation and Evolution of Ice Covers on Rivers, in: ASME-EIC Hydraulics Conference Paper No. 61-EIC-6. pp. 41–49.

Pariset, E., Hausser, R., Gagnon, A., 1966. Formation of Ice Covers and Ice Jams in

Rivers. J. Hydraul. Div. Proc. Am. Soc. Civ. Eng. 1–24.

Perham, R., 1983. Ice Sheet Retention Structures, in: Proc. from the IAHR Ice Symposium. Hamburg, Germany, pp. 339–348.

Peters, B.C., 2021. Investigation of the Ice Dam at Sundance Rapids on the Lower Nelson River. M.Sc. Thesis, University of Manitoba.

Petryk, S., 1995. Chapter 5: Numerical Modelling, in: Beltaos, S. (Ed.), River Ice Jams. Water Resources Publications, LLC, Highlands Ranch, Colorado, pp. 147–172.

Phelps, D.J., Coley, R.W., 1973. Flow Characteristics of the Outlet Channels of Lake Winnipeg for Natural and Regulated Channels, in: The 1st Canadian Hydraulics Conference. Edmonton, Canada.

Plymouth State Weather Center, 2019. Archived Surface Text Observations [WWW Document]. URL https://vortex.plymouth.edu/myo/sfc/textobs-a.html (accessed 6.8.21).

Pradhananga, S., Lutz, A., Shrestha, A., Kadel, I., Nepal, B., Nepal, S., 2020. Selection and downscaling of general circulation model datasets and extreme climate indices analysis. Manual, ICIMOD.

Province of Manitoba, 2021a. Lake Winnipeg [WWW Document]. URL https://www.gov.mb.ca/water/lakes-beaches-rivers/lake-winnipeg.html#:~:text=The Lake Winnipeg drainage basin,more than 7 million people.

Province of Manitoba, 2021b. Manitoba Drought Management Strategy.

Prowse, T., Alfredsen, K., Beltaos, S., Bonsal, B., Duguay, C., Korhola, A., McNamara, J., Pienitz, R., Vincent, W.F., Vuglinsky, V., Weyhenmeyer, G.A., 2011. Past and future changes in arctic lake and river ice. Ambio 40, 53–62. https://doi.org/10.1007/s13280-011-0216-7

Prowse, T.D., 1995. Chapter 2: River Ice Processes, in: Beltaos, S. (Ed.), River Ice Jams. Water Resources Publications, LLC, Highlands Ranch, Colorado, pp. 29–68.

Prowse, T.D., Beltaos, S., Gardner, J.T., Gibson, J.J., Granger, R.J., Leconte, R., Peters, D.L., Pietroniro, A., Romolo, L.A., Toth, B., 2006. Climate change, flow regulation and land-use effects on the hydrology of the Peace-Athabasca-Slave system; Findings from the Northern Rivers Ecosystem Initiative. Environ. Monit. Assess. 113, 167–197. https://doi.org/10.1007/s10661-005-9080-x

Reicosky, D.C., Winkelman, L.J., Baker, J.M., Baker, D.G., 1989. Accuracy of hourly air temperatures calculated from daily minima and maxima. Agric. For. Meteorol. 46, 193–209. https://doi.org/10.1016/0168-1923(89)90064-6

Richard, M., 2011. Field Investigation of Freshwater Frazil Ice Dynamics. Ph.D. Thesis, Laval University.

Rimsha, V.A., Donchenko, R.V., 1957. The investigation of heat loss from free water surfaces in wintertime (in Russian). Tudy Leningr. Gosud. Girdrol. Insti. 65, 58–83.

Schaefli, B. and Gupta, H. V.: Do Nash values have value?, Hydrol. Process., 21, 2075–2080, doi:10.1002/hyp.6825, 2007. Schönfelder, L. H., Bakken, T. H., Alfredsen, K. and Adera, A. G.: Application of HYPE in Norway., 2017. Seibert, J.: On the need for benchmarks in hydrological modelling, Hydrol. Process., 15(6), 1063–1064, doi:10.1002/hyp.446, 2001.

Schleussner, C., Lissner, T.K., Fischer, E.M., Wohland, J., Perrette, M., Golly, A., Rogelj, J., Childers, K., Schewe, J., Frieler, K., Mengel, M., Hare, W., Schaeffer, M., 2016. Differential climate impacts for policy-relevant limits to global warming : the case of 1.5◦C and 2◦C. Earth Syst. Dyn. 7, 327–351. https://doi.org/10.5194/esd-7-327-2016

Schönfelder, L. H., Bakken, T. H., Alfredsen, K. and Adera, A. G.: Application of HYPE in Norway., 2017. Seibert, J.: On the need for benchmarks in hydrological modelling, Hydrol. Process., 15(6), 1063–1064, doi:10.1002/hyp.446, 2001.

Sea-Bird Scientific, 2019. SBE 56 Temperature Sensor [WWW Document]. URL https://www.seabird.com/sbe-56-temperature-sensor/product-details?id=54627897760 (accessed 5.30.19).

Sen, P.K., 1968. Estimates of the Regression Coefficient Based on Kendall's Tau. J. Am. Stat. Assoc. 63, 1379–1389.

Shakibaeinia, A., Kashyap, S., Dibike, Y.B., Prowse, T.D., 2016. An integrated numerical framework for water quality modelling in cold-region rivers: A case of the lower Athabasca River. Sci. Total Environ. 569–570, 634–646. https://doi.org/10.1016/j.scitotenv.2016.06.151

Sharma, S., Magnuson, J.J., Batt, R.D., Winslow, L.A., Korhonen, J., Aono, Y., 2016. Direct observations of ice seasonality reveal changes in climate over the past 320-570 years. Sci. Rep. 6, 1–11. https://doi.org/10.1038/srep25061

She, Y., Hicks, F., Andrishak, R., 2012. The role of hydro-peaking in freeze-up consolidation events on regulated rivers. Cold Reg. Sci. Technol. 73, 41–49. https://doi.org/10.1016/j.coldregions.2012.01.001

Sheffield, J., Wood, E.F., 2007. Characteristics of global and regional drought, 1950-2000: Analysis of soil moisture data from off-line simulation of the terrestrial hydrologic cycle. J. Geophys. Res. Atmos. 112, 1–21. https://doi.org/10.1029/2006JD008288

Shen, H.S., Yapa, P., 1984. A unified degree-day method for river ice cover thickness simulation. Can. J. Civ. Eng. 12, 54–62. https://doi.org/10.1139/l85-006

Shen, H.T., 2016. River Ice Processes, in: Yang, C.T., Wang, L.K. (Eds.), Chapter 14, In Advances in Water Resources, Handbook of Environmental Engineering. Springer International Publishing. Humana Press, Inc., New Jersey, pp. 483–530.

Shen, H.T., 2011. A Study on the Need of Ice Sluice Gates for St. Lawrence/FDR Power Project. Department of Civil and Environmental Engineering, Clarkson University, Potsdam, NY, 13699-5710.

Shen, H.T., 2010. Mathematical modeling of river ice processes. Cold Reg. Sci. Technol. 62, 3–13. https://doi.org/10.1016/j.coldregions.2010.02.007

Shen, H.T., 2002. Development of a Comprehensive River Ice Simulation System, in: Proc. from the IAHR Ice Symposium. Dunedin, New Zealand.

Shen, H.T., Chen, Y.C., Wake, A., Crissman, R.D., 1993. Lagrangian discrete parcel simulation of two-dimensional river ice dynamics. Int. J. Offshore Polar Eng. 2, 328–332.

Shen, H.T., Goranka Bjedov, Daly, S., Lal, A.M.W., 1991. Numerical Model for Forecasting Ice Conditions on the Ohio River. https://doi.org/AD-A243 336

Shen, H.T., Ho, C.-F., 1986. Two-Dimensional Simulation of Ice Cover Formation in a Large River, in: Proc. from the IAHR Ice Symposium. Iowa, USA, pp. 547–558.

Shen, H.T., Shen, H., Tsai, S.-M., 1990. Dynamic transport of river ice. J. Hydraul. Rearch 28, 659–671.

Shen, H.T., Su, J., Liu, L., 2000a. SPH Simulation of River Ice Dynamics. J. Comput. Phys. 165, 752–770. https://doi.org/10.1006/jcph.2000.6639

Shen, H.T., Su, J., Liu, L., 2000b. SPH Simulation of River Ice Dynamics. J. Comput. Phys. 165, 752–770. https://doi.org/10.1006/jcph.2000.6639

Shen, H.T., Van DeValk, W.A., 1984. Field Investigation of St. Lawrence River Hanging Ice Dams, in: Proc. from the IAHR Ice Symposium. Hamburg, Germany, pp. 241–249.

Shen, H.T., Wang, D.S., 1995. Under cover transport and accumulation of frazil granules. J. Hydraul. Eng. 121, 184–195. https://doi.org/0.1061/(ASCE)0733-9429(1995)121:2(184)

Shen, H.T., Wang, D.S., Lal, A.M.., 1995. Numerical simulation of river ice processes. J. Cold Reg. Eng. 9, 107–118. https://doi.org/10.1061/(ASCE)0887-381X(1995)9:3(107)

Simoes, J., Clark, S.P., Ph, D., Eng, P., 2020. Quantification of Border Ice Growth on the Assiniboine River 34, 1–12. https://doi.org/10.1061/(ASCE)CR.1943-5495.0000200

Simonsen, C.P.S., Carson, R.W., 1977. Ice Processes During the Construction of Limestone Generating Station, in: Proc. from the Natonal Hydrotechnical Conference. Quebec City, Canada, p. 19.

Singh, S., Comfort, G., 1998. Expected thermal ice loads in reservoirs, in: Proc. from the IAHR Ice Symposium. Potsdam, USA, pp. 449–456.

Sodhi, D.S., Calkins, D.J., Deck, D.S., 1982. Model study of Port Huron ice control structure (wind stress simulation) (CRREL Report 82-9). Hanover, USA.

Stadnyk, T.A., MacDonald, M.K., Tefs, A., Déry, S.J., Koenig, K., Gustafsson, D., Isberg, K., Arheimer, B., 2020. Hydrological modeling of freshwater discharge into Hudson Bay using HYPE. Elem. Sci. Anthr. 8. https://doi.org/10.1525/elementa.439

Steffler, P., Blackburn, J., 2002. River2D - User Manual, University of Alberta.

Taylor, K.E., Stouffer, R.J., Meehl, G.A., 2012. An Overview of CMIP5 and The Exerpiment Design. Am. Meteorlogical Soceity 485–498. https://doi.org/10.1175/BAMS-D-11-00094.1

Tefs, A.A.G., 2018. Simulating hydroelectric regulation and climate change in the Hudson Bay drainage basin. M.Sc. Thesis, University of Manitoba.

Tefs, A.A.G., Stadnyk, T.A., Koenig, K.A., Déry, S.J., MacDonald, M.K., Slota, P., Crawford, J., Hamilton, M., 2021. Simulating river regulation and reservoir performance in a continental-scale hydrologic model. Environ. Model. Softw. 141. https://doi.org/10.1016/j.envsoft.2021.105025

Thériault, I., 2011. Romaine river ice cover, natural and post project accessibility, in: Proc. from the Workshop on River Ice. Winnipeg, Canada.

Thériault, I., Saucet, J.-P., Taha, W., 2010. Validation of the Mike-Ice model simulating river flows in presence of ice and forecast of changes to the ice regime of the Romaine river due to hydroelectric project, in: Proc. from the IAHR Ice Symposium. Lathi, Finland.

Timalsina, N., Beckers, F., Alfredsen, K., 2016. Modelling winter operational strategies of a hydropower system. Cold Reg. Sci. Technol. 122, 1–9.

Timalsina, N.P., Alfredsen, K.T., 2015. Impact of climate change on ice regime in a river regulated for. Can. J. Civ. Eng. 644, 634–644. https://doi.org/10.1139/cjce-2014-0261

Timalsina, N.P., Alfredsen, K.T., Killingtveit, Å., 2015. Impact of climate change on ice regime in a river regulated for hydropower 42, 634–644. https://doi.org/10.1139/cjce-2014-0261

Timalsina, N.P., Gebre, S.B., Alfredsen, K.T., 2013. Climate change impact on the river ice regime in a Norwegian regulated river, in: Proc. from the Workshop on River Ice. Edmonton, Canada.

Totaro, V., Gioia, A., Iacobellis, V., 2020. Numerical investigation on the power of parametric and nonparametric tests for trend detection in annual maximum series. Hydrol. Earth Syst. Sci. 24, 473–488. https://doi.org/10.5194/hess-24-473-2020

Turcotte, B., Burrell, B.C., Beltaos, S., 2019. The Impact of Climate Change on Breakup Ice Jams in Canada: State of knowledge and research approaches, in: Proc. from the Workshop on River Ice. Ottawa, Canada.

Tuthill, A., 2013. River Ice Control, in: River Ice Formation. Committee on River Ice Processes and the Environment; Canadian Geophysical Union, Hydrology Section, pp. 433–471.

Tuthill, A., 1999. Flow Control to Manage River Ice (Special Report 99-08). Hanover, USA.

Tuthill, B.A.M., Mamone, A.C., 1998. Structural Ice Control Alternatives for Middle Missisippi River. J. Cold Reg. Eng. 12, 202–220. https://doi.org/10.1061/(ASCE)0887-381X(1998)12:4(202)

Unduche, F.S., 2008. A Theoretical and Experimental Study of the Evolution of Surface Ice. Ph.D. Thesis, University of Manitoba.

United States Department of Agriculture, 2004. Chapter 11 - Snowmelt, in: Part 630 Hydrology - National Engineering Handbook. p. 50.

USACE, 2006. Engineering and Design: Ice Engineering.

Uzuner, M.S., Kennedy, J.F., 1972. Stability of Floating Ice Blocks. J. Hydraul. Div. ASCE HY 12, 2117–2133. https://doi.org/10.1061/JYCEAJ.0003500

van Rijn, L.C., 1984. Sediment Transport, Part III: Bed Forms and Alluvial

Roughness. J. Hydraul. Eng. 110, 1733–1754. https://doi.org/10.1061/(ASCE)0733-9429(1984)110:12(1733)

Wazney, L., Clark, S.P., Malenchak, J., 2019a. Laboratory investigation of the consolidation resistance of a rubble river ice cover with a thermally grown solid crust. Cold Reg. Sci. Technol. 157. https://doi.org/10.1016/j.coldregions.2018.10.001

Wazney, L., Clark, S.P., Malenchak, J., Knack, I., Shen, H.T., 2019b. Numerical simulation of river ice cover formation and consolidation at freeze-up. Cold Reg. Sci. Technol. 168. https://doi.org/10.1016/j.coldregions.2019.102884

Wazney, L.E., 2019. Investigation of River Ice Cover Formation Processes at Freeze-up. Ph.D. Thesis, University of Manitoba.

Wilson, S., Lees, K., Asadzadeh, M., 2020. Statistical modelling for the ratio of simulated flow using rating curve to measured flow during ice-on season for the Nelson River (report prepared for Manitoba Hydro).

Wojtowicz, A., Hicks, F., Andrishak, R., Brayall, M., Blackburn, J., 2009. 2-D Modeling of Ice Cover Formation Processes on the Athabasca River, AB, in: Proc. from the Workshop on River Ice. St. John's, Canada.

Yang, X., Pavelsky, T.M., Allen, G.H., 2020. The past and future of global river ice. Nature 577, 69–73. https://doi.org/10.1038/s41586-019-1848-1

Ye, Y., She, Y., 2021. A systematic evaluation of criteria for river ice breakup initiation using River1D model and field data. Cold Reg. Sci. Technol. 189, 1–18. https://doi.org/10.1016/j.coldregions.2021.103316

Zbigniewicz, H.S., 1997. Lake Winnipeg Regulation Ice Stabilization Program, in: Proc. from the Workshop on River Ice. Fredricton, Canada, pp. 43–53.

Appendix A: Field Monitoring Dates and Locations

Table A.1 – Summary of deployment locations and instrumentation types as part of the OLA river ice monitoring program.

Description of Location	Latitude	Longitude	Monitoring Year						
			2015-16	2016-17	2017-18	2018-19	2019-20	2020-2021	2021-2022
Jenpeg Forebay	54.4209	-98.0129	○●⊙	○●⊙	○●⊙	○●⊙	○⊙[6]●[7]	○●⊙	○●⊙
Manitou Rapids	54.4803	-98.0831	●	●[1]	●	●	⊙●◇	●[8]⊙	●⊙◈
05UB017	54.4206	-98.0121	○●	○●[2]	○●[4]	○●⊙	○●⊙	○●⊙	○●⊙
05UB702	54.4206	-98.0632	○●	○●	○●[5]	○●⊙	○●[7]⊙	○●⊙	○●⊙
05UB703	54.4582	-98.1113	○●	○●	○●⊙	○●⊙	○●⊙◆	○●⊙	○●⊙
05UB704	54.3887	-98.0632	○●	○●	○●⊙	○●⊙	○●⊙	○●⊙	○●⊙
Ominawin Bypass Channel	54.4317	-98.0875	N/A[3]	N/A[3]	●	●▲◇	●◇	●[8]	●◈
Saskatchewan Rapids	54.4991	-98.0404	N/A[3]	N/A[3]	N/A[3]	●▲◇	●⊙◇	●[8]⊙	●⊙◈
Manitou Island	54.4704	-98.0920	N/A[3]	N/A[3]	N/A[3]	N/A[3]	●⊙	●[8]⊙	N/A[3]
West Channel Point	54.4591	-98.0998	N/A[3]	N/A[3]	N/A[3]	N/A[3]	●	●[8]	N/A[3]
West Channel Island (levelogger)	54.4257	-98.1215	N/A[3]	N/A[3]	N/A[3]	N/A[3]	●◈	●[8]◈	N/A[3]
Jenpeg Weather Station	54.5265	-98.0333	○	○	○	○	○■	○■	○■

Legend
○Manitoba Hydro or Province of Manitoba Sensors
●Trail Camera
⊙Sea-Bird temperature sensor
■Radiation sensor
◈Solinst Levelogger
◆Solinst Barologger
▲Ice Core ◇Drone Footage

Notes
[1]Camera not deployed due to high water levels causing access issues.
[2]Camera lost due to beaver activity.
[3]No equipment deployed (N/A)
[4]Camera incorrectly deployed on motion-sensor setting, intermittent images available only.
[5]High frequency (5-min interval) images available from Nov 6 to 9, 2017. Photos are lost prior to Nov 6, 2017.
[6]Instrumentation failure (breached seal and flooded SeaBird).
[7]Instrumentation failure (unknown cause)
[8]Camera not active (no batteries installed due to COVID-19 restrictions)

Appendix B: Ice Roughness Reach Estimation

[Author's note: Appendix B describes the back-calculation of ice roughness from hydrometric data using a slope-area hydraulics method (Beltaos, 2011) along with OLA hydrometric data.]

Background

As a result of the hydraulic resistance of an ice cover, the same river reach can have a markedly higher water surface slope during winter relative to the open-water period. An example of this is shown on Figure B.1 for a river section of the OLA.

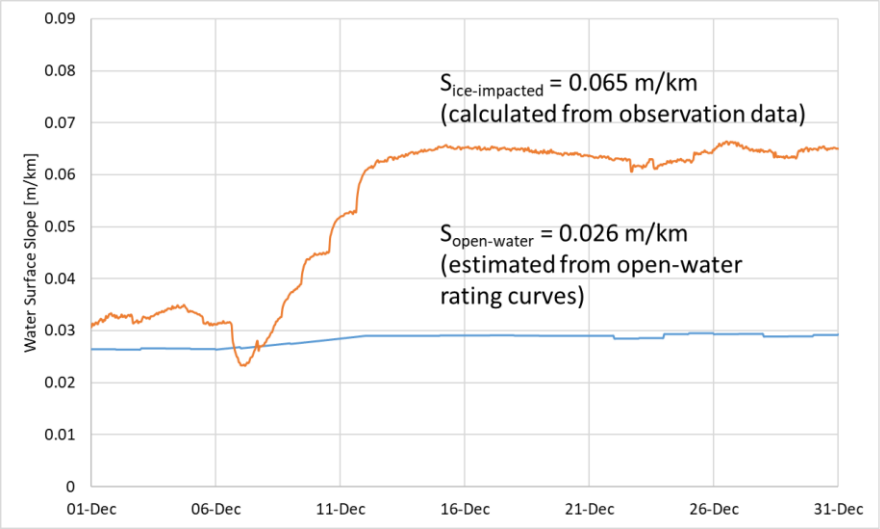

Fig B.1 – Comparison between ice-effected and open-water water surface slope.

Using these water surface slopes, channel bathymetry and estimates of bed roughness, the slope-area hydraulics method (Beltaos, 2011) can be applied to back-calculate values of ice roughness. This method was applied using OLA hydrometric data (monitoring stations shown as red stars on Fig B.2) across four reaches with different channel characteristics (reaches shown as coloured ovals on Fig B.2).

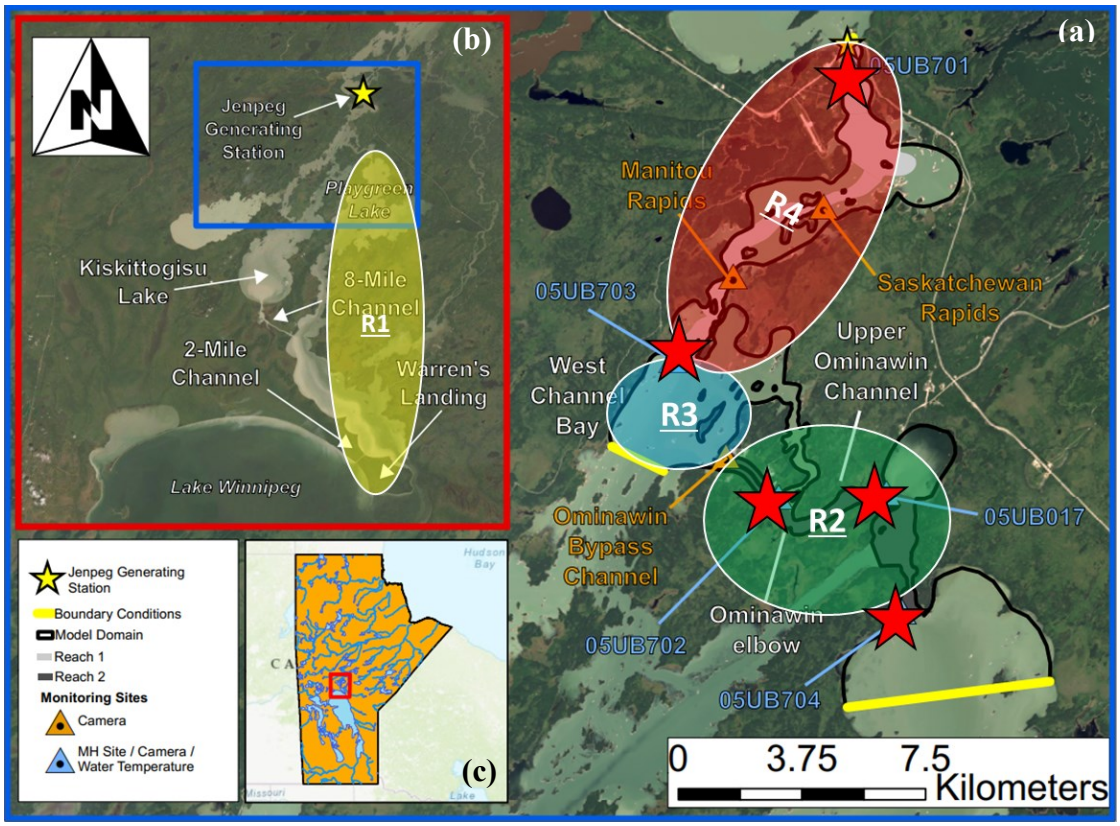

Fig B.2 – Map of hydrometric monitoring stations (red stars) and reaches R1 through R4 for ice roughness estimation (coloured ovals). [Image in (a) courtesy of the USGS, Landsat; base map in (b) from ArcGIS World Imagery, Surface Layer Credits: Source: Esri, DigitalGlobe, GeoEye, Earthstar Geographics, CNES/Airbus DS, USDA, AeroGRID, IGN, and the GIS User Community; vector data in (c) from Government of Manitoba 2001, Government of Canada 2017.]

Methodology

To pursue the slope-area hydraulics method, the following steps are required:

1) Define a cross-section of bathymetry representative of conditions at the hydrometric monitoring station. An example of which is shown on Fig B.3.

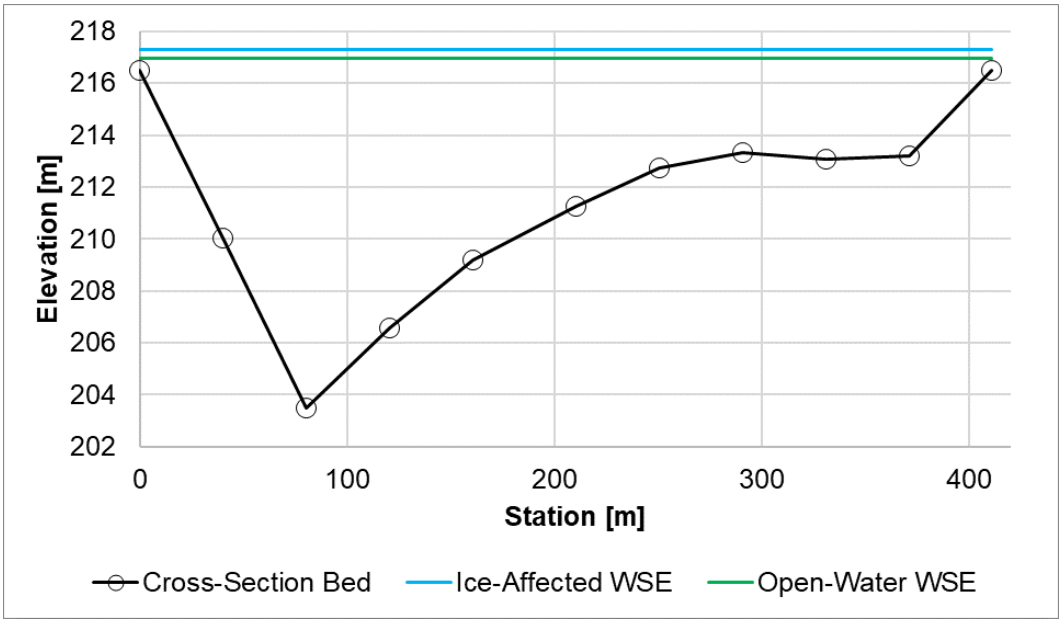

Fig B.3 – Example of bathymetric cross section along with open-water and ice-affected WSE observations.

2) Calculate the open-water composite Manning's coefficient using open-water hydrometric data (Eq B-1), where A_{XS} is the channel cross-sectional area [m^2].

$$Q = \frac{1}{n_c} A_{XS} R_h^{2/3} \sqrt{S} \qquad \text{Eq B-1}$$

3) Calculate the ice-covered composite Manning's coefficient (n_c):

   a. Assume a small initial ice thickness (e.g., 0.3 m).

   b. Assume the proportion of total Jenpeg flow that the reach receives (if necessary).

4) Apply Sabaneev equation to calculate n_i (Eq B-2)

$$n_c = \left(\frac{n_i^{\frac{2}{3}} + n_b^{\frac{3}{2}}}{2} \right)^{2/3} \qquad \text{Eq B-2}$$

Results

A summary of bed roughness (n_b) values calculated using Eq B-2 is summarized in Table B.1.

Table B.1 – Range of bed roughness calculated using hydrometric data from 1996 to 2018 for reaches shown on Fig B.3.

Roughness Zone	*Description*	*S_w Stations*	*n_b*	*Cross-Section*
R1	Playgreen Lake	RF005-UB704	0.041-0.047	UB704
R2	Upper Ominawin Channel	UB704-UB702	0.016-0.019	UB017
	Ominawin Bypass Channel	UB704-UB702	0.014-0.018	UB702
R3	West Channel Bay	UB702-UB703	0.041-0.049	UB703
R4	U/S Jenpeg Forebay	UB703-Forebay	0.026-0.029	UB701

Box-whisker plots of ice roughness values calculated using Eq B-1 and B-2 are shown on Fig. B.4.

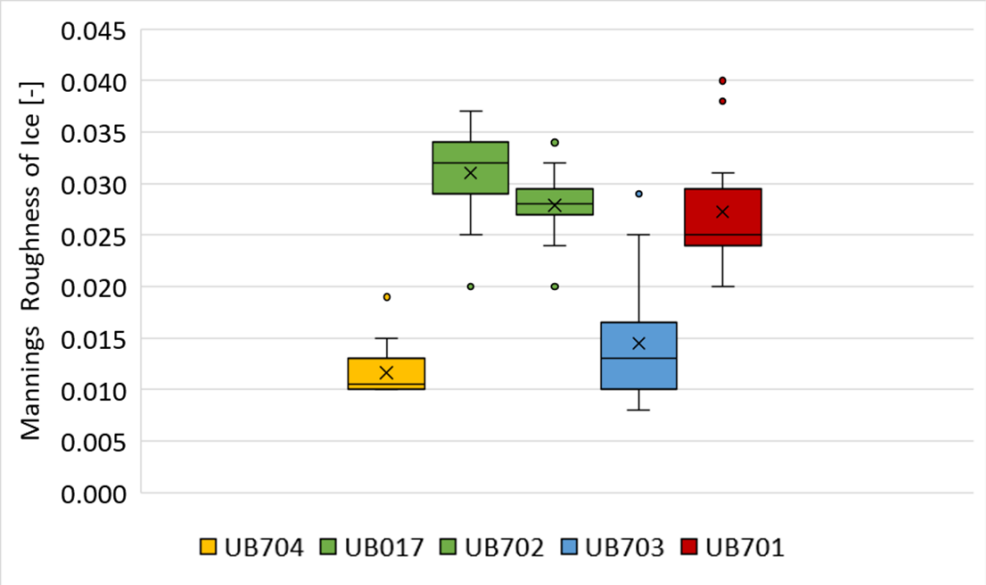

Fig B.4 – Box-whisker plots of Manning's ice roughness calculated for R1 (yellow), R2 (green), R3 (blue), and R4 (red) (see Fig. B.2).

Summary

There is a noticeable difference in ice roughness between channelized areas (R2 and R4 on Fig. B.2) and lake areas (R1 and R3 on Fig. B.2). Ice roughness estimates for lake areas (approximately 0.01 to 0.015) are consistent with calculations by Mann (1971) who estimated an OLA lake ice roughness of 0.013. Higher roughness estimates for channelized areas (approximately 0.02 to 0.04) reflect rougher ice conditions due to dynamic ice processes and localized hanging dam formations. It is noted that these values represent reach-averaged conditions, while localized roughness values at a particular location may vary considerably.

Appendix C: Open-Water and Ice-Affected Uncertainty

[Author's note: Appendix C summarizes a memo sent to Manitoba Hydro (December 20, 2020) describing how open-water error associated with the 3D Nelson River West Channel rating curves was determined. Small wording and style changes were made to be compatible with the format of this thesis. Supplementary detail is provided describing how error associated with discharge estimation at Jenpeg was calculated.]

Background

Research efforts at the University of Manitoba include monitoring, characterization and modelling of freeze-up processes on the Upper Nelson River between Lake Winnipeg and Jenpeg. As part of this research, Manitoba Hydro's Lake Winnipeg - Jenpeg 3D rating curves (sourced from the HERMES model; on the Lake Winnipeg datum) are being applied to generate hydraulic boundary conditions to simulate reduced channel discharge capacity through the winter months.

As per the details described in an email to Manitoba Hydro on November 23, 2020, these rating curves were tested for their suitability to generate the required boundary conditions. This was done by applying the rating curves during a period of constant Jenpeg flow immediately prior to ice stabilization. The range of these flows is reflective of the conditions observed during the winter season. During this constant flow period, we compared median calculated forebay WSE values from the rating curve to median observed forebay WSE values. While the analysis showed good agreement for most years, the forebay WSE calculated using the 3D rating curves was far too low for some years.

Methodology

In response to suggestions provided by Manitoba Hydro contacts, the following actions were taken:

- **Action 1:** Ensure datum corrections are applied (as necessary) to ensure datasets are on the same datum prior to comparison.

- **Action 2:** Modify MATLAB processing code with knowledge that the 3D rating curves are on the 'Lake Winnipeg Datum'.
- **Action 3:** Test application of the revised Jenpeg flow record ('JENPEG_GS_ADJ_FLOW_1977-2020.xlsx').

Results

The above three actions were applied by conducting the following tests:

- Test #1: Apply wind-eliminated Lake Winnipeg WSE and unadjusted flow record to back-calculate forebay WSE from the rating curve. Apply +0.169 m adjustment to compare with observed forebay WSE.
- Test #2: Apply wind affected Lake Winnipeg WSE at Montreal Point (RF001) and unadjusted flow record to back-calculate forebay WSE from the rating curve. Apply +0.169 m adjustment to compare with observed forebay WSE.
- Test #3: Apply wind-eliminated Lake Winnipeg WSE and revised flow record to back-calculate forebay WSE from the rating curve. Apply +0.169 m adjustment to compare with observed forebay WSE.

The error results from these calculations are summarized in Table C.1. Example years are shown on Figures C.1 and C.2, with comments found on the following page.

Table C.1 - Summary of error statistics for analysis.

Year	Duration of Constant Q @ Start of Ice Stabilization [days]	Constant Q @ Start of Ice Stabilization [m^3/s]	ΔWSE ($WSE_{OBS} - WSE_{SIM}$) [m] Test #1	Comments	ΔWSE ($WSE_{OBS} - WSE_{SIM}$) [m] Test #2	Comments	ΔWSE ($WSE_{OBS} - WSE_{SIM}$) [m] Test #3	Comments
1996	14	100000	-0.16	GOOD	see footnote 2	N/A	0	ERROR INCREASED DUE TO HIGH FLOW
1997	13	90000	0.03	GOOD	see footnote 2	N/A	0	ERROR INCREASED DUE TO HIGH FLOW
1998	see footnote 1	see footnote 1	see footnote 1	see footnote 1	see footnote 1	see footnote 1	see footnote 1	see footnote 1
1999	35	75000	0.15	GOOD	see footnote 2	N/A	0.280	ERROR INCREASED DUE TO HIGH FLOW
2000	27	80000	-0.04	GOOD	see footnote 2	N/A	0.123	GOOD
2001	35	85429	0.13	GOOD	see footnote 2	N/A	0.340	ERROR INCREASED DUE TO HIGH FLOW
2002	29	75000	0.03	GOOD	see footnote 2	N/A	0.180	ERROR INCREASED DUE TO HIGH FLOW
2003	see footnote 1	see footnote 1	see footnote 1	see footnote 1	see footnote 1	see footnote 1	see footnote 1	see footnote 1
2004	23	100000	-0.05	GOOD	see footnote 2	N/A	0.210	ERROR INCREASED DUE TO HIGH FLOW
2005	13	93462	0.200	HIGH FLOW? WIND?	0.11	**REDUCED ERROR FROM 0.2 to 0.11 m**	0.410	ERROR INCREASED DUE TO HIGH FLOW
2006	see footnote 1	see footnote 1	see footnote 1	see footnote 1	see footnote 1	see footnote 1	see footnote 1	see footnote 1
2007	14	110000	-0.27	HIGH FLOW? WIND?	0.09	**REDUCED ERROR FROM -0.27 to 0.09 m**	0.400	ERROR INCREASED DUE TO HIGH FLOW
2008	22	110000	-0.20	HIGH FLOW? WIND?	0.07	**REDUCED ERROR FROM -0.20 to 0.07 m**	0.260	ERROR INCREASED DUE TO HIGH FLOW
2009	12	90000	-0.16	HIGH FLOW? WIND?	0.07	**REDUCED ERROR FROM -0.16 to 0.07 m**	0.005	GOOD
2010	see footnote 1	see footnote 1	see footnote 1	see footnote 1	see footnote 1	see footnote 1	see footnote 1	see footnote 1
2011	15	95000	-0.01	GOOD	see footnote 2	N/A	0.300	ERROR INCREASED DUE TO HIGH FLOW
2012	13	70000	0.11	GOOD	see footnote 2	N/A	0.240	ERROR INCREASED DUE TO HIGH FLOW
2013	6	95000	-0.19	HIGH FLOW? WIND?	0.00	**REDUCED ERROR FROM -0.19 to 0.00 m**	0.190	ERROR INCREASED DUE TO HIGH FLOW
2014	7	100000	0.02	GOOD	see footnote 2	N/A	0.380	ERROR INCREASED DUE TO HIGH FLOW
2015	40	85000	0.04	GOOD	see footnote 2	N/A	0.270	ERROR INCREASED DUE TO HIGH FLOW
2016	20	100000	0.09	GOOD	see footnote 2	N/A	0.410	ERROR INCREASED DUE TO HIGH FLOW
2017	3	93333	-0.13	GOOD	see footnote 2	N/A	0.320	ERROR INCREASED DUE TO HIGH FLOW

Notes
[1]No identifiable constant flow period prior to ice stabilization, so this year was excluded from analysis.
[2]Error from Test #1 was within tolerance of error (0.5 ft.), so calculations not performed with wind-affected Lake Winnipeg data.

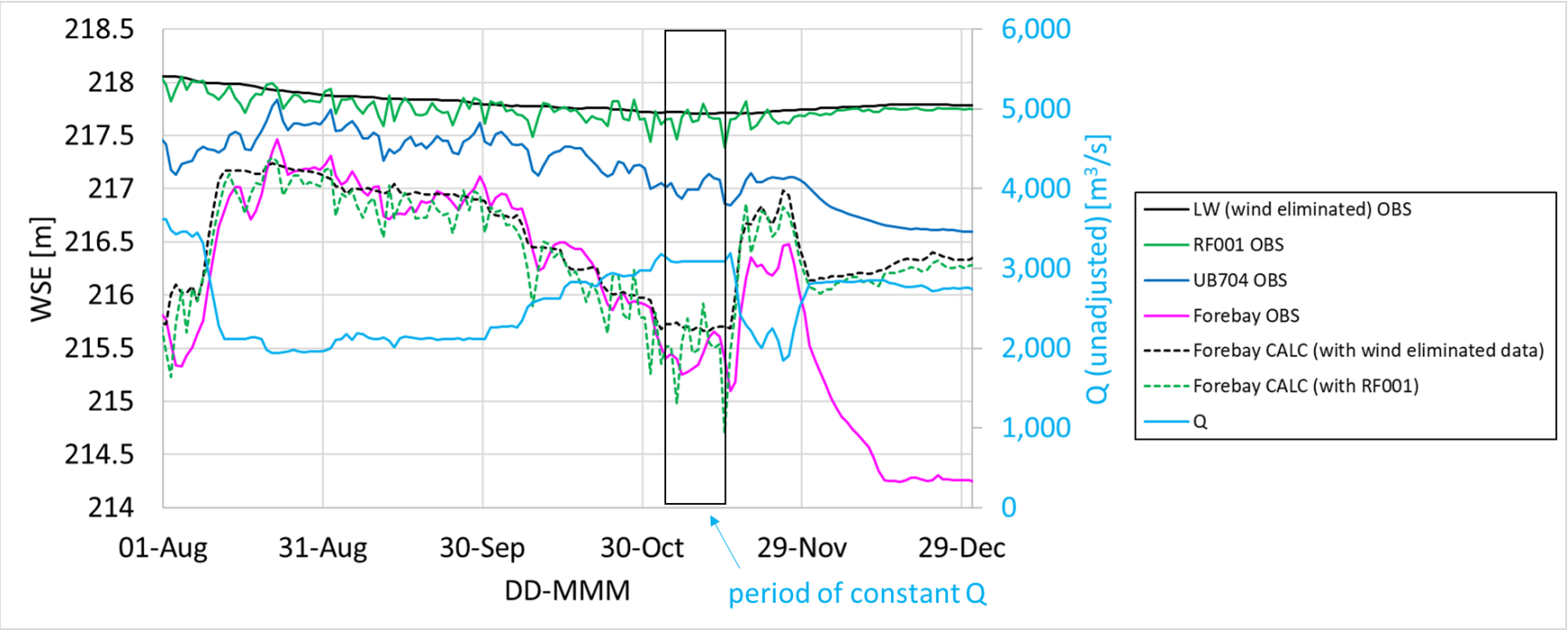

Fig. C.1 – Example of calculated forebay WSE for 2007 (higher error year).

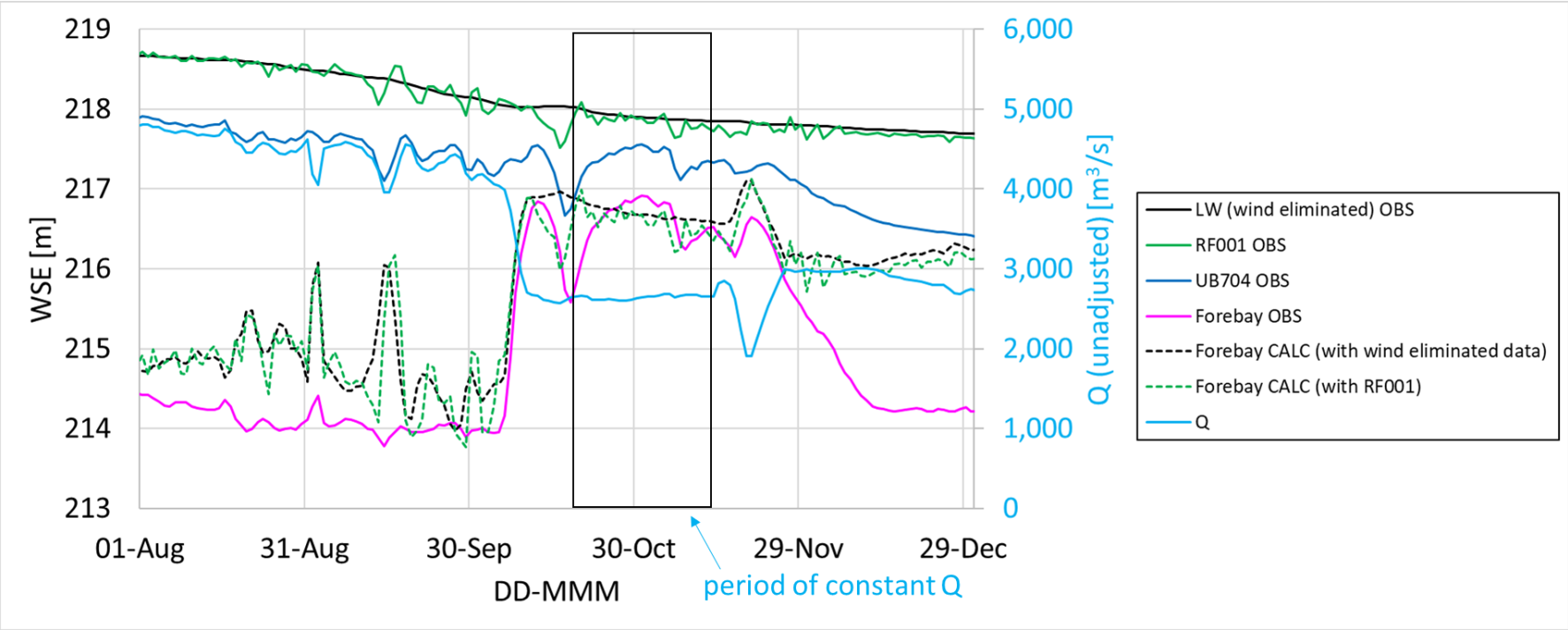

Fig. C.2 – Example of calculated forebay WSE for 2011 (lower error year).

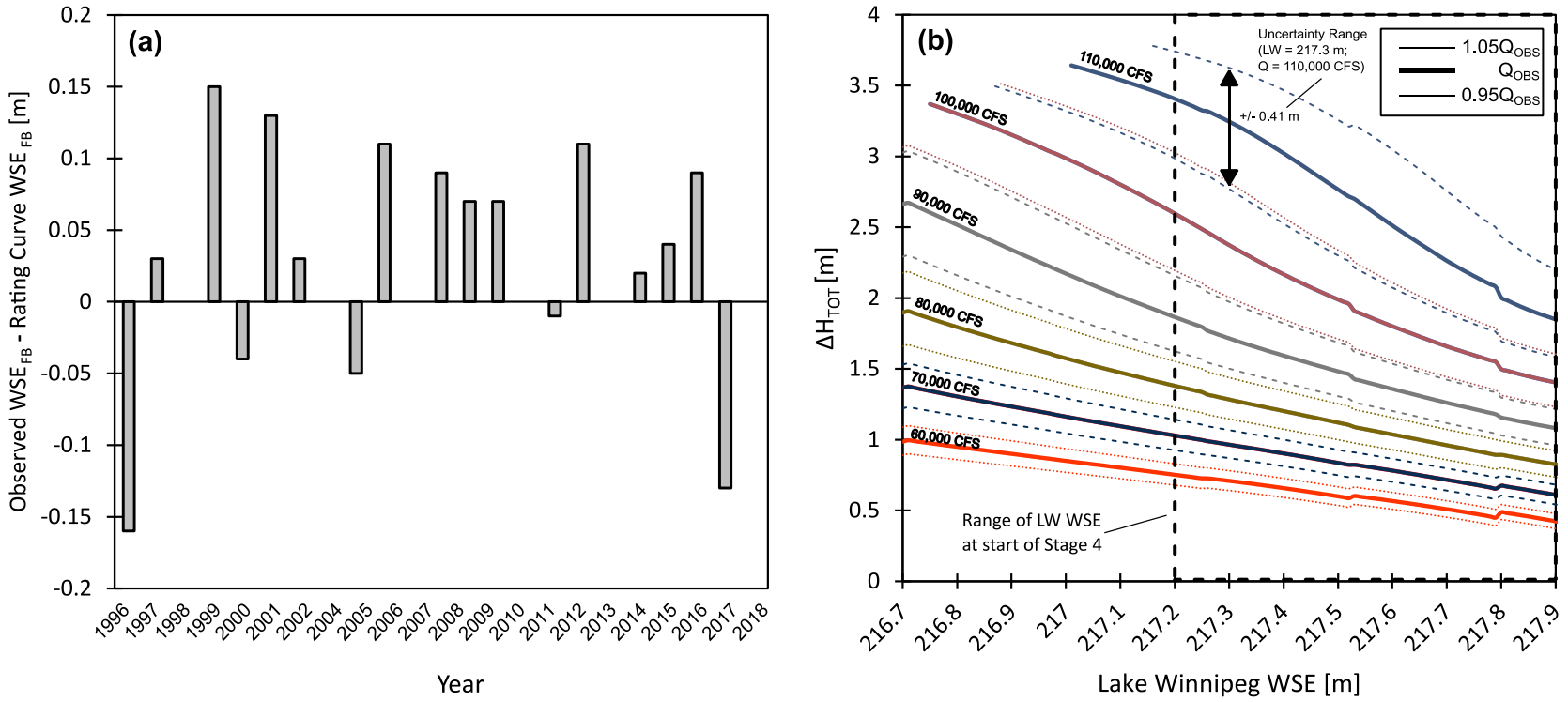

Fig C.3 – (a) Open-water error estimation using rating curves during constant *Q* and *WSE* period (estimated at 0.15 m). (b) Estimate of hydraulic head error introduced through flow estimation at Jenpeg (where true flow is estimated to be within +/- 0.05Q_{OBS}). When averaged for flow targets 60,000 CFS to 110,000 CFS, hydraulic head error introduced due to flow estimation is estimated to be 0.15 m. From this analysis, total acceptable hydraulic head error is assumed to be 0.3 m (0.15 m from rating curves, and 0.15 m from flow estimation uncertainty).

The following observations are made from the results:

- In Test #1, all years were within the selected error tolerance of 0.5 ft, except for the following years:
    - 2005, 2007, 2008, 2009, 2013
- Of the 5 years above, all were relatively high flow years (Q = 90,000 to 110,000 cfs). However, wind may be a more important factor in explaining higher errors during these years.
- In Test #2, by applying wind-affected data, errors were reduced in each of the 5 years above. In each case, error was reduced to be within the tolerance of 0.5 ft.
- In Test #3, the revised flow record was applied to rating curve calculations. In almost all years, resulting errors exceeded the selected tolerance of 0.5 ft. To apply this revised flow record, we would require a revised form of the 3D rating curves that account for these higher flows.
- Not shown are results from 1977-1995, where less data is available. The results were fairly consistent with 1996-2017 years, with higher errors in the early years of Jenpeg monitoring (1977-1982).
- **Using the results from this analysis, open-water error associated with rating curves is estimated to be 0.15 m (see Fig C.3a).**
- **It is suspected that Jenpeg discharge records may have error due to estimation errors (see Chapter 4). Using the 3D rating curves, error associated with discharge estimation is estimated to be an additional 0.15 m or more by calculating changes in hydraulic head over a range of discharge conditions (see Fig. C.3b). As such, the range of acceptable error in Chapter 4 was chosen as 0.3 m.**